UC San Diego
UC San Diego Electronic Theses and Dissertations

Title
Magnetization dynamics and spin diffusion in semiconductors and metals

Permalink
https://escholarship.org/uc/item/3sz7x6s6

Author
Cywiński, Łukasz

Publication Date
2007

Peer reviewed|Thesis/dissertation

eScholarship.org Powered by the California Digital Library
University of California

UNIVERSITY OF CALIFORNIA, SAN DIEGO

Magnetization Dynamics and Spin Diffusion in Semiconductors and Metals

A dissertation submitted in partial satisfaction of the

requirements for the degree Doctor of Philosophy

in

Physics

by

Łukasz Cywiński

Committee in charge:

Professor Lu Jeu Sham, Chair
Professor Leonid V. Butov
Professor Jorge E. Hirsch
Professor Deli Wang
Professor Edward T. Yu

2007

Copyright
Łukasz Cywiński, 2007
All rights reserved.

The dissertation of Łukasz Cywiński is approved, and it is acceptable in quality and form for publication on microfilm:

____

____

____

____

____

Chair

University of California, San Diego

2007

TABLE OF CONTENTS

Signature Page iii

Table of Contents iv

List of Figures vii

Acknowledgements ix

Vita, Publications, and Fields of Study xi

Abstract xiv

1 Introduction 1
A. Spintronics and magnetoelectronics in the previous millenium . . . 1
B. Overview of work presented in this dissertation 4
C. A reader's guide to the dissertation 7

2 Spin diffusion in semiconductors and metals: a general theory 9
A. Derivation of spin-dependent drift-diffusion equations from Boltzmann equation 10
B. Spin diffusion equations 20
1. Spin diffusion in a non-degenerate paramagnetic semiconductor 20
2. Spin diffusion in a degenerate ferromagnet 24

3 Spin injection and extraction in metal/semiconductor structures 26
A. Boundary conditions for spin currents at the interface of a metal and a semiconductor 27
1. Schottky barrier with homogeneous doping of the semiconductor 27
2. Schottky barrier with inhomogeneous doping for spin injection . 29
3. Calculation of the spin current through a square barrier 32
B. Single ferromagnet/paramagnet (F/N) junction: conductivity mismatch 37

4 A diffusive spin valve 41
A. One-dimensional calculation 42
B. Spin valve in a general geometry - a back-of-the envelope calculation 47

5 Lateral spin diffusion 50
A. Effective 1D diffusion formalism 50
B. Quantitative analysis of a lateral spin valve. 54
C. Acknowledgements 58

6 Mutli-terminal systems: Magnetic Contact Transistor and a logic gate 59
A. The principle of operation . . . 62
B. Results of modeling . . . 66
C. Fully polarized spin current and spin current without net charge current . . . 67
D. Five-terminal magneto-logic gate . . . 69
E. Acknowledgements . . . 71

7 Electric readout of magnetization dynamics . . . 72
A. The principle of operation . . . 72
B. Time-dependent formalism . . . 76
C. Results of calculations . . . 78
D. The dynamic readout of the outcome of a logic operation in the five-terminal system . . . 80
E. Acknowledgements . . . 82

8 Electric detection of light polarization . . . 83
A. System requirements for detection of light polarization . . . 84
B. Transport of photoexcited spin-polarized carriers . . . 87
C. Results and discussion in steady state . . . 88
D. The time dependent analysis . . . 93
E. Acknowledgements . . . 96

9 Ultrafast light-induced demagnetization in transition metals . . . 97
A. Previous work and phenomenology of the ultrafast demagnetization 98
B. Spin relaxation of quasiparticles - nonequilibrium Stoner model . . 103
1. Photoexcitation and its effect on single-particle excitations. . . . 104
2. Spin relaxation due to impurity and phonon scattering . . . 107
3. Estimate of Elliott-Yafet spin relaxation time from transport measurements in metals . . . 112
C. Carrier - spin wave interaction . . . 113
1. Comparison with the results of Koopmans et al. . . . 115
D. Summary . . . 116

10 Ultrafast demagnetization in the sp-d model: application to (III,Mn)V ferromagnetic semiconductors . . . 118
A. The sp-d model and its application to (III,Mn)V ferromagnetic semiconductors . . . 120
B. Light excitation of the carrier system in (III,Mn)V . . . 126
C. Model of the carrier bath . . . 128
D. Rate equations for the localized spin . . . 131
E. Demagnetization due to carriers in a single spin-split band . . . 135
1. The inverse Overhauser effect . . . 137
2. Carriers as a reservoir of angular momentum: $\Delta\mu$=0 . . . 138

3. The effects of the dynamic spin polarization of carriers: $\Delta\mu \neq 0$. 141
F. Demagnetization due to holes in the valence band of (III,Mn)V semiconductor . . . 144
G. Comparison with experimental results . . . 149
H. Summary . . . 152
I. Acknowledgements . . . 153

Appendix A. Derivation of the Master equation for the localized spin dynamics 154

Appendix B. $\mathbf{k} \cdot \mathbf{p}$ Hamiltonian for (III,Mn)V magnetic semiconductors . . . 162

Appendix C. Some symmetry properties of exchange-split bands in a cubic semiconductor . . . 166

Appendix D. Spin-flip transition rate in a 4 band spherical Luttinger model 168

Appendix E. Numerical calculations of densities of states and transition rates in a $\mathbf{k} \cdot \mathbf{p}$ model . . . 172

Bibliography . . . 175

LIST OF FIGURES

Figure 3.1: Band diagrams for a Schottky barrier 30

Figure 4.1: One-dimensional spin valve. 42
Figure 4.2: The spin current densities in a 1D spin valve. 43
Figure 4.3: The electrochemical potentials μ_s in the N channel of the 1D spin valve. 44
Figure 4.4: The magneto-resistive ratio of a one-dimensional spin valve for two channel lengths. 46

Figure 5.1: Lateral spin valve. 51
Figure 5.2: Magneto-resistive effect in a lateral spin valve. 56

Figure 6.1: A three-terminal Magnetic Contact Transistor. 62
Figure 6.2: Eletrochemical potentials in the MCT. 64
Figure 6.3: Right terminal current in the MCT with voltages tuned for the digital operation. 66
Figure 6.4: Current density in the vicinity of the right terminal of the MCT. 68
Figure 6.5: A five-terminal magneto-logic gate. 70

Figure 7.1: A Magnetic Contact Transistor modified for electric readout of magnetization dynamics. 73
Figure 7.2: Spin accumulation under the R contact and voltage inside it for different magnetization alignments of the L and M terminals. 75
Figure 7.3: Time-dependent current generated by magnetization dynamics. 79
Figure 7.4: A dynamical five-terminal magneto-logic gate and the electrochemical potentials in the semiconductor channel 81
Figure 7.5: Transient currents generated by the magneto-logic gate. . . 82

Figure 8.1: A detector of circular polarization of light. 86
Figure 8.2: Electrochemical potentials and current asymmetry coefficient for the steady state excitation of the light-polarization detector 90
Figure 8.3: Current asymmetry versus α and the magnitudes of the currents from both contacts in a polarization detector. 92
Figure 8.4: Time-resolved current response to light pulses alternating in polarization. 94

Figure 9.1: Typical magneto-optical trace of ultrafast demagnetization . 99
Figure 9.2: Spin-projected density of states in nickel. 106

Figure 10.1: The band structure of GaMnAs calculated using 8 band $\mathbf{k} \cdot \mathbf{p}$ model 127

Figure 10.2: Spin-flip transition rate in a single band model. 139
Figure 10.3: Spin-flip transition rate as a function of carrier density. . . 140
Figure 10.4: Demagnetization of the localized spins in a single band model for different energy relaxation times of carriers. 141
Figure 10.5: Demagnetization of the localized spins for different carrier spin relaxation times. 142
Figure 10.6: Valence band spin-resolved densities of states in GaMnAs and InMnAs. 145
Figure 10.7: Spin-flip transition rate W_{+-} in GaMnAs. 146
Figure 10.8: Demagnetization of the Mn spin in GaMnAs and InMnAs. 148

ACKNOWLEDGEMENTS

I would like to thank my advisor Lu Sham for giving me a lot of freedom in working on multiple projects. I have not always made the best use of this freedom, but he was patient, and he persistently guided me over these years. I have learned a lot during our weekly meetings.

Half of the work in this dissertation has been done in close collaboration with Hanan Dery, from whom I have learned many things about research. The other half of the dissertation has outgrown from a collaboration with Jun Kono and Jigang Wang. Their experiments have introduced me to the problem of ultrafast magnetization dynamics, and our conversations were always a source of inspiration for me. The constant encouragement which I got from Jun has got me through the ups and downs of my work on ultrafast demagnetization.

I have spent countless hours discussing science in our office with Parin Dalal, from whom I learned, among other things, about information theory. I have also benefitted from discussions with Harry Suhl, Joaquin Fernández-Rossier, Kenny Burch, Semion Saikin, Wang Yao, Fedir Kyrychenko and Vinay Tota.

Finally, I want to thank Alicja Pytlińska for teaching me mathematics and Włodzimierz Natorf for teaching me physics.

The text of Chapter 5, in part, is a reprint of the material as it appears in Hanan Dery, Łukasz Cywiński, and L.J. Sham, *Lateral diffusive spin transport in layered structures*, Phys. Rev. B **73**, 041306(R), © 2006 The American Physical Society. The dissertation author was a co-investigator and co-author of this article.

The text of Chapter 6, in part, is a reprint of the material as it appears in (1) Hanan Dery, Łukasz Cywiński, and L.J. Sham, *Spin transference and magnetoresistance amplification in a transistor*, Phys. Rev. B **73**, 161307(R), © 2006 The American Physical Society, in which the dissertation author was a co-investigator

and co-author; (2) Hanan Dery, Parin Dalal, Łukasz Cywiński, and L.J. Sham, *Spin based logic in semiconductors for reconfigurable large scale circuits*, Nature **447**, 573 © 2007 Nature Publishing Group, in which the dissertation author was a contributing investigator and author.

The text of Chapter 7, in part, is a reprint of the material as it appears in (1) Łukasz Cywiński, Hanan Dery, and L.J. Sham, *Electric readout of magnetization dynamics in a ferromagnet-semiconductor system*, Appl. Phys. Lett. **89**, 042105, © 2006 The American Institute of Physics, where the dissertation author was the primary investigator and author; (2) Hanan Dery, Parin Dalal, Łukasz Cywiński, and L.J. Sham, *Spin based logic in semiconductors for reconfigurable large scale circuits*, Nature **447**, 573 © 2007 Nature Publishing Group, in which the dissertation author was a contributing investigator and author.

The text of Chapter 8, in part, is a reprint of the material as it appears in Hanan Dery, Łukasz Cywiński, and L.J. Sham, *Spintronics for electrical measurement of light polarization*, J. Appl. Phys. **100**, 063713, © 2006 The American Institute of Physics. The dissertation author was a co-investigator and co-author of this article.

The text of Chapter 10, in part, is a reprint of the material as it appears in Łukasz Cywiński and L.J. Sham, *Ultrafast demagnetization in the sp-d model: a theoretical study*, arXiv preprint cond-mat/0703049, (to appear in Phys. Rev. B). The dissertation author was the primary investigator and author of this article.

VITA

August 11, 1978	Born, Warsaw, Poland
2002	Master of Science in Physics in Physics Warsaw University, Warsaw, Poland
2002	Teaching Assistant, Department of Physics University of California, San Diego
2003-2007	Research Assistant, Department of Physics University of California, San Diego
2007	Doctor of Philosophy University of California, San Diego

PUBLICATIONS

J. Wang, C. Sun, J. Kono, A. Oiwa, H. Munekata, Ł. Cywiński, and L.J. Sham, *Ultrafast quenching of ferromagnetism in InMnAs induced by intense laser irradiation*, Phys. Rev. Lett. **95**, 167401 (2005).

H. Dery, Ł. Cywiński, and L.J. Sham, *Lateral diffusive spin transport in layered structures*, Phys. Rev. B **73**, 041306(R) (2006).

H. Dery, Ł. Cywiński, and L.J. Sham, *Spin transference and magnetoresistance amplification in a transistor*, Phys. Rev. B **73**, 161307(R) (2006).

K. Dziatkowski, Ł. Cywiński, W. Bardyszewski, A. Twardowski, H. Saito, and K. Ando, *Influence of disorder on the optical absorption in semiconductors: Application to epitaxially grown III-V compounds*, Phys. Rev. B **73**, 235340 (2006).

Ł. Cywiński, H. Dery, and L.J. Sham, *Electric readout of magnetization dynamics in a ferromagnet-semiconductor system*, Appl. Phys. Lett. **89**, 042105 (2006).

H. Dery, Ł. Cywiński, and L.J. Sham, *Spintronics for electrical measurement of light polarization*, J. Appl. Phys. **100**, 063713 (2006).

J. Wang, C. Sun, Y. Hashimoto, J. Kono, G.A. Khodaparast, Ł. Cywiński, L.J. Sham, G.D. Sanders, C.J. Stanton, H. Munekata, *Ultrafast Magneto-Optics in Ferromagnetic III-V Semiconductors*, J. Phys.: Condens. Matter **18**, R501 (2006).

H. Dery, P. Dalal, Ł. Cywiński, and L.J. Sham, *Spin-based logic in semiconductors for reconfigurable large-scale circuits*, Nature **447**, 573 (2007).

Ł. Cywiński and L.J. Sham, *Ultrafast demagnetization in the sp-d model: a theoretical study*, preprint cond-mat/0703049, accepted for publication in Phys. Rev. B (2007).

FIELDS OF STUDY

Major Field: Physics

Studies in Theoretical Condensed Matter Physics.
Professor Lu Jeu Sham

ABSTRACT OF THE DISSERTATION

Magnetization Dynamics and Spin Diffusion in Semiconductors and Metals

by

Łukasz Cywiński

Doctor of Philosophy in Physics

University of California, San Diego, 2007

Professor Lu Jeu Sham, Chair

Spintronics is an emerging field of research focused on introducing the electron spin degree of freedom into electronics. Its aims include devising new means of magnetization manipulation in ferromagnets and creating systems in which the electrical expression of spin-related phenomena is possible. In this dissertation we present theoretical work important for both of these goals.

In a process of ultrafast light-induced demagnetization the magnetization of a ferromagnet decreases on a sub-picosecond time-scale following an excitation by a strong laser pulse. We present a theory of this phenomenon which is applicable to ferromagnetic (III,Mn)V semiconductors. Using it we qualitatively explain the experimental results obtained recently in these materials. We also give a theory of ultrafast demagnetization in transition metals, in which we put previously proposed approaches on a sound conceptual basis, and analyze a new mechanism of demagnetization due to emission of spin waves by hot carriers.

Recent progress in growth of metal-semiconductor interfaces has enabled efficient spin-polarized transport between metallic ferromagnets and semiconductors such as GaAs. We present a theory of diffusive spin transport in such metal-semiconductor structures. In contrast to popular one-dimensional approach, we take into account realistic two-dimensional lateral geometry of these systems. We also focus on room temperature regime. Our analysis of spin accumulation achievable in systems of sub-micron dimensions leads to a proposal of a new family of spintronic devices with multiple ferromagnetic terminals in contact with a semi-

conductor channel. We show that in a three-terminal "spin transistor" digital electric expression of spin accumulation is possible. We also calculate the time-dependent spin transport induced by rotation of one of the magnets in this system, and we show that electrical sensing of magnetization dynamics is realistic in metal-semiconductor structures. An analogous five terminal system can work as a reprogrammable logic gate, with the logic inputs and the gate functionality encoded in the directions of the ferromagnetic terminals. A system capable of electrical detection of circular polarization of light is also modeled. All these proposals will hopefully set new directions in applied spintronics research and stimulate new experiments.

1

Introduction

1.A Spintronics and magnetoelectronics in the previous millenium

Research on magnetism has always been one of the most important part of theoretical condensed matter physics. The different types of magnetic order (ferromagnetism, antiferromagnetism, etc.) are all caused by Coulomb interaction between the free and/or localized electrons in a given material. For this reason, a large part of many-body theory is occupied with explaining the origin of magnetic properties of materials. However, when theoretical physicists were working on subtle many-body spin-related problems (e.g. the Kondo effect in 60s and 70s), the research on the applications of magnetism was mostly a domain of classical physics. For example, the smallest ferromagnetic samples available then were large enough for magnetic domains to form, and the applied scientists working on e.g. magnetic recording were using a micromagnetic approach [1] to model the relevant properties of the magnets at hand.

The discovery of giant magnetoresistive effect (GMR) in late eighties [2, 3] can be considered a turning point in the relation between interesting microscopic (quantum) physics and the field of applied magnetism. GMR occurs in nanometer-thin multilayers of ferromagnetic and paramagnetic metals, and truly microscopic

theory of spin-polarized transport is needed to explain this effect [4]. Let us also mention that another physical effect present in such nano-sized multilayers, the coupling of the magnetizations of two ferromagnets separated by a paramagnet [5], also requires a quantum-mechanical explanation [6]. Within less than ten years from its discovery, the commercial devices using GMR were created [7]. Now practically every computer has a GMR read head in its hard drive.

The research on ferromagnetic metals has continued to bring fascinating results since then. The spin transfer effect, in which the spin-polarized current flowing between two ferromagnets with non-collinear magnetizations can switch the direction (or trigger a precessional motion) of one of the magnetizations, was first predicted theoretically [8, 9] and then observed (first experiment was reported in 1998 [10], for a review see Ref. [11]). A large progress in controlling the magnetization dynamics was made, with shortest reported magnetization switching time of a ferromagnetic particle on the order of 200 ps [12]. A discovery particularly important for this dissertation is the one of ultrafast light-induced demagnetization [13]. The excitation of a magnet by a strong laser pulse leads to a significant drop of magnetization on a time-scale of less than a picosecond. This is the fastest magnetization dynamics ever observed, and the physical mechanism governing it is not yet fully understood.

Another important development in spin-dependent transport in all-metallic structures was a discovery of tunneling magnetoresistance (TMR) effect at room temperature [14] in a device consisting of two ferromagnets separated by a tunneling barrier. TMR is used now in magnetic random-access memory (MRAM) devices, in which the bits of information are encoded in the magnetization alignments of TMR multilayer stacks of sub-micron size [15] (MRAM also relies on developments in fast precessional magnetization switching mentioned before). MRAM offers a non-volatile memory integrable on the same mother board with the microprocessor. However, it maintains the separation of functions between the new "magnetoelectronic" components (which are used for data storage) and the con-

ventional silicon based field-effect transistor electronics (used for logic operations). This brings us to the issue of spin physics in semiconductors.

The electronics is based on multi-terminal nonlinear devices (diodes, transistors), and semiconductors hold complete sway over this field. The reason for this is that due to the low carrier concentration the properties of semiconductors can be easily changed by either sample preparation (inhomogeneous doping) or applied stimuli (e.g. gate voltage changing the carrier concentration in the channel of a field-effect transistor (FET)). In a seminal article of Datta and Das [16] it was noted that the gate voltage could also influence the spin of the carriers in the channel of a FET through the Rashba effect (see e.g. [17]), which originates in the spin-orbit coupling present in the valence and conduction bands of a typical III-V semiconductor. If the spin-polarized current is injected and extracted by the source and the drain (which are assumed to be ferromagnetic), the gate voltage is predicted to modulate the current by influencing the precession of spins of ballistic electrons in the channel. Spin injection from a ferromagnetic to a paramagnetic metals had been shown in 1985 by Johnson and Silsbee [18], but in early nineties there were no experiments on spin polarized transport in semiconductors. The dynamics and relaxation of spin polarization created by optical excitation was an active area of research since the 70s [19], but electrical injection from a spin-polarized source (a ferromagnet) or transport of polarized carriers have not been experimentally achieved then.

Major experimental developments in spin physics of semiconductors occurred in late nineties. First, electron spin relaxation times of $\sim$100 ns were seen at low temperatures in GaAs [20], and the electrical transport of spin-polarized photoelectrons has been shown to occur on a length-scale of tens of microns [21]. Second, spin injection from Mn-doped diluted magnetic semiconductors into GaAs was achieved [22, 23, 24] in 1999. This was soon followed by successful spin injection from a metallic contact into a semiconductor [25]. The third development was a successful growth of a new class of ferromagnetic semiconductors: III-V materials

doped with Mn ions [26, 27]. The critical temperature in certain samples of GaMnAs was reported to be ∼110 K, and theoretical understanding of carrier-mediated ferromagnetism in these materials [28, 29, 30] gave hope for achieving the room-temperature ferromagnetism. Let us mention here, that the (III,Mn)V materials are not good semiconductors from the carrier transport point of view: they are are heavily p-type with hole concentration of the order of 10^{20} cm^{-3} and low mobility due to strong disorder. However, their magnetic properties are controlled by carrier concentration, and both the critical temperature [31] and the coercivity of InMnAs have been manipulated by voltage in a gated structure. This responsiveness to external stimuli is what justifies calling them ferromagnetic semiconductors instead of rather poor metals (the fact that they are semiconductor-based also matters, and because of this they form interfaces with paramagnetic semiconductors more easily than real metals).

All of the above have given a strong boost to the field, which was soon termed "spintronics" [32] (an earlier name of "magnetoelectronics" is associated more with all-metallic devices). An enormous amount of experimental and theoretical activity followed in last 7 years. Excellent reviews of the topic are now available. Reference [33] is probably the broadest, covering both metals and semiconductors (and including a very thorough overview if the history of all the relevant ideas and experiments). A book [34] focuses mostly on applications of metallic ("magnetoelectronic") structures, while Ref. [35] contains a detailed theoretical review of spin dynamics in semiconductors. Recent developments relevant for this dissertation will be discussed in the introductory sections of the following chapters of this work.

1.B Overview of work presented in this dissertation

In the historical sketch above one can see that the research in spintronics can be roughly divided into three subfields: (1) spin-dependent effects in "normal"

semiconductors (spin-orbit interaction in III-V semiconductors, spin transport including the spin Hall effect); (2) new phenomena associated with magnetism in metals (spin transfer torque, (ultra)fast magnetization dynamics); (3) physics of new magnetic material such as ferromagnetic semiconductors. All of these are, to a varying degree, represented in this dissertation.

The dissertation is divided into two largely independent parts. The first one, consisting of chapters 2-8, contains our research of spin transport and its electrical expression in hybrid metal-semiconductor structures. These investigations were inspired by a rapid experimental progress in spin injection and extraction between metals such as iron into semiconductors such as GaAs [36, 37, 38]. The main idea which we pursue in these chapter is that of the electrical expression of spin accumulation created in a semiconductor by spin injection and extraction through junctions with ferromagnets. We propose various systems with multiple magnetic terminals, the functionalities of which illustrate this idea. Specifically, we discuss: (a) both static and dynamic readout of magnetic memory by current measurement; (b) all-electrical sensing of magnetization dynamics; (c) a reprogrammable logic gate in which the gate functionality and the logic input is encoded in directions of magnetizations of four contacts; (d) a detector of circular polarization of light using the phenomenon of optical orientation in semiconductors and extraction of photoexcited carriers into the ferromagnetic leads. On the technical side, instead of using a popular one-dimensional approach to spin diffusion (see e.g. Ref. [39]), we developed a simple yet accurate formalism for calculating spin diffusion in realistic lateral systems. We applied it in our modeling of both steady state and dynamic (driven by rotation of ferromagnets) spin transport in the proposed systems.

We emphasize that in our work on spin transport in metal/semiconductor structures we have concentrated on room temperature regime, and we have confined ourselves to working with junction parameters very close to the experimentally realized ones. Because of the former restriction, our theoretical approach is a rather simple one, eschewing the intricate physics of transport in spin-orbit coupled bands

(e.g. Rashba interaction [17] or spin Hall effect [40]). Although the non-trivial effects of spin-orbit coupling on spin transport are fascinating, they are completely irrelevant at room temperatures in semiconductors such as GaAs. Thus our main effort in this field of research was to use a more limited set of physical resources to predict interesting spin-related effects observable at room temperature, and to devise realistic applications of them. We hope that our results will become an inspiration for future experiments. A rapid progress in the direction which we had investigated has already occurred [41, 42].

In the second part of the dissertation, consisting of chapters 9 and 10, we propose a theory of light-induced ultrafast demagnetization in transition metals (chapter 9) and in ferromagnetic (III,Mn)V semiconductors (chapter 10). Although the ultrafast demagnetization was discovered in Ni more than 10 years ago [13], there is yet no theory which is fully convincing and physically transparent (at least in our opinion). In chapter 9 we analyze two different mechanism which can lead to subpicosecond drop of magnetization in photoexcited itinerant ferromagnet. We build on a previously proposed [43] explanation in terms of Elliott-Yafet spin relaxation of electrons on a sound conceptual basis, and made a connection between this mechanism of demagnetization and the spin diffusion theory in ferromagnetic metals (discussed in chapter 2). Then we introduce a different approach, in which the demagnetization is caused by generation of spin waves by hot carriers. Although this model seems to us more physically appealing than the first, more theoretical work is needed to resolve which approach is more suitable for explanation of experiment in Ni and Fe. We hope that our work presented in chapter 9, by clarifying the previous theories and putting forth a new approach, will lead to new understanding of ultrafast demagnetization in transition metals.

Chapter 10 contains our theory of ultrafast demagnetization within the sp-d model of ferromagnetism. This work was motivated by our close collaboration with the experimental group of professor Junichiro Kono on ultrafast demagnetization in ferromagnetic (III,Mn)V semiconductors. This new class of magnetic materials

has garnered a lot of attention in the last decade, with hundreds of measurements of static magnetic and transport properties published, but only during the last two years there has been a progress in time-resolved experiments. We have worked closely with the experimentalists on many aspects of their measurements, with this effort culminating in writing together the first review article on time-resolved spectroscopy of (III,Mn)V semiconductors [44]. In chapter 10 we present a general theory of light-induced demagnetization in a system of localized spins coupled by exchange interaction to the spins of the itinerant carriers, and perform detailed calculations for ferromagnetic semiconductors InMnAs and GaMnAs. Our theory highlights the interplay between the nonequlibrium population dynamics of hot carriers, and spin-flip scattering between them and the localized spins. We obtain a qualitative agreement with experimental results in (III,Mn)V materials.

1.C A reader's guide to the dissertation

Chapters 2-8 are concerned with spin diffusion and electrical expression of spin accumulation in metal/semiconductor structures. In chapter 2 we derive the spin diffusion equations applicable to semiconductors at room temperature (when more subtle effects of spin-orbit interaction are blurred out), and to both ferromagnetic and paramagnetic metals. In chapter 3 we discuss the physics of spin injection and extraction through metal/semiconductor junction at room temperature. Then we discuss a simplest spintronic system, a two-terminal spin-valve in Chapter 4. There we also give an important example of the approximate calculation of spin accumulation (in section 4.B), which should help the reader develop an intuition on which the ideas for the systems discussed in chapters 6-8 are based. Chapter 5 contains more development of spin diffusion formalism, allowing for simple, approximate but accurate, calculation of spin accumulation in lateral systems (a semiconductors channel with magnetic contact of finite width on top of it). In this chapter we apply the new method of calculation to a lateral spin valve, and we discuss the

importance of a proper choice of system's geometry for an optimal operation (i.e. a large magneto-resistive effect).

In Chapter 6 we introduce a powerful concept of a multi-terminal system (a transistor), the principle of operation of which is the electrical expression of spin accumulation. Apart from a three-terminal transistor we present a five-terminal system which is capable of performing a logic operation (with logic inputs encoded in the magnetizations of the ferromagnetic contacts). In Chapter 7 we calculate the time-dependent currents induced in these multi-terminal systems by a rotation of the magnetization of one of the contacts, showing a possible method of electrical measurement of magnetization dynamics, and a dynamic readout of magnetic memory (or a result of a logic operation in a five-terminal system). Finally, Chapter 8 contains a description of a spintronic polarimeter (a detector of circular polarization of light).

Chapters 9 and 10 are concerned with theory of ultrafast light-induced demagnetization, and they are practically independent of the previous chapters (with one exception mentioned below). In chapter 9 we give an overview of experiments and previous theories of demagnetization in transition metals, and then present our contribution, which consists of clarification of a previously proposed model, and introduction of a new theory of excitation-induced carrier-magnon scattering. We also make a connection between a model of demagnetization based on Elliott-Yafet spin relaxation of electrons, and spin diffusion in ferromagnets, which is discussed in chapter 2.

In Chapter 10 we present a theory of ultrafast demagnetization in materials described by the sp-d model of ferromagnetism, with specific application to ferromagnetic (III,Mn)V semiconductors. This is the most theoretically involved part of the dissertation, both from analytical and numerical points of view. In order for the chapter to be more readable and efficient in conveying key physical messages, most technical details are contained in the following appendices.

2

Spin diffusion in semiconductors and metals: a general theory

In this chapter we will derive spin diffusion equations applicable to bulk semiconductors at room temperature and metals (para- and ferromagnetic). The caveats in the case of semiconductors are necessary because the spin-orbit interaction in III-V compounds leads to an effective spin-dependent Hamiltonian for carriers which has a non-trivial momentum dependence [17]. At room temperature in bulk samples it is well established that the "macroscopic" approach, in which the main role of spin orbit interaction is to relax the average carrier spin, is applicable. Actually, even at very low temperature, in spin injection experiments [38] the spin accumulation is seen to obey a simple diffusion equation (however, in order to account for spin precession due to applied strain [45] one has to use a microscopic Hamiltonian coupling the carrier spin to the lattice deformation). Equations more complicated than the ones derived below were obtained for 2D electrons at room temperature [46, 47], predicting e.g. the anisotropy of spin relaxation (in-plane and out-of plane components of spin polarization decaying on different time-scales). A subtler approach to deriving spin transport equation from the Boltzmann equation is necessary for describing the spin Hall effect [48, 49, 40]. However, this effect leads to a minute spin accumulation [50], and although it is

theoretically fascinating we are not concerned with it here. For our more practical purposes of describing the diffusion of spins injected from a ferromagnet, the approach described below is sufficient.

2.A Derivation of spin-dependent drift-diffusion equations from Boltzmann equation

In this section we will derive the macroscopic spin-dependent drift-diffusion equations from the Boltzmann equation. The main condition on which the derivation rests is that the spin relaxation time τ_{sr} should be much longer than the momentum relaxation time. We are also going to use the relaxation time approximation. Precisely, we will assume that the scattering is elastic and the material is isotropic (i.e. the probability of scattering from $\mathbf{k}$ to $\mathbf{k}'$ depends only on the common energy and the angle between the wave-vectors), and that the energy $\epsilon_s(\mathbf{k})$ for each spin subband depend only on the magnitude of the wave-vector $\mathbf{k}$. Under these assumptions, the relaxation time approximation is exact (see Ref. [51], chapter 16). However, the final results should be applicable in more general cases. The spin diffusion equation is clearly the simplest approach to the problem of spin transport, and its general form could be as well postulated (actually, in the first article [39] containing the form of spin diffusion equation presented below, the equation was simply written down without any discussion of its origin). Adding more realistic effects, like inelastic scattering (e.g. with phonons) or real band structure, can lead to more complicate formulas for different scattering times, but qualitatively the net result is going to be a redefinition of microscopic expressions for macroscopic parameters (e.g. diffusion constant and spin relaxation time). The latter are taken most often from experiments anyway.

An example of the resilience of the spin diffusion equation is the case of spin Coulomb drag [52, 53]. The Coulomb scattering does not affect the charge diffusion constant (as it conserves the total momentum of the carriers), but it renormalizes

the spin diffusion coefficient D_s. A more surprising example is the case of ferromagnetic materials (such as permalloy, $Ni_{80}Fe_{20}$) in which the spin-diffusion length is on the order of the electron mean free path. In such a case, the spin diffusion equation might not be applicable (surely the its justification given for metals in Ref. [54] is invalid). Somewhat surprisingly, the numerical calculations using the full Boltzmann equation have shown [55] that the macroscopic transport equation is accurate to a few percent.

We start from the Boltzmann equation for the spin-dependent distribution function $f_s(\mathbf{r},\mathbf{k},t)$ for electrons (charge $q{=}{-}e$):

$$\frac{\partial f_s}{\partial t} + \mathbf{v}\cdot\nabla_{\mathbf{r}} f_s - \frac{e\mathbf{E}}{\hbar}\cdot\nabla_{\mathbf{k}} f_s - \frac{e}{\hbar c}(\mathbf{v}\times\mathbf{B})\cdot\nabla_{\mathbf{k}} f_s = I_{s\mathbf{k}}\{f_s\} \tag{2.1}$$

where the electron velocity is

$$\mathbf{v} = \frac{1}{\hbar}\frac{\partial\epsilon(\mathbf{k})}{\partial\mathbf{k}} \quad .$$

In the subsequent analysis the last term on the left hand side of Eq. 2.1 (involving the **B** field) is going to be disregarded. The effect of magnetic field on the orbital motion is thus neglected. Magnetic field induced spin precession (not included above) is more relevant to spintronics, and it can be included in the spinor form of the Boltzmann equation (semiclassical transport equation for the spin density matrix), see e.g. Ref. [47].

The electric field **E** consists of both the external field, and a possible contribution from the local space charge. The problem of the presence of space charge will be addressed later on the level of drift-diffusion equations, when we discuss the so-called quasi-neutrality approximation.

The scattering integral on the right-hand side consists of spin-conserving term (for derivation see e.g. Ref. [51])

$$I_{s\mathbf{k}} = -\int \frac{d^3k'}{(2\pi)^3}\; W(s\mathbf{k}, s\mathbf{k}')\,(f_s(\mathbf{k}) - f_s(\mathbf{k}')) \;\; , \tag{2.2}$$

and a spin-flip term:

$$I_{sf,\mathbf{k}} = -\int \frac{d^3k'}{(2\pi)^3}\; W_{sf}(s\mathbf{k}, -s\mathbf{k}')\,(f_s(\mathbf{k}) - f_{-s}(\mathbf{k}')) \;\; . \tag{2.3}$$

The spin-flip scattering rate W_{sf} is usually much smaller than the spin-conserving scattering. In a paramagnetic material without magnetic impurities, the physical origin of spin relaxation is the spin-orbit interaction [19, 33]. In s-wave band this interaction is weak. For example, in a conduction band of a III-V semiconductor the spin-orbit interaction effects come from the $\mathbf{k}\cdot\mathbf{p}$ mixing [17] with the p-symmetry valence band (in which the spin-orbit splitting Δ_{SO} is quite large, typically 0.3 eV). However, even in the low-bangap materials such as InAs this is still a perturbative effect. For semiconductors at room temperature and paramagnetic metals it is safe to assume that the spin-flip scattering rate is much smaller than the ordinary spin-conserving scattering rate. As we have mentioned in the introduction to this chapter, we are not going to employ a microscopic spin-orbit Hamiltonian. If we had done this, the Boltzmann equation (2.1) would have to be written in the spinor notation, with electron density matrix $\hat{f}$ replacing the two distributions $f_{\pm}$ (see e.g. [56, 47]), and additional terms coupling the spin of electron in state $\mathbf{k}$ to its velocity would have appeared. In the regime of interest for us all these complications play a minor role, and we retain the spin-orbit interaction only in the spin-flip scattering term.

Assuming the isotropic material and elastic scattering (e.g. from impurities) we can derive relaxation-time expression for spin-conserving scattering. We write the $\delta f_{s\mathbf{k}}$ function as

$$\delta f_{s\mathbf{k}} = \mathbf{a}_s(\epsilon_{s\mathbf{k}})\cdot\mathbf{k} \tag{2.4}$$

where the vector $\mathbf{a}_s$ is parallel to the electric field driving the current. Following Ref. [51] we arrive at:

$$\int \frac{d^3k'}{(2\pi)^3} W(s\mathbf{k}, s\mathbf{k}')(f_s(\mathbf{k}) - f_s(\mathbf{k}')) = \frac{1}{\tau^m_{s\mathbf{k}}}(f_s(\mathbf{k}) - f^0_s(\mathbf{k})) \tag{2.5}$$

where f^0 is a *local* equilibrium distribution, and the transport momentum scattering time for spin s is given by

$$\frac{1}{\tau^m_{s\mathbf{k}}} = \int \frac{d^3k'}{(2\pi)^3} W(s\mathbf{k}, s\mathbf{k}')(1 - \hat{\mathbf{k}}\cdot\hat{\mathbf{k}'}) \ . \tag{2.6}$$

The spin-dependence of $\tau^m_{s\mathbf{k}}$ is relevant for the ferromagnetic materials, in which the densities of states for two directions of spin are different, and consequently the scattering times can differ.

Now let us come back to the Boltzmann equation (2.1). For simplicity we will assume that the spatial dependence of distribution function is limited to one dimension, e.g. $f{=}f(x,\mathbf{k},t)$. The spin-dependent distributions f_s are written in the following way:

$$\begin{aligned} f_{s\mathbf{k}}(x,t) &= f^0_{s\mathbf{k}}(x,t) + \delta f_{s\mathbf{k}}(x,t) \\ &= f^0(\epsilon_{s\mathbf{k}}) + \Delta f_s(x,\epsilon_{s\mathbf{k}},t) + \delta f_{s\mathbf{k}}(x,t) \end{aligned} \tag{2.7}$$

where f^0 is a *global* equilibrium distribution (thermal distribution of carriers in the material, without currents or spin accumulation), Δf_s describes spin accumulation and δf_s is the deviation from the *local* equilibrium (which generally is spin-dependent), given by $f^0_s{=}f^0 + \Delta f_s$. This local equilibrium distribution is simply a Fermi-Dirac function with a spatially dependent chemical potential $\mu^c_s(x)$ (the superscript c is for a chemical potential, in order to distinguish it with an electrochemical potential μ_s which we will introduce later). The deviation $\delta f_{s\mathbf{k}}$ fulfills the condition

$$\int \frac{d^3k}{(2\pi)^3} \delta f_{s\mathbf{k}} = 0 \ , \tag{2.8}$$

so that all the spin density variations are described by Δf_s. A similar separation of different contributions to the deviation from equlibrium (with Δf_s to linear order around f^0) is a cornerstone of a derivation of macroscopic spin diffusion equations presented in Ref. [54]. Next we linearize the Boltzmann equation around a local equlibrium f^0_s. This step deserves a comment: in the following we will neglect the terms proportional to $E\delta f$, but leave the expression involving $E\Delta f_s$. The existence of spin accumulation (nonzero Δf_s) is caused by the electric field, and strictly speaking this term is nonlinear in E. Nevertheless, the two contributions to the deviation from the global equlibrium (Δf_s and δf_s) are of very different character: δf_s represents a shift of the electron distribution function in the $\mathbf{k}$ space,

whereas Δf_s is a macroscopic spin accumulation, corresponding to smooth (on the length scales larger than the mean-free path) spatial dependence of chemical potentials $\mu_s^c(x)$ for both spins. The linearization around the local equilibrium is necessary in order to recover the drift-diffusion equations addressing the high electric field regime relevant in semiconductors [57]. Analogous equations for the case of electron and hole diffusion in bipolar structures have been successfully used since the beginnings of semiconductor physics [58].

First, let us derive the form of the scattering terms using the separation of $f_{s\mathbf{k}}$ given in Eq. (2.7). Within the relaxation time approximation with constant momentum relaxation time $\tau^m_{s\mathbf{k}}$ the spin-conserving scattering gives the term $-\delta f_{s\mathbf{k}}/\tau^m_{s\mathbf{k}}$. The spin-flip terms give two contributions. The first one involves Δf_s:

$$I^{(1)}_{sf,\mathbf{k}} = -\int \frac{d^3k'}{(2\pi)^3} W_{sf}(s\mathbf{k},-s\mathbf{k}')(\Delta f_s(\epsilon_{\mathbf{k}s}) - \Delta f_{-s}(\epsilon_{\mathbf{k}'-s}) \ . \tag{2.9}$$

We will deal with this term shortly, when we perform the $\mathbf{k}$ average of the Boltzmann equation. The second contribution to the spin-flip scattering involves δf_s:

$$I^{(2)}_{sf,\mathbf{k}} = -\int \frac{d^3k'}{(2\pi)^3} W_{sf}(s\mathbf{k},-s\mathbf{k}') \left[\delta f_{s\mathbf{k}} - \delta f_{-s\mathbf{k}'}\right] \ . \tag{2.10}$$

As before, we write $\delta f_{s\mathbf{k}}{=}\mathbf{a}_s(\epsilon_{s\mathbf{k}}) \cdot \mathbf{k}$ and obtain

$$I^{(2)}_{sf,\mathbf{k}} = -\frac{\delta f_{s\mathbf{k}}}{\tau_{s\mathbf{k}}} + \frac{\delta f_{-s\mathbf{k}}}{\tilde{\tau}_{s\mathbf{k}}} \ , \tag{2.11}$$

where the scattering times are given by

$$\tau^{-1}_{s\mathbf{k}} = \int \frac{d^3k'}{(2\pi)^3} W_{sf}(s\mathbf{k},-s\mathbf{k}') \ , \tag{2.12}$$

$$\tilde{\tau}^{-1}_{s\mathbf{k}} = \int \frac{d^3k'}{(2\pi)^3} W_{sf}(s\mathbf{k},-s\mathbf{k}') \, \hat{\mathbf{k}} \cdot \hat{\mathbf{k}}' \ . \tag{2.13}$$

Let us note the reason for spin-dependence of these times (it is not obvious in the notation above). In a ferromagnet the surfaces of constant energy are different for each spin $s{=}\pm$. For given s and $\mathbf{k}$ (with corresponding energy $\epsilon_{s\mathbf{k}}$), the energy-conserving delta function inside the transition rate W makes the surface of $\frac{d^3k'}{(2\pi)^3}$ integration depend on spin.

Finally, the Boltzmann equation linearized around local equilibrium reads:

$$\frac{\partial}{\partial t}(\Delta f_{s\mathbf{k}} + \delta f_{s\mathbf{k}}) + v_x\Big(\frac{\partial}{\partial x}(\Delta f_{s\mathbf{k}} + \delta f_{s\mathbf{k}}) - eE_x\frac{\partial}{\partial \epsilon}(f_0 + \Delta f_{s\mathbf{k}})\Big) = \\ = -\delta f_{s\mathbf{k}}(\frac{1}{\tau^m_{s\mathbf{k}}} + \frac{1}{\tau_{s\mathbf{k}}}) + \frac{\delta f_{-s\mathbf{k}}}{\tilde{\tau}_{s\mathbf{k}}} + I^{(1)}_{sf,\mathbf{k}} \ . \tag{2.14}$$

Now let us proceed to the derivation of drift-diffusion type equations. We want to integrate out the $\mathbf{k}$ dependence, and construct a set of equation for macroscopic functions of x and time [54, 56]. The $\mathbf{k}$ average of Δf_s is the nonequilibrium part of the spin density Δn_s

$$\Delta n_s(x,t) = \int \frac{d^3k}{(2\pi)^3}\Delta f_s(x,\mathbf{k},t) \ , \tag{2.15}$$

and the spin-s current is defined as

$$j_s(x,t) = -e\int \frac{d^3k}{(2\pi)^3} v_x \delta f_s(x,\mathbf{k},t) \ . \tag{2.16}$$

Note that only the "anisotropic" part of the deviation from equilibrium enters this expression, as the Δf_s contribution is isotropic in $\mathbf{k}$ space and does not contribute *directly* to the current (i.e. it does not enter the current definition above). The spin accumulation is going to lead to diffusive contribution to the current through the driving terms with spatial derivative on the left-hand side of Boltzmann equation.

The zeroth moment of the Boltzmann equation is obtained by integrating the both sides of Eq. (2.14) with respect to $\mathbf{k}$. In this way we obtain the continuity equation:

$$\frac{\partial}{\partial t}\Delta n_s(x,t) - \frac{1}{e}\frac{\partial}{\partial x} j_s(x,t) = -\frac{\Delta n_s}{\tau_{s,-s}} + \frac{\Delta n_{-s}}{\tau_{-s,s}} \ , \tag{2.17}$$

in which $\tau_{s,s'}$ is the spin-flip time (from spin s to s'), which we define below. Let us sketch how the right-hand-side of this equation was obtained from $\mathbf{k}$ integral of $I^{(1)}_{sf}$ term. We can write it in the following way

$$\begin{aligned}\int \frac{d^3k}{(2\pi)^3} I^{(1)}_{sf,\mathbf{k}} &= -\int \frac{d^3k}{(2\pi)^3}\int \frac{d^3k'}{(2\pi)^3} W_{sf}(s\mathbf{k}, -s\mathbf{k}')(\Delta f_s(\epsilon_{\mathbf{k}s}) - \Delta f_{-s}(\epsilon_{\mathbf{k}'-s})) \\ &= -\int d\epsilon \int d\epsilon' N_s(\epsilon) N_{-s}(\epsilon')\langle W_{s,-s}\rangle(\epsilon,\epsilon')\Big[\Delta f_s(\epsilon) - \Delta f_{-s}(\epsilon')\Big] \ ,\end{aligned}$$

where we have defined the band average of a quantity $A(\mathbf{k}s, \mathbf{k}'s')$:

$$\langle A(\mathbf{k}s, \mathbf{k}'s')\rangle(\epsilon, \epsilon') = \frac{\int \frac{d^3k}{(2\pi)^3} \int \frac{d^3k'}{(2\pi)^3} A(\mathbf{k}s, \mathbf{k}'s')\delta(\epsilon - \epsilon_{\mathbf{k}s})\delta(\epsilon' - \epsilon'_{\mathbf{k}'s'})}{N_s(\epsilon)N_{s'}(\epsilon')} \ , \tag{2.18}$$

in which the density of states for spin s is given by

$$N_s(\epsilon) = \int \frac{d^3k}{(2\pi)^3}\delta(\epsilon - \epsilon_{\mathbf{k}s}) \ . \tag{2.19}$$

Note that we have not used the assumption of elastic scattering here (which would enforce $\epsilon{=}\epsilon'$). If we invoke this, we obtain $\langle W_{s,-s}\rangle{=}\langle W_{-s,s}\rangle$. However, the spin-flip times in equation (2.17) can still be different. The integral of $I_{sf}^{(1)}$ involves a difference between occupation functions for two spins, each having an equilibrium (Fermi-Dirac) form, but with different spin-dependent chemical potential μ_s^c. To the lowest order in spin-splitting $\Delta\mu^c{=}\mu_+^c - \mu_-^c$ we have

$$\int \frac{d^3k}{(2\pi)^3} I_{sf}^{(1)} \sim \Delta\mu^c \ . \tag{2.20}$$

If the material is non-magnetic, we have the same energy dispersion for both spin directions, and $\Delta\mu^c$ is readily shown to be proportional to $\Delta n_+ - \Delta n_-$. Then we have $\tau_{s,-s}{=}\tau_{-s,s}$ in Equation (2.34). Additional care is needed [59] when considering a ferromagnet, in which the bands and densities of states can be very different for each spin. When we move a certain amount of carriers from one spin band to another, we create $\Delta n_s{=}{-}\Delta n_{-s}$, but the resulting shifts of chemical potentials are different in both bands if the densities of states are different. Because of this $\Delta\mu$ is expressed as a difference between non-equlibrium spin densities weighted by spin-dependent densities of states. For a degenerate ferromagnet we get for the spin-flip times $\tau_{s,-s}$ in Equation (2.34)

$$\frac{N_s(E_F)}{\tau_{s,-s}} = \frac{N_{-s}(E_F)}{\tau_{-s,s}} \ , \tag{2.21}$$

where $N_s(E_F)$ are the densities of states for each spin at the Fermi level .

The expressions for spin-flip times $\tau_{s,-s}$ are the distribution-dependent band-averages of spin scattering times $\tau_{s\mathbf{k}}$ defined before. A simplest approximation

would be to take $\tau_{s\mathbf{k}}$ independent of $\mathbf{k}$, and assume $\tau_{s,-s}{=}\tau_s$. However, below we will show that the details of relation between different microscopic ($\mathbf{k}$-dependent) spn scattering and the spin-flip times are not important for the macroscopic equations. As long as the momentum scattering time is by far the shortest time-scale in the problem, only the spin-flip times $\tau_{s,-s}$ matter. Let us only mention that in metals they are given by spin-flip scattering at the Fermi level (as usual in strongly degenerate systems), whereas in a non-degenerate semiconductor the spin-flip time involves the average of $\tau_{s\mathbf{k}}$ times in energy range of $k_B T$ above the bottom of the conduction band.

The calculation of the first moment with respect to v_x (in which we multiply the Boltzmann equation by v_x and integrate with respect to $\mathbf{k}$) is more subtle. The expression that has to be analyzed carefully is

$$\int \frac{d^3k}{(2\pi)^3}\, v_x^2\, \delta f_{s\mathbf{k}} \ . \tag{2.22}$$

Following Valet and Fert [54], we can use the cylindrical symmetry around the x direction, and expand the dependence δf_s on $\mathbf{k}$ in Legendre polynomials of $\cos\theta$, with θ being the angle between the x axis and the direction of $\mathbf{k}$. The "zero-angular momentum" term is absent in this expansion, as we have the condition $\int d^3k\, \delta f_s = 0$. If we assume that only the p-type component is present, i.e. $\delta f_s{\sim}v_x$, then the above integral is zero. The full expansion was treated in Ref. [54], where an infinite set of coupled equations was obtained. Our calculation of lowest moments of v_x corresponds to first two equations in this hierarchy. The decoupling of the first two equations from the terms of higher angular momentum depends on the smallness of the $\tau^m_{s\mathbf{k}}/\tau_{s\mathbf{k}}$ ratio. When it is small, the above troublesome term can be safely thrown out.

The averaged relaxation terms on the right-hand side of equation (2.14) are written in the following way

$$\int \frac{d^3k}{(2\pi)^3} v_x \frac{\delta f_{s\mathbf{k}}}{\tau_{s\mathbf{k}}} = \frac{j_s}{\tau_s} \tag{2.23}$$

where we have defined the average relaxation time

$$\frac{1}{\tau_s} = \frac{\int d^3k\, v_x \frac{\delta f_{s\mathbf{k}}}{\tau_{s\mathbf{k}}}}{\int d^3k\, v_x \delta f_{s\mathbf{k}}} \ . \tag{2.24}$$

Using this we arrive at

$$\begin{aligned} \frac{\partial}{\partial t} j_s - e\frac{\partial}{\partial x}\int \frac{d^3k}{(2\pi)^3} v_x^2 \Delta f_s &- e^2 E_x \int \frac{d^3k}{(2\pi)^3} v_x^2 \Big(-\frac{\partial}{\partial \epsilon}(f_0 + \Delta f_s)\Big) = \\ &= -j_s\big(\frac{1}{\tau_s^m} + \frac{1}{\tau_s}\big) + \frac{j_{-s}}{\tilde{\tau}_s} \\ &\simeq -\frac{j_s}{\tau_s^m} \ . \end{aligned} \tag{2.25}$$

In the last line we have made one more approximation. The momentum relaxation time τ_s^m is assumed to be much shorter than the times τ_s and $\tilde{\tau}_s$ which are related to scattering processes which change the spin. Later we are going to be interested in steady state solutions, or slow (compared to τ_s^m) dynamics. In such cases we can retain only the largest term on the right-hand side, namely $-j_s/\tau_s^m$ (we can also redefine τ_s^m and include a small correction from τ_s to this new transport relaxation time). The effects of cross-relaxation of two spin currents (terms with $\tilde{\tau}_s$) can be important at very short time-scales, comparable to τ_s^m. They have been analyzed in Ref. [60].

Let us rewrite the second term on the left-hand side in the following way. Under the differentation we can replace $\Delta f_s(x)$ by $f_s^0(x) = f^0 + \Delta f_s(x)$, which is the local-equilibrium (isotropic) part of the distribution function, given by Fermi-Dirac distribution with spatially-dependent chemical potential $\mu_s^c = \mu_0^c + \Delta\mu_s^c(x)$. Then we apply the chain rule:

$$\frac{\partial}{\partial x} f_s^0 = \frac{\partial}{\partial \mu_s^c} f_s^0 \frac{\partial \mu_s^c}{\partial x} = -\frac{\partial}{\partial \epsilon} f_s^0 \frac{\partial \mu_s^c}{\partial n_s} \frac{\partial n_s}{\partial x} \ , \tag{2.26}$$

so that now we have the same integral $A_s(x)$

$$A_s(x) = \int \frac{d^3k}{(2\pi)^3} v_x^2 \big(-\frac{\partial}{\partial \epsilon} f_s^0\big) \tag{2.27}$$

in the second and the third term.

Now we can derive the Einstein relation. We set the time derivative to zero and obtain a general form of the steady state current:

$$j_s(x) = \sigma_s(x)E_x + eD(x)\frac{\partial}{\partial x}n_s \ , \tag{2.28}$$

in which we define the conductivity $\sigma_s \equiv e^2 \tau_s^m A_s(x)$ and the diffusion constant $D_s(x) \equiv A_a(x)\tau_s^m \partial\mu_s^c/\partial n_s$. Both of them in general are spatially dependent, as they are proportional to the $A_s(x)$, which depends on x through $\mu_s^c(x)$. Without evaluating $A_s(x)$ we see that σ_s and D_s are connected by the Einstein relation:

$$D_s(x) = \frac{\sigma_s(x)}{e^2}\frac{\partial\mu_s^c(x)}{\partial n_s} \ . \tag{2.29}$$

Let us introduce here the concept of electrochemical potential $\mu_s(x)$. It is defined as:

$$\mu_s(x) = \mu_s^c(x) - e\phi(x) \ , \tag{2.30}$$

where $\mu_s^c(x)$ is the chemical potential for spin s and ϕ is the electrostatic potential. Using the above definition of D_s and Equation (2.28) we have the steady-state current:

$$j_s(x) = \frac{\sigma_s(x)}{e}\frac{\partial}{\partial x}\mu_s(x) \tag{2.31}$$

Using all of the above we can write a general form of time-dependent drift-diffusion equation. Together with the previously obtained continuity equation we have:

$$\frac{\partial}{\partial t}\Delta n_s(x,t) - \frac{1}{e}\frac{\partial}{\partial x}j_s(x,t) = -\frac{\Delta n_s}{\tau_{s,-s}} + \frac{\Delta n_{-s}}{\tau_{-s,s}} \tag{2.32}$$

$$\frac{\partial}{\partial t}j_s - \frac{\sigma_s(x)}{\tau_s^m}E_x - e\frac{D_s(x)}{\tau_s^m}\frac{\partial}{\partial x}n_s = -\frac{j_s}{\tau_s^m} \tag{2.33}$$

The steady state drift-diffusion equations are:

$$\frac{1}{e}\frac{\partial}{\partial x}j_s = \frac{\Delta n_s}{\tau_s} - \frac{\Delta n_{-s}}{\tau_{-s}} \tag{2.34}$$

$$j_s = \sigma_s E_x + eD_s\frac{\partial}{\partial x}\Delta n_s = \frac{\sigma_s}{e}\frac{\partial}{\partial x}\mu_s \ . \tag{2.35}$$

The relation between $\sigma_s(x)$ and $D_s(x)$ is given by the Einstein relation (2.29). The relation between μ_s^c and n_s depends on a system at hand (e.g. degenerate or non-degenerate).

2.B Spin diffusion equations

Now we discuss how the spin diffusion equations are derived from the drift diffusion equations. They basically come from plugging the Equation (2.35) into the Equation (2.34). The subtlety in this derivation comes from the issue of charge neutrality, i.e. whether the spin accumulation is accompanied by a creation of net spatial charge. A detailed discussion of quasi-neutrality for bipolar transport (drift and diffusion of electrons and holes) is given in Smith's book [58] and in Ref. [61]. The close analogy between bipolar and spin-polarized transport has been noticed by Yu and Flatté [57]. As the main focus of our attention are semiconductors at room temperature, we first discuss in detail the spin diffusion in a paramagnetic non-degenerate semiconductor, and then follow with discussion for ferromagnetic metals. The spin transport in non-degenerate ferromagnetic semiconductors has been analyzed e.g. in [62, 63, 64]. However, currently there are no semiconductors to which such theory would apply. The ferromagnetic semiconductors available now, such as GaMnAs [65], are strongly degenerate and p-type.

2.B.1 Spin diffusion in a non-degenerate paramagnetic semiconductor

In a paramagnetic semiconductor we can put the spin-flip times $\tau_{+,-}=\tau_{-,+}=2\tau_{\mathrm{sr}}$, defining the spin relaxation time τ_{sr}. The momentum transport relaxation time τ^m is the also same for both spins. The local equilibrium distribution function in a non-degenerate case is given by

$$f_s^0(x) = f^0 + \Delta f_s(x) = \exp\big(- \beta(\epsilon(\mathbf{k}) - \mu_s^c(x))\big) \ , \tag{2.36}$$

where $\beta=1/k_B T$ and $\mu_s^c=\mu_0^c + \Delta\mu_s^c$ with μ_0^c being the chemical potential in equilibrium. The density for spin s is then given by

$$n_s(x) = n_0/2 + \Delta n_s(x) = \frac{n_0}{2} \exp(\beta \Delta\mu_s^c(x)) \ , \tag{2.37}$$

with the equilibrium total density of carriers n_0. Using the above we can perform the $A_s(x)$ integrals in Eq. (2.27), and get the expression for conductivity

$$\sigma_s(x) = \frac{n_s(x)e^2\tau^m}{m} = n_s(x)e\nu \tag{2.38}$$

in which we have defined the mobility ν=$e\tau^m/m$. The Einstein relation in a non-degenerate system is then

$$\frac{eD}{\nu} = k_B T \ . \tag{2.39}$$

The electrochemical potential (with respect to μ_0^c in equilibrium) as a function of nonequilibrium part of the carrier density Δn_s is then given by

$$\mu_s = k_B T \ln\left(\frac{n_0/2 + \Delta n_s}{n_0/2}\right) - e\phi \tag{2.40}$$

$$\simeq k_B T \frac{\Delta n_s}{n_0/2} - e\phi \ , \tag{2.41}$$

where the second line is the linear approximation, valid for $|\Delta\mu_s^c|<k_B T$ (equivalently $|\Delta n_s|<n_0/2$).

In order to derive the spin diffusion equation, we plug the Equation (2.35) into the continuity equation (Eq. (2.34)), obtaining for s=$\pm$:

$$\frac{\partial n_s}{\partial x}\nu E_x + n_s \nu \frac{\partial E_x}{\partial x} + D\frac{\partial^2 n_s}{\partial x^2} = \frac{n_s - n_{-s}}{2\tau_{\rm sr}} \ . \tag{2.42}$$

Now we introduce the approximation of quasi-neutrality. If the net density of carriers becomes different than the equilibrium density n_0, an internal electric field is created (which should be distinguished from the external field imposed by attached leads, the divergence of which is zero in the channel). This electric field will induce currents counteracting the creation of space charge, and in most situations it can be assumed that the net charge density is zero

$$\Delta n_+ + \Delta n_- \approx 0 \ . \tag{2.43}$$

This is the approximation of quasi-neutrality. In the time domain, its validity can be gauged in the following way [58]. We neglect diffusion, and take the total current j=σE. We plug it into the continuity equation:

$$\frac{\partial j}{\partial x} = \frac{\partial}{\partial x}\sigma E = e\frac{\partial n}{\partial t} \ . \tag{2.44}$$

Now, we neglect the spatial dependence of σ=$n(x)e\nu$, and use the Poisson equation, thus obtaining

$$\frac{\partial}{\partial t}\delta n = -\frac{\sigma}{\epsilon\epsilon_0}\delta n = -\frac{\delta n}{\tau_d} \ , \tag{2.45}$$

where δn=$n - n_0$ and τ_d=$\epsilon\epsilon_0/\sigma$ is the dielectric relaxation time (with vacuum permittivity ϵ_0 and the dielectric constant of the semiconductor ϵ), which is below a picosecond even for a non-degenerate semiconductor with n_0=10^{16}nm^{-3}. Any deviation from neutrality decays to zero at this time scale.

When we include diffusion and spatial derivative of σ, it turns out that there exists a small net charge in regions close to the interfaces or where the density of dopants varies spatially (e.g. in p-n junctions). In order to deal with inhomogeneously doped structures, it is then necessary to solve the Poisson equation coupled with the transport equations. This procedure has been performed in studies of spin diffusion in bipolar systems [63, 66]. Spin transport in the presence of inhomogeneous electric field has also been calculated with the Boltzmann equation [67] without using the drift-diffusion approximation.

We are going to concentrate on homogeneously doped structures, where quasi-neutrality is a good approximation. Consequently, we set the derivative of electric field to zero in Eq. (2.42), and use $\Delta n_+ = -\Delta n_-$ to obtain the spin diffusion equation with electric field [57]:

$$\frac{\partial^2}{\partial x^2}(n_+ - n_-) + \frac{eE_x}{k_B T}\frac{\partial}{\partial x}(n_+ - n_-) = \frac{n_+ - n_-}{L^2} \ , \tag{2.46}$$

where we have used the Einstein relation (2.39), and defined the spin diffusion length L:

$$L = \sqrt{D\tau_{\rm sr}} \ . \tag{2.47}$$

In the linear regime (when $\Delta\mu_s$~Δn_s) the same diffusion equation as (2.46) holds for the splitting of the electrochemical potential $\Delta\mu$=$\mu_+ - \mu_-$. In the nonlinear regime of large spin accumulation (n_+ differing strongly from n_-) it is easier to solve the diffusion equation for n_s. However, boundary conditions are most often given in terms of μ_s, which are then nonlinear functions of n_s as in Eq. (2.40).

We discuss these boundary conditions for spin currents at interfaces of different materials in chapter 3. In the linear regime we have general form of solution for n_s and μ_s:

$$\mu_\pm = k_B T \frac{n_\pm - n_0/2}{n_0/2} - e\phi = \pm(Ae^{-\eta x/L_u} + Be^{\eta x/L_u}) - e\phi \ , \tag{2.48}$$

in which η=sgn(E_x) in exponents and the two distinct diffusion lengths, upstream L_u and downstream L_d (L_u<L_d) are given by

$$L_u = \left(\frac{1}{2L_E} + \sqrt{\frac{1}{4L_E^2} + \frac{1}{L^2}} \right)^{-1} \tag{2.49}$$

$$L_d = \left(-\frac{1}{2L_E} + \sqrt{\frac{1}{4L_E^2} + \frac{1}{L^2}} \right)^{-1} \tag{2.50}$$

where the length scale associated with electric field induced drift L_E is given by

$$L_E = \frac{eD}{|eE_x|\nu} \ . \tag{2.51}$$

A critical electric field, above which the effects of drift become stronger than isotropic diffusion is

$$E_c = \frac{k_B T}{e}\frac{1}{L} \ . \tag{2.52}$$

For such field voltage drop across one spin diffusion length L becomes equal to "thermal voltage" k_BT/e. Consequently, the effects of electric field become more pronounced at lower temperatures. An example is provided by experimental results in Ref. [38], where a clear asymmetry between up- and down-stream spin diffusion is visible in GaAs at T=4 K.

We have discussed the equation governing the spatial dependence of the splitting of the electrochemical potential $\Delta\mu$=$\mu_+ - \mu_-$. The average of electrochemical potentials μ_0=$(\mu_+ - \mu_-)/2$ is equal to $-e\phi$, so that we need to solve Poisson's equation in order to obtain it. In the case considered below in which we assume zero space charge in the semiconductor, we just need to consider Laplace's equation $\nabla^2\mu_0$=0, with appropriate boundary conditions at the boundaries with current-carrying contacts (following from the total current $\mathbf{j}$=$\sigma/e\nabla\mu_0$).

2.B.2 Spin diffusion in a degenerate ferromagnet

In a degenerate system the Einstein relation gives us

$$\sigma_s = e^2 D_s N_s(E_F) \ , \tag{2.53}$$

in which $N_s(E_F)$ is the density of states for spin s at the Fermi level. Writing the conductivity in such a way we have implicitly taken into account that in a metal it is practically impossible to change σ_s by creating a non-zero spin accumulation. The typical nonequilibrium spin densities are negligible compared to the total carrier density, and in the diffusion equation we can neglect the terms coming from spatial dependence of conductivity ($\partial n_s/\partial x$ in Equation (2.42)). Consequently, the spin diffusion in metals is unaffected by electric field, and the high-field strongly asymmetric spin diffusion discussed in the previous section exists only in semiconductors [57].

A net space charge created in a non-equilibrium situation is screened on a length scale l_{scr} ($l_{scr}^2 {=} D_s \epsilon\epsilon_0/\sigma_s$) which is of the order of an Angstrom in a metal. The previous discussion of the importance of the effects of non-neutrality in a time domain can be repeated using the spatial arguments, i.e. the fact that l_{scr} is much smaller than a spin diffusion length [59]. The carrier density and electrostatic potential vary on the length scale of l_{scr}, but the electrochemical potential given by

$$\mu_s = \frac{\Delta n_s}{N_s(E_F)} - e\phi \tag{2.54}$$

is smooth on the l_{scr} length scale [59]. The spin diffusion equations for μ_s are

$$\frac{\partial^2}{\partial x^2}\mu_s = \frac{\mu_s - \mu_{-s}}{L_s^2} \quad \Rightarrow \quad \frac{\partial^2}{\partial x^2}\Delta\mu = \frac{\Delta\mu}{L^2} \ , \tag{2.55}$$

where we have defined the spin-flip lengths $L_s {=} \sqrt{D_s \tau_{s,-s}}$ and the spin diffusion length $L^{-2} {=} L_+^{-2} + L_-^{-2}$. Using equations (2.21) and (2.53) we derive the expression for the effective diffusion constant D

$$D = \frac{\sigma_+ D_- + \sigma_- D_+}{\sigma_+ + \sigma_-} \tag{2.56}$$

and the spin diffusion length can be written exactly as before $L = \sqrt{D\tau_{\rm sr}}$ with the spin relaxation time given by

$$\tau_{sr}^{-1} = \tau_{+,-}^{-1} + \tau_{-,+}^{-1} \; . \tag{2.57}$$

The general solutions of the diffusion equations (2.55) are then given by

$$\mu_{\pm} = \pm \frac{1}{\sigma_{\pm}} (A e^{x/L} + B e^{-x/L}) - e\phi \; . \tag{2.58}$$

3

Spin injection and extraction in metal/semiconductor structures

Electrical spin injection (i.e. transfer of of spin polarization by electrical current) from a ferromagnet into a paramagnet was first achieved junctions of two metals by Johnson and Silsbee [18, 68]. The spin injection into semiconductors has proven to be a harder task. The early experiments were conducted in Russia on injection from a ferromagetic semiconductor $HgCr_2Se_4$ into InSb [69]. They have been mostly overlooked since then (with exception of a review [33], which contains a detailed account of all the efforts related to spin injection). In late 90s a successful spin injection at low temperatures from Mn-doped diluted ferromagnetic semiconductors [22, 23, 24, 70] gave new impetus to the field of semiconductor spintronics. Injection from ferromagnetic metals (most often iron) at temperatures up to the room temperature followed soon afterwards [25, 71, 37]. Initially the injection had quite low efficiency (2% in Ref. [25]), which was was later improved [71, 36, 72], with maximum reported value of 30% [36]. The rise in spin injection efficiency was achieved by a proper doping of the metal/semiconductor interface [73, 74]. Spin extraction was also seen (through optical measurement of spin accumulation) in forward-biased MnAs/GaAs junction [75].

During the last two years, there was a tremendous progress in both spin in-

jection *and extraction* in Fe/GaAs structures. The spin accumulation due to both spin injection from Fe and spin extraction from GaAs into Fe (a depletion of spins which can move more easily into the magnet) were imaged by Kerr spectroscopy [38]. Soon afterwards the spin accumulation in the semiconductor near the junction with a magnet has been sensed electrically [41, 42], proving that the current through the metal/semiconductor junction depends on spin polarization of electrons inside the semiconductor.

In section 3.A we outline the theory of spin transport between a ferromagnetic metal and a semiconductor through a Schottky barrier [73, 74]. In section 3.B we discuss the so-called "conductivity mismatch" problem [76, 77] (actually first described briefly in [78]) and set the stage for the analysis of the semiconductor spin valve following in the next chapter.

3.A Boundary conditions for spin currents at the interface of a metal and a semiconductor

In this section we are going to describe a model of metal/semiconductor junction, which we will use in the subsequent calculation of spin transport. We are going to start with a brief introduction to Schottky barriers (for more in-depth review, see e.g. Ref. [79]), and then consider a barrier modifications necessary for efficient spin transport.

3.A.1 Schottky barrier with homogeneous doping of the semiconductor

For most pairs of metals and semiconductors, the work functions (differences between the Fermi level and the vacuum level) are different. We will denote the difference between the metal and the semiconductor work function as E_B - the barrier height calculated from the Fermi level of the metal. In the most common case (which is of interest here), the work function of a metal is larger than the work function of a semiconductor (E_B>0). When the two materials are brought

into contact, the electrons start flowing from the semiconductor into the metal, resulting in the carrier depletion of a region near the junction. In the depleted region, we have a net positive charge of ionized donors, and on the metal side of the junction we have a net negative charge (where the surplus electrons exactly reside - in the metal close to the junction, or in the atomic layer of the junction, in the surface states - is not relevant for this discussion). The electric field created by such a dipole layer make the semiconductor band-edge energy position dependent, creating a barrier (see Figure 3.1a). The number of carriers that had to be swept from semiconductor into a metal (and thus the barriers width) is determined by an applied bias. In equilibrium, the Fermi levels of the two materials are aligned and there is no current flow. When bias V is applied, the Fermi level of the metal μ^F moves by $-eV$ relative to the semiconductor chemical potential μ^S, but the top of the barrier is still E_B above μ^F. The influence of bias changes on the shape of the barrier on the semiconductor side is shown in Figure 3.1a.

A simplest way to calculate the shape of the barrier is to use an abrupt approximation [79]. We assume, that for $x<d$ all the electrons are swept out, leaving behind a charge density en_D, where n_D is the concentration of donors. For $x>d$ we have a flat band with net charge density ρ=0. Using this, we obtain the depletion width:

$$d = \sqrt{\frac{2\epsilon\epsilon_0}{e^2 n_D}(\mu^S - eV + E_B)}\ , \tag{3.1}$$

and the conduction band profile E_C for $x<d$ (with $E_C(x>d)$=0 and interface at x=0):

$$E_C(x) = \frac{e^2 n_D}{2\epsilon\epsilon_0}x^2 - \frac{e^2 n_D}{\epsilon\epsilon_0}dx + \mu^S - eV + E_B \tag{3.2}$$

For Fe/GaAs junction we will employ a value of E_B=0.8 eV [74]. For homogeneous doping $n_D<10^{17}$ cm^{-3}, we have the depletion width $d>100$ nm. For such a wide barrier, the tunneling processes are completely irrelevant, and the current is due to a purely classical thermionic emission, which depends solely on the barrier height, not on its width (or shape, in general). For $V>0$ (forward bias), the height of the barrier seen by the electrons in the semiconductor is lowered (see Fig.

3.1a), and the current grows exponentially. On the other hand, for $V<0$ (reverse bias) the barrier experienced by electrons coming from the metal stops changing for $|V|>k_B T$, and the saturated current does not depend on V. The formulas for the current due to thermionic emission are [79]:

$$J_{th}(V) = J_S(e^{eV/k_B T} - 1) \tag{3.3}$$

$$J_S \propto T^2 e^{-E_B/k_B T} \; . \tag{3.4}$$

For doping densities $n_D \gg 10^{17}$ the tunneling starts to play a role, but for highest possible bulk doping levels (for $n_D=10^{19}$ cm^{-3} we have $d \approx 10$ nm) the typical current densities remain very small. The expression for the tunneling current is the same as the above formula, but with a different overall factor J_T (which now depends also on barrier thickness apart from its height) instead of J_S.

3.A.2 Schottky barrier with inhomogeneous doping for spin injection

For the purpose of efficient spin injection and extraction (leading to spin accumulation easily observable at room temperature), one has to consider an inhomogeneously doped Schottky barrier, where a thin region beneath the metal is ultra-heavily doped. This can be achieved by δ-doping [80, 81, 82], a technique in which a single monolayer of a semiconductor material near the interface is doped with a donor density impossible to achieve in the bulk material (in reality, the donors diffuse from a single monolayer, and spread out in the region of a couple of nanometers).

Let us assume that a δ-doping layer with planar density n_{2D} is placed a distance d_0 from the metal-semiconductor interface. If the doping density is given by

$$n^0_{\text{2D}}(d_0) = \epsilon\epsilon_0 \frac{E_B + \mu^S}{e^2 d_0} \; , \tag{3.5}$$

then the barrier shape is triangular, and its width for zero bias is given by d_0. For $d_0=3$ nm, $E_B=0.8$ eV, and $\mu^S=-0.1$ eV (corresponding to bulk $n=10^{16}$ cm^{-3}), we get $n^0_{\text{2D}} \approx 2 \times 10^{13}$ cm^{-2}. From practical point of view, in order to ensure the

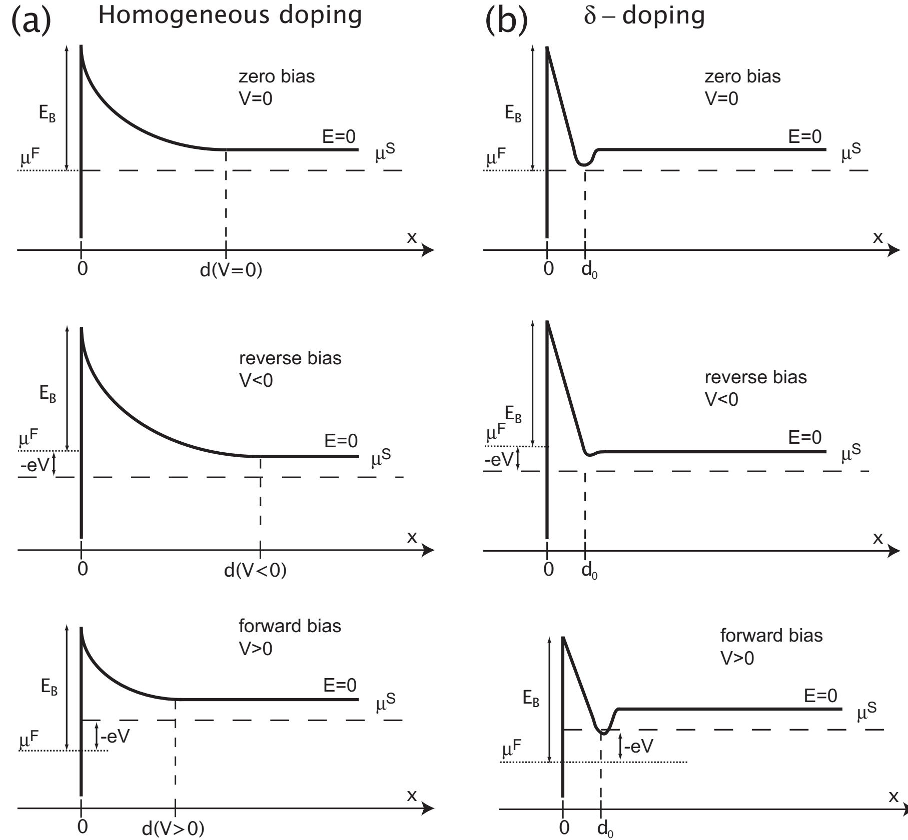

Figure 3.1: Band diagrams for Schottky barrier with (a) homogeneously doped semiconductor; (b) δ-doping at distance d_0 from the interface. Zero, reverse and forward bias are shown. In the calculations we set the zero of energy scale at the conduction band edge beyond the depletion region.

existence of thin tunneling barrier during the junction preparation, it is better to err on the side of overdoping rather than underdoping. If the real n_{2D} is larger than n^0_{2D}, not all of the doped electrons are going to be transferred into the metal surface, and the rest will remain close to the interface, creating a thin well in the energy profile of the band [80, 83] (see figure 3.1b). Under a forward bias, this well is going to deepen (or, if we have $n_{2D}{=}n^0_{2D}$, the well will appear). Under a reverse bias, the well is going to diminish, as more electrons will need to be swept out into the metal. The important thing is that the thickness of the barrier, and the state of the semiconductor beyond the well, are going to be practically unaffected by a small reverse bias. If there is no well, and $V{<}0$ is applied, additional depletion

occurs for $x>d_0$, affecting the bulk of the semiconductor. For example, for bulk doping $n_D=10^{16}$ cm^{-3}, and $V=-0.1$ V, the bottom of the conduction band at $x=d_0$ is going to be raised by approximately $e|V|$, and a depletion region between d_0 and $d\approx100$ nm is going to appear. Such a depletion region has been shown theoretically to be detrimental to both spin injection and extraction [84, 85].

We have seen that the presence of the thin well filled with electrons is inevitable at forward bias, and it enhances the tunneling current for reverse bias. Despite its significance, in the calculations below we are not going to explicitly include it, since we are going to concentrate on rather low biases and high temperatures. The electronic states inside the well have to be considered carefully for large forward biases, low temperatures and/or strongly overdoped interfaces. Then the self-consistent potential near the interface has bound states below the semiconductor's chemical potential μ^S, and they have to be taken into account explicitly into the calculation of the current [86].

In the following, we are going to calculate the tunneling current in a very simplified model of a thin ($d_0<10$ nm) Schottky barrier. Barriers of such thickness have not been developed yet in the Fe/GaAs system; recently $d_0\approx15$ nm has been achieved [36, 74] by heavy doping ($n_{3D}=5\cdot10^{18}-1\cdot10^{19}$ cm^{-3}) of the 15 nm thick layer next to the interface. The spin selectivity of such barriers has been demonstrated in spin-LED experiments, and the small bias conductances (per unit area) of the barriers were measured to be $G=4$ Ω^{-1}cm^{-2} at $T=10$ K [74] and $G>100$ Ω^{-1}cm^{-2} at room temperature [36].

In the calculation below we will get a typical barrier conductance per unit area $G\approx1000$ Ω^{-1}cm^{-2} at room temperature for biases of $|V|<0.1$ volts. The analysis of the semiconductor spin valve and its three-terminal extension in the following chapter will show that this is the order of magnitude of G which is necessary to achieve to even consider a possibility of application. Lower conductances are going to create spin accumulation which is negligible at room temperature, and increasing the applied voltage is ultimately going to lead to depolarization of the

injected current (due to enhanced scattering during the relaxation of injected high-energy electrons, see e.g. [87]). But the issue most important for three-terminal systems described in chapter 6 is the connection between the spin accumulation in the semiconductor and the spin currents through the barrier close to zero bias. For this case our neglect of effects connected with the electron well, and simplified treatment of the bias-dependence of the barrier width is justified. The barrier then needs to be close to being "optimally" doped, so that at zero bias we can neglect a depression in the band edge profile between the high barrier and the bulk non-degenerate region.

3.A.3 Calculation of the spin current through a square barrier

We are going to use an approach in which we treat both the semiconductor and the metal using an effective mass model, with a single spin-split band in a ferromagnet [88, 89, 90, 86]. Such an approach disregards the microscopic structure of the Fe/GaAs interface [91, 92], and it only takes into account the potential due to Schottky barrier. In the light of this approximation, and the fact that the physics of such ultra-heavily doped Schottky barriers remains largely unexplored and can hide many surprises, the calculation below should be treated as an estimate. Accordingly, we simplify the calculation as much as possible. We will use a square barrier of width d, which separates the non-degenerate semiconductor from a metal (the possible well next to the barrier is neglected). The square barrier underestimates the tunneling current for a given d compared to a more realistic triangular or parabolic barriers. However, the spin properties of the junctions do not depend on their shape, and the calculation for the triangular barrier simply gives larger conductances [83], while keeping the spin polarization of the current the same.

In our approach the two relevant parameters of the ferromagnet are the velocities of majority (spin s=+) and minority (s=−) electrons at the Fermi level v_{Fs}. We take them from [88]: the effective mass in Fe is taken as m_0 (the free elec-

tron mass), and the Fermi wave vectors for two spin directions are k_{+}=1.1 Åand k_{-}=0.42 Å. The assumption is that in the energy range of interest (of the order of $k_B T$ or the applied bias $e|V|$, whichever is larger) the velocities of electrons in metal are constant for each spin. This assumption is bound to break down at a certain value of bias, as the spin-resolved densities of states for ferromagnets such as Ni and Fe are definitely not smooth on an energy scale of more than 0.1 eV, see e.g. [93]. This is a reminder, that we should treat our calculation as an estimate and another reason to restrict ourselves to small biases.

The Schottky barrier is assumed to be square for the simplicity of calculation, with its height equal to the maximum height of the realistic barrier. The relations between chemical potentials, voltage, and bottom of conduction band in the bulk are depicted in Figure 3.1. The calculation of tunneling current is based on Landauer-Büttiker formalism, but the same formulas have been used in this context much earlier (see e.g [94]). The current density of electrons with spin s flowing from the semiconductor into the ferromagnet is

$$j_s^{FS} = -e \int_{k_x<0} \frac{d^3k}{(2\pi)^3} \; v_x \; T^s_{S\to F}(k_x, \mathbf{k}_\parallel, V) \; (f_s^S(E_S(\mathbf{k}) - f_s^F(E_S(\mathbf{k})) \; , \qquad (3.6)$$

where v_x is the velocity of the electron in the semiconductor, f_s^S and f_s^F are the occupation functions in the semiconductor and ferromagnet for spin s, $T^s_{S\to F}$ is the transmission probability for electron with spin s as a function of k_x in the semiconductor, and the vector $\mathbf{k}_\parallel$ in the plane of the interface. The latter is assumed to be conserved, i.e. we consider specular transmission. The above expression is written for the FS interface: the ferromagnet extending for $x < 0$ and semiconductors for $x > 0$ (as in Figure 3.1). For the SF interface the occupation functions should trade places.

Later we will see that the non-equlibrium spin splitting in the ferromagnet is negligible compared to the the bias eV and the spin splitting in the semiconductor. Anticipating this, we will use the same occupation function $f^F(E)$ for both spins in the metal. For the parabolic dispersion in the semiconductor Equation (3.6) can

be rewritten in the following way

$$j_s^{FS} = \frac{e}{\hbar^3}\frac{m_S}{4\pi^2}\int_0^\infty dE \int_0^E dE_x\ T^s(E_x, E, V)(f_s^S(E) - f^F(E))\ , \qquad (3.7)$$

where m_S is the effective electron mass in the semiconductor (m_S=0.067m$_0$ in GaAs), E is the total energy of the electron (with zero energy at the bottom of the conduction band far away from the barrier), and E_x is the part of the energy associated with motion in x direction in the semiconductor. The occupation functions are:

$$f_s^S(E) \;=\; f_{FD}(E, \mu_0^c + \Delta\mu_s^c) \qquad (3.8)$$

$$f^F(E) \;=\; f_{FD}(E, \mu_0^c - eV)\ , \qquad (3.9)$$

where $f_{FD}(E, \mu^c)$ is a Fermi-Dirac distribution function at energy E with chemical potential μ^c. μ_0^c is the average chemical potential in the semiconductor at the onset of the tunneling region, μ_0^c=$(\mu_+ + \mu_-)/2$. Without the depletion region beyond the barrier, and neglecting the possible existence of the well next to the interface, μ_0^c is a chemical potential of a bulk semiconductor (related to the equilibrium carrier concentration n_0). We identify the applied bias eV with the difference between μ_0^c and the chemical potential in the metal μ^F (see Figure 3.1). $\Delta\mu_s$ is the spin-dependent part of the total chemical potential for electrons with spin s. We are interested in the case when the semiconductor is non-degenerate ($\beta\mu_0 \gg 1$), when we can make an approximation:

$$f_s^S(E) \simeq e^{\beta(\mu_0+\Delta\mu_s)}e^{-\beta E} = \frac{n_s}{N_C}e^{-\beta E}\ , \qquad (3.10)$$

where n_s is the density of electrons with spin s and N_C is the effective density of states (for one spin direction):

$$N_C = \frac{1}{8}\left(\frac{2m_S k_B T}{\pi\hbar^2}\right)^{3/2}\ . \qquad (3.11)$$

Furthermore, we can also use a Maxwell-Boltzmann occupation function for $f^F(E)$ when $eV > k_B T + \mu_0 \approx \mu_0$. For carrier density of n=10^{16} cm^{-3} we have $\mu_0 \simeq -0.1$ eV

in GaAs. As we are going to restrict ourselves to small biases ($|V|$<0.1 volts), we can use the Maxwell-Boltzmann form of occupation function also in the metal.

Let us introduce the imaginary wave-vector κ (and the "barrier" velocity v_B=$\hbar\kappa/m_S$), which governs the decay of a wave function inside the square barrier:

$$\kappa(E_x) = \sqrt{\frac{2m_S}{\hbar^2}(E_B + \mu_0 - eV - E_x)}\ . \tag{3.12}$$

The value of κ is determined mostly by E_B≃0.8 eV. The dependence on E_x can be safely ignored, as the range of the relevant energies is about k_BT. We will retain the V dependence. A typical value of κ is then of the order of 1 nm^{-1}, so that for barrier width d=3 nm the exponential factor determining the magnitude of the transmission probability is

$$e^{-2\kappa d} \sim 10^{-3}\ . \tag{3.13}$$

For the triangular barrier the main difference is the reduction of the effective value of κ [83]. Using the semi-classical (WKB) approach, we can estimate that for small E_x and for a triangular tunneling barrier we have $\kappa_{\rm tr}$≃$2\kappa/3$. Thus, we get the same probability of tunneling if we replace the square barrier of thickness d with a triangular barrier of thickness $3d/2$.

Taking all of the above into account, the transmission probability T can be very well approximated by

$$T^s(E_x, V) = 16\, v_x\, v_{Fs}\, \frac{e^{-2\kappa d}}{v_{Fs}^2 + v_B^2}\ , \tag{3.14}$$

where

$$v_x = \frac{\hbar}{m_S}\sqrt{\frac{2m_S}{\hbar^2}E_x}\ . \tag{3.15}$$

Now we can calculate the spin-dependent current from Equation (3.7). Let us define the factor that depends on the properties of the ferromagnet:

$$A_s = \frac{v_{Fs}}{v_{Fs}^2 + v_B^2}\ . \tag{3.16}$$

In the model which we use here, v_B turns out to be much larger than v_{Fs}. Consequently, $A_s \propto v_{Fs}$, so that the spin with larger velocity at the Fermi energy in the ferromagnet is transported more easily through the barrier.

Finally, we arrive at j_s, which we present in two equivalent forms:

$$j_s^{FS} = \frac{8e}{m_S} A_s e^{-2\kappa d} k_B T \; n_s \Big(1 - e^{\beta(\mu^F - \mu_s)} \Big) , \tag{3.17}$$

$$= \frac{4e}{m_S} A_s e^{-2\kappa d} k_B T \; n_0 \Big(\frac{2n_s}{n_0} - e^{-\beta e V} \Big) , \tag{3.18}$$

$$= -j_s^{SF} , \tag{3.19}$$

in which $n_0 = n_+ + n_-$ is the total carrier concentration in the semiconductor, and we have used $eV = \mu_0^c - \mu^F$ and $2n_s/n_0 = \exp(\beta(\mu_s - \mu_0))$. In the above formulas, κ depends on V (through modified barrier height). Depending on the details of the interface doping, effective barrier width d can also change with the applied bias, especially for $V<0$ (reverse bias). Note that the total current bias dependence is determined by two competing exponential factors, $e^{-\beta eV}$ and $e^{-\kappa d}$, and it is possible that in certain voltage range the forward-bias current is going to be actually smaller than the reverse-bias current.

Let us discuss the spin currents close for $V \approx 0$ (i.e. $V < k_B T$). We assume that both $|\mu^F - \mu_s|$ and $|\mu_s - \mu_0|$ are smaller than $k_B T$. This corresponds to both the spin splitting in the semiconductor, and the applied bias smaller than $k_B T$.Then, to the first order we get for the spin currents (A,B=F,S):

$$j_s^{AB} \approx \frac{G_s}{e} (\mu_s^B - \mu_s^A) , \tag{3.20}$$

$$G_s = \frac{4e^2}{m_S} A_s e^{-2\kappa d} \; n_0 , \tag{3.21}$$

where we have defined a spin-dependent barrier conductance G_s. The spin-dependence of G_s comes from the A_s factor, and as we discussed above the ratio G_+/G_- is equal to the ratio of the velocities of carriers with different spin in the ferromagnet. For our parameters for Fe [88] we get

$$\frac{G_+}{G_-} \simeq 2 . \tag{3.22}$$

As we discuss in the following section, for barriers with low G the spin polarization of the injected current is determined by the ratio of barrier conductances for both

spins. The ratio of 2 agrees with the measurements of spin injection from Fe in to (Al,Ga)As done using the spin-LED setup [71, 36].

For a square barrier with $d \simeq 3$ nm (or triangular barrier of $d \simeq 5$ nm), carrier density $n = 10^{16}$ cm^{-3}, and barrier height $E_B = 0.8$ eV, we get $G_+ \approx 1900$ Ω^{-1}cm^{-2} and $G_- \approx 1200$ Ω^{-1}cm^{-2}. In the following, we will use G_s of this order of magnitude, with the ratio of G_+ to G_- set to 2.

3.B Single ferromagnet/paramagnet (F/N) junction: conductivity mismatch

In this section we consider a ferromagnet/paramagnet (F/N) junction in a one-dimensional geometry. We will use the spin diffusion equations derived in chapter 2 together with the boundary condition from equation (3.20). For $x<0$ we have the electrochemical potential in a ferromagnet given by :

$$\mu_{\pm}^{F} = \pm A_F \frac{eL_F}{\sigma_{\pm}^{F}} e^{x/L_F} + e\frac{J}{\sigma_F} x + \mu_0^F \ , \tag{3.23}$$

and for $x>0$ we have for the paramagnet:

$$\mu_{\pm}^{N} = \pm A_N \frac{2eL_N}{\sigma_N} e^{-x/L_N} + e\frac{J}{\sigma_N} x \ , \tag{3.24}$$

where we have set μ_0^N to zero. Depending on which is more convenient, A_F, A_N, and either J (the total current density) or μ_F^0 are to be determined. In the first case, $\mu_F^0 = -eV_F$ is the controlling parameter, and in the second case the total current is given. When the barrier is highly resistive, than the first choice of independent parameter is convenient: V_F can be identified with a bias applied to the junction. For F and N having lengths $d_{F,N}$ such that the potential drops in the bulk of the materials $|Jd_{F,N}/\sigma_{F,N}|$ are much smaller than V_F, practically all the potential drop across the structure occurs on the barrier, and is equal to V_F. When the interface resistance is not dominating, then if we want to use a bias voltage as a controlling parameter, we have to take into account the lengths of F and N materials and potential drops along them. As we now want to investigate the properties of the

junction alone for the wide range of its conductances, it is then more appropriate to use J as a controlling parameter.

At the interface between the two materials (x=0) we use the boundary condition for spin currents:

$$j_s(0) = \frac{G_s}{e}\left(\mu_s^N(0^+) - \mu_s^F(0^-)\right) , \tag{3.25}$$

where G_s are spin-dependent conductances of the barrier. In the previous section we have shown that such a boundary condition applies for metal-semiconductor junctions for $|\mu_s^N - \mu_s^F| < k_BT$ (equation (3.20)). The derivation of this boundary condition for metal/metal junctions is straightforward. We also use the condition of no spin scattering at the interface (continuity of spin current)

$$\Delta j^N(0^+) = \Delta j^F(0^-) , \tag{3.26}$$

where $\Delta j = j_+ - j_-$.

We calculate the profiles of electrochemical potentials and spin currents by solving a set of three linear equations, obtaining A_F, A_N and J. A parameter which has received a lot of attention in literature is the spin polarization of the current injected into the paramagnet, which is defined as

$$\alpha_j = \frac{\Delta j(0^+)}{J} . \tag{3.27}$$

In order to obtain a compact and easy to interpret expression for α_j it is useful to define the spin selectivity of the barrier γ_B and intrinsic spin polarization of the current in the ferromagnet γ_F

$$\gamma_B = \frac{G_+ - G_-}{G_+ + G_-} = \frac{\Delta G}{G} \tag{3.28}$$

$$\gamma_F = \frac{G_+^F - G_-^F}{G_F} \tag{3.29}$$

where $G_s^F = \sigma_s^F / L_F$, $G_F = G_+^F + G_-^F$. We also define the following quantities (using

the notation from Refs. [54, 95])

$$r_B = \frac{1}{1-\gamma_B^2}\frac{1}{G} \tag{3.30}$$

$$r_F = \frac{1}{1-\gamma_F^2}\frac{1}{G_F} \tag{3.31}$$

$$r_N = \frac{1}{G_N} = \frac{L_N}{\sigma_N} \ . \tag{3.32}$$

The above are the "spin resistances" of the barrier, the ferromagnet and the paramagnetic material, respectively. G is the barrier conductance (per unit area), G_F and G_N are the "spin depth" conductances of the F and N materials. With these we obtain the following expression for α_j:

$$\alpha_j = \frac{\gamma_B r_B + \gamma_F r_F}{r_B + r_F + r_N} \ . \tag{3.33}$$

From this equation we can see, that either the current in the ferromagnet has to be polarized ($\gamma_F \neq 0$) or the barrier has to be spin selective ($\gamma_B \neq 0$) for the spin injection to occur. This is obvious, but more interesting properties can be quickly gleaned from this expression. If there is no barrier (ohmic contact between F and N), then $r_B=0$, and we have

$$\alpha_j(r_B = 0) = \frac{\gamma_F r_F}{r_F + r_N} \ . \tag{3.34}$$

The maximum polarization is obtained in the limit of $r_N \ll r_F$: then α_j tends to γ_F. But for $r_N \gg r_F$, which is the case when N material is a semiconductor, and F is a metallic ferromagnet, the polarization of the current $\alpha_j \sim r_F/r_N$ is very small. This inability of injecting spin current from a ferromagnetic metal into a semiconductor has been termed "conductivity mismatch" [76] in 2000, and then it garnered a widespread attention. Soon after the publication of Ref. [76], it was noted in Ref. [77] that when a resistive barrier is present, and when r_B is the dominating resistance, then from Eq. (3.33) we immediately get that the polarization of injected current is restored if the barrier is spin-selective, and we have $\alpha_j \approx \gamma_B$.

As a historical note, let us mention that both the "conductivity mismatch" and the solution of this problem due to spin-selective resistive interface, have been first discussed in the article of Johnson and Silsbee from 1987 [78].

It turns out that polarization of injected current α_j is not the most important quantity for properly understood spin injection problem. More specifically, a finite value of α_J is necessary, but not sufficient for spintronic applications or even measurement of any spin effects. The spin polarization of current is not a directly observable quantity: it is the polarization of the carrier density (spin accumulation) which can be seen directly (e.g. in magneto-optical experiment), and which leads to magnetoresistive effects in the diffusive regime. A quantity which is more related to the real "spin efficiency" of the junction is the spin splitting in the N material at the interface expressed as a function of the total injected current:

$$\Delta\mu(0^+) = \mu_+(0^+) - \mu_-(0^+) = -2eJr_N\alpha_J \ . \tag{3.35}$$

As we have seen before, α_J becomes appreciable when r_B is the largest resistance in the system. In this situation, the current density $J{\sim}V/r_B$, where V is the applied voltage. So in the relevant regime w get

$$\Delta\mu(0^+) \sim \frac{r_N}{r_B} eV\alpha_J \ , \tag{3.36}$$

which shows that is we want the spin-splitting in the N channel to be an appreciable fraction of eV, then r_B should *not* be *much* larger than r_N.

Let us also note that in the most interesting regime of efficient spin injection from a metal into a semiconductor ($r_B{>}r_N{\gg}r_F$), the ratio of spin splittings at the F and N side is

$$\frac{\Delta\mu^F}{\Delta\mu^N} \propto \frac{r_F}{r_N} \ll 1 \ , \tag{3.37}$$

so it is a very good approximation to disregard $\Delta\mu^F$ and use a single value of μ^F in order to describe the metallic side of the junction. Then, the parameters of the bulk of the ferromagnet (σ_s^F,L_F) do not directly play any role in the calculation and the injection process is controlled by the junction parameters (two G_s or γ_B and r_B) and the N material parameters only. The microscopic structure of the ferromagnet of course still influences the properties of the junction. In the previous section we have shown how the interface spin selectivity γ_B is connected to the band structure of a ferromagnet in a simple model.

4

A diffusive spin valve

From a problem of spin injection (a single F/N interface) let us proceed to an investigation of a simplest two-terminal spintronic device. The term "spin valve" was introduced in Ref. [96] for a specific device using the giant magnetoresistive effect, but it is commonly used in a much broader sense. Here we use the term spin valve to denote a system with two ferromagnetic parts, the resistance of which depends on the alignment between the two magnetizations. One of the magnetizations is usually pinned (e.g. by exchange bias coupling [97] to an adjacent antiferromagnet), so that the external magnetic field can change the relative orientation of the two magnetizations, thus affecting the current flowing through the device. So it is a magnetically controlled "valve" for the current. Here we are going to be interested in a spin valve in which spin injection and extraction occurs, i.e. one of the ferromagnets is a source of the current, and the other is a drain (a spin valve-like system using a non-magnetic source and drain with two magnetic contacts influencing the carrier transport by proximity effect was also proposed [90, 98]). The two magnets are separated by a normal (paramagnetic) channel long enough that we can treat the spin transport inside it as diffusive. Finally, we will concentrate on the situation when the normal material is a semiconductor.

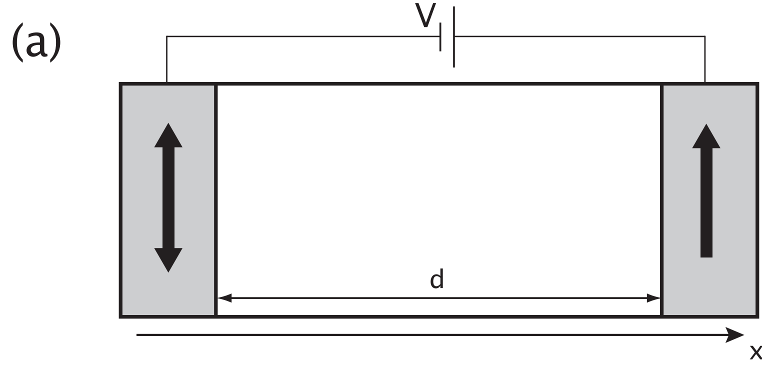

Figure 4.1: One-dimensional spin valve.

4.A One-dimensional calculation

A simple one-dimensional geometry shown in Figure 4.1 can be solved analytically [95], just like the case of the single F/N junction in the previous chapter. We set up equations for electrochemical potential in both ferromagnets (Eq. (3.23)) and in the semiconductor channel (Eq. (3.24)), and use the boundary conditions from Equations (3.25)-(3.26). This leads to a system of 6 linear equations to solve (we work in a regime in which the nonlinear effects on spin diffusion due to electric field can be neglected). Full analytical formulas are given e.g. in Ref. [95]. However, we can use the fact that for resistive barriers the splittings of the electrochemical potentials are very different in F and N: $\Delta\mu^F/\Delta\mu^N \sim r_F/r_N$. Thus we can neglect a very small spin splitting in F and use a single number to describe each of the ferromagnets: a potential in the L(R) terminal $\mu^{L(R)}$. Then we are left with only 4 equations. Here we will discuss the relevant qualitative features of their solutions.

Let us define two configurations of the magnetizations of the ferromagnetic contact: parallel one (P) and antiparallel (AP). Example plots of spin currents in the spin valve and electrochemical potentials inside the N chanel are shown in Figures 4.2 and 4.3 There are obvious differences between the P and AP case. For P, the same spin is more easily injected and extracted, and a current of uniform spin polarization flows through the channel (Figure 4.2). The spin accumulation

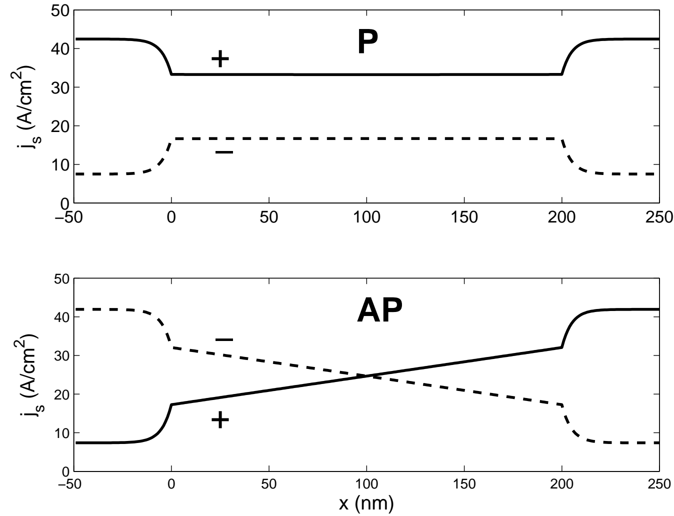

Figure 4.2: The spin current densities in a 1D spin valve. The solid line is the spin +, and the dashed line is the spin −. The semiconductor channel extends between x=0 and x=200 nm. In the AP configuration the left magnetization is reversed. The channel is GaAs at room temperature with carrier density n_0=10^{16} cm^{-3}. The barriers' total conductances per unit area are G=1000 Ω^{-1}cm^{-2}, and the ratio of spin conductances is G_+/G_-=2 (spin selectivity γ_B=1/3).

has opposite signs near the two contact, reflecting the accumulation of the preferred spin near the source, and its depletion near the drain (Figure 4.3). The situation looks very differently in the AP configuration. The current polarization changes sign in the middle of the channel; the source injects spin current of one sign, and the drain preferably extracts the current of the opposite spin polarization. However, the feature of crucial importance for us here is the fact that *the spin accumulation in AP is much larger than in P case* (see Figure 4.3). The average spin accumulation in P is zero, as it changes the sign in the channel, but when we compare the spin splittings of electrochemical potential near the contacts, we obtain

$$\frac{\Delta\mu^P}{\Delta\mu^{AP}} \propto \left(\frac{d}{2L_N}\right)^2 , \tag{4.1}$$

in which d is the length of the channel. A basic prerequisite for existence of any interesting two-teminal effects is $d<L_N$. Otherwise the spin information is

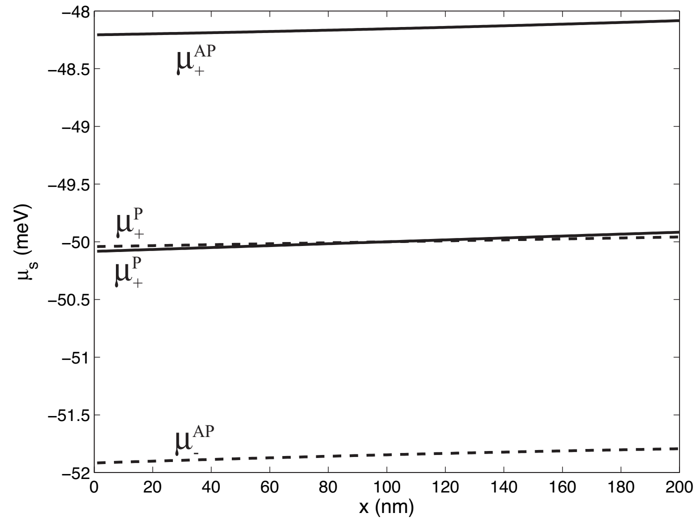

Figure 4.3: The electrochemical potentials μ_s in the N channel of the 1D spin valve. The parameters are the same as in Figure 4.2. The left contact has μ^L=−0.1 eV and the right contact is grounded (μ^R=0).

lost during the diffusion between the contacts, and we just have two uncoupled F/N junctions. Another observation is that despite this strong difference in spin accumulation between P and AP cases, the total currents I^P and I^{AP} are not significantly different. In fact, if we define the magnetoresistance coefficient MR as

$$MR \equiv \frac{I^P - I^{AP}}{I^P} \tag{4.2}$$

we obtain that to the lowest order in G/G_N it is given by

$$MR \sim 2\alpha_j^2 \frac{G}{G_N}\frac{L_N}{d} \ , \tag{4.3}$$

where $\alpha_j \simeq \gamma_B = (G_+ - G_-)/G$ in the regime of applicability of this formula. As an example, let us plug the numbers for non-degenerate GaAs at room temperature with carrier concentration $n=10^{16}\text{cm}^{-3}$. The mobility ν=5000 cm^2/Vs results in diffusion constant D=130 cm^2/s. The typical spin relaxation time at room temperature is $\tau_{sr}\simeq$80 ps [19] corresponding to $L_N \simeq 1$ μm. The spin-depth conductance is $G_N = \sigma_N / L_N \simeq 8 \cdot 10^4\ \Omega^{-1}\text{cm}^{-2}$. We use the spin selectivity γ_B=1/3 and the total

G=10^3 Ω^{-1}cm^{-2}. With these numbers we get MR=1% for a channel length d=200 nm. The latter length scale is an important practical limitation. It is close to the standard minimal size of industrial lithography, and also the smallest metal contacts in planar all-metallic structures have sizes of this order [99, 100].

The above results are an obstacle for using a metal/semiconductor system for magnetoresistive purposes. The MR ratio for any kind of application (e.g. hard disk read head) should exceed 10% in order to start competing with existing all-metal technologies like GMR or TMR. One possibility of increasing the MR ratio in a spin valve with semiconductor channel is to use barriers of lower resistance. Here a naive approach to the "conductivity mismatch" problem (the more resistive barrier, the better it is for spin injection) is shown to be inadequate, as the MR as a function of barrier G has been shown theoretically [95] to have a maximum at $G \sim G_N$. So the barriers optimal for MR effect have their conductances similar to the "spin-depth conductance" G_N of the channel. The last statement holds for a one-dimensional spin valve. An important generalization to the more realistic geometries will be presented in Chapter 5.

In Figure 4.4 we show MR as a function of the barrier conductance G for the parameters of Fe/GaAs system given above. A maximum of MR is about 10%. The optimal G can be approximated by:

$$G_{\mathrm{opt}} = G_N \frac{F+1}{2\sqrt{2F}} \;\Leftrightarrow\; r_B^{\mathrm{opt}} = r_N \sqrt{\frac{2}{1-\gamma_B^2}} \qquad (4.4)$$

where we have defined the barrier finesse $F \equiv G_+/G_-$. The maximal value of MR is obtained for this G_{opt}, and for short channels ($d \ll L_N$) it is approaching the absolute maximum for a given set of material parameters:

$$MR_{\mathrm{max}} = \gamma_B^2 = \left(\frac{\Delta G}{G}\right)^2 . \qquad (4.5)$$

The behavior in Figure 4.4 can be understood using the results of the discussion of the section 3.B. The decrease of MR for high G (low r_B) is due to conductivity mismatch, which makes the current injected into the semiconductor

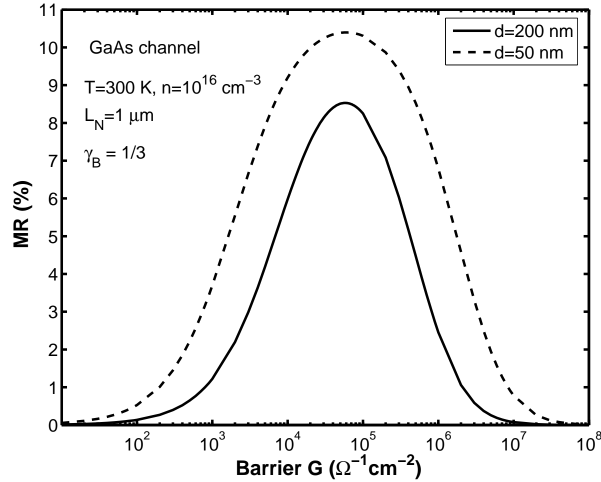

Figure 4.4: The magneto-resistive ratio of a one-dimensional spin valve for two channel lengths. The parameters of a Fe/GaAs system are given in the text.

unpolarized. On the other hand, for low G (large r_B) the current is polarized, but it is small. As we discussed in section 3.B, in this regime the spin accumulation in the semiconductor becomes very small. Every injected electron with unbalanced spin spends a long time in the channel before it tunnels out into the drain, and when this "dwell" time becomes larger than the spin relaxation time, the spin polarization in the N material is lost. With no spin polarization between the ferromagnets, there can be no difference between the current for P and AP. For more discussion see section 4.B

All this shows that the success of the diffusive spin valve with a semiconductor channel will require a significant progress in the control of the metal/semiconductor interface. Conductances at least an order of magnitude higher than the ones reported to date in Fe/(Al,Ga)As [36, 74] are needed, and the junction spin selectivity $\gamma_B \sim 1/3$ needs to be maintained or improved. Also, having a longer spin diffusion length L_N would be helpful - and the prospect of long L_N is exactly what has been attracting attention to the semiconductor spintronics. Quite probably, in order for semiconductors to challenge the position that all-metal devices have in the field of magnetoelectronic applications (read-heads, MRAM), spin injection into silicon

(in which a very long L_N is expected) will have to be shown. An important step od growing contacts of optimal resistance between a ferromagnet and Si has been done recently [101], but in this work the spin polarization of the current has not been measured. Spin injection of hot electrons into silicon and magnetoresistive effect in a spin valve with 10 μm long silicon channel were reported in May of 2007 [102].

However, instead of waiting for more experimental breakthroughs we can try to do our best using currently available system parameters (e.g. $G \approx 1000\ \Omega^{-1}\text{cm}^{-2}$). An important step is to move beyond a passive two-terminal device such as a spin valve, and consider a spin-transistor system, in which additional external stimuli can control the magnetoresistive effects. A proposal of this kind, which is predicted to work in a diffusive regime at room temperature will be presented in chapter 6. But before this, let us deepen our understanding of the spin valve, and analyze a more realistic geometry than a purely one-dimensional system considered until now.

4.B Spin valve in a general geometry - a back-of-the envelope calculation

Let us use the approximations described in the previous Sections in the case of a spin valve having a general 3D geometry. We consider a paramagnetic (N) channel of finite volume V with two ferromagnets connected by junctions of area A each. We assume that (a) the dimensions of the N channel are less than spin diffusion length L_N in every direction, and (b) the barriers are resistive enough so that μ_s have discontinuities at the interfaces. Because of the former assumption we can approximate μ_s inside N as constant. Furthermore, we will neglect a small $\Delta\mu^N$ splitting in the P configuration (and of course $\Delta\mu^F$=0 is a perfect approximation). Let us write the electrochemical potentials in the channel as $\mu^N_{\pm}=\mu_0 \pm \Delta\mu/2$. The

spin currents entering the channel through the source (S) are

$$I_{\pm}^{S} = A\frac{G_{\pm}^{S}}{e}(\mu_0 \pm \Delta\mu/2 - \mu^S) \ , \tag{4.6}$$

with μ^S being the electrochemical potential in the source. The current leaving the channel into the drain (D) is

$$I_{\pm}^{D} = A\frac{G_{\pm}^{D}}{e}(-\mu_0 \mp \Delta\mu/2) \ , \tag{4.7}$$

where we have set μ^D=0, so that the bias applied to the device is μ^S/e. In the P configuration we have G_s^D=G_s^S and in the AP the spin conductances of the drain are reversed: G_s^D=G_{-s}^S. The current flowing through the system is conserved (I^S=I^D) and so within our approximations we get that μ^0=$\mu^S/2$ both for P and AP configuration. In order to determine $\Delta\mu^{AP}$ we have to consider the spin relaxation in the channel. The difference in spin polarizations of the drain and source currents is related to the number of spin flips per unit time:

$$-\frac{1}{e}(\Delta I^S - \Delta I^D) = \frac{A}{e^2}(\Delta G \mu^S - G\Delta\mu^{AP}) = V\frac{\Delta n}{\tau_{\rm sr}} \ , \tag{4.8}$$

where ΔI=$I_+ - I_-$, ΔG=$G_+^S - G_-^S$, G is the total barrier conductance, n_s is the (uniform) density of electrons with spin s, Δn=$n_+ - n_-$, and τ_{sr} is the spin relaxation time. Now we use the Einstein relation (Eq. (2.29)) for a paramagnet:

$$D = \frac{\sigma_N}{e^2}\frac{\partial\mu}{\partial n} \quad \Rightarrow \quad \Delta n \simeq \frac{\sigma_N}{De^2}\Delta\mu \ , \tag{4.9}$$

and derive the formula for $\Delta\mu^{AP}$ which is valid for any paramagnetic material (degenerate or non-degenerate):

$$\Delta\mu^{AP} = \frac{\Delta G \mu^S}{\frac{V}{2AL_N}G_N + G} \ . \tag{4.10}$$

The expression for the MR ratio is given by

$$MR = \frac{I_P - I_{AP}}{I_P} = \frac{\Delta G}{G}\frac{\Delta\mu^{AP}}{\mu^S} \ , \tag{4.11}$$

$$= \left(\frac{\Delta G}{G}\right)^2 \frac{1}{1 + \frac{V}{2AL_N}\frac{G_N}{G}} \ . \tag{4.12}$$

From the above formula we can see the following. (1) Spin accumulation ($\Delta\mu^{AP}{\neq}0$) is necessary for non-zero MR; (2) the MR depends only on geometry and barrier/channel properties - in the considered limit of low electric fields it does not depend on applied bias; (3) for large MR the ratio V/AL_N has to be small, quantifying the influence of the channel volume and the contact area; (4) in the limit of $G/G_N{\ll}1$ we obtain

$$MR = 2\Big(\frac{\Delta G}{G}\Big)^2 \frac{AL_N}{V}\frac{G}{G_N} \ , \tag{4.13}$$

which for the 1D channel ($A/V{=}d$) gives Equation (4.3).

The formulas for MR given above can only describe the case when channel is small enough for the approximation of constant μ_s to work. In section 5.B we will include the spatial dependence of the electrochemical potentials and show that it leads to a *non-monotonic* behavior of MR with contact size and channel volume.

5

Lateral spin diffusion

The most technologically convenient geometry of a small spintronic or electronic system is a lateral one, in which current-carrying contacts (leads) are deposited on top of a planar channel. A spin valve in such a geometry is presented in Figure 5.1. Despite the fact that practically all the experiments are done in such a configuration (for metallic systems see e.g. Ref. [99], for systems using diluted magnetic semiconductors see e.g. Ref. [103]), majority of the calculations are performed using a simple 1D model described in Chapters 3 and 4. There are a few exceptions: in Ref. [104] a numerical calculation of spin-current distribution in a metallic spin valve was done, and in Ref. [105] uniform spin injection from finite-size contacts was considered. Below we give a simple yet accurate formalism which can be used to calculate analytically the lateral spin diffusion in systems with (relatively) resistive junctions.

5.A Effective 1D diffusion formalism

In this section we analyze the lateral geometry (like the one if Figure 5.1), in which the system is uniform along the z direction. We are thus left with a problem of two-dimensional spin diffusion. The equations for electrochemical potentials are:

$$\nabla^2 \mu_s(x,y) = \frac{\mu_s(x,y) - \mu_{-s}(x,y)}{(L_s)^2} \ , \tag{5.1}$$

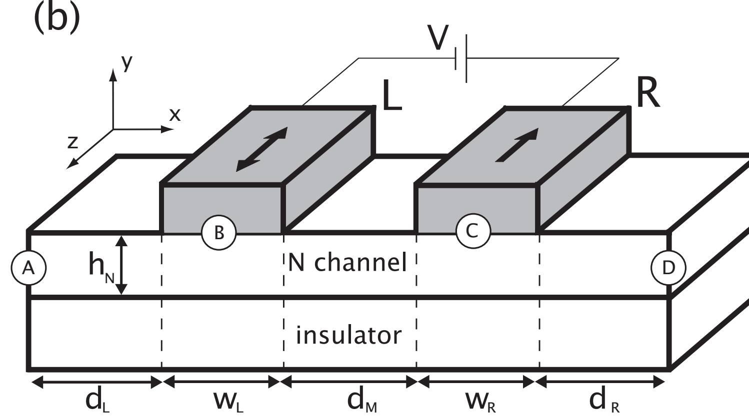

Figure 5.1: Lateral spin valve. The labels A-D denote different interfaces at which the boundary conditions have to be specified. The dashed lines divide the system into stacks of layers (see the text).

where the characteristic distance of spin-flip for spin $s{=}\pm$ is $L_s{=}\sqrt{D_s\tau_s}$, with τ_s the spin flip time and D_s is the diffusion constant of carriers with spin s (see Section 2.A). Let us remind that the measurable spin diffusion length L, on the scale of which the spin splitting $\Delta\mu{=}\mu_+{-}\mu_-$ changes, is given by $L^{-2}{=}L_s^{-2}+L_{-s}^{-2}$. As discussed in Chapter 2, such equations hold for ferromagnetic and normal metals [59], and also for non-degenerate semiconductors with the additional condition of a small electric field [57]. The boundary conditions at the interfaces are:

$$\sigma_s^i\left(\widehat{n}^i\cdot\nabla\mu_s^i\right)=G_s^{i,k}(\mu_s^k-\mu_s^i)=-\sigma_s^k\left(\widehat{n}^k\cdot\nabla\mu_s^k\right), \tag{5.2}$$

where σ_s^i and $\widehat{n}^i$ refer to conductivity of ith segment of the structure and its outward interface normal, respectively, and $G_s^{i,k}$ is the spin-dependent barrier conductance. The segments can be layers (N channel and F contacts in Figure 5.1) or sections of a single layer (N channel divided by dashed lines in Figure 5.1). With the boundary conditions specified at the outer terminals, the two coupled differential equations for μ_s can be solved numerically (results in a 3D metal structure are shown in [104]). The case of Ohmic contacts, when the current density is strongly spatially inhomogeneous, can probably be only analyzed quantitatively in such a way. However, for the resistive barriers of interest for us, a very accurate analytical

approach can be derived.

We want to reduce the essential feature of a 2D current flow to a 1D effective description. We define the vertical (with respect to y) average of μ_s in each layer:

$$\xi_s^i(x) \equiv \frac{1}{h^i}\int_{y_0^i}^{y_1^i} dy \mu_s^i(x,y) \ , \tag{5.3}$$

with h^i being the thickness of the layer between its boundaries (y_0^i, y_1^i). We perform the same kind of vertical average of Eq. (5.1), and use the boundary conditions from Eq. (5.2) to obtain

$$\begin{aligned} \frac{\partial^2 \xi_s^i(x)}{\partial x^2} &= \frac{\xi_s^i(x) - \xi_{-s}^i(x)}{(L_s^i)^2} + \frac{G_s^{i,i+1}}{\sigma_s^i h^i}\Big[\mu_s^i(x,y_1^{i+}) - \mu_s^{i+1}(x,y_1^{i+})\Big] \\ &+ \frac{G_s^{i-1,i}}{\sigma_s^i h^i}\Big[\mu_s^i(x,y_0^{i+}) - \mu_s^{i-1}(x,y_0^{i-})\Big] \ . \end{aligned} \tag{5.4}$$

For sufficiently thin layers, $\mu_s^i(x,y)$ may be replaced by its vertical average $\xi_s^i(x)$. The conditions for validity of such a replacement can be gauged by expanding μ_s along the y axis in Eq. (5.3):

$$\begin{aligned} \xi_s^i(x) &= \frac{1}{h^i}\int_{y_0^i}^{y_1^i} dy \Big[\mu_s^i(x,y_0^i) + (y-y_0^i)\frac{\partial}{\partial y}\mu_s^i|_{y_0^i} + \frac{1}{2}(y-y_0^i)^2\frac{\partial^2}{\partial y^2}\mu_s^i|_{y_0^i} + ...\Big] \\ &\simeq \mu_s^i(x,y_0) + \frac{h^i G_s^{i-1,i}}{2\sigma_s^i}\Big[\mu_s^i(x,y_0^{i+}) - \mu_s^{i-1}(x,y_0^{i-})\Big] + \mu_s^i(x,y_0^{i+})\frac{(h^i)^2}{6L_s^2} \ , \end{aligned}$$

where in the last term we have used the diffusion equation to make an approximation

$$\frac{\partial^2 \mu_s}{\partial y^2} \sim \frac{\mu_s}{L_s^2} \ . \tag{5.5}$$

The same expansion can be made around $y{=}y_1^i$ point. Now we can see, that under the conditions

$$h \ll \frac{\sigma_s}{G_s} \ , \tag{5.6}$$

$$h < L_s \ , \tag{5.7}$$

we can simply disregard the y dependence of μ_s. Replacing all the μ_s^i by layer-averaged ξ_s^i we get a set of coupled one-dimensional equations for $\xi_s^i(x)$ potentials

in all the layers:

$$\frac{\partial^2 \xi_s^i(x)}{\partial x^2} = \frac{\xi_s^i(x) - \xi_{-s}^i(x)}{(L_s^i)^2} + \frac{G_s^{i,i+1}}{\sigma_s^i h^i}\Big[\xi_s^i(x) - \xi_s^{i+1}(x)\Big] + \frac{G_s^{i-1,i}}{\sigma_s^i h^i}\Big[\xi_s^i(x) - \xi_s^{i-1}(x)\Big] \ . \quad (5.8)$$

In this way we have transformed a 2D diffusion into an effectively 1D problem. In a general case, theses equations can be solved numerically. However, if the conductivities σ_s can be taken as constant, the Equation (5.8) is a linear differential equation for ξ_s and we can solve it analytically. In the following we will concentrate on such a case. This means, that we will assume that the splitting of electrochemical potential in a semiconductor is smaller than $k_B T$, so that we can make an approximation $\sigma_s(x) \simeq \sigma_N/2$.

We now divide the lateral transport into regions of vertical stacks (denoted by dashed lines in Figure 5.1). Consider a region with a vertical stack of N_L layers. For example, in the region of width w_L covered by the left lead in Fig. 5.1, we have $N_L = 2$ excluding the insulator. Transport in the layers of the stack is governed by $2N_L$ coupled members of Eq. (5.8), which in the matrix form are simply

$$(\partial^2/\partial x^2)\boldsymbol{\xi} = \mathbf{M} \cdot \boldsymbol{\xi} \, , \quad (5.9)$$

with the column vector $\boldsymbol{\xi}$ of elements ξ_s^i and the positive definite matrix $\mathbf{M}$ of elements from Eq. (5.8). The general solution of the homogeneous equation form

$$\boldsymbol{\xi}(x) = \mathbf{1}(a + bx) + \sum_{j=1}^{N_L - 1} \mathbf{v_j} \Big(p_j e^{\lambda_j x} + q_j e^{-\lambda_j x} \Big), \quad (5.10)$$

where $\mathbf{1}$, a column of ones, is an eigenvector of $\mathbf{M}$ with zero eigenvalue and $\mathbf{v_j}$ is an eigenvector with eigenvalue λ_j^2. The connection of the vertical stacks to the outside of the system and to each other is maintained by the boundary conditions. Between stacks they are given by the continuity of $\xi_s(x)$ and their first derivatives (currents) through each homogeneous layer. At the outermost boundaries (like A and D in Fig. 5.1) the conditions are prescribed by the external driving terms of the electrochemical potential in the form of either a constant voltage maintained at an electrode, or an injection current (possibly zero) through an interface. Applying

currents/voltages to B and C interfaces results in the presence of inhomogenous terms in Eq. (5.9). These boundary conditions provide a unique set of solutions for the parameters a, b, p_j, q_j in Eq. (5.10). This method offers a considerable simplification compared to solving the 2D spin diffusion equation for the same planar structure, and yet it includes the influence of the contacts of finite lateral size on the current flow beneath and between them. In the following, we will apply this method to the semiconductor spin-valve from Figure 5.1. An example of application to an all-metallic system is given in Ref. [106].

5.B Quantitative analysis of a lateral spin valve.

In the spin valve the current is passed between the two magnetic contacts (through B and C interfaces Fig. 5.1). As we are working with quite resistive barriers, we will use the voltage difference between the two metals as a control parameter. We divide the normal channel into sections belonging to 5 vertical stacks as shown in Fig. 5.1. In the middle section of the channel, the solution is

$$\xi_{\pm}(x) = (e/\sigma_N)Jx + \xi \pm (p_c e^{x/L_N} + q_c e^{-x/L_N}), \tag{5.11}$$

where J, ξ, p_c and q_c are constants to be determined by the boundary conditions. The total current flowing between the two leads is $I = Jh_N l_z$, where l_z is the length of the structure in the z direction. For the two sections outside the footprint defined by the two leads, we introduce the notion of the "open" versus "confined" geometry depending on whether $d_L, d_R \gg$ or $\ll L_N$. In both geometries the net charge current flows only between the leads B and C. This means that the outside sections lack the linear term of Eq. (5.11). In the open geometry the spin polarization extends noticeably outside of the footprint between B and C, reducing the spin accumulation beneath the contacts.

As we have discussed before, we can neglect the tiny spin splitting in the ferromagnets. Furthermore, due to the difference of conductivities between the metallic contacts and the semiconductor channel, we can safely disregard the spatial vari-

ation of $\xi^F(x)$, and use constant electrochemical potentials $\xi^F_{L,R}$ in the left (L) and right (R) ferromagnets. The eigenvalues of the spin diffusion equations in the semiconductor are given by

$$\lambda^2_{(s,c)} = [\alpha + 1 \pm \sqrt{1+\beta^2}]/(2L_N^2) \ , \tag{5.12}$$

where the + sign corresponds to the s ("spin") mode and the $-$ sign corresponds to the c ("charge") mode. The two dimensionless parameters α and β are

$$\alpha = 2L_N^2(G_+ + G_-)/(\sigma_N h_N), \tag{5.13}$$

$$\beta = 2L_N^2(G_+ - G_-)/(\sigma_N h_N). \tag{5.14}$$

α and β are non-zero only in the channel regions beneath the contacts. Note that the ratio β/α is equal to the barrier spin selectivity γ_B. The electrochemical potential in the semiconductor layer beneath the ferromagnet is given by

$$\xi_\pm(x) = \xi^F + (1\pm\lambda)\Big[pe^{\lambda_s x} + qe^{-\lambda_s x}\Big] + (\lambda \mp 1)\Big[re^{\lambda_c x} + se^{-\lambda_c x}\Big], \tag{5.15}$$

where p, q, r and s are constants to be determined by boundary conditions and $\lambda = \cot[\frac{1}{2}\tan^{-1}\beta]$. We consider the case of robust spin injection in which α and β are comparable. If $\alpha \ll 1$, then $\lambda_c \ll 1/L_N$ and $\lambda_s \sim 1/L_N$. The s-mode decays on the spin diffusion length scale, and it corresponds to spin accumulation ($\lambda \gg 1$ in this case). If $\alpha \gg 1$, then both eigenvalues are nearly independent of L_N, and neither of the eigenvectors is a pure spin mode (as $\lambda \simeq 1$). The inhomogeneity of injection along the contacts dominates then the spatial dependence of $\xi_s(x)$.

To illustrate the effect of the contact width on the magnetoresistive (MR) effect, we use the parameters of the Fe/GaAs system given in the previous chapter (with the carrier density n=$4 \cdot 10^{15}$ cm^{-3} in GaAs). The thickness of the N channel is h_N=100 nm, and the inner channel length is d_m=200 nm. These structure parameters correspond to the values of α=1/3 and $|\beta|$=1/9. The calculated MR is shown in Fig. 5.2(a) as a function of the contact width, where for simplicity we have used w=w_L=w_R. We note the deleterious effect of the open geometry (dashed

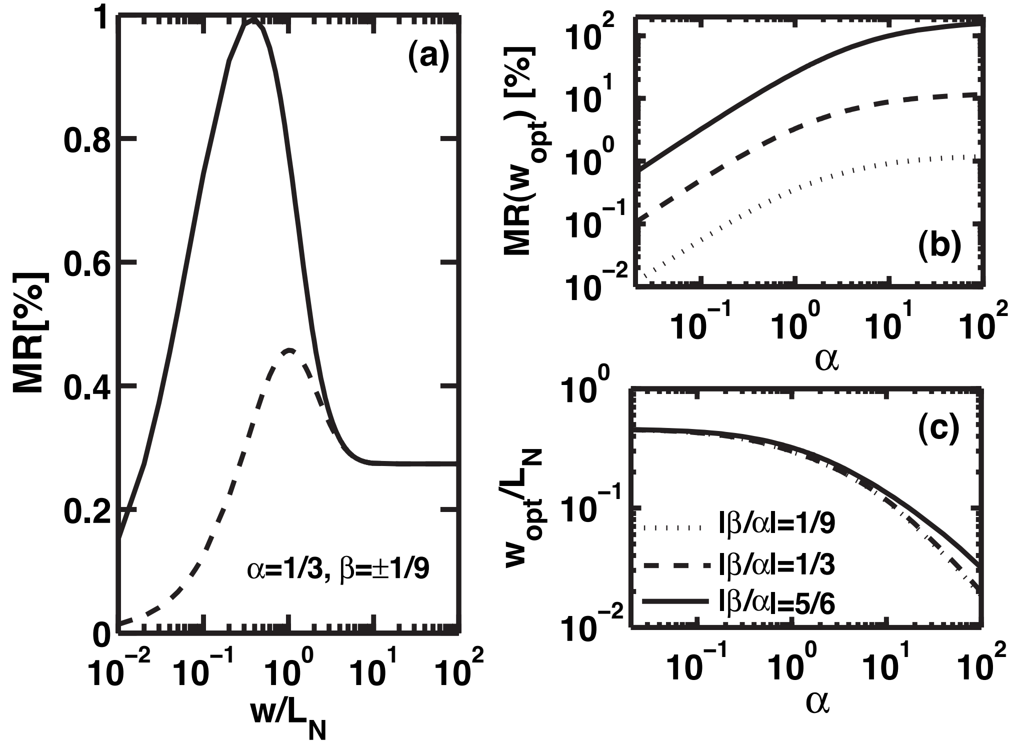

Figure 5.2: (a) Magneto-resistive effect versus the contact width of a GaAs channel at 300K. The solid (dashed) line denotes a confined (open) structure. (b) Magneto-resistive effect versus α for three cases of spin selectivity, β/α in the confined geometry, calculated for the optimal contact width corresponding to the same α value shown in (c).

line) compared with the confined geometry (solid line) because of the weaker spin accumulation in the semiconductor channel which produces the MR effect. Let us mention that for these parameters the effective 1D method presented here gives results indistinguishable from the results of a 2D numerical calculations which we have also performed.

It is interesting to see again the existence of the maximum of MR, which this time occurs for a certain optimal contact size w_{opt}. This effect arises out of the balance between spin injection and spin relaxation in the channel. The spin accumulation in the normal conduction channel is built up from injection along the width of the ferromagnetic contact. When this width is very small there is simply not enough current (notwithstanding its finite polarization) to significantly split

the spin-dependent electrochemical potentials. Then, according to the discussion from section 4.B the MR effect is small. For relatively small w we are in the "constant $\Delta\mu$ limit", and we can use Equation (4.12). According to it, the MR increases with w until the w-dependent part of the denominator in Eq. (4.12), namely

$$\frac{h_N(d+2w)}{L_N w}\frac{G_N}{G} \ , \tag{5.16}$$

either saturates or becomes smaller than 1. Further increase of w is going to lead to decrease of MR, as we eventually have to take into account the spatial dependence of μ_s. So we expect the optimal contact width $w_{\rm opt}$ to be smaller when h_N/G is small (α is large), and this is borne out by results shown in Figure 5.2c, where we have $w_{\rm opt}/L_N \simeq 2/\alpha$ for $\alpha \gg 1$. Finally, when the contact width w exceeds the spin diffusion length L_N, the build-up of spin accumulation from vertical injection along the width of the contact beyond L_N becomes ineffective, so that $\Delta\mu$ in the middle of the structure (between the contacts and under their inner edges) saturates. Thus the MR effect approaches an asymptotic value. Then the difference between the open and confined structures is removed, and the solid and dashed lines in Fig. 5.2a merge. As we expect from the previous derivations, the magnitude of MR for the optimal contact width depends on the spin selectivity of the barriers, β in Eq. (5.14), as illustrated in Fig. 5.2b. On the other hand, Fig. 5.2c shows a much weaker dependence on the spin selectivity of the optimal contact width. The ratio $w_{\rm opt}/L_N$ depends only on α defined in Eq. (5.14). For parameters used in Fig. 5.2a we have $\alpha \ll 1$, and the optimal contact width $w_{\rm opt}/L_N$ is approximately 6/5 or 3/8 for the open or confined geometry, respectively (these number come from a tedious analytical calculation best left to programs like *Mathematica*). These results enable the extraction of the spin diffusion length of a test material by measuring the MR of several structures with different contact widths from the same growth.

5.C Acknowledgements

The text of Chapter 5, in part, is a reprint of the material as it appears in Hanan Dery, Łukasz Cywiński, and L.J. Sham, *Lateral diffusive spin transport in layered structures*, Phys. Rev. B **73**, 041306(R), © 2006 The American Physical Society. The dissertation author was a co-investigator and co-author of this article.

6

Mutli-terminal systems: Magnetic Contact Transistor and a logic gate

In Chapters 4 and 5 we have analyzed the spin valve, which is a passive two-terminal device. By “passive” we mean that although the current through the valve depends on the P/AP alignment of the magnets, the value of the MR ratio is set by the geometry of the device and cannot be manipulated by some external stimulus (e.g. the MR effect does not depend on the applied bias, at least as long as electric field effects [57] are not important).

A three-terminal device (a transistor) is a cornerstone of electronics. In a transistor, the current between the two terminals is controlled by a voltage applied to the third terminal. Equivalently we can say that the resistance between two terminals is controlled by the third terminal. Thus, the name of *trans*ferable res*istor*. In a bipolar transistor, the base-emitter voltage controls the current of minority carrier which can cross the pn (or np, depending on polarity of the transitor) junction between the emitter and the base region. Due to the geometry of the device, most of these carriers are actually swept into the collector (creating a collector current I_C), and a much smaller current I_B enters the base. The final

outcome is often summed up as "small I_B current controls the large I_C current", but a physical explanation is that the base-emitter voltage provides the control of both currents, which are proportional to each other: $I_C/I_B \equiv \beta$, where β is the current gain coefficient (typical value of β is 100). In the field-effect transistor (FET), the voltage applied to the gate changes the resistance of the channel between source and drain, including the possibility of switching the source-drain current on and off. The modern electronics is now completely dominated by field-effect transistors, specifically the so-called Complementary Metal-Oxide-Semiconductor (CMOS) technology, in which FETs with both n-type and p-type channels are employed.

In recent years, many types of "spin transistors" have been proposed theoretically. The most famous is the simple "current modulator" proposed by Datta and Das [16] in 1990, in which the electric field of the gate together with spin-orbit interaction in the small-bandgap semiconductors (Rashba effect, see e.g. Ref. [17]) controls the precession of spins of ballistic electrons injected and extracted by ferromagnetic contacts. Despite a large experimental effort (and innumerable theoretical papers on modeling of variations of the Datta-Das transistor) the conclusive demonstration of the device operation has remained elusive. Let us mention some of the other proposed semiconductor spin-transistors. A diffusive version of a Datta-Das system has been put forth [107]. Magnetic unipolar [108] and bipolar transistors [63, 109, 64] (both of which require non-degenerate magnetic semiconductors) have been analyzed. Another proposal was that of a spin transistor without any ferromagnetic elements [110], which relies exclusively on strong spin-orbit interaction experienced by electrons in low bandgap materials such as InAs. There was also a proposal of bypassing the problems with efficient spin injection (which were more serious at that time than they are now) and using a proximity effect of a ferromagnetic gate [90, 98].

Motivated by a rapid progress in spin injection and extraction in structures consisting of ferromagnetic metals and semiconductors [38, 41, 42], we present a

proposal of a three-terminal system [111], which we predict to operate at room temperature using realistic numbers for spin injection across Fe/GaAs interface. In chapter 4 we have seen that despite the large difference between the spin accumulation in P and AP configurations of a spin valve, the MR effect remains very small for barrier conductances G smaller than the spin depth conductance of the channel G_N. The main idea it to use a third ferromagnetic contact in order to sense the qualitative difference between spin splittings for two alignments of remaining two contacts. The only feature necessary in such a system is the spin selectivity of barriers between the channel and all three contacts (allowing for spin injection and extraction by every contact). Because of this we have termed it a "Magnetic Contact Transistor" (MCT).

Let us mention that a similar system has been known for some time in the field of all-metal magnetoelectronics as a non-local spin valve [112, 99, 100]. However, the third contact in a non-local spin valve is used as a passive floating terminal (essentially a spin dependent voltage probe). In the MCT all the contacts are active terminals controlled by applied voltages. The possibility of control is closely related to the use of the non-degenerate semiconductor as a paramagnetic channel. Due to very small concentration of carrier compared to metals, spin injection can lead to spin splittings of electrochemical potentials of the order of milivolts in the channel. Then, the voltages supplied with mV accuracy can efficiently tune the magnetoresitive effect measured in one of the terminals.

The basic physical principle behind the operation of the MCT, which is the direct electrical expression of the spin accumulation in the semiconductor, is then used in section 6.D to propose a magneto-logic gate (MLG). In this system the logic input is encoded in the magnetization orientations of 4 metallic contacts, and the fifth ferromagnetic contact is used to sense the magnitude of the resulting spin accumulation, which encodes the logic output of the gate.

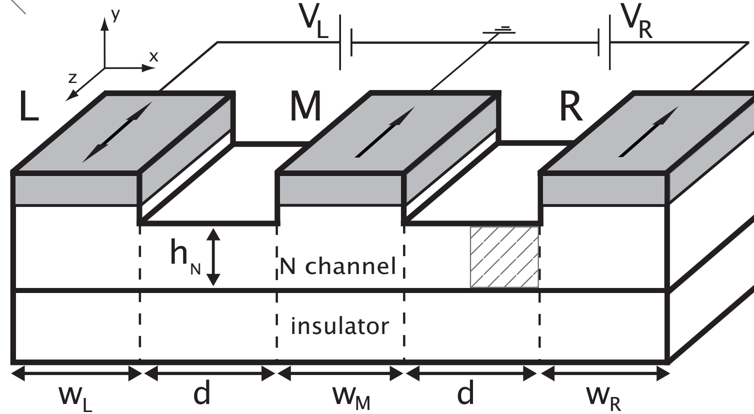

Figure 6.1: A three-terminal Magnetic Contact Transistor. The spin currents in the marked area close to the right magnet are shown in Figure 6.4 (see text for details).

6.A The principle of operation

A schematics of the proposed system is shown in Figure 6.1. Since we will use the spin accumulation in the channel, the outer edges of the channel are removed, so that we are in the "confined" geometry (see Chapter 5). We let the left ferromagnet (L terminal) be a "soft" magnetic layer, the magnetization of which can be easily flipped. The middle (M) and right (R) magnets have parallel magnetizations. They can be pinned by exchange bias [97], so that only the L magnet changes its orientation due to an external magnetic field. Alternatively, the shapes (aspect ratios) of M and R can be chosen in such a way that their coercivities differ from the L magnet (this will work when the magnetic anisotropy is dominated by shape anisotropy, e.g. in permalloy). The P and AP configurations denote, respectively, the L magnetization parallel and antiparallel to that of the M and R. Now we have two voltages, V_L and V_R, controlling the I_L and I_R currents (with the value of I_M following from current conservation).

In order to explain the principle of operation, let us first consider at situation in which the R terminal is disconnected (e.g. the wire leading to it is cut). Then the L and M contacts constitute a spin valve analyzed in previous chapters, with

voltage V_L applied to it. Upon change of the orientation of the L magnet (between P and AP with respect to M), the current I_L changes slightly, but the average spin splitting of electrochemical potential in the channel $\Delta\xi$ varies between two very different values (inside the channel we use ξ_s for the layer-averaged electrochemical potential). Let us remind that beneath the injecting and extracting contacts we have $\Delta\xi^P/\Delta\xi^{AP}\propto(l/2L_N)^2$ (see Chapter 4), with effective length of the active channel covered by L and M terminals $l\approx d+w_L+w_M$. The spins accumulated beneath the M terminal diffuse out to the right, but if $d\ll L_N$ the spin accumulation beneath the R magnet is going to be practically the same as beneath the M contact. For $w_R\ll L_N$ the ξ_s beneath R can be assumed to be constant. Let us write the electrochemical potentials as

$$\xi_\pm^{P,AP} = \xi^{P,AP} \pm \frac{1}{2}\Delta\xi^{P,AP} \ , \tag{6.1}$$

where $\Delta\xi$ is the spin splitting and ξ is the average value of electrochemical potential. Now, if we connect the R terminal and apply any voltage V_R, the situation inside the channel will change in general. But we are interested in choosing V_R such that there is only a small (possibly zero) I_R current. Then the spin accumulation determined by a larger I_L injected into the channel remains practically unaffected. For such a voltage applied to R, we have the total current entering the R contact (with A being the contact area and $\mu_R{=}-eV_R$):

$$I_R^{P,AP} = \frac{GA}{e}(\mu_R - \xi^{P,AP}) - \frac{\Delta GA}{e}\frac{\Delta\xi^{P,AP}}{2} \ , \tag{6.2}$$

and the corresponding spin current

$$\Delta I_R^{P,AP} = \frac{\Delta GA}{e}(\mu_R - \xi^{P,AP}) - \frac{GA}{e}\frac{\Delta\xi^{P,AP}}{2} \ . \tag{6.3}$$

By a proper choice of μ_R we can make $I_R{=}0$. Let us denote $\mu_0^{P,AP}$ as the value of electrochemical potential in R magnet that quenches the total current in this contact:

$$\mu_0^{P,AP} = \xi^{P,AP} + \frac{\Delta G}{G}\frac{\Delta\xi^{P,AP}}{2} \ . \tag{6.4}$$

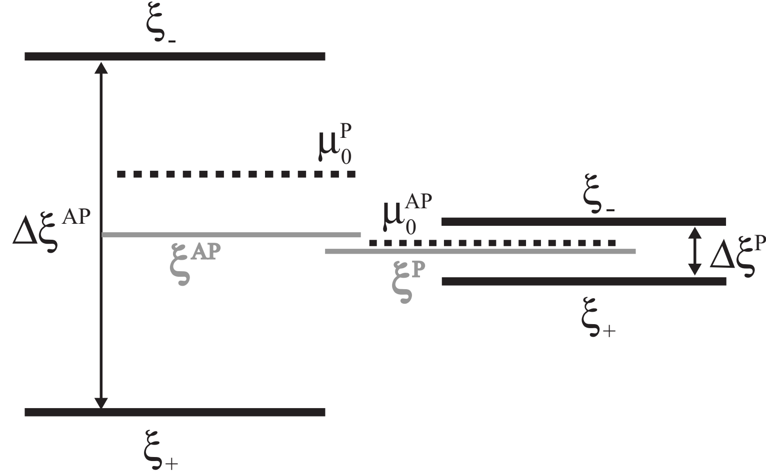

Figure 6.2: The alignment of electrochemical potentials (ξ_s) in the channel beneath the R contact and the potential inside the R terminal which make I_R equal to zero (μ_0). The grey lines are the average values of the electrochemical potential in the channel. Their change between P and AP configurations is much less prominent than the change in splittings $\Delta\xi$.

.

In the following derivations we will disregard a small value of $\Delta\xi^P$ and set

$$\Delta\xi^P \approx 0 \; . \tag{6.5}$$

The last piece of information that we need is the fact that when the barriers are the most resistive elements in the circuit, we have

$$\xi^P \approx \xi^{AP} \approx \frac{-eV_L}{1 + R_L/R_M} \; , \tag{6.6}$$

where R_L and R_M are the resistances of the L and M contacts, respectively. So the average electrochemical potential is roughly the same for both magnetization configurations. This can be shown to the first order in G/G_N in a 1D model, and also holds very well in the realistic lateral case. It can be seen in Figure 6.2, where an example lineup of ξ_s under the right magnet is shown.

After all this preparation, we can immediately derive the following. In either P or AP alignment of L and M magnets, we can bias the R terminal in such a way that the current flowing through it is zero. If we then flip the L magnetization,

a finite I_R current will flow. This is a consequence of large spin accumulation in AP configuration, and spin selectivity of the barrier ($\Delta G \neq 0$). The "on" current is given by

$$I_R^{on} = \pm \frac{\Delta G}{e} \frac{\Delta \xi^{AP}}{2} \tag{6.7}$$

where we have the (+) sign for the case when I_R^{AP} was quenched and the (-) sign when the R voltage was chosen so that I_R^P=0. Thus, we have found a way to *digitize the MR effect in the R contact.* Instead of some finite ratio of P and AP currents, we can have zero current for one and a finite current for the other configuration.

The "digitization" holds for the MR effect measured in the third (R) terminal. The larger currents in the other two (L and M) have a small relative change when we alternate between P and AP configurations. Yet these contacts do almost all of the job of injecting and extracting spin-polarized currents. We can say that we have transferred the magneto-resistive effect to the third contact, where we can tune it by V_R voltage. In Ref. [111] we have called this *spin transference.* An alternative term of "transferable magnetoresistance" underlines the connection to the standard transistors. Actually, we can draw an analogy between the Magnetic Contact Transistor (MCT) and the bipolar transistor. In the latter case, the transistor action results from attaching two p-n diodes back to back into a pnp or npn structure, where the common base width must be smaller than the recombination diffusion length. A longer base would beget two uncoupled diodes devoid of amplification effects. We can look at the MCT as two spin valves with a common middle terminal. If the width of this common contact is smaller than the spin diffusion length L_N, we create a system capable of amplifying the MR effect of each spin valve. However, the MCT does not amplify currents, and it is a linear device in a sense that all the currents depend linearly on both applied voltages. But, as a spintronic device, it is also sensitive to the additional discrete degree of freedom (magnetization configuration), and the flexibility provided by two controlling voltages allows us to manipulate the magnetoresistive effect associated with changing the magnetizations.

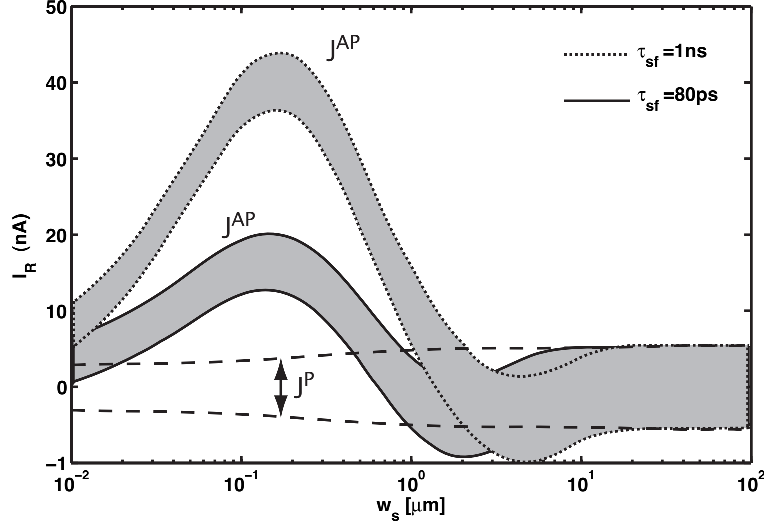

Figure 6.3: Right terminal current versus the middle terminal width for the left terminal magnetization parallel (P) and antiparallel (AP) to the other two magnets. $V_L = 0.1V$ and V_R is adjusted for each w_s so that $I_R^P = 0$. Upper and lower curves of each set show the current densities for V_R±0.2 mV. The dashed lines are the values for I_R^P around zero current. The solid and dotted lines show the currents for I_R^{AP} for two different spin relaxation times. The middle contact width, separation between the contacts and the channel thickness are w=d=2h=0.2 μm, and the areas of the L and R contacts are 1 μm^2.

6.B Results of modeling

We have modeled the MCT shown in Figure 6.1 using the lateral diffusion formalism from Chapter 5. We have also performed the numerical calculations of a 2D diffusion equation, and the agreement with an effective 1D method confirmed its accuracy. For the calculations we have used parameters of room temperature GaAs with carrier density n=$4 \cdot 10^{15}$ cm^{-3}, and spin relaxation time τ_{sr}=80 ps (with corresponding spin diffusion length L_N=1 μm). The barriers have total conductance G=3000 Ω^{-1}cm^{-2}and spin selectivity γ_B=1/3 (equivalent to G_+/G_-=2). The dimensions of the system are the following: the thickness of the N layer h_N=100 nm, the distance between the contacts d=200 nm, the widths of L and R contacts w_L=w_R=200 nm. The areas of L and R contacts are 1 μm^2. In Figure 6.3 we show the current I_R^{AP} calculated for V_R such that I_R^P=0, as a function of the middle

contact width. For large w_M, equivalent to uncoupled spin valves, the MR effect is lost. Again, as in case of the spin valve, there is an optimal value of w_M for which the desired effect is maximized. The resulting I_R^{AP} currents are about 10 nA for room temperature GaAs parameters and for an optimal width $w_M \simeq 200$ nm. The I_L and I_M currents are of the order of 1 pA for this w_M. In this figure we also show the analogous results for a longer spin relaxation time $\tau_{sr}=1$ ns. Spin relaxation times of nanoseconds and longer can be seen in GaAs at temperatures below 100 K [20], and are expected in Si at room temperature.

Another important feature which we have taken into account in the calculations shown in Figure 6.3 is the presence of noise in the system. For the obtained values of I_R currents, the main contribution to the current fluctuations comes from the Johnson (thermal) noise, which for highly resistive barriers that we have dominates over the shot noise. The mean square of the voltage (or current) fluctuation depends on the bandwidth of interest. For a characteristic time of measurement t_m the bandwidth is $\delta f \sim 1/t_m$. In a given bandwidth, we have for the thermal noise the fluctuation of the voltage across the resistor $\langle V^2 \rangle = 4 k_B T R \delta f$. In order to estimate the noise in the system we take a resistance of the contact of 1 μm^2 area which is R=$0.3 \cdot 10^5$ Ω. If we take 100 MHz bandwidth, we get a 0.2 mV voltage noise. In Figure 6.3 we calculate the “on” and “off” I_R currents taking such a fluctuation of V_R into account. Of course, the voltage source applied to the contact needs to have a smaller intrinsic noise.

6.C Fully polarized spin current and spin current without net charge current

Let us note some interesting features of the current flowing into the R contact for V_R chosen in a way discussed above. Firstly, the “on” current is fully spin polarized, i.e. carriers of one spin are entering the contact, while the carriers of the opposite spin are leaving it. It can be seen from Figure 6.2 in which the μ_0

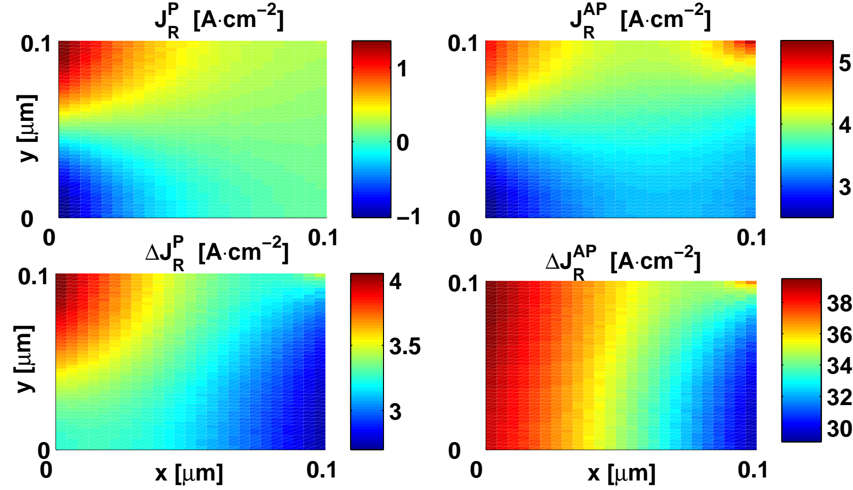

Figure 6.4: Spatially resolved x component of the current density at the right half of the right channel (the region marked in Figure 6.1). Note the different scales for each figure. The upper panels show the zero and finite net charge currents for the parallel and antiparallel configurations, respectively (0 versus $\sim$3.5Acm^{-2}). The lower panels show the amplification of ΔJ=j_+−j_- due to the difference in electrochemical potential splitting. The parameters are as in Fig. 6.3 with optimal source width and τ_{sp}=80 ps.

adjusted in the contact lies between the two ξ_s in the channel. The two opposing currents of spin up and down do not cancel each other exactly, and we are left with a finite net I_R. Secondly, in the "off" state, when V_R is adjusted so that the net I_R=0, there is a non-zero spin current flowing into the R terminal:

$$\Delta I_R^{off} = \frac{\Delta\xi^{P,AP}}{2e}\frac{\Delta G^2 - G^2}{G}A \ . \tag{6.8}$$

The currents of electrons with both spins flow in the opposite directions, canceling the net particle current, but adding to a net flow of spin polarization. A similar effect was predicted in a lateral structure with non-magnetic source and drain and two ferromagnetic gates, into which the current could leak [98].

A finite spin current entering a ferromagnet can lead to the reversal or precession of the magnetization, if the polarization of injected spins is non-collinear with the magnetization axis of the magnet [8, 9]. This is a so-called spin-torque effect. This effect has been observed in an metallic non-local spin valve [113]. The mag-

netization of a floating terminal (zero net charge current through it) was switched by a spin current flowing into it.

In Figure 6.4 we show the plots of x component of current densities and their polarizations in the semiconductor channel in the 100 nm section left of the right contact (see Figure 6.1). The V_R voltage is adjusted so that I_R^P=0. In the upper panels one can see the zero and finite net current flowing in P and AP configurations (in P case the current flows in the opposite directions near the top and the bottom of the channel). In the lower panels we show the amplification of spin polarization of current ΔJ_x from P to AP (according to Equation (6.8) ΔI is proportional to $\Delta\xi$).

6.D Five-terminal magneto-logic gate

The three-terminal MCT can be used for electric readout of a bit of memory encoded in a magnetization direction of the L terminal. But the same physical principle of operation can be harnessed to achieve a more complicated functionality. In Figure 6.5 we present a scheme of a five-terminal system, in which the electric sensing of spin accumulation is used to perform a logic operation, i.e., two bits of input are converted to a binary output signal. Let us mention that spintronic logic gates have been proposed in purely metallic systems [114], but ours is the first realistic proposal which employs semiconductors as active elements of the system.

The system presented in figure 6.5 works in the following way. The charge currents are flowing between two pairs of terminals (X and A, Y and B), between which the bias V_{dd} is applied. Depending on the alignment of these pairs of magnets, different patterns of spin accumulation are created in the channel. As in the case of the MCT, the middle contact (M) can be used to directly express the differences in the average spin accumulation beneath it.

The logic inputs are encoded by magnetization directions of A,B,X, and Y terminals. We will concentrate on the case in which A and B magnetizations

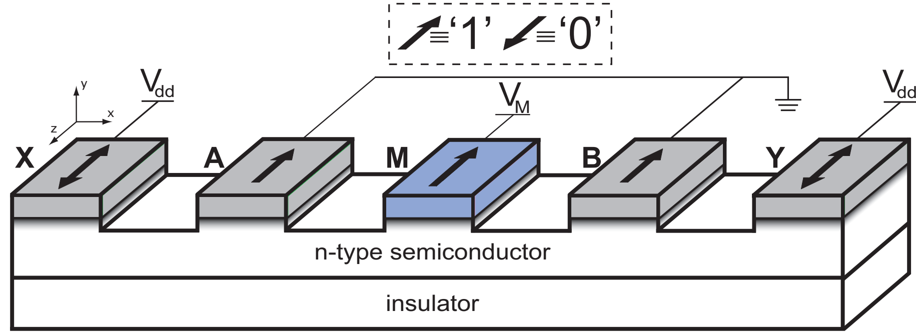

Figure 6.5: A five-terminal magneto-logic gate. The logic inputs '0' and '1' are encoded by magnetization direction of the A,B,X,Y terminals (see text for details). As shown here, the gate is set to work as a NAND operation between X and Y (A and B are fixed to '1' values).

are preset, defining the logic function of the gate. This reprogrammability is an important feature of magnetization-based logic. X and Y are then the logic inputs, and the current from the (properly biased) M contact gives the result of the logic operation. Let us focus on an example of the NAND gate. Any other logic function can be realized by using a finite number of such gates. For the NAND operation, A and B magnets are set parallel to each other (their direction defining the logical '1'). If both X and Y magnets are set to '1' direction, the spin accumulation beneath the M contact is small (as the spin injection and extraction occurs between pairs of parallel magnets). The voltage V_M is tuned so that the I_M current is zero. If either X or Y are set to '0', there is a larger spin accumulation created and a finite I_M=I_{10} will flow. When both X and Y are set to '0', a current I_M=I_{00}=$2I_{10}$ will result (the spin accumulation is additive in the linear regime). Now the "digitization" of the response achieved in the MCT is lost, but if the I_{10} and I_{00} currents can discerned, then we can assign the logical '1' to the large output current, and '0' to the smaller current. Thus we electrically read out the result of the NAND(X,Y) operation. Further details, and a discussion of a dynamic readout scheme which could be used in a large-scale circuit, is presented in section 7.D of Chapter 7.

6.E Acknowledgements

The text of Chapter 6, in part, is a reprint of the material as it appears in (1) Hanan Dery, Łukasz Cywiński, and L.J. Sham, *Spin transference and magnetoresistance amplification in a transistor*, Phys. Rev. B **73**, 161307(R), © 2006 The American Physical Society, in which the dissertation author was a co-investigator and co-author; (2) Hanan Dery, Parin Dalal, Łukasz Cywiński, and L.J. Sham, *Spin based logic in semiconductors for reconfigurable large scale circuits*, Nature **447**, 573 © 2007 Nature Publishing Group, in which the dissertation author was a contributing investigator and author.

7

Electric readout of magnetization dynamics

In the previous chapter we have shown how in a multi-terminal system we can manipulate the response of the current to the alignment of magnetizations of the contacts. In this chapter we will explore the possibility of a *dynamical* read-out scheme in such a system based on a time-dependent analysis of the lateral spin diffusion. In response to time dependence of one of the magnetizations (e.g. its rotation), a transient current in a terminal (the rotated one, or another) is triggered. The three-terminal system can then be used as an electric sensor of magnetization dynamics. This is described in sections 7.A-7.C. An alternative application is given in section 7.D, in which the transient current response is used to read-out the outcome of the logic operation in a five-terminal magneto-logic gate (MLG) introduced in section 6.D of the previous chapter.

7.A The principle of operation

The three-terminal system is shown in Figure 7.1. The difference with respect to the MCT described in chapter 6 is the fact that the R terminal is now connected to a capacitor C. Hence, in the steady state there is no I_R current. The bias is

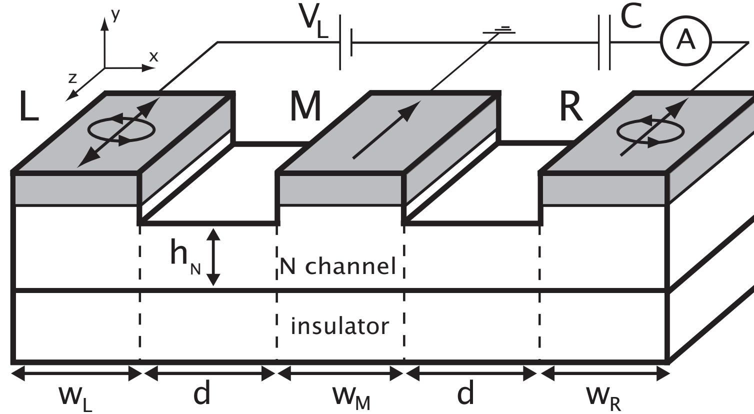

Figure 7.1: A Magnetic Contact Transistor modified for electric readout of magnetization dynamics. The right (R) terminal is connected to the capacitor C. When one of the magnetizations becomes time-dependent, the transient currents flow out of the R contact. The dimensions used for calculations are h_N=100 nm, w_L=w_M=w_R=400 nm, d=200 nm and the length in z direction l_z=2 μm.

applied between the L and M terminals, and there is a current flowing between them at all times. The voltage on the capacitor depends on the alignment of L and M magnetizations as well as on the spin selective properties of the R terminal, as in the non-local spin valve effect. In the following we fix the M terminal magnetization (e.g. by exchange bias pinning).

In order to change the magnetizations of L and R terminals “on the chip”, the planar structure can be augmented by a set of current-carrying lines known from MRAM devices [15]. In MRAM, there are wide metallic strips (so-called ‘bit’ and ‘word’ lines) running above and below the magnets that are to be addressed. The upper and lower wires are at a 90 degrees angle, so that every magnet is (when looking from above) located at an intersection of two wires. In order to switch its magnetization, the current pulses are passed through the appropriate bit and word lines. These currents generate transient local magnetic fields (through Ampere’s law) which can switch the magnetization of the addressed terminal. The two lines are necessary for addressing purposes in a matrix consisting of many MCTs. Only the magnet located at the intersection of two lines is switched.

The other magnets over (under) which the activated current-carrying line passes are unaffected, as the current magnitudes are such that a magnetic field from a single line is unable to switch the magnetization. Furthermore, using the two lines (giving two perpendicular magnetic fields which add up) is advantageous because the presence of magnetic field components non-collinear with the magnet's easy axis aids the fast switching [115].

We will discuss two possible modes of operation for this system. In the first mode, the magnetization of L contact is perturbed, and its dynamics drives a current in the R contact. This leads to the possibility of an all-electrical measurement of magnetization reversal. In the second mode, the L magnetization represents a bit of memory, and the rotation of the R contact triggers a transient current, the magnitude of which is related to the relative alignment of L and M magnetizations.

The principle of operation is the same as in the static MCT, with the additional complication of allowing for changes of R magnetization direction. In the steady state we have thus four possible configurations of magnetization. The spin accumulation in the channel is determined by the alignment of L and M terminals. In each situation, the voltage on the capacitor (equal to the potential in the R contact) is such that there is no net I_R. A schematic plot of electrochemical potentials ξ_s in the channel beneath the R contact and the potentials μ_R inside the R magnet is shown in Figure 7.2. Let us repeat here Equation (6.4) for the R contact:

$$\mu_R = \xi + \frac{G_+^R - G_-^R}{G_+^R + G_-^R}\frac{\Delta\xi}{2} \ . \tag{7.1}$$

When the L magnetization is rotated, $\Delta\xi$ changes, and when R magnet is switched, G_+^R and G_-^R trade places. In both cases, the potential μ_R ceases to give zero net current, and a transient current charges the capacitor until a new steady state is reached. A full flip of either L or R magnet leads to a transition of μ_R between a pair of dashed lines in Figure 7.2. If the RC time constant of the entire circuit is shorter than a time-scale of magnetization dynamics, it is possible to trace out the magnetization dynamics by electrical means. If $\Delta\xi$ is unchanged (when only R is

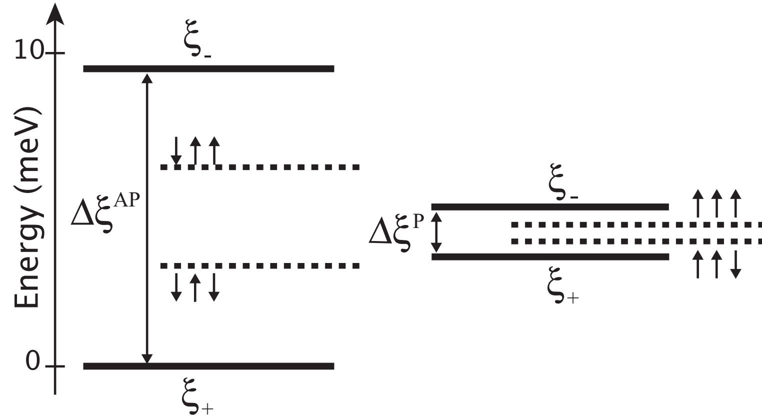

Figure 7.2: Spin accumulation under the R contact and voltage inside it for antiparallel (AP) or parallel (P) magnetization alignment of the L and M terminals. Solid lines are the spin-dependent electrochemical potentials in the semiconductor channel beneath the R contact. Dashed lines are the values of electrochemical potential μ_R in the R contact in the steady state, depending on the R direction, with arrows denoting the alignment of three magnets.

rotated), then the signal is expected to differ strongly in magnitude depending of the L/M alignment, due to the ratio of spin splittings in P and AP configuration of L and M magnets. This leads to a dynamical readout of the L magnetization direction by rotating the R magnet.

For the electrical tracing of L magnetization dynamics, both M and R magnets should be pinned in the same direction. In the case of the dynamical readout of L/M alignment, we need to write separately the memory bit (direction of L magnet) and read by rotating the R magnet. A proper choice of different coercivities of two magnets and magnetic field pulses should allow for separate addressing. The half-selection (unintentional perturbation of magnetization) of L when rotating R should be diminished, in order not to mix the signal from the L dynamics with the readout of L alignment.

7.B Time-dependent formalism

In order to model the transient behavior, we need to add the time dependence to the formalism of lateral spin diffusion. We are going to be interested in time-scales of a least tens of picoseconds. The fastest magnetization reversal time is about 100 ps [12]. A typical period of magnetization precession in ferromagnetic resonance is also of this order of magnitude. Magnetization switching times used in commercial devices are of the order of a nanosecond. Consequently, we will use an adiabatic approximation with respect to the processes occurring on a much faster (sub-picosecond) time scales: the momentum scattering and dielectric relaxation. We can then neglect the time derivative in Equation (2.33), and plug in the resulting expression for j_s into the continuity equation (2.32). In this way we obtain a time-dependent diffusion equation for the spin accumulation Δn=$n_+ - n_-$. In the linear regime (spin accumulation much smaller than the total carrier density), we also have a diffusion equation for spin-splitting of electrochemical potential $\Delta\mu$. We integrate out the y dependence of $\Delta\mu(x, y)$ like in Chapter 5, and obtain the diffusion equation for the spin splitting $\Delta\xi$=$\xi_+ - \xi_-$:

$$\frac{\partial \Delta\xi}{\partial t} = D\frac{\partial^2 \Delta\xi}{\partial x^2} + \frac{\beta_i(t)}{\tau_{sr}}(\mu_i^F - \xi) - \frac{\alpha_i}{2\tau_{sr}}\Delta\xi - \frac{\Delta\xi}{\tau_{sr}}. \tag{7.2}$$

The meaning of the $\beta_i(t)$ parameter of i-th layer is discussed below. Next we use the fact that the dielectric relaxation (about 100 fs for non-degenerate semiconductor with n_0=10^{16} cm^{-3}) is much faster than the time-scale of magnetization dynamics and spin diffusion, and assume quasi-neutrality n the channel at all times ($n_+(t) + n_-(t)$=0). In the linear regime under consideration (when $\Delta\xi$<$k_B T$) the average electrochemical potential μ=$(\mu_+ + \mu_-)/2$ is equal to $-e\phi$ (where ϕ is an electrostatic potential). At every moment of time μ fulfills the Laplace equation, with boundary conditions given by currents at the interfaces. In the time-dependent case these include also a displacement current connected with charging of the barrier capacitance C_B. A Schottky barrier is basically a dipole layer, and its capacitance can have a strong effect on dynamics of currents on time scales of

interest here. In order to take the displacement current in the barrier into account, the boundary condition for spin current has to be modified in the following way:

$$j_s = \frac{G_s}{e}(\mu^F(t) - \mu_s(t)) + \frac{c_B}{2e}\frac{\partial}{\partial t}(\mu^F(t) - \mu(t)) \ , \tag{7.3}$$

where μ^F is an electrochemical potential in a metal (its spin splitting neglected as usual) and c_B is the barrier capacitance per unit area. The second term in the above equation represents the carriers which flow towards the barrier, but do not tunnel through it. Instead, they stay in the semiconductor close to the barrier, making the depletion region slightly thinner or wider. An equal amount of opposite charge is brought to the metal surface. The charge involved in this process is negligible compared to the charge already swept out of the depletion region (which determines the width of the Schottky barrier), and we can keep c_B constant. For small spin splitting (so that the conductivities $\sigma_+ \simeq \sigma_-$) the same amount of carriers of each spin is going to be brought from the channel into the barrier, thus the displacement current is the same for each spin in Equation (7.3). The equation for layer-averaged ξ is obtained as in Chapter 5:

$$\frac{\partial^2 \xi}{\partial x^2} = -\frac{\alpha_i}{2L_N^2}(\mu_i^F - \xi) + \frac{\beta_i(t)}{4L_N^2}\Delta\xi - \frac{c_B}{\sigma h}\frac{\partial}{\partial t}(\mu_i - \xi) \, . \tag{7.4}$$

and the right hand side of Eq. (7.4) is non-zero only under the contacts.

The dynamics of magnetization in a contact is parametrized by a single parameter $\beta(t)$, which characterizes the contact polarization only along the z axis. If we deal with a coherent precession of magnetization then this is an approximation. In principle, one should perform calculations of diffusion of spin accumulation treated as a vector quantity [47], and take into account the noncollinearity of spins and the magnets in the tunneling process [116, 117, 89]. However, for tunneling barriers the non-trivial effects of this noncollinearity (the "mixing conductance" in [116]) are expected to be small, and the only thing that matters is the average polarization along the z direction in the channel. Then we can model the influence of the contact with magnetization making an angle θ with the z axis by assuming that

$\beta\sim\Delta G\cos\theta$. On the other hand, if the magnetization reversal is incoherent (e.g. proceeding by nucleation of domains with opposite magnetization), the parameter $\beta(t)$ describes an area average of spin-selectivity of magnetically inhomogeneous contact, and again β can be taken as proportional to the z component of the contact's magnetization.

Summarizing, the magnetization dynamics of ith contact translates into time-dependence of β_i, driving the spin diffusion in Eq. (7.2) and electric potential in the channel in Eq. (7.4). From ξ_s we calculate the current I_R flowing into the right contact and charging the capacitor C, and consequently the electrochemical potential of the R terminal μ_R=$-eV_R$ changes according to dV_R/dt=I_R/C.

7.C Results of calculations

For the calculations, we use the parameters of GaAs at room temperature from the previous sections, with doping n_0=10^{16}cm^{-3}. The dimensions of the system are given in Figure 7.1. Again we employ the experimentally verified [36] spin selectivity G_+/G_-=2, but in order to achieve signal stronger than noise we take the barrier conductance to be G=$10^4\,\Omega^{-1}$cm^{-2}. For such barriers of 1 μm^2 area and 10 nm thickness, R_B=10 kΩ and C_B=10 fF . The external capacitance is taken as C=40 fF, and the resulting RC time is about 1 ns. The applied voltage V_L is 0.1 V.

In Figure 7.3a we present the calculated I_R induced by a reversal of the L magnet from AP to P alignment relative to M. The reversal is parametrized by $\beta_L(t)$=$\beta_0\cos(2\pi t/T)$, with different reversal times T. The shape of the I_R current pulse follows closely the time-dependence of β_L, which is proportional to the z component of the L magnetization. The time-integrated current is the same for any reversal time, and it is given by a change of the charge on a capacitor C needed to switch the R terminal potential between a pair of levels shown as dashed lines in left and right parts of Figure 7.2.

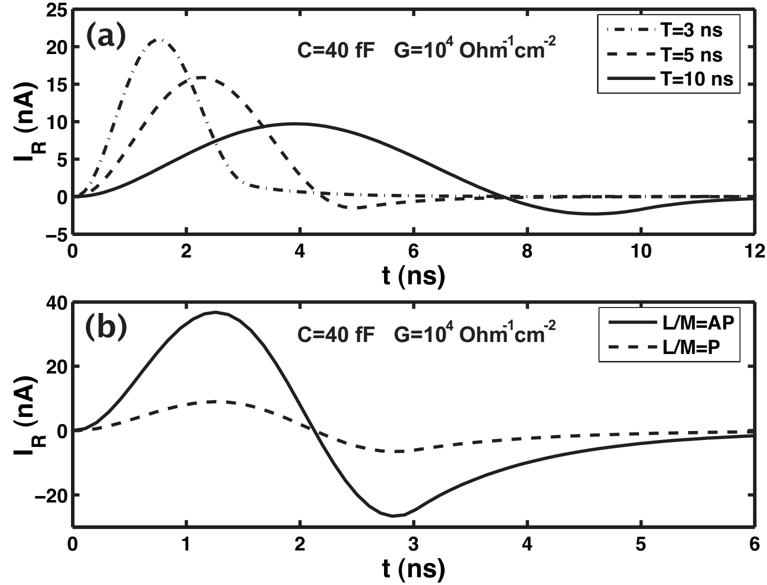

Figure 7.3: (a) R current signal for reversal of L magnetization occurring on time-scale of 3, 5 and 10 ns starting from AP alignment of L relative to M magnet. (b) R current signal for 2π rotation of R magnet for P and AP alignments of L and M magnets. The period of rotation is 3 ns.

In Figure 7.3b the transient I_R for the 2π rotation of R occurring in 3 ns is shown. While the average current is zero, the average power of the current pulse is much higher for the L/M=AP than for P. Two signals of such clearly different magnitude can be easily distinguished, provided that the stronger signal is above the noise level (dominated by Johnson noise in our system). In Figure 7.3b the power of AP pulse is slightly above the noise power in 0.3 GHz bandwidth.

The above calculations show that metal/semiconductor system could be used to sense the dynamics of magnetization rotation by electrical means. However the problem of noise is more pronounced in the dynamical case. The operation of the static MCT could be demonstrated in the laboratory using the currently available metal/semiconductor spin injecting junctions (as we can always decrease the bandwidth until the signal becomes stronger than noise). Here the characteristic time-scale of magnetization reversal sets the minimum bandwidth. Even for rotations slower compared to the ones achieved in MRAM devices, we need more

transparent barriers in order to make signal at least comparable to the noise.

Let us note that the possibility of performing operations described above is closely related to the use of a semiconductor channel. In an all-metal MCT the concept of operation still holds, but the swings of μ_R are orders of magnitude smaller, and in order to achieve measurable current we would have to use a macroscopic capacitor. Clearly, for the dynamical MCT to work we need a semiconductor, and we need relatively low resistance tunneling barriers. Significant steps towards making such metal-semiconductor contacts have been made recently [101].

7.D The dynamic readout of the outcome of a logic operation in the five-terminal system

The dynamic approach to the readout of magnetization alignment presented above can also be used in a magneto-logic gate (MLG) introduced in Section 6.D. In Figure 7.4a the modified MLG is presented. The middle (M) contact is connected to the capacitor C_M, and the rotation of the M magnetization creates a transient current $I_M(t)$, the magnitude of which gives the outcome of the logic operation. For a NAND operation described in Section 6.D, A and B magnets are fixed in the '1' direction (see Figure 7.4a). The profiles of the electrochemical potentials in the semiconductor channel are shown in Figure 7.4b for different directions of X and Y magnets (the X='0', Y='1' configuration results in a mirror image of the X='1', Y='0' shown by the blue lines in the Figure). As we discussed in the previous sections of this chapter, the rotation of the contact connected to the capacitor (M terminal in this case), creates a transient current, the magnitude of which is proportional to the spin accumulation beneath the contact. For the case presented in Figure 7.4, the amplitude of the $I_M(t)$ oscillation is two times larger for X='0' and Y='0' compared to the case when one of them is '0' and the other is '1' (for '11' case the current is negligible). This is shown in Figure 7.5. Reference [118] contains a detailed account of how this transient current can

be captured by an external electronic circuit, and then used to control a suitable write operation applied to magnetic contact of the another gate.

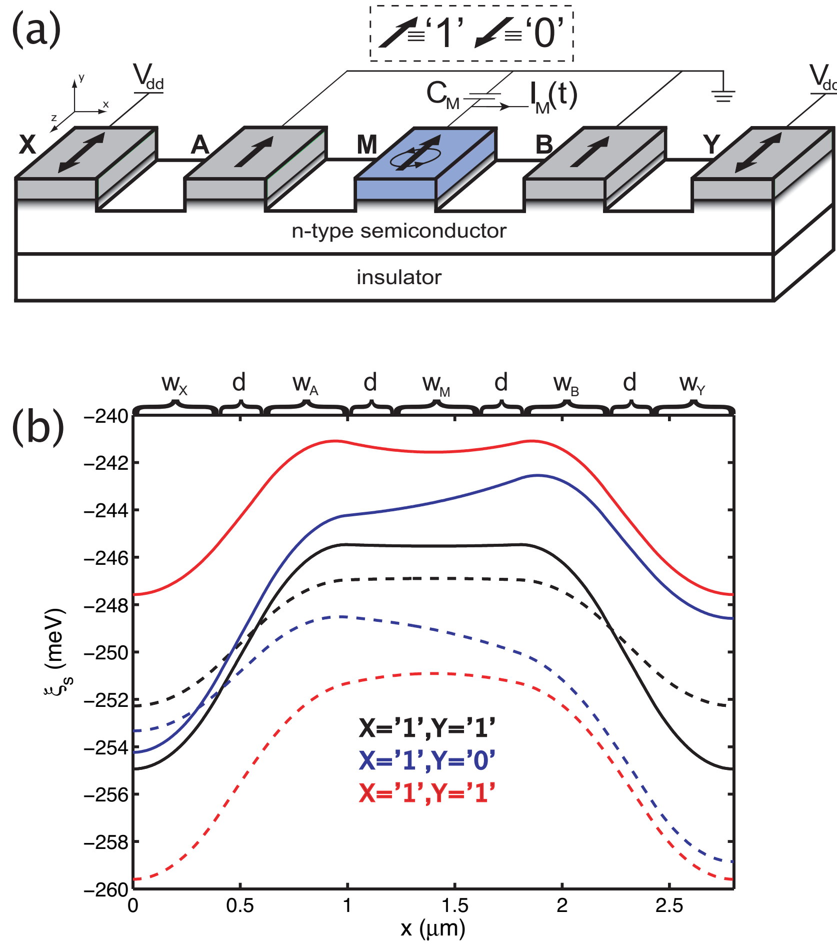

Figure 7.4: (a) A dynamical five-terminal magneto-logic gate. A and B contacts are preset so that the logic operation of the gate is NAND(X,Y). The rotation of the magnetization of the middle (M) contact triggers a current pulse $I_M(t)$, which gives the logic output of the gate. (b) The electrochemical potentials ξ_s in the semiconductor channel (solid lines for s=+, dashed lines for s=−). The applied voltage V_{dd}= 0.5 V, the semiconductor is GaAs with doping n_0=10^{16} cm^{-3}, the barriers have total conductances G=1000 Ω^{-1}cm^{-2} and G_+/G_-=2.

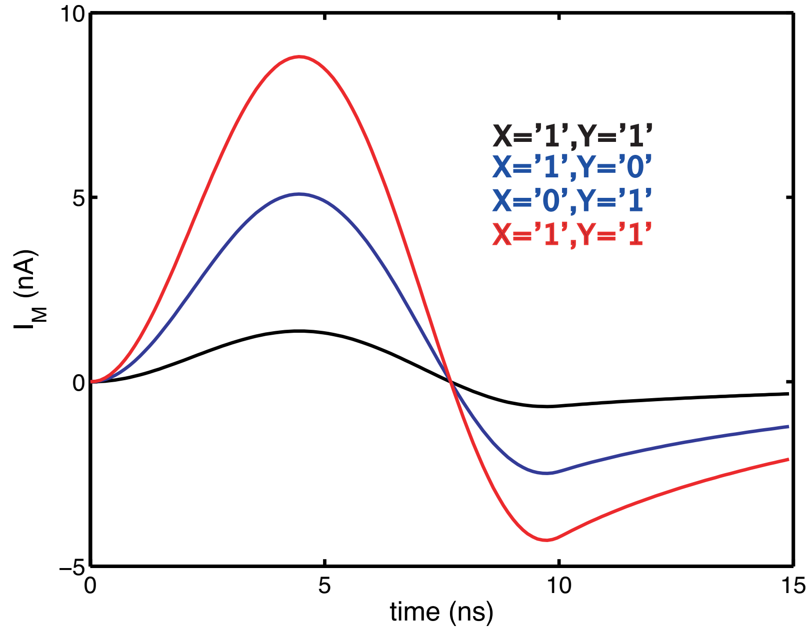

Figure 7.5: The transient currents $I_M(t)$ generated by the 10 ns long 2π rotation of the M magnetization. The capacitance C_M=40 fF, and the other parameters are the same as in Figure 7.4.

7.E Acknowledgements

The text of Chapter 7, in part, is a reprint of the material as it appears in (1) Łukasz Cywiński, Hanan Dery, and L.J. Sham, *Electric readout of magnetization dynamics in a ferromagnet-semiconductor system*, Appl. Phys. Lett. **89**, 042105, © 2006 The American Institute of Physics, where the dissertation author was the primary investigator and author; (2) Hanan Dery, Parin Dalal, Łukasz Cywiński, and L.J. Sham, *Spin based logic in semiconductors for reconfigurable large scale circuits*, Nature **447**, 573 © 2007 Nature Publishing Group, in which the dissertation author was a contributing investigator and author.

8

Electric detection of light polarization

Although silicon is expected to be a very good material for spintronic application due to a very large spin diffusion length, most of the experimental progress in the last decade has occurred in III-V semiconductors. The existence of *optical orientation* [19] in these direct band-gap materials has allowed optical sensing of spin accumulation, and practically all the major experiments in semiconductor spintronics have relied on the optical techniques. The selection rules for optical transitions near the Γ point in a III-V semiconductor are such that the absorption of circularly polarized light leads to photoexcitation of spin-polarized electrons and holes. Conversely, when recombination of spin-polarized carriers occurs, the emitted light is circularly polarized. In the presence of spin-polarized carriers, the absorption (and thus also the refractive index) for two circular polarization becomes different near the band gap, leading to magneto-optical activity. The spin accumulation can be measured by either Kerr reflection or Faraday rotation, which are caused by difference in optical constants for two circular polarizations of light. Seminal experiments in semiconductor spintronics have relied on these phenomena. Long spin relaxation time of electrons ($\sim$100 ns) in n-GaAs at low temperatures was measured by first creating the carriers with polarized light, and

then measuring the time-resolved Faraday rotation [20]. Both spin injection into a semiconductor [22, 23, 71, 36] and spin extraction for the opposite current direction [75, 38] were also seen through magneto-optics. The spin injection experiments are especially important for this chapter, since they have used a spin light emitting diode (spin-LED) setup, in which the polarization of emitted light was caused by *electrical* spin injection into a semiconductor . In the following, we will present a theoretical demonstration how the spin polarization of photoexcited electrons may be determined by electrical means in a system consisting of a semiconductor and two ferromagnetic contacts. Such a system could have a device application as a compact sensor of circular polarization of light. Unlike the currently used polarimeters, it does not require any additional optical elements, such as beam splitters and photoelastic modulators [119].

Before we present the details of our system, let us mention other works on connection between photoexcitation and spin transport. Žutić, Fabian, and Das Sarma have worked out the theory of spin generation by polarized light in p-n junctions made of paramagnetic and/or ferromagnetic semiconductors [120, 62, 66]. Such a spin-photovoltaic effect has been observed in a p-n heterojunction of n-AlGaAs/p-InGaAs [121]. Experiments were also conducted in structures consisting of a single junction of a semiconductor and a ferromagnet, in which the spin-polarized photocurrent was injected from a semiconductor into the ferromagnetic metal [122, 123, 124]. The electrical expression of spin polarization in our two-contact scheme is predicted to be much stronger compared to the difference in photocurrents for two light polarizations in a single contact device.

8.A System requirements for detection of light polarization

The system is shown in Figure 8.1. It consists of a stack of semiconductor layers (a substrate transparent to light with frequency of interest, and a p-n junction

above it) covered with a two ferromagnetic contacts (left (L) and right (R) one), and a metallic gate in between them. The beam of light propagates along the y direction (the growth direction of the semiconductor stack) from the side of the transparent substrate. It becomes absorbed inside the p-n junction, in which the photoexcited electrons and holes are separated. The total thickness of the p-n junction H is comparable to light penetration depth (about a micron for photon energy light slightly above the band gap of a typical semiconductor), so that most of the photons are absorbed. The electrons are swept upwards towards the gate and the electrodes, and they accumulate in n-type channel of thickness h. The effective spin diffusion length is large in the presence of a strong electric field in the junction (see Chapter 2), and we assume that all the photoelectrons are harvested into the n channel without an appreciable loss of their spin polarization. Note that $h \ll H$, so that the density of the spin-polarized electrons in this region is larger than the average density in the whole p-n junction at the moment of excitation. The photocurrent is split through two Schottky barriers with ferromagnets of opposite magnetizations. As in the previous chapters, the barriers are assumed to be very thin due to modification by heavy interfacial doping. The spin selectivity of the metal-semiconductor contacts leads to the dependence of the photocurrent injected into the ferromagnet on the relative orientation of the magnet's magnetization and the spin polarization of the photoelectrons. The two ferromagnets have antiparallel magnetizations, so that for a given circular polarization of light one of them will extract larger photocurrent than the other. The measurement of the two currents leads to an electrical sensing of the polarization of the absorbed light.

The choice of the semiconductor materials is governed by the light wavelength of interest. The transparent substrate should have the band gap larger than the energy of the photons. For the light-absorbing material, the lower and upper bounds for the light frequency are set, respectively, by the threshold of band gap transitions and by the onset of transitions between the split-off valence band and the conduction band. In this energy range a there is strong optical orientation in a III-V semi-

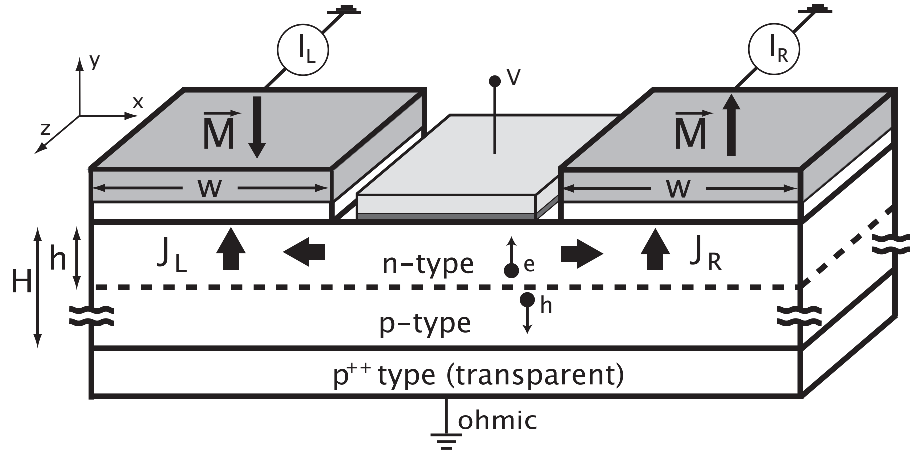

Figure 8.1: A detector of circular polarization of light. The magnetizations of the ferromagnetic contacts are along the z direction perpendicular to the channel plane. The metal gate between the contacts is separated from the channel by a thin insulating barrier. The n-type channel has thickness h, which is smaller than the overall thickness H of the light-absorbing semiconductor (note that the p-type region can have thickness much larger than h).

conductor. In the bulk material, the heavy and light hole bands are degenerate, leading to optical excitation of both types of holes. In order to quantify the spin polarization the beam intensity is decomposed into two generating terms of photo-excited electrons I_+ and I_- which correspond, respectively, to electrons with spin up and spin down. The resulting spin polarization is $\rho \equiv (I_+ - I_-)/(I_+ + I_-) = \pm 1/2$ where the sign depends on the helicity of light [19].

The metallic gate between the terminals is essential to the stability of the system. It screens the in-plane electric field due to excess electrons in the channel by bringing “mirror” charges to the metal surface adjacent to the insulator. The screening is effective for a high aspect ratio between the channel length and the thickness of the insulating barrier separating it from the gate. Consequently, the system is electrostatically stable as in MOSFET devices, and the transport along the axis connecting the ferromagnets may be assumed to be purely diffusive. The gate may have an additional role if the p-n junction of Fig. 8.1 is replaced by an

alternate design with a unipolar doped structure. In this case the gate should be biased so that a charge accumulation (inversion) layer is formed if an n-doped (p-doped) semiconductor is used. In such a case, the gate electric field in the semiconductor replaces the built-in field of the p-n junction in the function of sweeping the electrons into the conduction channel.

The scale of the system is set by the spin diffusion length, about 1 μm in GaAs at room temperature, which limits the travel distance of the spin-polarized electrons in the system. For high detection efficiency, the thickness h of the conduction channel should be much less than the spin diffusion length. The width of the gate (equal to the separation between the two magnetic contacts) must also be less than the diffusion length. According to the discussion of the lateral spin valve in Chapter 5, in order to have a larger spin accumulation beneath the contacts the pillar structure (a "closed" geometry) is used.

8.B Transport of photoexcited spin-polarized carriers

The polarized light beam creates non-equilibrium spin-dependent components of the density Δn_s, s=$\pm$ for spin up or spin down. The spin accumulation is then Δn=$\Delta n_+ - \Delta n_-$. In order to simplify the numerical procedures and extract analytical expressions when possible we consider weak excitations, i.e. Δn_s much smaller than the carrier concentration in the paramagnetic channel at equilibrium, n_0. In this regime the electrochemical potential μ_s is linear in Δn_s. There is no charge neutrality in the channel (where electrons are accumulated), but the electric field is screened by the gate. The time-dependent spin diffusion equations are derived just like in the previous chapters, with the addition of the term corresponding to the optical generation of carriers of spin s denoted by I_s (generated density per unit time). The continuity equation is then given by

$$\frac{\partial \Delta n_s}{\partial t} = \frac{1}{e} \nabla \cdot \mathbf{j}_s - \frac{\Delta n_s - \Delta n_{-s}}{2\tau_{\mathrm{sr}}} + I_s \ . \tag{8.1}$$

As before we average the (electro)chemical potential over the thickness of the channel, and using a very simplified approach to transport in the vertical direction (the electrons swept up from the p region are added to the effective photogeneration term I_s) we obtain

$$\frac{\partial \xi_s}{\partial t} = D\frac{\partial^2 \xi_s}{\partial x^2} + \frac{2DG_s}{h\sigma}(\mu_F - \xi_s) + \frac{2k_BT}{n_0}I_s \ , \tag{8.2}$$

where σ is the conductivity of the n channel, μ_F is the electrochemical potential in the metal (we include the possibility of applying the bias $V_F{=}{-}\mu_F/e$), and the term involving the barrier conductances G_s is present only for parts of the channel covered by ferromagnets. The k_BT factor multiplying the effective photogeneration rate I_s is specific to the case of non-degenerate electrons.

8.C Results and discussion in steady state

We introduce the total electron generation rate I_T and the spin generation rate I_D

$$I_T = I_+ + I_- \qquad\qquad I_D = I_+ - I_- \ , \tag{8.3}$$

and using the notation introduced in Chapter 5 we obtain the steady state solution beneath the contacts for spatially uniform photoexcitation:

$$\begin{aligned} \xi_\pm \ &= \ (1 \pm \lambda)\Big[Ae^{\lambda_s x} + Be^{-\lambda_s x}\Big] + (\lambda \mp 1)\Big[Ce^{\lambda_c x} + Fe^{-\lambda_c x}\Big] \\ &\quad + \mu_{L(R)} + \frac{2k_BTL_{sc}^2}{Dn_0}\frac{(\alpha \mp \beta)(I_T \pm I_D) + 2I_T}{\alpha^2 - \beta^2 + 2\alpha} \ . \end{aligned} \tag{8.4}$$

Between the magnets (beneath the gate) we have the following general form of the solution:

$$\xi_\pm(x) = A_c + B_c x \pm \left(C_c e^{\frac{x}{L_N}} + F_c e^{-\frac{x}{L_N}}\right) - \frac{k_BT}{Dn_0}\left(\frac{I_T}{2}x^2 \mp I_D L_N^2\right) \ . \tag{8.5}$$

The unknown coefficients in the above general solutions ($A, .., F$ and $A_c, ..., F_c$) are determined by conditions of continuity of ξ_s and its first derivative at boundaries between the sections of the channel. In addition, the derivatives of ξ_x (which are

proportional to spin-resolved currents) vanish at the outer boundaries. The total currents flowing into the ferromagnets are:

$$I_L = l_z \sum_{s=\pm} \int_L \frac{G_s^L}{e} \Big[\mu_L - \xi_s(x)\Big] dx$$
$$I_R = Z \sum_{s=\pm} \int_R \frac{G_s^R}{e} \Big[\mu_R - \xi_s(x)\Big] dx \quad (8.6)$$

where l_z denotes the contact length along the z direction and the integrals are performed under the contacts.

The key discriminant for the light polarization direction is the current asymmetry (CA) coefficient defined as $CA \equiv |I_L/I_R - 1|$, where we assume that the currents have been balanced by a small voltage adjustment when the light is unpolarized. We have performed our calculations using the parameters of a GaAs/Fe system at room temperature. The equilibrium electron concentration in the n-type GaAs channel is taken to be $n_0 = 2 \cdot 10^{15}$ cm^{-3} and the effective channel thickness h=100 nm. The barrier conductances are $G_+ = 2G_- = 500\ \Omega^{-1}$cm^{-2} for one contact, and the roles of + and − are switched for the other one. In the channel, the semiconductor diffusion coefficient D is 180 cm^2/sec and the mobility ν=7000 cm^2/V-sec. The semiconductor spin relaxation time is $\tau_{\rm sr}$=80 ps [19], with corresponding spin diffusion length L_N=1.2 μm. Accordingly, the dimensionless quantity α=1. The spin selectivity of the barriers $\gamma_B = \beta/\alpha$ is set to 1/3, according to the spin-injection experiments in Fe/GaAs system [71, 36].

Fig. 8.2 shows the electrochemical potential profiles in the semiconductor channel for excitation level at which the nonequilibrium density is $\delta n_+ + \delta n_- \simeq 0.04 n_0$. This corresponds to light with $\hbar\omega$=1.5 eV (band gap of GaAs) and power of about 1 W/cm^2, when the light is absorbed in a layer of 1 μm thickness and all the photoelectrons are then drawn into the 100 nm thick n-type channel. The separation of the ferromagnets is d=200 nm and the contact widths are $3L_N/8$=450 nm. Using these parameters we obtain a ∼15% difference between the left and right ferromagnet currents. In Figure 8.2a we see from the slopes of the electrochemical potentials that spin-up electrons move towards the right ferromagnet

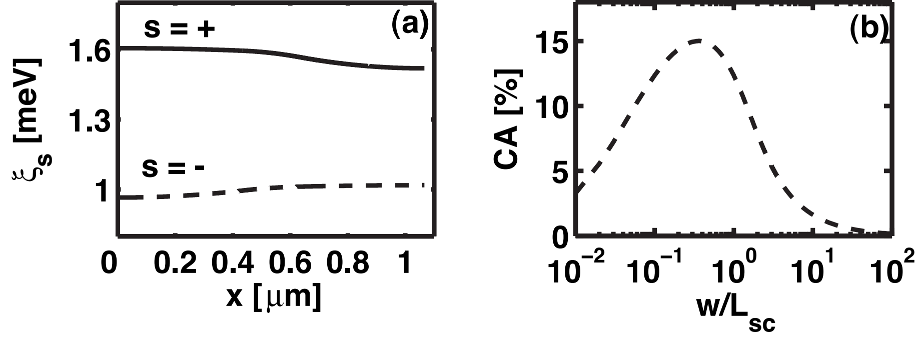

Figure 8.2: (a) The steady state profiles of the electrochemical potentials. The resulting right current (I_R) is 15% higher than the left current (I_L). (b) The corresponding current asymmetry (CA) coefficient as a function of the ferromagnetic contact width w. For all cases, α=1, spin selectivity β/α=1/3, the temperature is 300K, μ_L=μ_R, and the same weak intensity level is used. The sub-gate region is centered and extends over 200 nm.

(and spin-down electrons go in the opposite direction). The right contact extracts preferentially spin-up carriers. Flipping the helicity results in a mirror image of the spatial profile and in switching the roles of ξ_+ and ξ_-. The larger current is extracted from the side with the larger spin depletion. Fig. 8.2b shows the dependence of CA on the ferromagnetic contact width w with an optimal value relative to the spin diffusion length.

Analogously to the discussion from Chapter 5, the existence of a peak in the CA may be understood by the behavior in two extreme cases. For very wide contacts ($w \gg L_N$) most of the current in each contact is due to electrons excited beneath it, and only a small fraction of electrons (the ones excited in the middle section of the system) can “choose” which contact to tunnel into. On the other hand, very small contacts cannot extract the polarized carriers fast enough from the channel. More discussion from the time-dependent point of view follows below in Section 8.D.

Let us mention that although the principle of operation of our proposal is straightforward, it is different than the existing electrical measurement scheme with a single ferromagnetic contact on top of the semiconductor layer [123, 122]. If

the contacts are separated by less than the spin diffusion length than the spin accumulation profile in the channel ”senses“ the antiparallel contacts. Consequently, the difference in the relative current magnitude from each terminal is sharper compared to the difference in photocurrents for different light polarizations in a single contact scheme.

In Figure 8.3a we show the value of CA for the optimal value of the contact width as a function of α for three different values of barrier spin selectivity $|\gamma_B|=|\beta/\alpha$. The fixed parameters are the spin diffusion length L_N=1.2 μm and the ferromagnets' separation $d = L_N/6$. Curves for different values of ρ and γ_B show that the CA is proportional to $\rho\gamma_B$, and that it is independent of the excitation level in the linear regime ($|\Delta n_{\pm}| \ll n_0$). The linear dependence on γ_B comes from the difference between two currents being linear in the spin selectivity. We recall that in lateral spin valves electrons traverse two barriers leading to quadratic dependence of magneto-resistive effect on γ_B (see Eq. 4.3). In the detector scheme the role of one ferromagnetic contact (injector) is replaced by the photexcitation process (ρ), and in a properly designed system the carriers may “select” their preferable extracting terminal.

The optimal contact widths w_{opt} for which these CA values were obtained are plotted in Fig. 8.3c. The lowering of w_{opt} with increasing α can be understood in the following way. For highly conductive contacts, the inhomogeneity of extraction dominates the spatial dependence of spin densities. This means that electrons coming from the gate region will immediately leave the channel when reaching the contact as it would be the path of minimal resistance. Moreover, the photo-excited electrons which are created beneath the far edge of the contact will go into this contact, and never explore the rest of the channel by diffusion. Thus, they do not have the chance to contribute to the current asymmetry. We also note that w_{opt} is weakly dependent on the spin selectivity of the barriers. This observation simplifies the procedure for choosing the contact width as α can be easily obtained from the I-V curve of the junction without need of the knowledge of β, which is

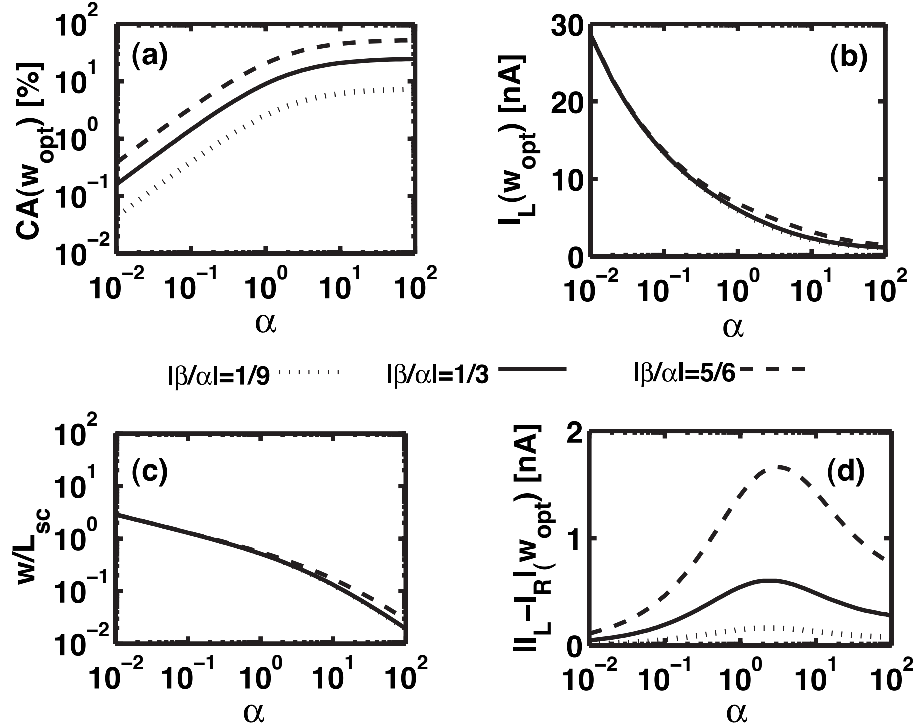

Figure 8.3: (a) current asymmetry versus α for three cases of spin selectivity. (b) and (d) are, respectively, the current from the left contact and the magnitude of the current difference between the left and right contacts. All calculations are done for a structure with an optimal contact widths shown in (c). The spin diffusion length is L_N=1.2 μm and the separation between the ferromagnetic contacts is d=0.2 μm.

harder to measure.

Fig. 8.3b and Fig. 8.3d show, respectively, the current from the left contact and the magnitude of the current difference between the left and right contacts for excitation with left-hand circular polarization. The semiconductor parameters and the light intensity are the same as before (Fig. 8.2). The contact length along the z axis of Fig. 8.1 is 1 μm. Although we are using the same excitation level the current is reduced with α as the optimal contact width becomes smaller (thus diminishing the total volume of the light-absorbing region). For the case of $|\gamma_B|$=5/6 and $\alpha \geq 10$ the CA is about 50%.

8.D The time dependent analysis

The circular polarization of a pulse of light may also be determined by this spintronic system. We start by a numerical simulation of the time-dependent diffusion (Eq. (8.2)). The initial condition corresponds to a quiescent medium: $\Delta n_s(x, y, t = 0)$=0. Figure 8.4 shows the currents through the two ferromagnetic contacts as a result of excitation by two consecutive Gaussian-shaped pulses of opposite polarization. The width of the pulses is 100 ps. In Figure 8.4a the pulse repetition rate is 0.5 GHz, with all the parameters as in Fig. 8.3, and the average light power of 5 W/cm^2 (calculated using the same assumptions as in the steady-state case). In Fig. 8.4b we use barrier conductances ten times larger, and 1 GHz repetition rate with average light power of 10 W/cm^2. In both cases, the peak power is 40 W/cm^2. The contact widths have been optimized in both cases according to the steady state analysis above. Accordingly, in the higher conductance barriers case (lower panel) the contact widths are equal to $L_N/6$. The contact length along the z axis in Fig. 8.1 is 1 μm.

The electrical noise is dominated by thermal fluctuations, as the shot noise is irrelevant at predicted current levels. The pulses of 100 ps amount to a bandwidth of 10 GHz so that the Johnson-Nyquist current fluctuations in the highly resistive contacts are of the order of 10 nA. This value is comparable with the difference between I_R and I_L hence sets an lower bound for the pulse widths. In order to improve the performance one should either improve the CA as discussed previously, use stronger excitations in order to improve the signal to noise ratio, or use longer light pulses to decrease the noise bandwidth.

There is ∼100 ps (∼20 ps) lag between the peak of the light pulse (not shown) and the peak of the current in Figure 8.4a(b). This lag is caused by a finite time which is needed for electrons to leave the channel by tunneling through the barriers. A simple estimate of the time associated with the flush-out of the photoexcited carriers is obtained in the following way. We set up equations for time-dependence

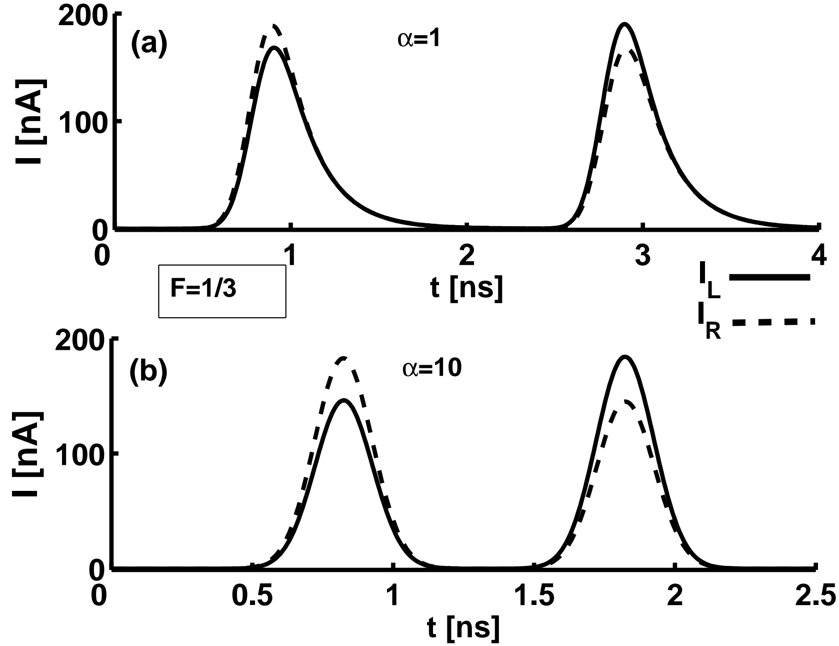

Figure 8.4: Time-resolved current response to light pulses alternating in polarization. The solid (dashed) line is from the left (right) magnetic contact. (a) Low conductance barriers with the light pulse rate is 0.5 GHz and the two pulses centered at 0.8 ns and 2.8 ns. (b) Barriers of higher conductance with the repetition rate is 1 GHz with two pulses centered at 0.8 ns and 1.8 ns.

of spin densities after an instantaneous excitation, neglecting the diffusion inside the channel and assuming a spatially uniform distribution. Integrating out the x and y coordinates in the continuity equation (Eq. (8.1)) yields,

$$\frac{\partial \Delta n_s}{\partial t} = \frac{1}{e}\frac{w}{(2w+d)h}(j_L + j_R) - \frac{\Delta n_s - \Delta n_{-s}}{2\tau_{\mathrm{sr}}} \ , \tag{8.7}$$

where j_L and j_R are the average current densities at the interfaces. In order to express the currents in terms of the non-equilibrium densities, we use of the boundary conditions relating the electrochemical potentials to the tunneling currents and employ the relation between the chemical potential and the non-equilibrium density in the linear regime. We arrive at the following equations for the total photoexcited density δn=$\Delta n_+ + \Delta n_-$ and for the photoexcited spin polarization

Δn=$\Delta n_+ - \Delta n_-$:

$$\frac{\partial}{\partial t}\delta n = -\frac{\delta n}{\tau_f}\ , \qquad \frac{\partial}{\partial t}\Delta n = -(\frac{1}{\tau_f} + \frac{1}{\tau_{\rm sr}})\Delta n\,, \tag{8.8}$$

in which the carriers "flush-out" time τ_f is given by

$$\tau_f = \frac{(2w+d)h}{w}\frac{\sigma}{2D(G_+ + G_-)} = \frac{2w+d}{w}\frac{\tau_{\rm sr}}{\alpha}\ . \tag{8.9}$$

The total current out of the system is proportional to δn, so it decays exponentially with time-constant τ_f. This time constant is spin independent and depends only on the total resistances of the FM/semiconductor barriers and of the semiconductor layer. The difference $I_L - I_R$ is proportional to the spin accumulation Δn, and decays on a time-scale of $\tau_{\rm CA}^{-1}$=$\tau_{\rm sr}^{-1} + \tau_f^{-1}$. These results agree very well with the numerical calculations using the full time-dependent diffusion equation. We can see that the time-scale after which an excited system returns to its equilibrium state is given by τ_f, which limits the repetition rate of light pulses. It is also favorable to have τ_f<$\tau_{\rm sr}$, so that the photoelectrons leave the channel before losing their spin polarization; the time-scale on which the CA effect disappears is bounded from above by the spin relaxation time $\tau_{\rm sr}$. However, too short τ_f is also undesirable. The explanation of this leads to an alternative understanding of the optimal contact size discussed for the steady state case.

In order to analyze the effect of short τ_f, we have to relax the simplifying approximation of uniformity of Δn_s, and we reintroduce the diffusion processes. A typical time for the density perturbation to propagate through distance l is $\tau_{\rm diff}$~l^2/D. If the carriers tunnel into each of the contacts faster than they diffuse between them, both contacts do not "sense" each other. The time-integrated CA will vanish in such a case, as electrons leave the channel through the nearer contact, and the average I_L and I_R currents will be the same. The requirement for τ_f to be smaller than $\tau_{\rm sr}$ but larger than $\tau_{\rm diff}$ leads to inequalities:

$$\frac{l^2}{L_N^2}\alpha < \frac{2w+d}{w} < \alpha\ , \tag{8.10}$$

where $l = w + d$ is a typical distance on which an electron has to diffuse to get from under one contact to another. From the above inequalities, we can qualitatively recover the results of Fig. 8.3a and Fig. 8.3c. For $\alpha < 2$, the spin relaxation is faster than the flush-out time and the right hand side of the inequality is violated. Consequently, further reduction of α results in weaker CA effect in agreement with the steady state behavior shown in Fig. 8.3a. In the limit of large α, it is possible to satisfy the left hand side of the inequality by shrinking the contact width compared with the gate width: $w < d$. The diffusion process is faster than the flushing time if w is smaller than $L_N^2/(d\alpha)$. The spin flip processes are of no importance on these time scales as long as $L_N > d$ so that the right part of the inequality is fulfilled. The CA is maximal in this regime, and $w_{\text{opt}} \propto 1/\alpha$, as one can see in Fig. 8.3d. Satisfying both conditions of the inequality results in high CA effect which in steady state corresponds to the plateau of Fig. 8.3a. The time domain analysis clarifies the relatively weak dependence of w_{opt} on the spin selectivity. This is seen from the fact that the flush-out time, the diffusion time, and the spin relaxation time involve only α, L_N, and the length scales of the structure in hand.

8.E Acknowledgements

The text of Chapter 8, in part, is a reprint of the material as it appears in Hanan Dery, Łukasz Cywiński, and L.J. Sham, *Spintronics for electrical measurement of light polarization*, J. Appl. Phys. **100**, 063713, © 2006 The American Institute of Physics. The dissertation author was a co-investigator and co-author of this article.

9

Ultrafast light-induced demagnetization in transition metals

When an itinerant ferromagnet is excited by a short (∼100 fs) pulse of light, its magnetization drops by a sizable fraction in less than a picosecond. The first observation [13] of such an effect in nickel was a surprise, as it had been believed that the time-scale of magnetization dynamics is given by a spin-lattice (phonon-magnon scattering) relaxation time, which is of the order of tens of picoseconds [125, 126, 127]. During last ten years, similar ultrafast effects have been observed in transition metals such as Ni [13, 128, 129, 130, 131, 132], Fe [133, 134], Co [135, 136] and $CoPt_3$ [137, 138, 139]. In most of these works time-resolved magneto-optics was employed, but the ultrafast dynamics of magnetization is confirmed by other techniques, such as second harmonic generation [128], spin-resolved photoemission [130, 136], and THz generation caused by time-dependence of macroscopic magnetization [131, 134].

In Section 9.A we review the experimental results in metals and existing theories of the ultrafast magnetization dynamics. There we also present our understanding of the phenomenology of the process. We work within a "minimal"

model of an itinerant ferromagnet, in which the relevant excitations are single-particle excitations (SPEs), which can be envisioned within the band picture, and the collective modes (spin waves). In section 9.B we describe the influence of laser pulse excitation on SPEs, and we analyze the role of spin-flip scattering of SPEs (Elliott-Yafet spin relaxation) on in light-induced demagnetization demagnetization. In section 9.C we discuss the coupling between the SPEs and the spin waves.

A theory of ultrafast light-induced demagnetization in the sp-d model (which is not a reliable "minimal" model for transition metals) is presented in Chapter 10.

9.A Previous work and phenomenology of the ultrafast demagnetization

With the exception of the THz emission, all the experimental methods probe the magnetization dynamics indirectly, by coupling to the electronic states of the material [140]. Problems with interpretation of obtained signals are specific to each experimental method. Most attention has been paid to the artifacts in the magneto-optical (MO) response caused by carrier excitation effects, which have been termed "dichroic bleaching" effects. They have been shown to contribute significantly to the time-resolved Kerr response for degenerate pump and probe measurements in Ni [129]. A theoretical calculation [141] of magneto-optical response of non-equilibrium electrons in Ni confirmed that the Kerr response at very short time-scale does not correspond to the sample magnetization. On the other hand, the results of Kerr and Faraday measurements for different probe wavelengths in $CoPt_3$ did not any apparent dichroic bleaching, suggesting that the significance of these effects varies between different materials. It seems that in order to gauge the correlation between the magneto-optical signal and magnetization dynamics during the first couple hundreds of femtoseconds, a careful calculation of optical

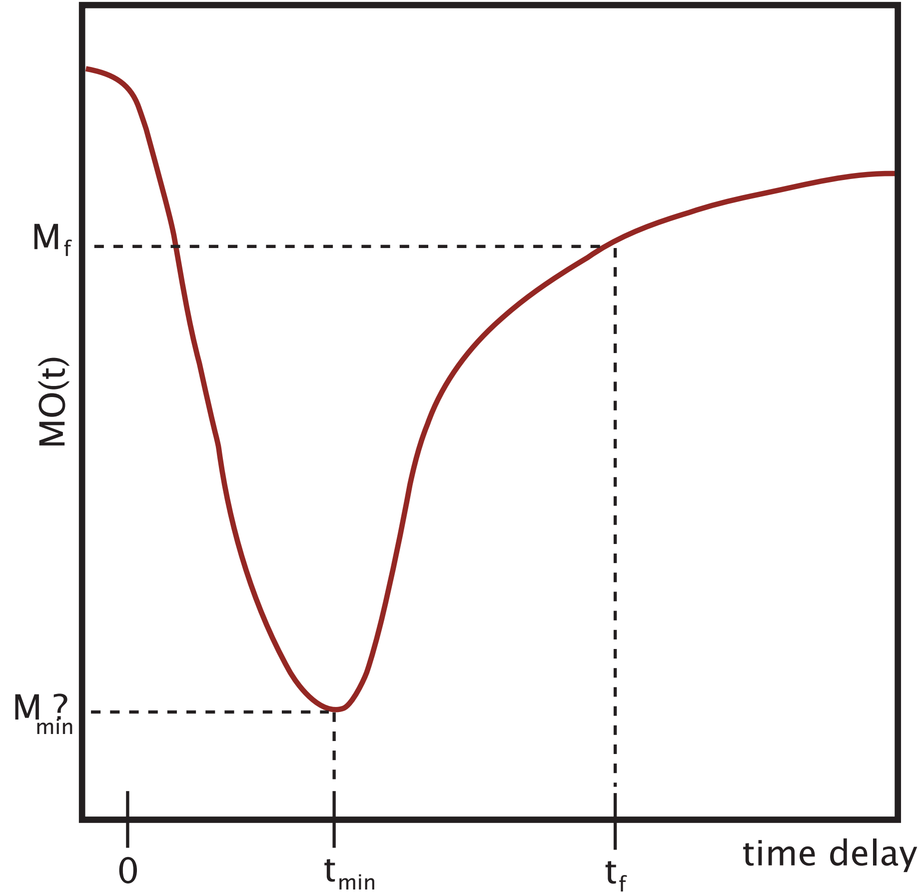

Figure 9.1: Typical magneto-optical (MO) response of a transition metal ferromagnet excited by a strong pump pulse at t=0. The values of $t_{\rm min}$ are between 300 fs and 2 ps in different experiments. It is unclear if the MO signal at $t_{\rm min}$ is proportional to the macroscopic magnetization $M_{\rm min}$. On the other hand, for times larger than $t_{\rm f}\sim$1 ps the MO signal corresponds to real magnetization, the dynamics of which for $t>t_{\rm f}$ is due to heat diffusion, spin-lattice relaxation, and slow precession about a thermally modified easy axis (on a time-scale of hundreds of picoseconds). Typical values of $M_{\rm f}$ seen in experiments correspond to a drop of magnetization of at least a couple percent.

transitions and carrier dynamics is necessary.

In the magneto-optical experiments, the MO signal is seen to decrease immediately after the light pulse and reaches a minimum $t_{\rm min}$, which is between 300 fs [129] and 2 ps [13] (see Figure 9.1). Then the MO signal recovers partially at slightly later time $t_{\rm f}\sim$1 ps, and the subsequent dynamics is much slower (spin-lattice relax-

ation, heat diffusion, and magnetization precession triggered by heating-induced change in anisotropy). According to the preceding discussion, it is unclear to what extent the minimum of MO signal at $t_{\min}$ is a dichroic bleaching artifact (especially for $t_{\min} \ll 1$ ps), so it is hard to say how much exactly the magnetization decreases during this time. On the other hand, it is easy to check that after t_{f} the MO signal agrees with the expected value of the equilibrium $M_{\mathrm{f}}=M(T_{\mathrm{f}})=M_0\sqrt{1-T_{\mathrm{f}}/T_{\mathrm{c}}}$ for the final temperature of the metal T_{f} (T_{c} is the critical temperature). This result follows from calculating the energy injected into the sample (from pulse fluence, the absorption coefficient and sample thickness) and using the total specific heat of a metal (e.g. $C_{\mathrm{Ni}}=4\cdot 10^6$ J/Km^3 for nickel) to get the final temperature T_{f}. $M_{\mathrm{f}}(T_{\mathrm{f}})$ calculated in this way agrees quite well with the demagnetization at $\sim$1 ps delay seen in Refs. [13, 129, 132]. Furthermore, in Ref. [129] it was shown, that for $t \geq 1$ ps the MO signal could be well fitted by calculated changes of the equilibrium magnetization $M(T)$ due to heat diffusion. As we discuss below, the electrons (SPE) equilibrate with the lattice on the time-scale of energy relaxation time $\tau_{\mathrm{E}} \simeq 0.5$ ps. The magnetization achieves equilibrium with both the carriers and the lattice slightly later, about a picosecond after the laser pulse. The mechanism of this spin-related equilibration process is our main subject here. Since the experimental results at shortest time-scales are often controversial, we want to de-emphasise the question of what is the ultimate shortest time of magnetization dynamics, and concentrate on the physical mechanism of the heating of the magnetization on a time scale of a picosecond.

Initially, the apparent ultrafast decrease of magnetization seen in MO experiments was interpreted as a rise of "spin temperature", and fitted using a phenomenological three-temperature model [13, 142]. In this approach the system is divided into three reservoirs: carriers, lattice and spins. Excitation by light amounts to injecting energy into the carrier system. Just after the light pule and carrier thermalization, the carriers can have a very high electronic temperature T_e (possibly higher than the critical temperature). Each reservoir is described by

its temperature, and phenomenological equations are written down for heat flow between each pair of reservoirs:

$$C_e(T_e)\frac{dT_e}{dt} = -G_{el}(T_e - T_l) - G_{es}(T_e - T_s) + P(t) \ , \quad (9.1)$$

$$C_s(T_s)\frac{dT_s}{dt} = -G_{sl}(T_s - T_l) - G_{es}(T_s - T_e) \quad (9.2)$$

$$C_l(T_l)\frac{dT_l}{dt} = -G_{el}(T_l - T_e) - G_{sl}(T_l - T_s) \ . \quad (9.3)$$

The subscripts e,s, and l denote the electronic, spin and the lattice reservoirs, respectively. The corresponding heat capacities are denoted by C_a and the coupling constants are G_{ab}. The influence of the optical pulse on the electronic system is described by the absorbed power $P(t)$.

Physical underpinnings and time-scales of two of the G_{ab} couplings are known. For carrier-lattice (electron-phonon) interaction see, e.g., Refs. [143, 144], and for spin-lattice interactions see Ref. [127]. A new ingredient, a direct carrier-spin coupling G_{es} has to be postulated in order to explain the ultrafast demagnetization. Apart from the lack of detailed microscopic understanding of such carrier-spin coupling, there are two major deficiencies of the three-temperature model. The first is that treating carriers and spins as separate entities is a controversial starting point for the transition-metal itinerant ferromagnets. If such an approach is possible, the nature of an effective separation into subsystems should be elucidated. The second shortcoming is the fact that that only the energy transfer between reservoirs is considered. As the key phenomenon to be described is the change of magnetization, a correct physical description should involve the mechanism according to which the angular momentum (spin and orbital) is exchanged between the subsystems [140, 145].

Apart from a phenomenological three-temperature model, a microscopic theory based on Hubbard model with orbital degeneracy embedded into a crystal field has also been proposed [146, 142]. In this approach the cooperative effect of a coherent laser field and the spin-orbit coupling is calculated, resulting in predictions for magnetization dynamics during the ~100 fs time of the light pulse.

Time-resolved photoemission experiments [130], in which the spin splitting of d bands is monitored, show that a large part of the reduction in exchange splitting occurs well after the laser pulse. This shows that the possible laser field assisted process is certainly accompanied by further demagnetization due to dynamics of the system itself, without the assistance of the laser field. A similar approach to laser-controlled spin dynamics in antiferromagnets [147] looks more promising in light of recent experimental developments in these materials [148]. Here we are going to treat the optical excitation as a source of incoherent ultrafast heating of the electronic population, and we will concentrate on the magnetization dynamics after the carrier thermalization.

Recently, Koopmans et. al. (Refs. [43, 145]) have proposed another theoretical model of demagnetization in itinerant transition-metal ferromagnets. In these works the carriers (assumed spinless in Ref. [43]) have been assumed to interact with a separate spin system (an ensemble of two-level systems). The nature of this separation into carrier and "pure spin" degrees of freedom is unclear. A process of Elliott-Yafet [149, 150] spin relaxation has been proposed to be the driving force of the demagnetization process, and the scattering of carriers with impurities and phonons has been considered. Furthermore, an idea that there is a connection between the ultrafast demagnetization and Gilbert damping [1, 151] of slow (typical period $\sim$100 ps) magnetization precession has been put forth in Ref. [43]. In Section 9.B we will critically assess the relevance of the Elliott-Yafet spin relaxation for demagnetization process. In Section 9.C we will introduce another mechanism of demangetization, based on SPE-magnon interaction, and we will re-examine the idea of the connection between ultrafast dynamics and Gilbert damping in this context.

A "minimal" model of an itinerant ferromagnet which we study takes into account two types of low-energy excitation of the electronic system. The first are the single-particle excitations (SPEs), or electron-hole excitations. In such an excitation a state occupied in the equilibrium distribution is emptied (a hole is created),

and another electron is added in a different state. If the net carrier spin is changed, this is a Stoner excitation [152]. These SPEs are directly created by absorption of the laser pulse. For them we can talk about Elliott-Yafet spin relaxation, and the electronic temperature T_e describes their distribution after the thermalization. The second type of excitations are collective spin excitations: spin waves (magnons). They can be envisioned as linear combinations of a large number of single-particle Stoner excitations [153]. We can assign to them a "spin" temperature T_{sw}, which characterizes the distribution of bosonic spin-wave excitations. The spin waves are coupled to the SPEs [152, 154], and we are going to argue that fast heating of the quasiparticles leads to a generation of spin waves. In our opinion, this is a natural explanation of ultrafast demagnetization in transition metals, which also provides a link between the demagnetization and Gilbert damping of slow magnetization precession.

9.B Spin relaxation of quasiparticles - nonequilibrium Stoner model

In the process of optical absorption only the single-particle excitations are directly affected. A natural setting for the discussion of their dynamics is a band (Stoner) model of an itinerant ferromagnet [152]. The deficiencies of this model as the overall description of itinerant ferromagnetism are well known: it predicts much too large Curie temperatures [155] and gives a wrong temperature dependence of magnetization at low temperatures (a correct description requires the spin waves, see e.g. [51]). Clearly, the Stoner excitations are not the most important kinds of magnetization fluctuations (and including the spin waves is not the whole story either, see e.g. Ref. [156]).

9.B.1 Photoexcitation and its effect on single-particle excitations.

Before the excitation, the system is in equlibrium at temperature T_0, which we take as room temperature (as in most of the experiments). The bands are spin-split, and for simplicity we assume the spin-projected densities of states D_s (per atom) to be rigidly split by exchange energy Δ. The numbers of electrons with majority (s=↑) and minority (s=↓) spin per atom are denoted by N_s. The splitting is proportional to the magnetization: $\Delta = UM$, with $M = N_\uparrow - N_\downarrow$ in the units of μ_B, and the on-site (Hubbard) Coulomb energy U.

A laser pulse creates a nonequilibrium distribution of electrons and holes for energies E in the range $|E - E_\mathrm{F}| < \hbar\omega$, with typical photon energy $\hbar\omega$=1.5 eV. The subsequent dynamics of the quasiparticles has been a subject of many studies, see e.g. Refs. [157, 158]. The quasiparticles excited far away from E_F scatter very quickly by Coulomb interaction with the rest of the Fermi sea, and their achieves the Fermi-Dirac form with an elevated electronic temperature T_ei after the thermalization time τ_th. This time is of the order of 100 fs in metals, e.g. τ_th=80 fs in Ni [159]. It scales with the carrier temperature after thermalization as T_{ei}^{-2}, so that the thermalization becomes faster with increasing excitation level. As the carrier distribution approaches the thermal form, the energy transfer into the lattice (carrier-phonon scattering) becomes more effective [157]. When the thermalization is fast enough, we can assume that there is practically no transfer of energy into the lattice during τ_th, and energy relaxation through phonon emission follows after the thermalization. The energy relaxation occurs on time-scale τ_E. Typical energy relaxation time is close to a picosecond, with the latest value reported for Ni being $\tau_\mathrm{E} \approx 0.3 - 0.4$ ps [159].

For fluence $F \simeq 1$ mJ/cm^2 and 10 nm thick Ni film a 4% drop of magnetization after 1 ps was observed [129]. Using the optical constants of Ni (or the fraction of photons absorbed f_{abs} given in Ref. [129]) we get that the pump pulse injects the energy of 0.01 eV/atom into the electronic system. In another experiment [132], light pulse with fluence F=5 mJ/cm^2 impinging on 30 nm thick film led to ∼15 %

demagnetization, and we calculate the injected energy to be ∼0.04 eV/atom. Let us note, that the demagnetization ΔM in Ni for 1 ps time delay has been shown [132] to be roughly linear with pump fluence for F<20 mJ/cm^2. The results of Ref. [129] fit roughly the same linear relationship, after correcting for different sample thickness. If we write the final equilibrium temperature of the sample as $T_{\rm f}{=}T_0+\Delta T_{\rm f}$ with T_0 being the room temperature, then for injected energy of 0.01 (0.04) eV/atom we get $\Delta T_{\rm f}$ equal to about 40 (150) K. As we have noted before, the magnetization at ∼1 ps time delay agress with the equlibrium value of $M(T_{\rm f})$.

In order to convert the optically injected energy into the changes of electronic temperature $\Delta T_e{=}T_{ei}-T_0$ we need to know the electronic specific heat $c_e{=}\gamma T_e$ for T_e around room temperature. A low temperature value of the γ coefficient in Ni is 10^3 J/K^{2}m^3, but as the total density of states at the Fermi level changes significantly with temperature (due to the temperature dependence of the exchange splitting), so does the γ coefficient. A room temperature value of $\gamma{=}3.8\cdot10^3$ J/K^{2}m^3 was measured in Ni [160], and a value of $\gamma{=}6\cdot10^3$ J/K^{2}m^3 was calculated [142]. Using these two values of γ as lower and upper bounds, we can derive the range of changes of electron temperature corresponding to a given energy change using the total energy of electrons $E(T){=}E(T{=}0)+\frac{1}{2}\gamma T_{ei}^2$. For excitation corresponding to ∼4% demagnetization we get an increase of the electronic temperature ΔT_e between 70 and 110 K, whereas for excitation corresponding to ∼15% demagnetization we get ΔT_e between 260 and 330 K.

In the following, we will concentrate on the low-fluence case when $\Delta T_e{\leq}100$ K, for which the demagnetization of a few percent is seen. We will assume that the numbers of excited electrons of both spins is the same. In nickel this is supported by calculation of band-by-band decomposed optical absorption [141]. We will also neglect the spin relaxation of quasiparticles during the fast thermalization. Then, immediately after the end of the pump pulse (the pulse time is usually comparable to the thermalization time) we have an excited system of quasiparticles described by temperature $T_{\rm ei}$, but $N_\uparrow$ and $N_\downarrow$ (and thus the magnetization) are the same as

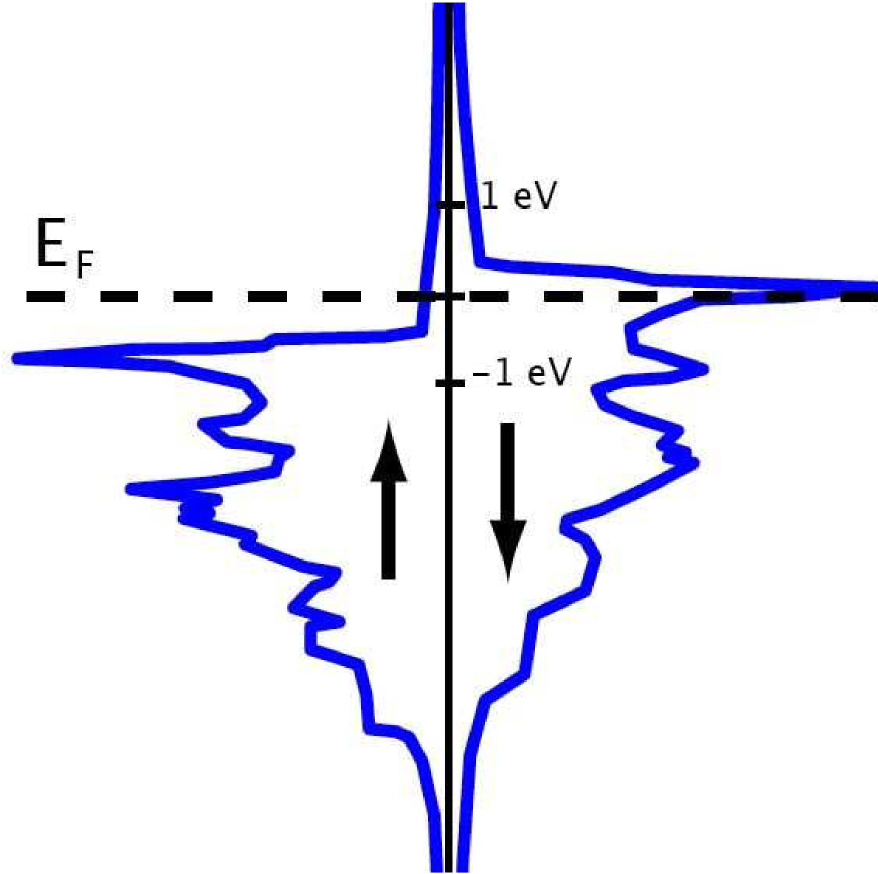

Figure 9.2: Spin-projected density of states in Ni from (from Ref. [93]). Majority (minority) spin is denoted by $\uparrow(\downarrow)$. The zero of energy is at the Fermi level E_{F}.

before the excitation.

In Ref. [43] the elevated electronic temperature T_e was assumed to be the sole cause of spin-flip scattering. As we discuss below, for the Elliott-Yafet spin relaxation to occur, is not enough to specify the temperature of SPEs. The quasiparticle system has to be out of its *internal* spin equilibrium, i.e., the chemical potentials μ_s for minority and majority spins have to be unequal. It has to be stressed, that for SPE spin scattering it is the chemical potential imbalance $\Delta\mu{=}\mu_\uparrow - \mu_\downarrow$, not the elevated T_e itself, which is the driving force for spin-flip scattering of carriers leading to a net change of magnetization.

For the simple model of excitation described above, we derive an estimate of $\Delta\mu$ using the Sommerfeld expansion [51, 152]. To the lowest order in temperatures,

the spin-splitting of chemical potentials is given by

$$\Delta\mu = \frac{\pi^2}{6}k_B^2(T_{ei}^2 - T_0^2)\Big[\frac{D'_\downarrow(\mu_0)}{D_\downarrow(\mu_0)} - \frac{D'_\uparrow(\mu_0)}{D_\uparrow(\mu_0)}\Big] \,, \tag{9.4}$$

where μ_0 is the common chemical potential before the excitation. Although from the above expression it might seem that any sign of $\Delta\mu$ is allowed, the negative sign would imply that the equilibrium magnetization would increase with rising temperature, which is very unlikely (see Ref. [152], chapter 12). Let us remark, that the requirement of the thermodynamic stability of the finite magnetization in the Stoner model puts certain (often complicated) restrictions on the allowed form of the spin-split densities of states [155, 161, 162], and $\Delta\mu>0$ can be derived from them in the limit of small magnetization.

Using the calculated densities of states D_s for Ni [163] we derive an estimate for $\Delta\mu$ corresponding to ΔT_e=100 K. Taking into account the reduced spin splitting at room temperature by rigid shifting of D_s, we estimate $\Delta\mu<10$ meV.

9.B.2 Spin relaxation due to impurity and phonon scattering

Now we consider the spin-dependent scattering of the excited SPEs. We take into account only the processes involving the SPEs and the lattice: electron-impurity and electron-phonon scattering. These correspond to Elliot-Yafet relaxation of the electronic spin into the lattice. The scattering w of SPEs with the spin waves, in which the spin is transferred from one kind of electronic excitation to the other, will be considered in the next section. The Boltzmann-like spin-flip rates for both impurity and electron-phonon scattering are proportional to $\Delta\mu$, and they depend weakly on T_e, the temperature of SPEs. For electron-impurity scattering, as long as $k_\mathrm{B}T_e$ and $\Delta\mu$ are smaller than the energy scale on which the densities of states $D_s(E)$ change appreciably, we get (see Chapter 2)

$$\frac{\partial N_\uparrow}{\partial t} = -\frac{\delta N_\uparrow}{\tau_{\uparrow\downarrow}} + \frac{\delta N_\downarrow}{\tau_{\downarrow\uparrow}} = -\frac{\partial N_\downarrow}{\partial t} \,, \tag{9.5}$$

in which δN_s are the nonequilibrium parts of the density of carriers with spin s. The spin flip scattering times $\tau_{ss'}$ are T_e-independent under the conditions given

above, and they are connected one to another by the following relation (see Chapter 2 or Ref. [59]):

$$\frac{\tau_{\uparrow\downarrow}}{D_{\uparrow}(\mu_0)} = \frac{\tau_{\downarrow\uparrow}}{D_{\downarrow}(\mu_0)} \ . \tag{9.6}$$

For the spin relaxation due to phonon scattering we follow the standard treatment of electron-phonon scattering (see Ref. [143], chapter 8.3) and modify it to include the spin-flip processes. We generalize the Eliashberg-MacMillan function $\alpha^2 F$ [143, 144] used in description of electron-phonon scattering, to the case of spin-flip scattering in a ferromagnet (the spin-flip Eliashberg function for a paramagnet was introduced in Ref. [164]). The Eliashberg function corresponding to spin flip from spin s to s' is defined as

$$\alpha^2 F_{ss'}(\epsilon, \epsilon', \Omega) = \frac{1}{\hbar D_s(\epsilon)} \sum_{\mathbf{k},\mathbf{k}'} |M^{ss'}_{\mathbf{k}\mathbf{k}'}|^2 \delta(\epsilon - \epsilon_{\mathbf{k}s})\, \delta(\epsilon' - \epsilon_{\mathbf{k}'s'})\, \delta(\Omega - \omega_{\mathbf{k}\mathbf{k}'}) \tag{9.7}$$

where $M^{ss'}_{\mathbf{k}\mathbf{k}'}$ is the matrix element for spin-flip scattering due to electron-phonon interaction, and $\omega_{\mathbf{k}\mathbf{k}'}$ is the frequency of the phonon with the wave vector $\mathbf{k} - \mathbf{k}'$. The index $\mathbf{k}$ includes the band index in the case of multiple bands. Below we use a standard approximation of taking both ϵ and ϵ' equal to the Fermi energy, which here we take as μ_0, the chemical potential before the excitation. After some manipulation (along the lines of Ref. [143], chapter 8.3) we get for the spin-flip scattering:

$$\begin{aligned} \frac{\partial N_{\uparrow}}{\partial t} &= -2\pi D_{\uparrow}(\mu_0) \int d\Omega \alpha^2 F_{\uparrow\downarrow}(\Omega) \Big[2n(T_l, \Omega)\Delta\mu - (\hbar\Omega + \Delta\mu) n(T_e, \hbar\Omega + \Delta\mu) \\ &\quad + (\hbar\Omega - \Delta\mu) n(T_e, \hbar\Omega - \Delta\mu) \Big] \ , & (9.8) \\ &\simeq -2\pi D_{\uparrow}(\mu_0) \int d\Omega \alpha^2 F_{\uparrow\downarrow}(\Omega) \Big[\frac{2k_{\mathrm{B}}T_l}{\hbar\Omega} + 1 - \frac{\hbar\Omega}{3k_{\mathrm{B}}T_e} \Big] \Delta\mu \ , & (9.9) \end{aligned}$$

where $n(T, E)$ is the Bose-Einstein distribution at temperature T and energy E, and we have used the high temperature approximation in the second expression (to the lowest order in $\hbar\Omega / k_{\mathrm{B}} T_e$). In the equation for $\partial N_{\downarrow}/\partial t$ we exchange the spin indices and change the sign of $\Delta\mu$. Note that the product $D_s \alpha^2 F_{s,-s}$ is the same for both directions of spin s (see Eq. (9.7)).

Now let us define the nonequlibrium part of the magnetization, δM:

$$\delta M \equiv \delta N_\uparrow - \delta N_\downarrow = 2\delta N_\uparrow = \frac{2\Delta\mu}{D_\uparrow^{-1}(\mu_0) + D_\downarrow^{-1}(\mu_0)} \ . \tag{9.10}$$

This δM is a difference between the actual magnetization M and its equilibrium value at temperature T_e *while keeping the spin splitting of the bands* Δ *constant.* δM is then a function of both T_e, and the value of M itself:

$$\delta M(M, T_e) = M - M_0(\Delta = UM, T_e) \ , \tag{9.11}$$

where M_0 is obtained by filling the bands spin-split by Δ with carriers of temperature T_e up to a common chemical potential.

Both the impurity scattering and the phonon scattering lead to the same form of the equation for δM. which we write as

$$\frac{\partial}{\partial t}\delta M = -\frac{\delta M}{\tau_{\rm sr}} \ , \tag{9.12}$$

where $\tau_{\rm sr}$ is the spin relaxation time, and the same equation holds for $\Delta\mu$. We have already encountered this equation in our analysis of spin diffusion in Chapter 2. The derivation of microscopic formulas shows that as long as $k_{\rm B}T_e$ and $\Delta\mu$ are smaller than the energy scale on which D_s change appreciably, the spin relaxation time $\tau_{\rm sr}$ is a constant. Thus, the same $\tau_{\rm sr}$ applies to equations for $\Delta\mu$ of the order of μeV created by spin injection, and to equations for $\Delta\mu$ of the order of meV for spin relaxation of SPE excited by light.

In the next section we estimate $\tau_{\rm sr}$ from the transport experiments, from which the spin diffusion length in a ferromagnet can be inferred. Actually, the value derived from the spin diffusion length is a lower bound on $\tau_{\rm sr}$ above, since we exclude the scattering with spin waves from $\tau_{\rm sr}$ defined in this section. However, before we give our estimate of $\tau_{\rm sr}$, let us analyze in more detail how the magnetization dynamics follows from Eq. (9.12).

The $\partial/\partial t$ derivative in Eq. (9.12) accounts for the change in δM due to spin flip scattering, and so the equation for the dynamics of the magnetization M reads

$$\frac{dM(t)}{dt} = -\frac{M(t) - M_0(M(t), T_e(t))}{\tau_{\rm sr}} \ , \tag{9.13}$$

where $M_0(M, T_e)$ is the magnetization calculated for bands spin-split by $\Delta(t) = UM(t)$ (in the rigid-shift approximation) and carrier temperature T_e. The time dependence of $T_e(t)$ needs to be solved for, e.g. using a two-temperature model. As a simplification we can assume that T_e simply decays exponentially, with time constant $\tau_{\rm E}$, towards the final equilibrium temperature $T_{\rm f}$.

In the regime of moderate excitation in which we work, using the D_s of Ni [163] we get that just after SPE thermalization we have $\delta M{\simeq}{-3}\cdot 10^{-3}$ $\mu_{\rm B}$/atom. Using the magnetization of Ni at room temperature equal to $M(T{=}0)\times\sqrt{1-T/T_c}{=}0.35$ $\mu_{\rm B}$/atom (with $T_c{=}$ 631 K), we get $\delta M/M{\simeq}3\%$. Let us consider some limiting cases of behavior of Eq. (9.13) for such a value of inital δM, and for T_e decaying towards $T_{\rm f}$ with a characteristic time constant $\tau_{\rm E}$ (which is about 0.5 ps in Ni).

If $\tau_{\rm sr}{\gg}\tau_{\rm E}$, there is no ultrafast demagnetization within the Elliott-Yafet based model. In about a picosecond the electronic and lattice temperatures settle at $T_{\rm f}$, while the magnetization is practically unchanged. However, the spins of electrons are still out of equilibrium, albeit with $\Delta\mu$ given by Eq. (9.4) with $T_{ei}{=}T_{\rm f}$. Then, the spin relaxation proceeds, and after a time of the order of $\tau_{\rm sr}$ the magnetization achieves the final equlibrium value $M_{\rm f}(T_{\rm f})$.

For the other extreme case, $\tau_{\rm sr}{\ll}\tau_{\rm E}$, we have the possibility of significant ultrafast demagnetization. Now it is important to consider how $M_0(M, T_e)$ changes when M is decreasing, and T_e is kept (approximately) constant. It is easy to see that when the band splitting Δ is decreased, the splitting of chemical potentials $\Delta\mu$ goes up. Consequently, M_0 goes down, and the total magnetization M is relaxing towards a "moving target" of M_0. For example, when initial $\Delta\mu{=}10$ meV, $\delta M/M{=}3\%$. When magnetization actually changes by this δM, an additional splitting of $\Delta\mu{\simeq}7$ meV is created by shifting of majority and minority bands with respect to each other (here we have used the value of room temperature exchange splitting $\Delta{=}0.25$ in Ni from Ref. [130]). Let us note that it is possible to show within the Stoner model that $\Delta\mu$ cannot increase in this process. The condition

for stability of magnetization M is (see e.g. Ref. [155]):

$$2U < \frac{1}{D_{\uparrow}(\mu_0)} + \frac{1}{D_{\downarrow}(\mu_0)} \ , \tag{9.14}$$

and together with Eq. (9.10) this forces $\Delta\mu$ to decay in time when the exchange splitting $\Delta = UM$ is decreasing. However, it is clear that due to changes of M_0 the demagnetization can continue for a time longer than $\tau_{\rm sr}$. Investigation of possible behavior of $M(T)$ for various parameters, such as the shapes of D_s around the initial μ_0 and the ratio of times $\tau_{\rm sr}/\tau_{\rm E}$ is left for future research. The question of whether it is possible for $M(t)$ to initially "overshoot" $M_{\rm f}$ (as it is suggested by the magneto-optical experiments) is especially worth investigating.

Finally, for $\tau_{\rm sr} \approx \tau_{\rm E}$ we expect the demagnetization ΔM during time $\tau_{\rm E}$ to be of the order of initial δM (assuming that the effects of decaying $T_e(t)$ making $\Delta\mu$ smaller and decreasing M_0 making $\Delta\mu$ larger roughly cancel each other). This initial drop might not be enough to reach the real equilibrium $M(T_{\rm f})$, and further demagnetization at constant $T_e = T_{\rm f}$ might occur.

In Section 9.B.3 we derive an estimate of $\tau_{\rm sr} \simeq 0.4$ ps, which is very close to the measured $\tau_{\rm E} \simeq 0.4$ ps [159]. Using our estimate of $\Delta\mu \leq 10$ meV and densities of states from Ref. [163] we get $\delta M/M \leq 3\%$. This is comparable to the observed $\Delta M/M \simeq 4\%$ [129].

To summarize, simple estimates of the significance of the Elliott-Yafet spin relaxation process for ultrafast demagnetization show that this mechanism should be taken into account. However, it is rather improbable that this is the sole explanation of demagnetization. As we have noted before, this approach to demagnetization is expected to work as well as the Stoner model does, and the Stoner model is well known to be not reliable at finite temperatures. For example, deriving the $M(T)$ dependence in the spirit of the above equations leads to T^2 behavior at low temperatures. This is not observed, instead the Bloch $T^{3/2}$ law due to spin waves is seen. A mechanism of ultrafast demagnetization beyond the nonequilibrium Stoner model discussed in this section is given in Section 9.C.

9.B.3 Estimate of Elliott-Yafet spin relaxation time from transport measurements in metals

The derivation and discussion of spin diffusion equations is given in Chapter 2. In a ferromagnetic material the spin relaxation time τ_{sr} is given by

$$\tau_{\text{sr}} = e^2 L^2 \frac{\sigma_{\uparrow}^{-1} + \sigma_{\downarrow}^{-1}}{D_{\uparrow}^{-1} + D_{\downarrow}^{-1}} = \frac{4e^2 L^2}{\sigma(1-\beta^2)(D_{\uparrow}^{-1} + D_{\downarrow}^{-1})} \ , \tag{9.15}$$

where L is the spin diffusion length, the densities of states D_s are taken a the Fermi level, σ_s are spin-resolved conductivities, and β is the spin-asymmetry of conductivity defined by equations:

$$\sigma_{\uparrow(\downarrow)} = \frac{\sigma}{2}(1 + (-)\beta) \ , \tag{9.16}$$

in which σ is the total conductivity.

Using the above, and given the total conductivity of a ferromagnet, the spin polarization of the current inside it (parametrized by β), and the densities of states at the Fermi level we can derive the spin-flip times from the spin diffusion length. We will use a value of L≈20 nm for Ni obtained [165] from GMR measurements at low temperatures (T=4 K). We use the densities of states from available calculations [163, 93], and conductivity σ_{Ni}=$1.6 \cdot 10^5\ \Omega^{-1}\text{cm}^{-1}$. For β we use a value for permalloy ($Ni_{79}Fe_{21}$) from Refs. [166, 167], as the values for pure Ni are not available. With all these we get

$$\tau_{\text{sr}}^{\text{Ni}} \approx 0.4\,\text{ps} \ . \tag{9.17}$$

This could be considered an upper bound for spin flip times in Ni at room temperature (we generally expect more scattering at higher temperatures), with the caveat of uncertainty in β and the fact that N_s can change significantly with growing T due to the decrease of the band spin-splitting. Thus, the above value should be treated as a rough estimate.

9.C Carrier - spin wave interaction

In this section we sketch an alternative approach to magnetization dynamics. We consider the interaction between the SPEs heated by the laser and the spin waves. An excitation of a spin wave corresponds to a decrease of the magnetization by one unit of $\mu_{\rm B}$, so that the magnetization in units of $\mu_{\rm B}$/atom is given by

$$M = M_{\rm sat} - \frac{1}{N}\sum_{\mathbf{q}} n_{\rm sw}(\omega_{\mathbf{q}}) \ , \tag{9.18}$$

where $M_{\rm sat}$ is the saturation magnetization, N is the number of atoms, $\omega_{\mathbf{q}}$ is the frequency of the magnon with wave vector $\mathbf{q}$, and $n_{\rm sw}$ is the distribution function of spin waves. If the spin wave system is in the state of internal thermal equibrium at temperature $T_{\rm sw}$, then $n_{\rm sw}$ is the Bose-Einstein distribution $n(\omega_{\mathbf{q}}, T_{\rm sw})$.

We use a general form of the model Hamiltonian describing the coupling between the spin waves and the single particle excitations [154]:

$$H_{\text{e-sw}} = \sum_{\mathbf{kq}\,n,n'} V_{\mathbf{kq}}^{nn'} \left(a^\dagger{}_{\mathbf{q}} c^\dagger{}_{n\mathbf{k}} c_{n'\mathbf{k}+\mathbf{q}} + a_{\mathbf{q}} c^\dagger{}_{n'\mathbf{k}} c_{n\mathbf{k}-\mathbf{q}} \right) \ , \tag{9.19}$$

where $a^\dagger_{\mathbf{q}}$ and $a_{\mathbf{q}}$ are creation and annihilation operators for bosonic spin waves, $c^\dagger_{n\mathbf{k}}$ and $c_{n\mathbf{k}}$ are the operators for fermionic single-particle excitations (electrons near the Fermi energy), $V_{\mathbf{kq}}^{nn'}$ are matrix elements describing the coupling of two kinds of excitations, and n,n' label different bands.

In the simplest possible case of a single spin-split band the band indices n,n' correspond to the two possible spin directions. In a usual textbook treatment we have then $V^{ss'} \sim \delta_{s,-s'}$, and one gets that for bands spin-split by Δ the spin waves with $\hbar\omega_{\mathbf{q}} < \Delta$ cannot be scattered by electrons. However, in the presence of spin-orbit coupling it is possible [154] for the spin wave to be created/annihilated without changing the "spin" label of an electronic state (the electronic eigenstates are not pure spin states in the presence of spin-orbit interaction). Due to such non-spin-flip scattering even the magnons with small $\mathbf{q}$ can interact with SPEs.

From the coupling of small-$\mathbf{q}$ spin waves to the SPEs follows a model for the Gilbert damping of magnetization precession [151, 154]. A uniform precession can

be identified with an out-of-equilibrium population $\delta n_{\mathbf{q}}$ of the spin wave modes with small $\mathbf{q}$ (large wavelength). The decay rate $\gamma_{\mathbf{q}}$ of $\delta n_{\mathbf{q}}$ calculated from a Boltzmann-like scattering approach is

$$\gamma_{\mathbf{q}} = \frac{2\pi}{\hbar} \sum_{\mathbf{k},n,n'} |V^{nn'}_{\mathbf{kq}}|^2 \big(f(\epsilon_{n'\mathbf{k}-\mathbf{q}}) - f(\epsilon_{n\mathbf{k}})\big)\, \delta(\epsilon_{n\mathbf{k}} - \epsilon_{n'\mathbf{k}-\mathbf{q}} - \hbar\omega_{\mathbf{q}}) \ , \tag{9.20}$$

where $f(\epsilon)$ is the Fermi-Dirac distribution of electrons of energy ϵ. An analogous expression for the spin wave damping can be derived from the RPA treatment of the Hubbard model [156, 168], justifying the use of an effective magnon-SPE Hamiltonian from Eq. (9.19).

The Gilbert damping coefficient α is related to the spin wave decay rate in the following way [154]:

$$\alpha = \lim_{\mathbf{q}\to 0} \frac{\gamma_{\mathbf{q}}}{2\omega_{\mathbf{q}}} \ . \tag{9.21}$$

This definition makes sense, i.e. it leads to a finite value of α, because for small $\omega_{\mathbf{q}}$ Equation (9.20) gives $\gamma_{\mathbf{q}} \sim \omega_{\mathbf{q}}$. This is basically a phase-space argument (the initial and final electron energy has to be inside the energy layer having $\hbar\omega_{\mathbf{q}}$ thickness around the Fermi energy), which holds when $\hbar\omega_{\mathbf{q}}$ is smaller than the energy on which the densities of states change, and for the matrix element $V^{nn'}_{\mathbf{kq}}$ constant for the wave-vectors involved (both initial and final electron wave vectors are $\sim k_{\mathrm{F}}$). These conditions should hold for $\omega_{\mathbf{q}}$ of the order of tens of THz ($\hbar\omega$ od the order of 10 meV) as well as for $\omega_{\mathbf{q}}$ of the order of 1 GHz, which corresponds to a typical precession frequency in ferromagnetic resonance experiments. Thus, we will assume in the following that

$$\gamma_{\mathbf{q}} = 2\alpha\omega_{\mathbf{q}} \tag{9.22}$$

holds for energies $\hbar\omega_{\mathbf{q}}$ comparable to $k_{\mathrm{B}}T_e$ of the excited carriers.

In the case of light-induced demagnetization we face a problem complementary to the Gilbert damping case. Above we have calculated the decay rate of nonequilibrium occupation of the long-wavelength spin wave mode, assuming the equilibrium distribution of electrons. For demagnetization, we have to calculate the generation rate of spin waves due to nonequilibrium distribution of carriers.

Using the same Boltzmann-like approach, we get for the magnetization dynamics due to spin wave generation the following expression:

$$\frac{dM}{dt} = -\frac{1}{N}\sum_{\mathbf{q}} \gamma_{\mathbf{q}}\Big(n(\omega_{\mathbf{q}}, T_e) - n(\omega_{\mathbf{q}}, T_{\rm sw})\Big) \ , \tag{9.23}$$

where $n(\omega, T)$ is the Bose-Einstein distribution at temperature T, and $T_{\rm sw}$ is the temperature of spin waves. In the above expression we have made a rather crude simplifying assumption that during the demagnetization spin waves maintain a thermal distribution at time-dependent "spin" temperature $T_{\rm sw}(t)$. We also use the spin wave dispersion given by

$$\hbar\omega_{\mathbf{q}} = Aq^2 \ , \tag{9.24}$$

with spin stiffness A, and we employ Eq. (9.22) arriving at

$$\frac{dM}{dt} = -\frac{\alpha k_{\rm B}^{5/2}}{2\pi^2\hbar n A^{3/2}}\Gamma\big(\frac{5}{2}\big)\xi\big(\frac{5}{2}\big)\left[T_e^{5/2} - T_s^{5/2}\right] \ , \tag{9.25}$$

where n is the density of atoms, and $\xi(x)$ is the Riemann function [169]. This formula is a large step forward from the purely phenomenological three temperature model presented before. It connects the magnetization dynamics to the electronic temperature T_e and the "spin" temperature $T_{\rm sw}$, which is identified here with the temperature describing the distribution of spin waves. The coupling coefficient is connected to macroscopic quantities: Gilbert damping α and spin stiffness A.

9.C.1 Comparison with the results of Koopmans et al.

In Ref. [43] the characteristic demagnetization time $\tau_{\rm M}$ was derived in the following way. A weak excitation was assumed, and a constant T_e was used. The demagnetization time was then defined as

$$\tau_{\rm M}^{-1} = \frac{\frac{dM}{dt}\big|_{t=0}}{\Delta M(t=\infty)} \ , \tag{9.26}$$

where $\Delta M(t{=}\infty)$ is the total demagnetization. Within their model (which we consider oversimplified), the authors of Ref. [43] obtained

$$\tau_{\rm M} \approx \frac{\hbar}{k_{\rm B}T_C}\frac{1}{\alpha} \ , \tag{9.27}$$

in which T_C is the critical temperature. For nickel, the above expression gives $\tau_{\rm M}$= 100 fs.

We derive the expression for $\tau_{\rm M}$ within our model, assuming $\Delta T_e \ll T_0$ and using Eq. (9.18) to obtain $\Delta M(t{=}\infty)$. To the lowest order in $\Delta T_e/T_0$ we get

$$\tau_{\rm M} = \frac{\hbar}{k_{\rm B}T_0}\frac{1}{\alpha}\,\frac{3}{5}\frac{\Gamma\left(\frac{3}{2}\right)\xi\left(\frac{3}{2}\right)}{\Gamma\left(\frac{5}{2}\right)\xi\left(\frac{5}{2}\right)} \approx 0.78\,\frac{\hbar}{k_{\rm B}T_0}\frac{1}{\alpha}\ . \tag{9.28}$$

This formula is analogous Eq. (9.27), with the crucial difference of the initial temperature T_0 replacing the critical temperature T_C. Since the demagnetization experiments are conducted at room temperature, which is of the same order as T_C (e.g. in Ni we have T_C=631 K), the order-of-magnitude agreement between the above $\tau_{\rm M}$ and the observed time-scale of initial drop in magnetization still holds. Using the value of α=0.038 in Ni [43] we get that at room temperature $\tau_{\rm M}\approx$0.5 ps, which is in qualitative agreement with the experimental results. Although our estimate for $\tau_{\rm M}$ is similar to the value of 100 fs derived in Ref. [43], we deem our approach to be more realistic for itinerant ferromagnets than the model used in Ref. [43].

9.D Summary

In this chapter we have presented an outline of a theory of ultrafast light-induced demagnetization in transition metals. We have considered two mechanisms of decay of magnetization due to heating of carriers (single-paticle excitations) by a laser pulse.

The first is basically a non-equlibrium extension of the Stoner (band) model of ferromagnetism. The magnetization changes due to Elliott-Yafet (EY) spin relaxation of carriers scattering with impurities and phonons. The necessary condition for EY spin scattering to occur is the creation of a splitting of chemical potential for two spins, $\Delta\mu$. This splitting is caused by heating of carriers, and its magnitude depends on the shape of spin-projected densities of states at the Fermi level.

The characteristic time-scale on which the magnetization changes is given by spin-relaxation time τ_{sr} which is bounded from below by the spin relaxation time used in the theory of spin diffusion (see Chapter 2). It is important to note that this time is independent of the excitation level, at least as long as it is moderate (in the lower range of pump fluences used in experiments). Using the values of τ_{sr} inferred from transport measurements, we have estimated the maximal change of magnetization $\Delta M/M \leq 3\%$ for Ni with excitation corresponding to a rise of electronic temperature $\Delta T_e \simeq 100$ K. The experimental result is $\Delta M/M \simeq 4\%$. Since in deriving our estimate we have consistently erred on the side of too large ΔM, we cannot say that the EY mechanism provides a full explanation of the experiments. It seems that it could be important, and it deserves further exploration, e.g. by doing calculations using more accurate densities of states. However, due to the well-known unreliability of the Stoner model at finite temperatures, it is unclear whether a more detailed investigation of this approach is going to lead to more realistic results.

The second mechanism is the excitation of spin waves by hot carriers. In contrast to the EY process, magnetization change in this mechanism is directly driven by the rise of the electronic temperature T_e. We use the definition of characteristic demagnetization time τ_{M} from Ref. [43], and arrive at a simple expression connecting the Gilbert damping constant α and the initial temperature of the ferromagnet with τ_{M}.

10

Ultrafast demagnetization in the sp-d model: application to (III,Mn)V ferromagnetic semiconductors

In Chapter 9 we have discussed the ultrafast light-induced demagnetization in transition metals. Recently, an analogous phenomenon, including a complete destruction of ferromagnetic order in less than a picosecond, has been observed in (III,Mn)V ferromagnetic semiconductors [170, 44]. In these materials, the ferromagnetism is described by the sp-d model [171, 172, 173], in which the localized spins (formed by d-shell electrons of Mn ions) are coupled by exchange interactions with the spins of the carriers (electrons of s symmetry and holes of p symmetry). This clear-cut separation into the systems of carriers (which are directly excited by light) and the localized spins (which provide most of the macroscopic magnetization) allows for formulation of the physically transparent theory of ultrafast demagnetization. In our model, the excited carriers are described by an elevated electronic temperature, which leads to enhancement of the spin-flip scattering rate between the localized spins and the carriers' spins. The resulting transfer of the

angular momentum from the localized spins to the carriers is termed the "inverse Overhauser effect". If the nonequilibrium spin polarization injected into the carriers' system is relaxed fast enough by spin relaxation (due to the spin-orbit interaction experienced by the carriers), the localized spin system can be siginificantly demagnetized during the carriers' energy relaxation time.

In Section 10.A we introduce the sp-d model, give some basic information about the (III,Mn)V semiconductors, and discuss the mean-field theory of ferromagnetism in these materials. In Section 10.B we discuss the specific features of the photoexcitation process in ferromagnetic semiconductors such as GaMnAs. Section 10.C contains the description of our approach to the modeling of the hot carrier bath. The main differences with respect to usual treatment is that we allow for the presence of the dynamic spin polarization of carriers, and that the carriers' temperature T_{e} changes on the time-scale of the energy relaxation of carriers. Then in Section 10.D we outline the derivation of the rate equations for the dynamics of the localized spin coupled to the carrier bath (the details are given in Appendix A). The transition rates are due to spin-flip scattering with the carrier spins, and they depend on the instantaneous state of the carrier system at a given time. This derivation generalizes to the non-stationary case the results from Ref. [174], in which the heating of Mn spins by electrons excited by cw light was considered in a (II,Mn)VI based quantum well. The rate equations have to be augmented by a phenomenological treatment of the bath dynamics. In Section 10.E we calculate the ultrafast demagnetization using a simplified band structure (a single spin-split band), introduce the equations governing the carrier dynamics, and discuss how the energy and spin relaxation of carriers influences the demagnetization process. Complications introduced by valence band-structure of a ferromagnetic semiconductor are discussed in Section 10.F, where we use an effective Hamiltonian [175] model of the spin-split valence band to calculate the hole-Mn spin-flip transition rate. Finally, we discuss the connection to the experiments (Refs. [170, 44]) in Section 10.G.

Although many features which we discuss are specific to the (III,Mn)V ferromagnetic semiconductors, the general results are directly applicable to any system described by analogous s(p)-d(f) model, in which the indirect (carrier-mediated) exchange interaction between localized spins dominates over other mechanisms of d-d coupling (e.g. superexchange). However, when the non-carrier-mediated d-d exchange coupling is strong (e.g. in the europium chalcogenides [176]), the starting point of the calculation should not be the interaction of a single spin with the carriers (which is our approach here), but the enhancement of the carrier-magnon scattering. A similar treatment should be applied to a recent measurement [177] of the ultrafast magnetization dynamics in GaMnAs excited with the pump fluence 3 orders of magnitude smaller than in Ref. [170]. In this case, our assumption of complete obliteration of the carrier-mediated exchange coupling by excitation of carriers might not hold, and spin-wave modes of coupled Mn spins should be the starting point of the calculation.

10.A The sp-d model and its application to (III,Mn)V ferromagnetic semiconductors

A model of ferromagnetism ideally suited for investigation of magnetization quenching induced by excitation of carriers is the sp-d model. In this approach, most of the macroscopic magnetization comes from the localized d-shell spins (or f shells, in case of the rare earth elements), which are coupled by an exchange interaction to itinerant s or p carriers. This model was introduced independently by Zener [172, 173] and by Vonsovskii [171] in order to describe the transition metals, but was abandoned when the lack of sharp separation into s carriers and d spins in metals was understood. Later, the s-d(f) model was succesfully applied to magnetic semiconductors such as the chalcogenides of europium [176]. Recently, it has been again used in itinerant ferromagnets, in order to analyze the situations in which an interplay between the transport and magnetic properties is critical.

Examples include spin-transfer torque [11] and an enhancement of Gilbert damping in a magnet due to pumping of spin currents into adjacent non-magnetic material [178].

Most importantly for us, the p-d model is describes the basic physics of ferromagnetism in diluted magnetic semiconductors (DMS). These materials are created by doping a small ($x\sim5\%$) molar fraction of magnetic ions (most often Mn) into a non-magnetic host semiconductor. The DMS based on II-VI materials, such as CdTe, were researched intensively since the seventies (for a review of work until 1988 see e.g. Refs. [179, 180]). The d shells of doped magnetic ions form localized spins, which are coupled by the isotropic sp-d exchange interaction to the carriers: the Hamiltonian of the interaction is $\hat{H}_{sp-d} \sim \gamma \hat{\mathbf{S}} \cdot \hat{\mathbf{s}}$, with the exchange constant γ and the localized and carrier spins denoted by $\hat{\mathbf{S}}$ and $\hat{\mathbf{s}}$, respectively. This exchange interaction causes the giant Zeeman splittling of the carriers bands in magnetic fields. Also, in the presence of free carriers the sp-d interaction could lead to a carrier-mediated exchange interaction between the localized spins. The simplest form of such an interaction is RKKY, named after Rudermann, Kittel, Kasuya, and Yosida, who have proposed it in the fifties for a system of nuclear magnetic moments interacting by hyperfine contact interaction (having the same Hamiltonian as the sp-d exchange) with the conduction electrons. However, the carrier concentrations achievable in bulk (II,Mn)VI materials are too low for carrier-mediated exchange to dominate over antiferromagnetic superexchange [181] interaction between the localized spins. As a consequence, the II-VI based DMS were either paramagnets, or spin glasses at very low temperatures and high magnetic ion concentrations. Only in 1997 the RKKY-driven ferromagnetism was seen in a CdMnTe quantum well modulation-doped with holes [182, 183], but the Curie temperature was of the order of only one Kelvin.

Ferromagnetism was seen at much higher temperatures in III-V semiconductors doped with Mn, specifically $Ga_{1-x}Mn_xAs$ and $In_{1-x}Mn_xAs$ [26, 27], and critical temperature of 110 K was achieved in GaMnAs in the end of nineties [28] (a

current record is $\sim$ 170 K in GaMnAs). In (III,Mn)V materials the Mn ions are acceptors (when they substitute the cations), and their d shells can be treated as well-localized 5/2 spins [65]. For a molar fraction x~5% of Mn, the concentration of holes if on the order of 10^{20} cm^{-3} (strong compensation due to defects acting as donors inherent in these materials has to be taken into account in order to derive this number). At these hole densities a mean-field theory of Zener [172, 173, 28, 29] has been successful in describing many features of ferromagnetism in these materials. It correctly predicts the critical temperature T_{cr}, increasing trend in T_{cr} with the density of carriers, and magnetic anisotropies [175]. A derivation of the critical temperature in the Zener model is sketched below. A recent review of the theory of these materials is Ref. [175]. Here we use the simplest effective model of these materials, in which the sp-d interaction is added to the host Hamiltonian.

The strong correlation between the presence of the delocalized (or at least weakly localized) holes and ferromagnetic ordering of Mn spins has been firmly established experimentally. The optical induction of ferromagnetic transition (through cw photoinjection of holes) has been shown [184], and the critical temperature and the coercive field has been altered by changing the density of holes in InMnAs by applying the gate voltage [31, 185]. Most importantly for us, the sub-picosecond light induced demagnetization has been recently observed in InMnAs [170] and GaMnAs [44]. A complete quenching of ferromagnetic order was achieved in InMnAs for pump fluences above 10 mJ/cm^2. This should be contrasted with behavior in Ni, where the demagnetization saturates at higher fluences while not reaching the complete demagnetization [132]. Since the carrier concentration is much lower in ferromagnetic semiconductors as compared to metals, their magnetization is more amenable to manipulation by external stimuli.

The Hamiltonian of the sp-d model consists of the single-particle carrier part $\hat{H}_C$, localized spin part $\hat{H}_S$ and the sp-d coupling $\hat{H}_{CS}$:

$$\hat{H} = \hat{H}_C + \hat{H}_S + \hat{H}_{CS} \ . \tag{10.1}$$

We do not explicitly consider the carrier-carrier interaction , carrier-phonon inter-

action, and the lattice dynamics. However, these interactions are included phenomenologically in our treatment of the carrier bath below (Section 10.C). The carrier part of the Hamiltonian is given by

$$\hat{H}_C = \sum_{n\mathbf{k}} \epsilon_{n\mathbf{k}} a^{\dagger}{}_{n\mathbf{k}} a_{n\mathbf{k}\sigma} \ , \tag{10.2}$$

where n is the band index, $\mathbf{k}$ is the wave-vector, and $\epsilon_{n\mathbf{k}}$ is the energy. In the case of (III,Mn)V semiconductors, the valence band structure near the Γ point can be obtained from a $\mathbf{k}\cdot\mathbf{p}$ model, such as 6×6 Luttinger Hamiltonian commonly used in these systems [29] (see Appendix B for details of this approach). Although the ferromagnetic semiconductors are known to be heavily disordered, we have neglected the disorder potential in Eq. (10.2). If the disorder can be treated perturbatively, then its influence on the treatment below is not expected to be strong, as we work in the regime of very strong excitation of carriers, in which more subtle features of bands are going to be averaged out anyway. On the other hand, if the effects of disorder are non-perturbative (e.g. the holes are in an impurity band rather than in the host valence band, as it has recently been suggested in Ref. [186]), a new energy dispersion (e.g. a single weakly dispersive band) should be introduced in Eq. (10.2).

The localized spin Hamiltonian $\hat{H}_S$ includes Zeeman coupling to the external magnetic field. In the ferromagnetic phase, the splitting of the localized spin S due to exchange interaction with carriers exceeds the typical Zeeman splitting, and the only role of the Zeeman term is to choose the direction of the magnetization. We disregard possible S-S exchange coupling by mechanisms other [181] than indirect carrier-mediated exchange.

Finally, the exchange coupling is given by

$$\hat{H}_{CS} = -\frac{\gamma}{V} \sum_{l} \sum_{n\mathbf{k},n'\mathbf{k}'} \hat{\mathbf{S}}_l \cdot \langle n\mathbf{k}|\hat{\mathbf{s}}|n'\mathbf{k}'\rangle \, e^{i(\mathbf{k}'-\mathbf{k})\mathbf{R}_l} \ a^{\dagger}_{n\mathbf{k}} a_{n'\mathbf{k}'} \ , \tag{10.3}$$

where $\hat{\mathbf{S}}_l$ is the spin operator of localized spin at $\mathbf{R}_l$, $\hat{\mathbf{s}}$ is the carrier spin operator and γ is the exchange constant. In the literature on diluted magnetic semiconductors, the γ parameter is called α and β for the conduction and valence band

electrons, respectively [179]. The typical values in (III,Mn)V materials are $\alpha \approx 10$ and $\beta \approx -50$ meV·nm^3. The exchange energy J per unit cell is $J = N_0 \gamma$, where N_0 is the density of the cations. Accordingly, $N_0 \alpha \approx 0.2$ eV and $N_0 \beta \approx -1$ eV.

For a single band, the sum over n states is simplified to

$$\hat{H}^1_{CS} = -\frac{\gamma}{V} \sum_l \sum_{\mathbf{k},\mathbf{k}'} \hat{\mathbf{S}}_l \cdot \hat{\mathbf{s}}_{\mathbf{k}\mathbf{k}'} \, e^{i(\mathbf{k}'-\mathbf{k})\mathbf{R}_l} \ , \tag{10.4}$$

where the scalar product of spin operators can be expressed using spin ladder operators as:

$$\hat{\mathbf{S}}_l \cdot \hat{\mathbf{s}}_{\mathbf{k}\mathbf{k}'} = \frac{1}{2}(\hat{S}^+_l \hat{s}^-_{\mathbf{k}\mathbf{k}'} + \hat{S}^-_l \hat{s}^+_{\mathbf{k}\mathbf{k}'}) + \hat{S}^z_l \hat{s}^z_{\mathbf{k}\mathbf{k}'} \ , \tag{10.5}$$

and the explicit form of carrier spin operators is

$$\hat{s}^z_{\mathbf{k}\mathbf{k}'} = \frac{1}{2}(a^\dagger{}_{\mathbf{k}\uparrow} a_{\mathbf{k}'\uparrow} - a^\dagger{}_{\mathbf{k}\downarrow} a_{\mathbf{k}'\downarrow}) \tag{10.6}$$

$$\hat{s}^+_{\mathbf{k}\mathbf{k}'} = a^\dagger{}_{\mathbf{k}\uparrow} a_{\mathbf{k}'\downarrow} \ , \ \ \hat{s}^-_{\mathbf{k}\mathbf{k}'} = a^\dagger{}_{\mathbf{k}\downarrow} a_{\mathbf{k}'\uparrow} \ . \tag{10.7}$$

We assume the magnetization (the average localized spin) in the z direction, and treat the sp-d Hamiltonian in a mean-field approximation. The mean-field felt by the carriers is obtained by performing the simplest virtual crystal disorder averaging of localized spins positions:

$$\hat{H}^{mf}_C = -n_i \gamma \langle S_z \rangle \sum_{n,n',\mathbf{k}} \langle n\mathbf{k} | \hat{s}^z | n'\mathbf{k} \rangle a^\dagger{}_{n\mathbf{k}} a_{n'\mathbf{k}} \ , \tag{10.8}$$

where n_i is the density of localized spins and $\langle S_z \rangle$ is the average localized spin. The energy of the carrier spin splitting is defined as

$$\Delta = -n_i \gamma \langle S_z \rangle \ . \tag{10.9}$$

The typical value of Δ in GaMnAs and InMnAs with the highest critical temperatures is of the order of 0.1 eV. On the other hand, by averaging Eq. (10.3) with respect to the carriers we arrive at

$$\hat{H}^{mf}_S = \delta \sum_l \hat{S}^z_l \ , \tag{10.10}$$

where the energy splitting of different m levels of a localized spin is

$$\delta = -n_c \gamma \langle s_z \rangle \ , \tag{10.11}$$

with n_c the carrier density and $\langle s_z \rangle$ the average carrier spin. The typical magnitude of δ in (III,Mn)V materials is of the order of 1 meV. When the localized spins are magnetized along one of the high-symmetry directions of the crystal (which we labeled as z), the average carrier spin is collinear with them (see Appendix C for derivation), and the above equations are consistent.

In the mean-field theory of ferromagnetism [187, 28, 29, 188, 30, 175] only the two averaged fields $\langle S_z \rangle$ and $\langle s_z \rangle$ are taken into account, and the free energy of their interaction is minimized. For temperatures below the critical temperature T_{cr}, the gain in energy from polarization of the two spin systems outweighs the free energy penalty due to decreased entropy of the ordered state, and the system becomes magnetized. The derivation of the critical Curie temperature T_{cr} is a simple exercise in the application of the mean-field theory to two coupled spin systems, which was actually first given published in 1963 [187]. The magnetization of the localized spins due to the exchange interaction with the carriers is given by a Brillouin function B_S for spin S [51], with S=5/2 in GaMnAs and InMnAs:

$$\langle S_z \rangle = -S B_S(\delta S / k_B T) = S B_S(n_c \gamma \langle s_z \rangle S / k_B T) \ . \tag{10.12}$$

On the other hand, the non-zero value of average carrier spin $\langle s_z \rangle$ entering the above equation is caused by the effective field due to the localized spins:

$$\langle s_z \rangle = -\frac{\chi \Delta}{(g\mu_B)^2 n_c} = \frac{\chi n_i \gamma \langle S_z \rangle}{(g\mu_B)^2 n_c} \ , \tag{10.13}$$

in which χ is the magnetic susceptibility of the carriers. We plug Eq. (10.13) into Eq. (10.12), and expand the Brillouin function for small values of its arguments ($B_S(x) \approx \frac{S+1}{3S} x + O(x^3)$), obtaining the critical temperature

$$k_B T_{cr} = \frac{n_i S(S+1) \gamma^2 \chi}{3(g\mu_B)^2} \ . \tag{10.14}$$

In a single parabolic band the susceptibility χ is proportional to $n_c^{1/3}$. This explains qualitatively the observed increase of T_{cr} with increasing hole concentration. However, in order to reproduce the observed trends in Curie temperature for different hole-doped ferromagnetic semiconductors, it is essential to go beyond the single-band model and to include the spin-orbit coupling in calculation of χ [28, 29, 30].

10.B Light excitation of the carrier system in (III,Mn)V

To construct a model of the excited carrier bath, it is helpful to first analyze qualitatively the process of carrier photoexcitation in ferromagnetic semiconductors. The cw (magneto)optical spectra of GaMnAs are qualitatively different from results in pure GaAs, as they show very strong effects of disorder [189, 190, 191, 192]. There is no gap in the absorption, which is at least of the order of 10^4 cm^{-1} for all energies [191]. The origin of strong absorption inside the host gap is a matter of controversy (see Figure 10.1). It has been proposed that the additional optical transitions are between the valence band and the dispersionless levels (located about 0.7 E_g above the valence band) originating from As antisites or Mn interstitials [193]. Transitions terminating inside the Mn derived impurity band ∼0.1 eV above the valence band edge have also been suggested [194, 191, 186].

In addition, the role of the inter-valence band transitions is increased in the disordered material, in which the **k**-selection rule is relaxed. As a result, the absorption of light with energy smaller than the bandgap of the host material leads to a strong excitation in the valence band, which occurs due to inter-valence transitions, and due to possible transitions from below the Fermi energy into the localized states within the gap. The initial distribution of photoholes is expected to be very broad, determined only by energy conservation (not by **k**-selection). We are going to use the broadness of the distribution of the carriers after the excitation and their total number as free parameters of the theory. Some flexibility in the used values of total hole density immediately after the excitation p is also justified by

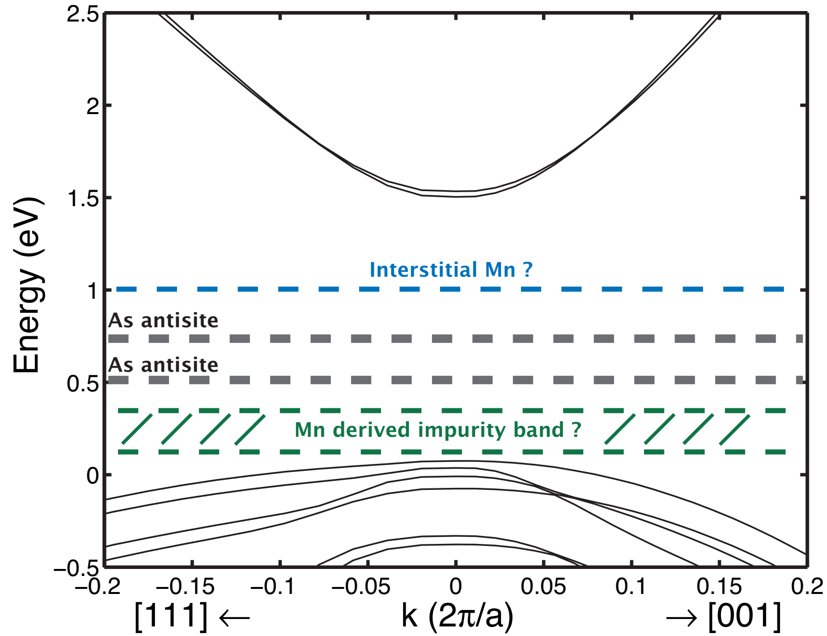

Figure 10.1: The band structure of GaMnAs (solid lines) calculated using 8 band $\mathbf{k} \cdot \mathbf{p}$ model with mean-field sp-d exchange interaction ($|\Delta|$=0.15 eV). The dotted lines denote the possible positions of midgap energy levels of different origins. In the model without an impurity band, the Fermi energy is typically around −0.1 eV for hole density $p \sim 10^{20}$ cm^{-3} (the zero of energy is at the top of the valence band without the exchange splitting).

the fact that the initial densities p_0 are usually known with the order of magnitude accuracy. A typical width of hole distribution after excitation used in the following is of the order of 0.1 eV, a value comparable to the exchange splitting of the valence band. In Section 10.G we use the experimental data to argue that the above energy scale is sensible.

The optical experiments in InMnAs are limited to samples with very small Mn concentrations [195] or energies above the fundamental bandgap [196]. The role of different defects has not been investigated as closely as in GaMnAs, but the observed [44] ultrafast electron trapping time suggests that InMnAs does have a large concentration of midgap defects characteristic for low-temperature grown III-V semiconductors. We can also use the results of this chapter to argue for

the presence of strong transitions involving the valence band and states not in the conduction band, on the ground that the number of states available for optical transitions in the conduction band is far too small to explain the demagnetization results.

This picture of photoexcitation is confirmed by the ultrafast demagnetization measurements [44] in GaMnAs excited by 0.6 eV pump, far below 1.5 eV bandgap of GaAs . The results are similar to the ones observed [170] in InMnAs (bandgap of 0.4 eV) excited by the same pump beam, showing that excitation into the conduction band plays a minor role in the demagnetization process.

10.C Model of the carrier bath

According to the discussion in the previous section, immediately after the photoexcitation the distribution of carriers is very broad. We will approximate it by a thermal distribution described by carrier temperature T_{e}. in Section 10.G we estimate the initial $T_{\mathrm{e}}\approx 1000$ K for demagnetization experiments from Ref. [170].

The interaction between the carriers and the localized spins produces a mean-field part (Eq. (10.8)) and a secondary term corresponding to simultaneous flips of the itinerant and localized spins. The latter causes exchange of angular momentum between the excited carriers and the localized spin system. Due to the spherical symmetry of the sp-d Hamiltonian, the sp-d interaction alone conserves the total spin, and it can only move the spin polarization from one system to another. The mechanism of this transfer of spin is going to be described in detail in the next section. Now we concentrate on the features of the carrier bath which are specific to the case at hand: the possibility of dynamic spin polarization and the energy relaxation of carriers.

The spin transferred into the carrier system is not conserved due to the spin-orbit interaction. In its presence the scattering within the electronic system is accompanied by spin relaxation [33] (ultimately into the lattice). However, the

spin relaxation occurs on a finite time-scale $\tau_{\rm sr}$. If the rate at which the carriers relax their spins is smaller than the rate at which angular momentum is injected into the carrier population, there is a dynamic spin polarization of the carriers. In this case the average carrier spin deviates from the mean-field value determined by Δ splitting of the bands. In the case when the carriers occupy a single spin-split band, there is a simple way of introducing the dynamic polarization into our formalism. We assume that populations for both spin directions are described by Fermi-Dirac distributions with the common temperature $T_{\rm e}$ but different quasi-chemical potentials μ_s (spin s=$\uparrow$,$\downarrow$). This is equivalent to saying that we coarse-grain the dynamics on a time-scale larger than the time in which the energy is redistributed within the carrier system (by carrier-carrier scattering), and we explicitly consider only the slower processes: spin relaxation of carriers and energy transfer into the lattice. It is similar to the situation encountered in semiconductor lasers, where the processes of thermalization of electrons and holes separately occur faster than the recombination, and the resulting globally out-of-equilibrium situation can be described by using the quasi-equilibrium form of the carrier distribution, with different quasi-chemical potentials for electrons and holes.

The above approximation of having a single band split into two subbands with definite spin character is valid when the spin-splitting is larger than the spin-orbit interaction energy (as the latter always leads to some mixing of spin states). In the case of the valence band of the (III,Mn)V semiconductor, the spin-orbit interaction ($\Delta_{so}\simeq$0.3 eV) cannot be treated as a small perturbation compared to the exchange splitting of bands ($\Delta\simeq$0.1 eV). We analyze the dynamical spin polarization in this case in Section 10.F.

As we discuss in detail in the following sections, dynamic polarization of carriers affects the spin-flip scattering rate. This is a back-action effect of the S system on the carrier system: demagnetization of localized spins causes the dynamic polarization of carriers, which in turn influences the rate of transfer of angular momentum between the systems. Additionally, as the average S spin changes in

time, so does the Δ splitting of the carrier bands.

Apart from the dynamic polarization effects, we also have to take into account that the carriers are not in thermal equlibrium with the lattice, and in the first picoseconds after the photoexcitation they are described by a temperature different than the lattice. We model the carrier-phonon interaction (leading to the cooling of carriers) and carrier-carrier scattering (maintaining the thermal distribution) phenomenologically. In metals, the electron-phonon energy relaxation time is a couple hundreds of femtoseconds [157, 159]. In semiconductors, the regime of excitation as strong as used in Ref. [170] to demagnetize InMnAs, has not been investigated in detail. Theoretical calculations of energy relaxation of holes deep in the valence band indicate that emission of optical phonons is very efficient for these states [197]. Calculated emission of 7 phonons during a picosecond should correspond to significant cooling of the carriers. Naïve extrapolation of energy-loss curves [198] to hole temperatures of $\sim$1000K also gives a sub-picosecond energy relaxation time. In the following, we will use an energy relaxation time τ_{E} of the order of picosecond, and assume $T_{\mathrm{e}}(t) = T_{\mathrm{e}}(0)\exp(-t/\tau_{\mathrm{E}})$. More generally, the carrier and lattice temperatures could be solved for using a two-temperature model [144]. However, in the case of (III,Mn)V semiconductors the rise in lattice temperature due to heat transfer from the carriers described by such T_{e} is quite small, so that the final common temperature of carriers and the lattice is less than 100 K. As we discuss in detail further on, such a temperature corresponds to very slow demagnetization dynamics, and for the purpose of calculating the ultrafast process, we can then assume that the carrier temperature simply decays towards zero.

In the following, all the averages with respect to carrier degrees of freedom will be taken using a density matrix of non-interacting electrons $\hat{\rho}_C$, which is not necessarily of the equilibrium form, but remains diagonal in the basis of carrier Hamiltonian's eigenstates $|\alpha\rangle$=$|n\mathbf{k}\rangle$ (with the mean-field spin splitting taken into

account). These averages are denoted as $\langle ... \rangle_C \equiv \mathrm{Tr}_C\{\hat{\rho}_C ...\}$, and they are given by

$$\langle a^\dagger{}_\alpha a_\beta \rangle_C = \delta_{\alpha\beta}\ f_\alpha \quad (10.15)$$

$$\langle a^\dagger{}_\alpha a_\beta a^\dagger{}_\gamma a_\delta \rangle_C = \delta_{\alpha\beta}\delta_{\gamma\delta}\ f_\alpha f_\gamma + \delta_{\alpha\delta}\delta_{\beta\gamma}\ f_\alpha(1 - f_\beta) \quad (10.16)$$

where f_α is the average occupation of α state. In a single-band model, the $\alpha ... \delta$ indices refer to $|s\mathbf{k}\rangle$ states with spin s=↑,↓, and $f_{s\mathbf{k}}$ is a Fermi-Dirac function at temperature T_e with spin-dependent chemical potential μ_s.

10.D Rate equations for the localized spin

The framework of the sp-d model allows for clear separation of carrier (C) and localized spin (S) systems. The mean-field parts of their mutual interaction are given by Eq. (10.8) and (10.10). The spin-splitting Δ of the carriers' band is proportional to the instantaneous $\langle S_z \rangle$, and the splitting δ of localized spins changes with the average carrier spin $\langle s_z \rangle$. We assume that any correlation between localized spins beyond the mean-field Zener approach is obliterated by the strong scattering of excited carriers. Each localized spin feels the dynamics of the other spins only through their average value, which influences the state of the carrier system (its spin splitting Δ). Essentially, we consider an ensemble of paramagnetic S spins interacting with a bath, the properties of which depend on the average S. The ferromagnetism enters only as an initial condition: the S system is polarized at t=0. Below we derive the equations for the dynamics of the average S spin due to the interaction with the carrier bath, the state of which depends on the average S.

The Hamiltonian of the localized S spins and the carriers system is written as

$$\hat{H}_{S-C} = \hat{H}_0 + \hat{V} = \hat{H}_C + \hat{H}_C^{mf} + \sum_l (\delta \hat{S}_l^z + \hat{V}_l) \ , \quad (10.17)$$

where $\hat{H}_C$ is the carrier band Hamiltonian (Eq. (10.2)), $\hat{H}_C^{mf}$ is the mean-field spin-splitting from Eq. (10.8), δ is the mean-field localized spin splitting defined in

Eq. (10.11) and the spin-flip term of l-th localized spin $\hat{V}_l$ comes from part of sp-d interaction which is off-diagonal in $\hat{S}^z$ basis. We write it in the following way:

$$\hat{V}_l = \hat{S}_l^+ \hat{F}^- + \hat{S}_l^- \hat{F}^+ \tag{10.18}$$

where $\hat{F}^\pm$ are proportional to the ladder operators of carrier spin. In the general case of multiple bands (as in Eq. (10.3)) we have

$$\hat{F}^\pm = -\frac{\gamma}{2V} \sum_{n\mathbf{k},n'\mathbf{k}'} \langle n\mathbf{k}|\hat{\mathbf{s}}^\pm|n'\mathbf{k}'\rangle a^\dagger{}_{n\mathbf{k}} a_{n'\mathbf{k}'} \ , \tag{10.19}$$

whereas for a single band we have

$$\hat{F}^{+(-)} = -\frac{\gamma}{2V} \sum_{\mathbf{k},\mathbf{k}'} a^\dagger{}_{\mathbf{k}\uparrow(\downarrow)} a_{\mathbf{k}'\downarrow(\uparrow)} \ . \tag{10.20}$$

Now we follow a standard way of deriving the Master equation for the density matrix of the localized spin system interacting with a carrier bath (see e.g. Ref. [199]). The total density matrix of the system is assumed to factorize into the carrier and localized spin density operators:

$$\hat{\rho}(t) \approx \hat{\rho}_C(t)\hat{\rho}_S(t) \ , \tag{10.21}$$

and the Liouville equation for time-dependence of $\hat{\rho}(t)$ is turned into an equation for $\hat{\rho}_S(t)$ by tracing out the carrier degrees of freedom. However, unlike in standard treatment [199], the state of the carrier bath changes in time, as discussed in the previous section.

The usual derivation of the Master equation implies coarse-graining of the system dynamics on time-scale Δt longer than the correlation time of the bath τ_c. This is the condition on which the Markov approximation rests. For the gas of carriers described by the effective temperature $k_B T_\mathrm{e} \approx 0.1$ eV, we can expect this time to be of the order of a few femtoseconds. Let us define a time-scale τ_ρ in which changes in the carriers' density matrix $\hat{\rho}_C(t)$ occur. The contributions to the evolution of $\hat{\rho}_C(t)$ are as follows. The carrier temperature changes appreciably during energy relaxation time $\tau_\mathrm{E} \sim 1$ ps. The spin splitting of the band $\Delta(t)$ is

proportional to the average localized spin $\langle S(t)\rangle$, which we expect to decrease during a characteristic demagnetization time τ_{M}. The build-up of the dynamic spin polarization of the carriers is determined by two processes: transfer of spin from the S system occurring during the aforementioned time τ_{M}, and the spin relaxation of carriers characterized by time τ_{sr} (for very short τ_{sr} there is no dynamical polarization). Now we will assume that all these result in the time τ_ρ much larger than the bath correlation time τ_c, so that we can choose our coarse-graining step Δt so that

$$\tau_c \ll \Delta t \ll \tau_\rho \ . \tag{10.22}$$

In such a case, at each coarse-grained time-step t_n we can derive a Master equation with carriers described by $\hat{\rho}_C(t_n)$ treated as approximately constant during Δt. In this way we can use the Markov approximation locally in time, having separated the "macroscopic" back-action of the localized spin system on the bath, which occurs on a longer time-scale. The Master equation for the localized spin density matrix $\hat{\rho}_S$ is then derived exactly as in the usual case (see Ref. [199]), only with the transition rates depending on time t_n. The details of the derivation are given in Appendix A. We write the equations in the continuum limit, keeping in mind that they cannot be used for times shorter than Δt, thus obtaining the following rate equations for the diagonal elements of the localized spin density matrix

$$\begin{aligned}\frac{d}{dt}\rho^S_{m,m} &= -(W_{m-1,m}+W_{m+1,m})\rho^S_{m,m} \\ &\quad +W_{m,m+1}\rho^S_{m+1,m+1}+W_{m,m-1}\rho^S_{m-1,m-1}\ ,\end{aligned} \tag{10.23}$$

where $W_{n,m}$ is the transition rate from m to n level of the localized spin induced by sp-d interaction with the carriers. The time dependence of the transition rate is understood for clarity. Then the average localized spin evolves according to

$$\frac{d}{dt}\langle S_z(t)\rangle = \sum_m m\frac{d}{dt}\rho^S_{m,m}\ . \tag{10.24}$$

The general formula for $W_{m,m\pm1}$ is (see Appendix Afor detailed derivation)

$$W_{m,m\pm1}(t) = \frac{1}{\hbar^2}S^{\mp}_{m,m\pm1}\int_{-\infty}^{\infty}dt'\, e^{\pm i\delta t'/\hbar}C^{>}_{\mp\pm}(t;t')\ , \tag{10.25}$$

in which the matrix element (squared) for the flip of the localized spin in Eq. (10.25) is given by

$$S^{\mp}_{m,m\pm1} = S(S+1) - m(m\pm1) \ , \tag{10.26}$$

where S is the magnitude of the localized spin. The correlation function of the carriers $C^{>}_{ij}(t;t')$, with i,j=$\pm$, is given by (reverting to the coarse-grained notation with t_n replacing t)

$$C^{>}_{ij}(t_n;t') = \mathrm{Tr}_C\{\hat{\rho}_C(t_n)\tilde{F}^i_n(t_n+t')\tilde{F}^j_n(t_n)\} \ , \tag{10.27}$$

where$\mathrm{Tr}_C\{...\}$ is the trace with respect to the carrier states and $\tilde{F}^i_n(t'')$ are operators defined in Eqs. (10.19) and (10.20) written in the "local" interaction picture at coarse-grained time t_n:

$$\tilde{F}^i_n(t'') = \exp\left\{\frac{i}{\hbar}\hat{H}_0(t_n)t''\right\}\hat{F}^i(t'')\exp\left\{-\frac{i}{\hbar}\hat{H}_0(t_n)t''\right\} \ , \tag{10.28}$$

where $\hat{F}^i(t'')$ is the Schrödringer picture operator, and $\hat{H}_0(t_n)$, defined in Eq. (10.17), depends on the coarse-grained time t_n through the mean-field spin splittings δ and Δ. These correlation functions $C^{>}_{ij}(t;t')$ decay for t' larger than the correlation time τ_c, which has to be much shorter than the time on which $\hat{\rho}_C(t)$ changes. For this reason the integration domain in Eq. (10.25) is effectively $t' \in (-\tau_c, \tau_c)$. In this range of t', the above definitions of $C^{>}_{ij}$ and $\hat{F}^i(t)$ make sense.

In the general case of the multiple bands the transition rates are given by:

$$\begin{aligned} W_{m,m\pm1} \ &= \ \frac{\gamma^2}{4}\frac{2\pi}{\hbar}S^{\mp}_{m,m\pm1}\sum_{nn'}\int\frac{\mathrm{d}^3k}{(2\pi)^3}\int\frac{\mathrm{d}^3k'}{(2\pi)^3}|\langle n'\mathbf{k}'|\hat{s}^{\pm}|n\mathbf{k}\rangle|^2 f_{n\mathbf{k}}(1-f_{n'\mathbf{k}'}) \\ &\quad \times\delta(\tilde{\epsilon}_{n\mathbf{k}} - \tilde{\epsilon}_{n'\mathbf{k}'} \pm \delta) \ , \end{aligned} \tag{10.29}$$

where n and n' are labeling the subbands, $f_{n\mathbf{k}}$ is the occupation of $|n\mathbf{k}\rangle$ state, and $\tilde{\epsilon}_{n\mathbf{k}}$ are the band energies with the mean-field exchange interaction with localized spins taken into account. The distribution functions, energies $\tilde{\epsilon}_{n\mathbf{k}}$, and δ depend implicitly on time, as we discussed before.

For a single spin-split band we replace n and n' by two spin indices and recover the formula given by us in Ref. [170]. An analogous expression has been used in

Ref. [174], where heating of the Mn spins by photoelectrons was considered in a paramagnetic (II,Mn)VI quantum well. Actually, in the case of carriers being a true reservoir of energy and polarization, Eqs. (10.23) and (10.29) were derived originally by Korringa [200] in order to describe the relaxation of nuclear spins coupled to carriers' spins by hyperfine interaction.

The rate equation (10.23) has to be augmented by equations governing the dynamics of the carrier distribution function $f_{n\mathbf{k}}$. A discussion of these additional equations follows in the next section.

10.E Demagnetization due to carriers in a single spin-split band

Let us concentrate now on a model of a single spin-split band of s symmetry. From it, we deduce the general features of the behavior of the system in a simple way. The treatment of the dynamical polarization of carriers is especially transparent in this case. We make use of the distribution functions f_s for spin s=↑,↓ characterized by two different chemical potentials μ_s and a common temperature T_{e} (see Sec. 10.C).

We define reduced transition rates W_{+-} and W_{-+} given by $W_{m,m-1}$ and $W_{m,m+1}$, respectively, with the localized spin matrix elements $S^{\pm}_{m,m\mp1}$ removed (see Eq. (10.29)). In a single band with spin-splitting Δ, the transition rate W_{+-} can be rewritten using the spin-resolved densities of states $D_s(E)$:

$$W_{+-} = \frac{\gamma^2}{4}\frac{2\pi}{\hbar}\int dE\, f_{\uparrow}(E)(1-f_{\downarrow}(E-\delta)) \times D_{\uparrow}(E)D_{\downarrow}(E-\delta) \; , \tag{10.30}$$

and W_{-+} is obtained by exchanging the spins and changing the sign of δ. Manipulating the explicit forms of occupation functions we obtain a generalization of the detailed balance condition to the case of different chemical potentials for two spin

directions:

$$\frac{W_{-+}}{W_{+-}} = e^{\beta_e(\delta-\Delta\mu)} \ , \tag{10.31}$$

where $\beta_e{=}1/k_B T_\mathrm{e}$ and $\Delta\mu{=}\mu_\uparrow - \mu_\downarrow$ is the spin splitting of the carriers' chemical potential. For $\mu_\uparrow{=}\mu_\downarrow$ we recover the usual detailed balance condition.

When the localized $S{=}1/2$, Eq. (10.24) can be transformed into the Bloch-like equation for the dynamics of average localized spin $\langle S_z(t)\rangle$:

$$\frac{d}{dt}\langle S_z(t)\rangle = -\frac{\langle S_z(t)\rangle - S_0(t)}{T_1(t)} \ , \tag{10.32}$$

where $S_0(t)$ is the *instantaneous* equilibrium value of the spin, given by the transitions rates at time t:

$$S_0(t) = \frac{1}{2}\frac{W_{+-}(t) - W_{-+}(t)}{W_{+-}(t) + W_{-+}(t)} = -\frac{1}{2}\tanh\left\{\beta_e(t)(\delta(t) - \Delta\mu(t))\right\} \ , \tag{10.33}$$

and the relaxation time is given by

$$T_1(t) = (W_{+-}(t) + W_{-+}(t))^{-1} \ . \tag{10.34}$$

Note that in applications to (III,Mn)V semiconductors we are going to be interested in the regime of $\beta_e\delta{\ll}1$ and in the localized spin $S{=}5/2$. If the dynamic spin splitting also fulfills $\beta_e\Delta\mu{\ll}1$, we can approximate the Eq. (10.24) *for any magnitude of spin S* by the following expression:

$$\frac{d}{dt}\langle S_z(t)\rangle \simeq -2W_{+-}(t)\langle S_z(t)\rangle \ . \tag{10.35}$$

For the conditions considered below, this equation gives a very good description of the initial stage of the localized spin dynamics, in which the carrier temperature is very high. When the temperature drops so that the above inequalities are violated, one has to solve the full eqs. (10.23) and (10.24) for $S{>}1/2$, and the Bloch equation (10.32) for $S{=}1/2$.

We now introduce the phenomenological equations describing the dynamics of the carrier bath. The time dependence of T_e comes from the cooling of carriers by phonon emission, and we model it by a simple decay (see Section 10.C)

$$T_\mathrm{e}(t) = T_\mathrm{e}(0)\, e^{-t/\tau_\mathrm{E}} \ , \tag{10.36}$$

where τ_{E} is the energy relaxation time of highly excited carriers. The changes of chemical potentials are governed by a second phenomenological equation for the dynamics of the average carrier spin $\langle s_z(t)\rangle$:

$$\frac{d}{dt}\langle s_z(t)\rangle = -\frac{n_i}{n_c}\frac{d}{dt}\langle S_z(t)\rangle - \frac{\langle s_z(t)\rangle - s_0(\Delta, T_{\mathrm{e}})}{\tau_{\mathrm{sr}}} \ . \tag{10.37}$$

The first term on the right describes the transfer of angular momentum by spin-flips (with n_c/n_i being the ratio of the carrier density to the localized spin density), and the second term describes the relaxation (on time scale τ_{sr}) of the average carrier spin towards the instantaneous equilibrium value s_0 determined by the spin splitting Δ and the carrier temperature T_{e}. The above set of single-band equations was used in Refs. [170] and [44] to qualitatively model the demagnetization in (III,Mn)V semiconductors [170, 44].

10.E.1 The inverse Overhauser effect

The demagnetization process described by the above equations occurs in the following way. We model the absorption of a ~100 fs light pulse as an instantaneous increase of concentration and temperature of carriers. The heating of the carriers by a pulse of light modifies the spin-flip transition rates W_{+-} and W_{-+}. The broader the carrier distributions (the higher the T_{e}), the larger these rates. When the dynamic spin splitting $\Delta\mu$ is zero, the detailed balance of transition rates tells us that the localized spin is going to evolve towards a new value corresponding to a high temperature T_{e}. This final value of $\langle S_z\rangle$, and the rate at which it is approached, change with the decrease of the carrier temperature. In addition, the possible build-up of polarization of the carriers changes the spin-flip transition rates in such a way that the spin transfer is blocked, and without spin relaxation in the carrier system a "polarization bottleneck" occurs. This is analogous to the "magnetic resonance bottleneck" known in electron spin resonance of localized moments in metals [201]. In the latter, the resonance spectrum of the localized spins is changed when the spin relaxation of carriers is long enough for the two

spin systems to become "locked" together in precession. Here, in the extreme case of very slow spin relaxation, the initial demagnetization can result in a flip of all the carriers of one spin direction, leaving the carrier system in a "dynamic half-metallic state". After such a saturation of demagnetization process, the rate of spin flip is determined by the (low) rate of the carrier spin relaxation.

The basic principle of demagnetization is analogous to the well-known Overhauser effect [202], in which the itinerant spins are optically pumped, and this injected polarization is transferred by s-d type interaction to the localized spins. Although the original Overhauser effect involves pumping of angular momentum into one of the spin populations, the essence of the effect is taking one spin population out of equilibrium with another, and thus inducing the transfer of angular momentum between them. One generalization of the Overhauser effect was proposed and realized experimentally by Feher [203, 204]. The idea was to heat up the electrons by passing a current through the sample in order to induce spin-flips between the electrons spins and nuclear spins. Depending on the parameters of both spin systems, increase of either nuclear spin polarization [203] or electron polarization [205] is predicted. The "inverse Overhauser effect" presented here is related to the latter: by heating up the carriers, we induce the transfer of angular momentum from the localized spins to the electron (hole) spins.

10.E.2 Carriers as a reservoir of angular momentum: $\Delta\mu$=0

We first analyze the case in which the carrier spin relaxation is so fast that the carriers are a good sink of polarization, so that $\Delta\mu$=0 at each moment of time. The occupation factors f_s are the same for both spins, and are characterized by the time varying temperature T_e and chemical potential μ.

When the temperature is not too high, i.e., $k_B T_\mathrm{e}$ is smaller than the energy scale on which the densities of states change appreciably (but still much larger than localized spin splitting δ), the transition rate (10.30) can be approximated

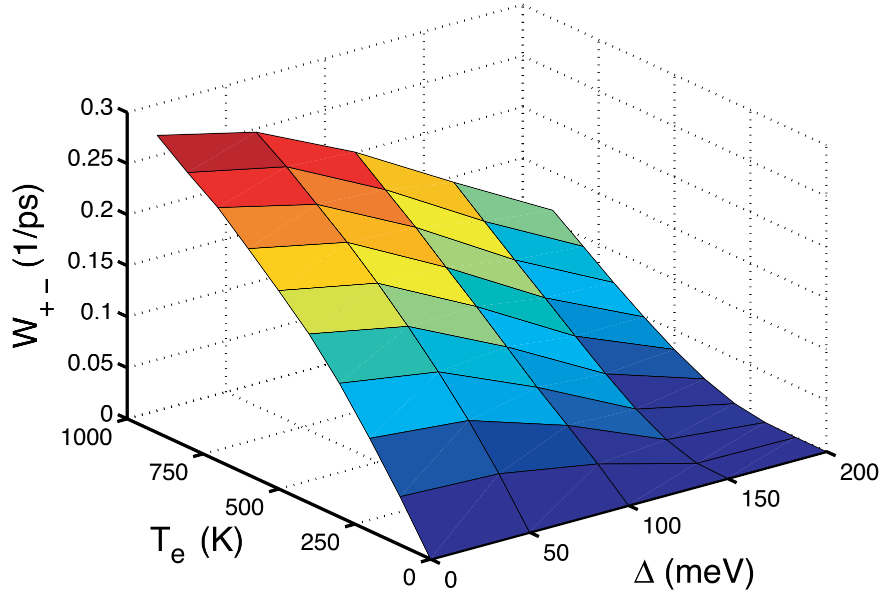

Figure 10.2: Transition rate W_{+-} in a single parabolic band with effective mass $m_{\rm eff}$=1 and γ=50 meV·nm^3 as a function of carrier temperature and band splitting Δ. The concentration of carriers is 10^{20} cm^{-3}.

by

$$W_{+-}(t) \approx \frac{\gamma^2}{4}\frac{2\pi}{\hbar}k_B T_{\rm e}(t) D_+(\mu) D_-(\mu) \; . \tag{10.38}$$

It shows that the rate of demagnetization scales with $T_{\rm e}$, and that large densities of states for both spins around the Fermi level are needed. Together with the γ^2 scaling, this shows that in (III,Mn)V ferromagnetic semiconductors the holes (having larger mass and exchange constant) are much more effective in the demagnetization process than the electrons.

Fig. 10.2 and 10.3 illustrate the dependence of W_{+-} from Eq. (10.30) on temperature $T_{\rm e}$, spin splitting Δ, and carrier concentration. We use the density of states of a parabolic band, with effective mass $m_{\rm eff}$=1, which roughly corresponds to the density-of-states mass in the valence band of GaMnAs. W_{+-} goes to zero for low carrier temperature, when phase-space blocking limits the number of states which can scatter. It also decreases for increasing spin-splitting Δ, when the num-

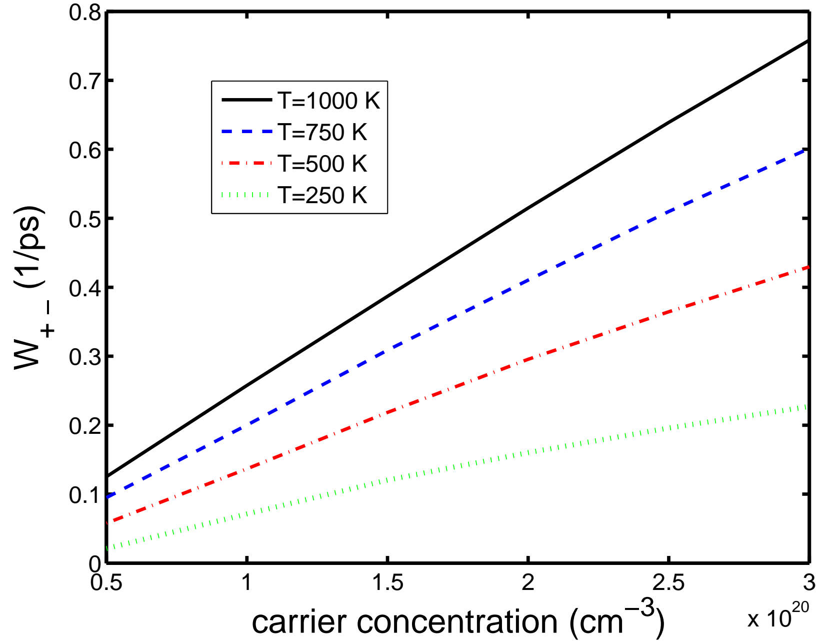

Figure 10.3: Transition rate W_{+-} for Δ=0.15 eV and different carrier temperatures, as a function of carrier density. Other parameters are the same as in Figure 10.2

ber of minority spins available for spin-flip goes down. This effect is stronger for smaller carrier concentrations and lower temperatures. For $T_{\rm e}$ close to 1000 K the corresponding characteristic time T_1 is of the order of a picosecond. Whether a full demagnetization occurs depends on the rate of energy relaxation of carriers. If the carrier temperature does not drop significantly within the time $T_1(0)$ (calculated at the initial carrier temperature $T_{\rm e}$), then a significant demagnetization occurs on this time-scale. On the other hand, if the $T_{\rm e}$ changes strongly on the scale of $T_1(0)$, then we have to solve our equations with $W_{+-}(t)$ updated according to carrier temperature changes from Eq. (10.36). We are interested in the dynamics occurring during the first picosecond. When $T_1(t)$ becomes much larger than 1 ps, then for our purposes the demagnetization process is effectively stopped. Such an effect of cooling of carriers on demagnetization is illustrated in Figure 10.4. For all energy relaxation times τ_E the initial slope of $\langle S_z(t)\rangle$ is the same, given approximately by Eq. (10.38) evaluated for $T_{\rm e}(0)$, but the time at which the demagnetization ceases

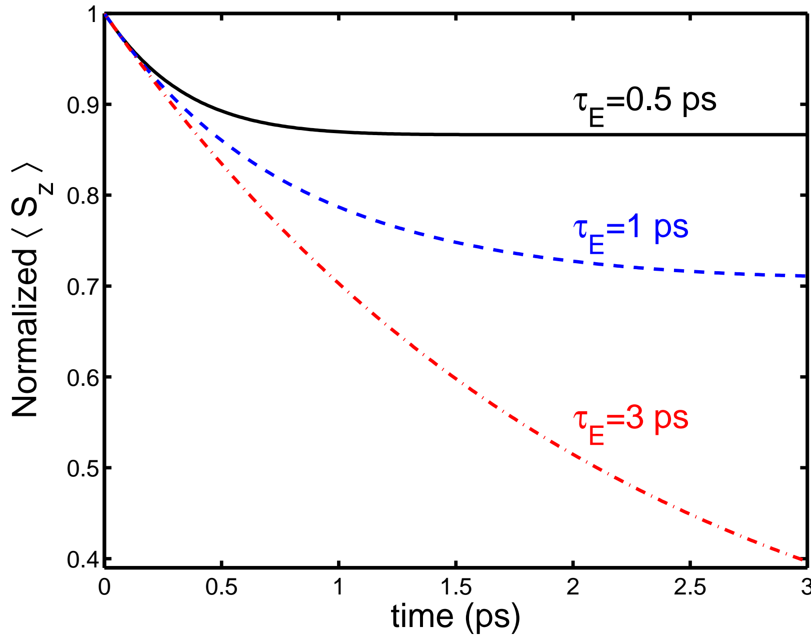

Figure 10.4: Demagnetization of the localized spins S=5/2 (normalized to 1) in a single band model with m_{eff}=1 and γ=50 meV·nm^3 for different energy relaxation times of carriers. The concentration of carriers n_c=10^{20} cm^{-3}, and the density of localized spins is such that the band splitting Δ=150 meV (corresponding to $x\approx$0.055 in GaMnAs).

and the saturation value depend on τ_E. This shows that the time-scale on which the ultrafast demagnetization occurs can be given by τ_{E}, which is not related to magnetic properties of the material. From this point of view, it is not the fact that the magnetization drop occurs in less than a picosecond which is interesting. Instead it is the *magnitude* of the demagnetization which demands explanation.

10.E.3 The effects of the dynamic spin polarization of carriers: $\Delta\mu\neq 0$

The efficiency of the "inverse Overhauser effect" is limited by the finite spin relaxation time of the carriers. Each spin flip which leads to the demagnetization, if not followed by carrier spin relaxations, diminishes the phase space available for next transition of this kind. The result is the decrease of the net number of spin-flips during the time τ_{E}, which translates into smaller total demagnetization.

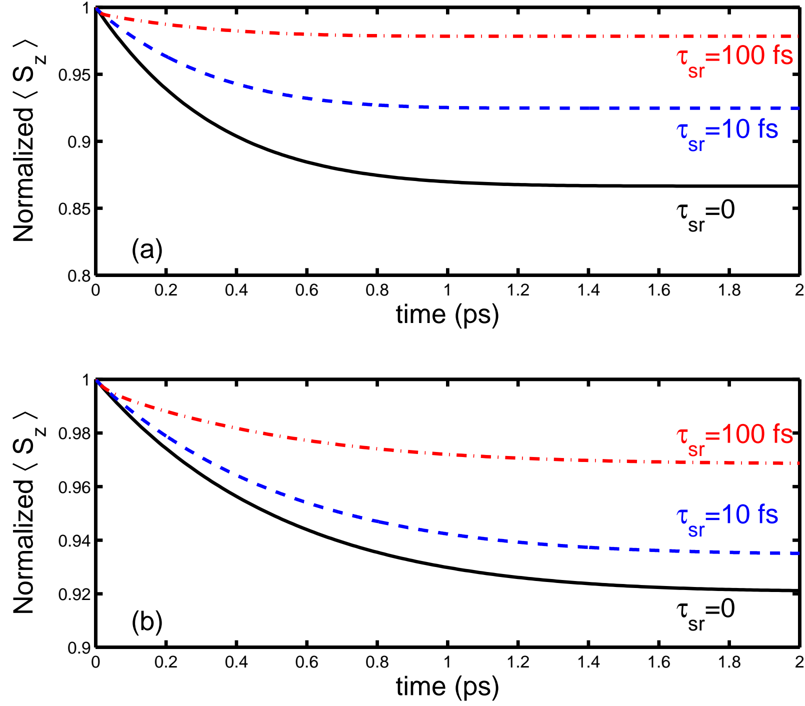

Figure 10.5: Demagnetization of the localized spin S for different carrier spin relaxation times, with energy relaxation time τ_{E}=0.5 ps. The effective mass of a single spin-split band is (a) m_{eff}=1 and (b) m_{eff}=0.5. All the other parameters are same as in Fig. 10.4. The total drop in magnetization becomes smaller for longer carrier spin relaxation times.

Let us concentrate on the case in which W_{+-} is the transition which leads to the demagnetization of the localized spins. The corresponding electron spin flip is from spin $\uparrow$ to $\downarrow$, so that the demagnetization of S spins leads to $\Delta\mu<0$. In the limit of negligible δ and $\Delta\mu$ smaller than $k_B T_{\mathrm{e}}$, we can approximate Eq. (10.30) by

$$W_{+-}(t) \approx \frac{\gamma^2}{4}\frac{2\pi}{\hbar}k_B T_{\mathrm{e}}(t) D_+(\mu_\downarrow) D_-(\mu_\downarrow) \times\left(1+\frac{\Delta\mu}{2k_B T_{\mathrm{e}}}+...\right) . \tag{10.39}$$

From this we see that W_{+-} decreases in the presence of dynamic spin polarization.

When $|\Delta\mu|$ becomes comparable to $k_B T_\text{e}$, W_{+-} goes to zero.

A rough estimate of what τ_sr is short enough to be considered instantaneous can be given assuming a constant density of states D for both spins. The localized spin splitting is then $|\delta|=|\gamma\Delta|D/2$, and the second term in Eq. (10.37), corresponding to spin relaxation can be written as $D\Delta\mu/2n_c\tau_\text{sr}$. We want it to dominate over the first term (spin transfer from localized S), for $\Delta\mu$ small enough that the transition rate W_{+-} is still unaffected by such dynamic spin splitting, i.e. for $\Delta\mu \ll k_B T_\text{e}$. The resulting inequality is

$$\frac{Dk_B T_\text{e}}{4Sn_i} > W_{+-}(\Delta\mu \approx 0, T_\text{e})\tau_\text{sr} \ , \tag{10.40}$$

which means that the ratio of the density of carriers available for the spin flip to the localized spin density is larger than the product of spin-flip rate and carrier spin relaxation time. Using Eq. (10.38) we can transform this inequality into a very simple, but physically less intuitive form:

$$\tau_\text{sr} < \frac{\hbar}{4\pi\delta} \ , \tag{10.41}$$

In (III,Mn)V semiconductors for typical value of localized spin splitting δ is a couple of meV, the spin relaxation time has then to be smaller than 100 fs for spin bottleneck to become unimportant.

The "spin bottleneck" effect is illustrated in Figure 10.5, where calculated $\langle S_z(t)\rangle$ are plotted for different values of carrier spin relaxation time τ_sr. The bottleneck effect is stronger in Figure 10.5a, where the effective mass m_eff=1 and carrier concentration n_c=10^{20} cm^{-3}. In Figure 10.5b, where m_eff=0.5, the difference between results for τ_sr=10 fs and τ_sr=0 is smaller. When the effective mass m_eff is smaller, while keeping n_c and Δ the same, the average carrier spin is decreased, as the Fermi energy becomes larger compared with Δ. Then δ is smaller, making the inequality (10.41) easier to fulfill.

10.F Demagnetization due to holes in the valence band of (III,Mn)V semiconductor

For the case of (III,Mn)V semiconductors the carriers relevant for ultrafast demagnetization are the holes. If they reside in an impurity band, the single band theory described above could be applied, but currently there is no simple quantitative model for this case. Below we perform calculations for the case of holes residing inside the valence band. We use an "effective Hamiltonian" model [29, 175] in which a mean-field p-d term from Eq. (10.8) is added to the 6 band Luttinger Hamiltonian (see Appendix B). In this way we can analyze quantitatively the influence of the strong spin-orbit interaction on the spin-flip transition rate.

A typical plot of energy dispersions in (III,Mn)V calculated by $\mathbf{k}\cdot\mathbf{p}$ method with exchange splitting Δ=0.15 eV is shown in Figure 10.1. The corresponding spin-resolved densities of states are shown in Figure 10.6. Their calculation is described in Appendix E. In order to calculate the W_{+-} transition rate we cannot use Eq. (10.30) which requires only the densities of states. In the p symmetry band the matrix elements of carrier spin ladder operators $\hat{s}^{\pm}$ are non-trivial due to spin-orbit coupling, and cannot be neglected. The full Eq. (10.29) has to be used.

The presence of strong spin-orbit interaction suppresses the spin-flip transition rate, compared to the value predicted by Eq. (10.30). If we disregard for a moment the orbital parts of the $|n\mathbf{k}\rangle$ eigenstates, the squared matrix element $|\langle n'\mathbf{k}'|\hat{s}^{-}|n\mathbf{k}\rangle|^2$ is maximal when the spin part of $|n\mathbf{k}\rangle$ state is $|\uparrow\rangle$, and the spin part of $|n'\mathbf{k}'\rangle$ is $|\downarrow\rangle$. If both states contained equal mixtures of spin up and down, the squared matrix element would be 1/4. When the orbital parts of the states are taken into account, the spin-orbit interaction diminishes the matrix elements between the states with different spin character, because it aligns orthogonal orbital wave functions (of different orbital angular momentum l) with opposite spins s. In the limit of infinite spin-orbit interaction, a spin-flip between pure spin-up and spin-down states is impossible, because the orbital parts of $|n\mathbf{k}\rangle$ states are exactly

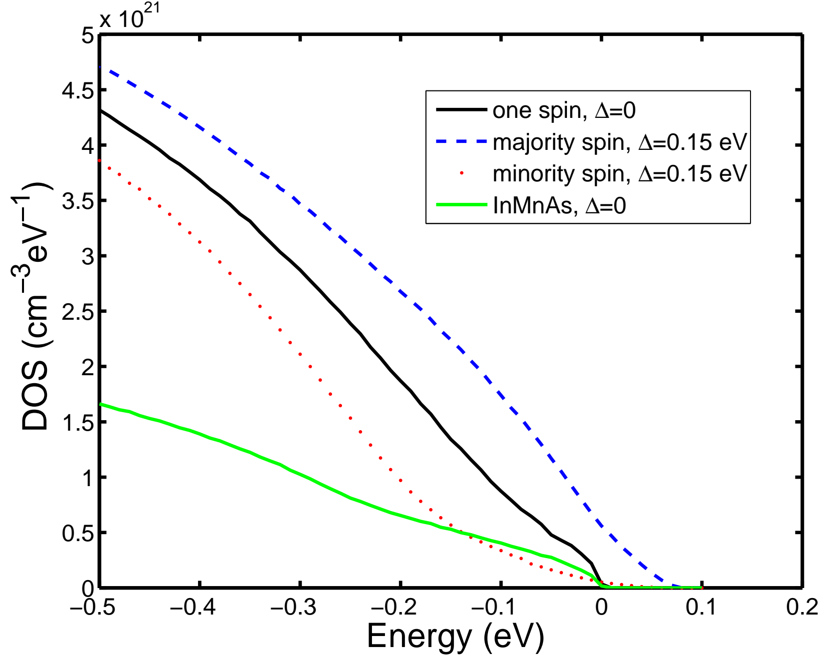

Figure 10.6: Valence band spin-resolved densities of states in GaMnAs. The solid lines are for single spin with Δ=0 in GaMnAs and InMnAs. Dashed and dotted lines are majority and minority spin for splitting Δ=0.15 eV in GaMnAs.

orthogonal. This limit is realized in the case of the 4 band Luttinger Hamiltonian for the holes. We have evaluated analytically the spin-flip transition rate in the spherical 4×4 Luttinger model at zero spin splitting, and obtained that the result of the exact Eq. (10.29) is smaller by a factor of 5/18 than the value obtained from densities of states in Eq. (10.30) (see Appendix D for derivation). This sets a limit on how much the spin-orbit interaction can suppress the transition rates for small Δ in the full 6 band model.

For the actual calculation of the time-dependence of magnetization, we have evaluated the transition rates from Eq. (10.29) using the band-structure obtained from the 6×6 Luttinger Hamiltonian (for the details of the numerical procedure see Appendix E). In all the following calculations, we have put δ=0, which is justified by the smallness of δ in ferromagnetic semiconductors, and the fact that we are primarily interested in the regime of high T_{e}, where δ can be completely

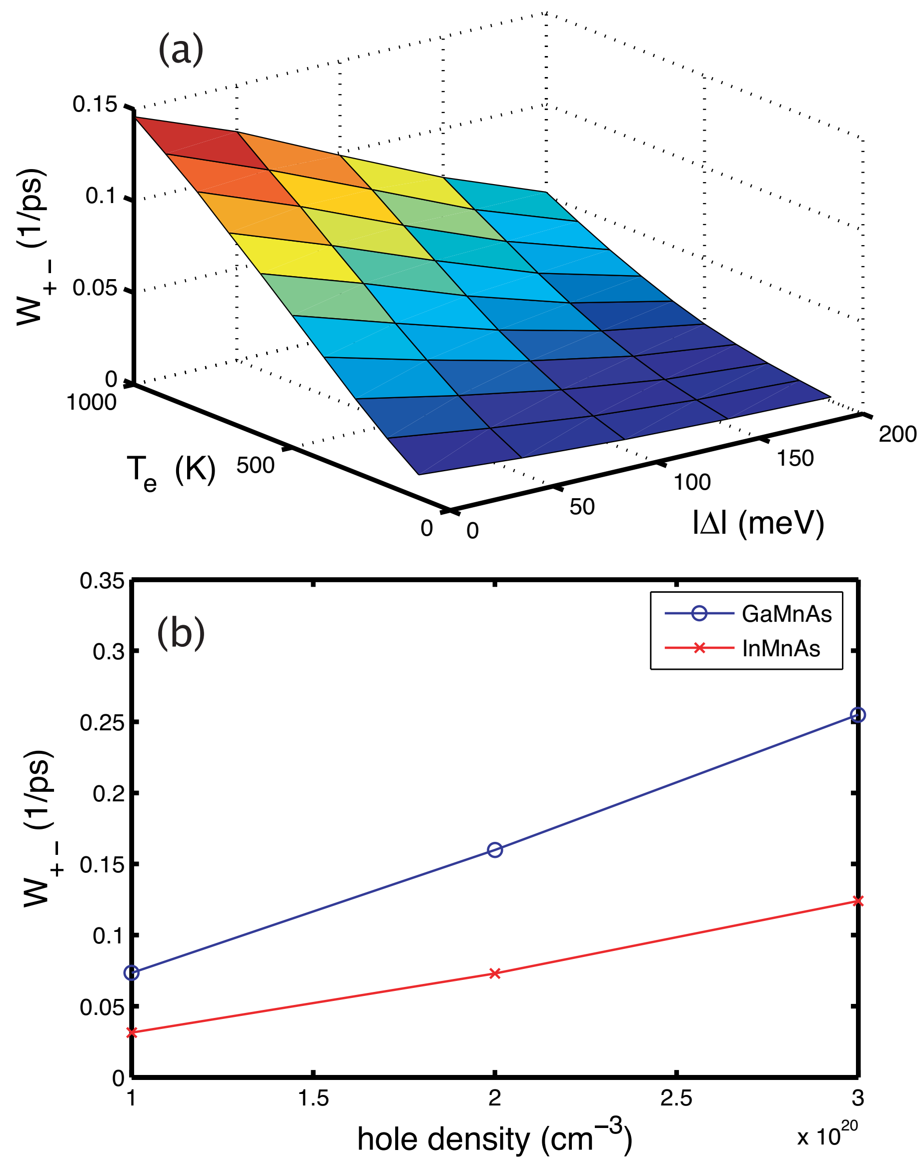

Figure 10.7: (a) Reduced transition rate W_{+-} in GaMnAs for hole density p=10^{20} cm^{-3} and no dynamic polarization of holes ($\Delta\mu$=0). Analogous plots for other values of p and for InMnAs look qualitatively similar, only the overall magnitude of W_{+-} changes. (b) Hole density dependence of W_{+-} at T_{e}=1000 K and spin splitting Δ=−0.15 eV (the lines are guides for the eye).

disregarded. In Figure 10.7 we plot W_{+-} for GaMnAs and InMnAs for various carrier temperatures, exchange splittings and hole densities. The transition rates are larger for GaMnAs, which can be traced mostly to larger density of states in the valence band compared to InMnAs.

The presence of strong spin-orbit interaction makes including the dynamic spin polarization of carriers much harder than in a single-band case (discussed in Section 10.E.3). Due to a large spin-orbit splitting $\Delta_{\text{SO}}\simeq 0.3-0.4$ eV the $|n\mathbf{k}\rangle$ states have mixed spin character even in presence of exchange splitting $\Delta\approx 0.1$ eV, and a simple introduction of different distribution functions f_s for two spin directions is not possible. Performing an ensemble Monte Carlo calculation of dynamics of strongly excited holes [206] with spin degree of freedom taken into account is a vast undertaking beyond the purpose of this investigation. We resort to an approximate method of including the effects of non-zero $\Delta\mu$.

Above we have calculated the exact transition rates for $\Delta\mu=0$. We have also calculated the corresponding W_{+-} assuming constant matrix elements and only taking spin-resolved densities of states calculated from Luttinger Hamiltonian (Eq. (10.30)). The inclusion of matrix elements leads to decrease of W_{+-} by a factor of 0.25-0.3 in the most relevant range of high T_{e} and $\Delta\simeq 0.1$ eV (not shown). We assume that this ratio of exact and DOS-derived W_{+-} also holds in the case of a finite $\Delta\mu$ (but small compared to E_F and $k_B T_{\text{e}}$). We have calculated the demagnetization with finite spin relaxation time of the holes using the properly down-scaled transition rates from Eq. (10.30) with finite $\Delta\mu$. The results are shown in Figure 10.8. The effect of spin bottleneck on demagnetization is clearly very weak for $\tau_{\text{sr}}\leq 10$ fs. For $\tau_{\text{sr}}=100$ fs the total demagnetization is diminished by $\sim$50% compared to the case of short τ_{sr}. These results agree with estimates from the inequality (10.41), which is fulfilled for $\delta\sim 1$ meV and $\tau_{\text{sr}}=10$ fs.

In the presence of the strong spin-orbit interaction, the hole spin relaxation is expected to be very fast, occurring on the momentum scattering time-scale [19]. For example, in pure GaAs the spin relaxation of holes was measured to be about

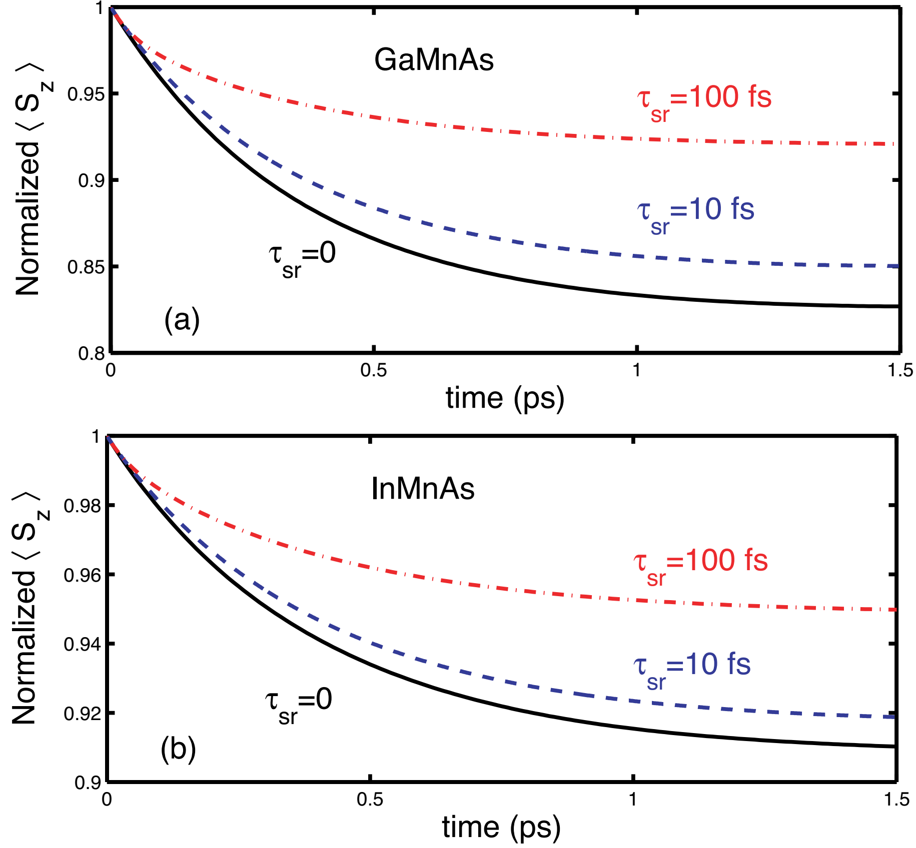

Figure 10.8: Demagnetization of the Mn spin in (a) GaMnAs and (b) InMnAs. The solid lines are calculated using the exact transition rates at $\Delta\mu$=0 (dynamical spin polarization of carriers is neglected). The dashed lines come from the approximate calculation including the finite hole spin relaxation time $\tau_{\rm sr}$ (see text for details). The initial temperature of holes if $T_{\rm e}$=1000, the hole density is p=3 × 10^{20} cm^{-3}, the exchange integral β=−50 meV·nm^3, and the molar fraction of Mn is x=0.054 (initial spin splitting Δ=−0.15 eV). The energy relaxation time $\tau_{\rm E}$ is 0.5 ps.

100 fs at room temperature [207]. The calculated [208] momentum scattering of holes in GaMnAs at low temperature is about 10 fs, and it is expected to be shorter when the holes are highly excited. There is one caveat in the case of exchange spin-split bands in (III,Mn)V. The lifting of the heavy-light hole degeneracy by confinement in quantum wells makes the spin relaxation time longer [209, 210], with measured values of 4 ps for holes close to Γ point in modulation-doped GaAs quantum wells [211]. An analogous effect is expected in exchange-split bands. However, for the carrier densities and temperatures under consideration we are

mostly interested in spin relaxation of holes with quite large wavevectors ($|\mathbf{k}|\approx 1-3$ nm^{-1}). For such large $|\mathbf{k}|$ the effect of lifted degeneracy on spin relaxation becomes much weaker [210]. For example, at a wavevector of this magnitude in the direction perpendicular to the magnetization the band-mixing terms in the Luttinger Hamiltonian overcome the p-d interaction, and the spin splitting becomes negligible. Taking all this into account it is reasonable assume that in an excited and disordered sample the hole spin relaxation time should be shorter than in pure GaAs.

In the experiments on (III,Mn)V spin lifetimes of electrons between 1 ps in highly excited InMnAs [212, 213] and 30 ps in much more weakly excited GaMnAs [214] were seen. To the best of our knowledge, no signal attributable to hole spin relaxation has ever been seen on a time-scale of the temporal resolution of the experiments. If $\tau_{\rm sr}\leq 10$ fs, the measurements would be particularly challenging due to time-resolution constraints on the laser pulse time. Also, at such time-scale the carrier dynamics is in the non-Markovian regime [215], and $\tau_{\rm sr}$ is a typical time-scale of the spin-dependent correlated relaxation dynamics.

In Fig. 10.8 we can see that for $\tau_{\rm sr}<100$ the spin bottleneck effect is qualitatively unimportant, and it becomes negligible for $\tau_{\rm sr}=10$ fs.Without the bottleneck, we obtain a typical magnitude of demagnetization in (III,Mn)V within a picosecond to be of the order of 10%. For the same carrier density, initial $T_{\rm e}=1000$ K and $\tau_{\rm E}=0.5$ ps, the drop in magnetization is more pronounced in GaMnAs (20% demagnetization) than in InMnAs (10%). A discussion of the connection between these calculations and experiments follows below.

10.G Comparison with experimental results

We can estimate the initial temperature of carriers in experiments on InMnAs from Ref. [170] in the following way. There are two time-scales in demagnetization: an ultrafast one (<1 ps), and a subsequent much slower (~100 ps) demagnetiza-

tion due to spin-lattice relaxation. For example, for pump fluence of 3 mJ/cm^2, an ultrafast quenching of $\sim$ 50% of magnetization was followed by a complete demagnetization 100 ps later. On the latter time-scale we can safely use a thermal description of the spin system. The full demagnetization means that the localized spin temperature T_S had risen above the Curie temperature, which was 50 K in the sample used. This tells us that 100 ps after the excitation the lattice temperature T_L was at least 50 K. The energy (per atom), which had to be transferred into the lattice to heat it up from initial temperature T_i (before the excitation) up to the final T_L is given by

$$\Delta E_L = \int_{T_i}^{T_L} c_L(T) dT \ , \tag{10.42}$$

where c_L is the specific heat of the lattice (per atom), which in the temperature range of interest is given by the Debye formula:

$$c_L(T) = \frac{12\pi^4}{5} k_B \left(\frac{T}{\Theta_D}\right)^3 \ , \tag{10.43}$$

where Θ_D=280 K is the Debye temperature of InAs.

The energy transferred into the lattice needs now to be related to the energy deposited initially by the light pulse into the valence band. In the process of absorption, the energy of the pump photon ($\hbar\omega$=0.6 eV) is split into a kinetic energy of a created hole and an energy of an excited state within a gap (we disregard the photoelectrons because the low density of states in the conduction band makes this excitation channel insufficient to explain the experiments). The Fermi level before the excitation is situated between 0.1 and 0.3 eV below the top of the valence band for hole densities of 10^{20} and 3×10^{20} cm^{-3}, respectively. Thus, the energies of the newly created holes are a sizable fraction of the photon energy. As a rather safe estimate we will take the fraction of the pump pulse energy imparted to the holes as R=1/4.

Now we can derive an estimate of the carrier temperature $T_\mathrm{e}(0)$ just after the absorption of the pump pulse. We assume that after 100 ps all the absorbed energy has been transferred to the lattice. The observed spin temperature T_S is larger than

$50K$, and gives a lower bound for the final lattice temperature T_L. We calculate the energy given to the lattice using Eqs. (10.42) and (10.43), with initial T_i=10 K and final T_L=50 K A fraction R of this energy was excess kinetic energy of holes in the valence band after the excitation. Using the density of states of InMnAs with Δ=0.15 eV calculated before, we obtain the temperature of carriers which gives such an excess energy. In this way we obtain an estimate of the initial T_{e}, which we find to be between 1500 and 1000 K for hole densities changing between 10^{20} and 3×10^{20} cm^3. The analogous calculation in GaMnAs gives T_{e} smaller by a factor of 2 (due to the larger density of states). These results justify our use of a typical initial T_{e}=1000 K.

Let us now address the corresponding demagnetization in InMnAs for pump fluence of 3 mJ/cm^2. The hole concentration before the excitation is about 3×10^{20} cm^{-3}, estimated from critical temperature of 50 K and magnetization measurements [170]. After the excitation the total number of holes is larger but, because the initial p is not certain, we will simply use a value of total p=3×10^{20} cm^{-3}. The measured sample was a 25 nm thick layer of InMnAs grown on GaSb. For such thickness, the confinement leads to formation of hole subbands, with typical energy spacing between them of the order of 10 meV. This confinement energy is much less than the disorder broadening and the thermal spread of photoexcited carriers (both $\sim$0.1 eV), so that our calculation of spin-flip transition rates using the bulk band-structure should be a good approximation. In the previous section, we have seen that for p=3×10^{20} cm^{-3} the sub-picosecond drop in magnetization is about 10%. Experimentally a 50% drop in Kerr signal was observed within $\sim$200 fs after the pump pulse. The step-like character of the magnetization drop is not reproduced by our theory, which predicts a smoother demagnetization. However, the carrier-induced artifacts (termed “dichroic bleaching” in Ref. [129]) obscuring the magnetization dependence of the magnetooptical signal are possible at very short time-scale. The magnitude of the total demagnetization is in qualitative agreement with our calculations.

For pump fluence of 10 mJ/cm^2, for which a complete quenching of ferromagnetic order is observed, the role of multi-photon absorption processes becomes pronounced, and photocarriers are created in a very large region of the Brillouin Zone (as in experiments from Ref. [216], where a pump with $\hbar\omega$=3.1 eV was used in GaMnAs). Our $\mathbf{k}\cdot\mathbf{p}$ model with "rigid" spin splitting (i.e. $\mathbf{k}$-independent exchange constant) is not applicable far away from the Γ point. Also, for very strong excitation the assumption of quasi-thermal distribution of holes can fail.

In GaMnAs the experiments show a similar behavior [44] after 1 picosecond, with 30% magnetization drop for fluence of $\sim$8 mJ/cm^2. This value is very close to the predictions of our theory for p=3 $\times$ 10^{20} cm^{-3}. For the same fluence InMnAs was already nearly completely demagnetized. Although our theory predicts larger demagnetization in GaMnAs than in InMnAs, in order to make meaningful comparisons one has to achieve comparable excitation parameters (total p and T_e after the pulse).

10.H Summary

We have presented the investigation of the ultrafast demagnetization induced by an incoherent light excitation in a system described by the sp-d model. The physical picture of demagnetization is very transparent, with sp-d interaction providing the mechanism of spin transfer from the localized spins into the system of excited carriers. This process is closely related to effects known from systems of electronic and nuclear spins coupled by hyperfine contact interaction, and thus we have termed it the inverse Overhauser effect. The demagnetization basically comes from very fast T_1 relaxation of the localized spins due to sp-d interaction with the hot carriers' spins. In a simple one-band model the rate of spin flip scattering of itinerant and localized spins is proportional to the square of the sp-d exchange constant, the product of electronic densities of states at Fermi energy for two spin directions, and the temperature of the carriers. Due to the carrier

temperature dependence, the rapid demagnetization can occur only for a time of the order of energy relaxation time τ_{E}. Thus, the sub-picosecond time scale of the demagnetization process simply comes from the characteristic time of carrier-phonon interaction. The total magnitude of demagnetization during the τ_{E} time depends only on the spin-flip scattering efficiency if the carrier system is a good spin sink, i.e. the carrier spin relaxation time τ_{sr} is shorter than the time-scale on which the dynamic spin polarization of carriers builds up. A long τ_{sr} leads to spin bottleneck that suppresses the demagnetization.

A large part of the discussion was aimed at the specific case of (III,Mn)V semiconductors. There, a non-trivial band structure with spin-orbit interaction has to be taken into account. We have performed the calculations of spin-flip transition rate using an effective $\mathbf{k}\cdot\mathbf{p}$ Hamiltonian approach. An approximate calculation of the effects of dynamical spin polarization of holes has been used to argue that the holes can be treated as a perfect sink for the angular momentum transferred from the localized spins. A qualitative agreement with demagnetization experiments in these materials was obtained: the theory shows that the magnetization can drop by $\sim$10% within the energy relaxation time of the holes. More theoretical and experimental work on electronic and optical properties of (III,Mn)Vs, will be necessary in order to better reconcile experiments and theory.

10.I Acknowledgements

The text of Chapter 10, in part, is a reprint of the material as it appears in Łukasz Cywiński and L.J. Sham, *Ultrafast demagnetization in the sp-d model: a theoretical study*, arXiv preprint cond-mat/0703049, (to appear in Phys. Rev. B). The dissertation author was the primary investigator and author of this article.

Appendix A

Derivation of the Master equation for the localized spin dynamics

General theory: Redfield equation with time-dependent coefficients

The Hamiltonian of the localized S spin and the carriers system is written as

$$\hat{H}_{S-C} = \hat{H}_0 + \hat{V} = \hat{H}_C + \hat{H}_C^{mf} + \delta \hat{S}^z + \hat{V} \ , \tag{A.1}$$

where $\hat{H}_C$ is the carrier band Hamiltonian (Eq. (10.2)), $\hat{H}_C^{mf}$ is the mean-field spin-splitting from Eq. (10.8), δ is the mean-field localized spin splitting defined in Eq. (10.11) and the spin-flip term of the localized spin $\hat{V}$ is coming from part of sp-d interaction which is off-diagonal in $\hat{S}^z$ basis:

$$\hat{V} = \hat{S}^+ \hat{F}^- + \hat{S}^- \hat{F}^+ \equiv \sum_i \hat{S}^i \hat{F}^i \ , \tag{A.2}$$

with carrier spin-flip operators $\hat{F}^{\pm}$ operators given by Eq. (10.19). In this equation we have introduced a general notation with i index labeling different pairs of products of the spin system S^i and the bath F^i operators. In the case at hand here, the same index i denotes *different* raising/lowering indices of F and S operators. This notation is slightly cumbersome, but it is general and it will allow for a quick transition to a different set of operators in the definition of $\tilde{V}$ (e.g. sometimes it is more convenient to write $\tilde{V}$=$\tilde{S}^x \tilde{F}^x + \tilde{S}^y \tilde{F}^y + \tilde{S}^z \tilde{F}^z$). We will keep it throughout

this section for the sake of generality, and use the specific form of $\hat{V}$ in the next section.

We express all the operators in the interaction picture with respect to some reference time t_0. We employ a notation in which a Schrödringer picture operator $\hat{A}$ is denoted by $\tilde{A}(t)$ in the interaction picture. The density matrix of the whole system (localized spins and carriers) is given in the interaction picture by

$$\tilde{\rho}(t) = \hat{U}^{-1}(t, t_0)\ \hat{\rho}(t)\ \hat{U}(t, t_0)\ , \tag{A.3}$$

where the free evolution operator $\hat{U}_0(t, t_0)$ is given by:

$$\hat{U}_0(t, t_0) = \mathcal{T} \exp\Big(-\frac{i}{\hbar} \int_{t_0}^{t} \hat{H}_0(t) \Big)\ , \tag{A.4}$$

in which $\mathcal{T}$ denotes the time-ordering operator. The operators $\tilde{A}(t)$ are defined analogously. The time-dependence of $\hat{H}_0(t)$ comes from the mean-field spin splittings Δ and δ, which change during the magnetization dynamics. However, if the difference $t - t_0$ is smaller than the characteristic time on which $\hat{H}_0(t)$ changes, we can use instead of Eq. (A.4) a simpler expression without the time-ordering. Let us define the temporally "local" interaction picture for times t sufficiently close to a certain time t_n:

$$\tilde{A}_n(t) = \exp\Big(\frac{i}{\hbar}\hat{H}_0(t_n)(t - t_n)\Big)\hat{A}(t) \exp\Big(-\frac{i}{\hbar}\hat{H}_0(t_n)(t - t_n)\Big)\ . \tag{A.5}$$

The above expression is a good approximation to the Eq. (A.3) with t_0=t_n for $t - t_n$ short enough for H_0 to be approximated by a constant.

The derivation relies on the fundamental Markovian assumption of very short time-scale of the bath "memory" (quantified by the bath correlation time τ_c defined below) compared to the characteristic time-scales of the dynamics of the system (the localized spins) interacting with the bath (the carriers). We coarse-grain the time into steps $t_{n-1}, t_n, t_{n+1}, ...$ which are separated by intervals Δt fulfilling the inequalities:

$$\tau_c \ll \Delta t \ll \tau_\rho\ , \tag{A.6}$$

in which the characteristic time-scale of the total system dynamics τ_ρ appears. The time Δt is long enough for the bath fluctuations to become uncorrelated, but short compared to the time on which the density matrix changes (so that we can put $\hat{\rho}(t_n)\approx\hat{\rho}(t_{n-1})$). Our goal is to derive the equation of motion for the localized spin density matrix which holds on the time-scale of Δt.

The exact equation for the dynamics of the total density matrix (in the interaction picture) is the Liouville equation:

$$\frac{\partial\tilde{\rho}(t)}{\partial t} = -\frac{i}{\hbar}[\tilde{V}(t),\tilde{\rho}(t)] \ . \tag{A.7}$$

The localized spins are described by a reduced density matrix $\tilde{\rho}_S$ defined by

$$\tilde{\rho}_S(t) = \mathrm{Tr}_C\{\tilde{\rho}(t)\} \ , \tag{A.8}$$

in which the trace is taken with respect to the carriers (C) degrees of freedom. The interaction picture is taken with respect to a certain time t_{n-1} (in Eq. (A.3) we put t_0=t_{n-1}). We integrate the Liouville equation from t_{n-1} to t_n (one coarse-graining step forward):

$$\tilde{\rho}(t_n) = \tilde{\rho}(t_{n-1}) - \frac{i}{\hbar}\int_{t_{n-1}}^{t_n}[\tilde{V}(\tau),\tilde{\rho}(\tau)]d\tau \ . \tag{A.9}$$

Then we plug this expression back into the original equation and trace out the bath degrees of freedom, obtaining the equation for the localized spin density matrix:

$$\frac{\partial}{\partial t}\tilde{\rho}_S(t_n) = -\frac{i}{\hbar}\mathrm{Tr}_C\Big\{[\tilde{V}(t_n),\tilde{\rho}(t_{n-1})]\Big\} - \frac{1}{\hbar^2}\int_{t_{n-1}}^{t_n}\mathrm{Tr}_C\Big\{[\tilde{V}(t_n),[\tilde{V}(\tau),\tilde{\rho}(\tau)]]\Big\}d\tau \ . \tag{A.10}$$

Now we assume that the density matrix $\tilde{\rho}$ can be simply factorized in the localized spin (S) and the carrier bath (C) density matrices:

$$\tilde{\rho}(t) \approx \tilde{\rho}_C(t)\tilde{\rho}_S(t) \ , \tag{A.11}$$

and we define the bath average of the operator $\tilde{A}(t)$ as

$$\langle\tilde{A}(t)\rangle_{t_n} \equiv \mathrm{Tr}_C\{\tilde{\rho}_C(t_n)\tilde{A}(t)\} \ . \tag{A.12}$$

The first term on the right-hand side of the Eq. (A.10) is zero, because

$$\langle \tilde{V}(t_n) \rangle_{t_{n-1}} \sim \langle \tilde{F}^{\pm} \rangle_{t_{n-1}} = 0 \ , \tag{A.13}$$

for the average localized spin $\langle \mathbf{S} \rangle$ oriented along one of high-symmetry directions of the crystal (see Appendix C). In the second term we note that under the integral the density matrix $\tilde{\rho}(\tau)$ is needed for times $\tau \in [t_{n-1}, t_n]$. According to our assumptions, $\tilde{\rho}$ does not change significantly in such a time period, and we can simply replace $\tilde{\rho}(\tau)$ by $\tilde{\rho}(t_n)$ in Eq. (A.10). Thus we obtain a closed equation for $\tilde{\rho}(t_n)$:

$$\begin{aligned} \frac{\partial}{\partial t}\tilde{\rho}_S(t_n) &= -\frac{1}{\hbar^2}\int_{t_{n-1}}^{t_n} \langle [\tilde{V}(t_n), [\tilde{V}(\tau), \tilde{\rho}_S(t_n)]] \rangle_{t_n} \, d\tau \\ &= -\frac{1}{\hbar^2}\int_{0}^{\Delta t} \langle [\tilde{V}(t_n), [\tilde{V}(t_n - t'), \tilde{\rho}_S(t_n)]] \rangle_{t_n} \, dt' \end{aligned} \tag{A.14}$$

where in the second line we have changed the integration variable to $t'{=}t_n{-}\tau$. Since we assume that $\Delta t{=}t_n - t_{n-1}$ is short enough for the change in the total density matrix $\tilde{\rho}(t_n) - \tilde{\rho}(t_{n-1})$ to be small, and consequently $H_0(t){\approx}H_0(t_n){\approx}\ H_0(t_{n-1})$, we can use the “local” interaction picture (Eq. (A.5)) for the operators in the above equations.

Now we plug in the explicit form of the localized spin-bath interaction from Eq. (A.2), and after some algebra we arrive at the Master equation:

$$\begin{aligned} \frac{\partial}{\partial t}\tilde{\rho}_S(t_n) = -\frac{1}{\hbar^2}\sum_{i,j}\int_0^{\Delta t} dt' \Bigg(& [\tilde{S}^i(t_n), \tilde{S}^j(t_n - t')\tilde{\rho}_S(t_n)]\, C^{>}_{ij}(t_n; t') + \\ & - [\tilde{S}^i(t_n), \tilde{\rho}_S(t_n)\tilde{S}^j(t_n - t')]\, C^{<}_{ij}(t_n; t') \Bigg) \ , \end{aligned} \tag{A.15}$$

where we have defined the correlation functions:

$$C^{>}_{ij}(t_n; t) = \langle e^{iH_0(t_n)t/\hbar}\hat{F}^i e^{-iH_0(t_n)t/\hbar}\,\hat{F}^j \rangle_{t_n} = \langle \tilde{F}^i_{n-1}(t_n)\tilde{F}^j_{n-1}(t_n - t) \rangle_{t_n} \tag{A.16a}$$

$$C^{<}_{ij}(t_n; t) = \langle \hat{F}^j\, e^{iH_0(t_n)t/\hbar}\hat{F}^i e^{-iH_0(t_n)t/\hbar} \rangle_{t_n} = \langle \tilde{F}^j_{n-1}(t_n - t)\tilde{F}^i_{n-1}(t_n) \rangle_{t_n} \tag{A.16b}$$

They are defined just like the usual correlation functions (see e.g. Ref. [143]), only the operators are in the “local” interaction picture at time t_n. After introducing

the correlation functions C_{ij} we can define the bath correlation time τ_c as such that for $|t|>\tau_c$ the correlation functions defined above are practically zero. The use of the "local" interaction picture is justified by the fact that τ_c is much smaller than the time on which H_0 changes. Now we can see, that the derivative of $\tilde{\rho}_S$ at time t_n depends only on the history of the bath for times at most τ_c before t_n. Since $\Delta t \gg \tau_c$, we can as well extend the limits of dt' integration to infinity. We also revert from a coarse-grained to a continuous time notation, with time t replacing t_n. We only have to remember not to use our equations to investigate the dynamics on time-scale smaller than $\Delta t \gg \tau_c$. The Master equation for the localized spin density matrix is finally given by:

$$\frac{\partial}{\partial t}\tilde{\rho}_S(t) = -\frac{1}{\hbar^2}\sum_{i,j}\int_0^\infty dt' \Bigg([\tilde{S}^i(t), \tilde{S}^j(t-t')\tilde{\rho}_S(t)]\, C^>_{ij}(t;t') + - [\tilde{S}^i(t), \tilde{\rho}_S(t)\tilde{S}^j(t-t')]\, C^<_{ij}(t;t') \Bigg) \ . \tag{A.17}$$

The derivation of the equations for different elements of the localized spin density matrix is a rather tedious exercise. The matrix elements are

$$\tilde{\rho}^S_{mm'}(t) = \langle m|\tilde{\rho}_S(t)|m'\rangle \ , \tag{A.18}$$

with m,m' labeling the different energy levels of the localized spin in the mean-field $\delta\hat{S}_z$. A general form of the Master equation for $\tilde{\rho}^S_{mm'}$ derived using the above approximations is known as the Redfield equation [217, 218, 199], which we write below after reverting to the Schrödringer picture

$$\frac{d}{dt}\hat{\rho}^S_{nm}(t) = -i\omega_{nm}\hat{\rho}^S_{nm}(t) + \sum_{ab}\mathcal{R}_{nmab}(t)\hat{\rho}^S_{ab}(t) \ , \tag{A.19}$$

where $\mathcal{R}_{nmab}(t)$ are the elements of the Redfield tensor and $\omega_{nm}=(E_n - E_m)/\hbar$, with the energies E_n of the localized spin experiencing the mean-field exchange splitting. In the standard case (see e.g. [218, 199]) the elements of the Redfield tensor are constants. Here, their time dependence comes from the dynamics of the bath. They can be written as

$$\mathcal{R}_{nmab}(t) = -\sum_k(\Gamma^+_{nkka}(t)\delta_{mb} + \Gamma^-_{bkkm}(t)\delta_{na}) + \Gamma^+_{bmna}(t) + \Gamma^-_{bmna}(t) \ , \tag{A.20}$$

where

$$\Gamma^{+}_{mabn}(t) = \frac{1}{\hbar^2} \sum_{ij} S^{i}_{ma} S^{j}_{bn} \int_0^\infty dt'\, e^{-i\omega_{bn} t'}\, C^{>}_{ij}(t;t') \ , \tag{A.21a}$$

$$\Gamma^{-}_{mabn}(t) = \frac{1}{\hbar^2} \sum_{ij} S^{j}_{ma} S^{i}_{bn} \int_0^\infty dt'\, e^{-i\omega_{ma} t'}\, C^{<}_{ij}(t;t') \ , \tag{A.21b}$$

and S^{i}_{nm} are the matrix element of the localized spin operators between different eigenstates of $\hat{S}_z$.

Let us define the Fourier transform of the correlation function:

$$C_{ij}(t;\omega) = \int_{-\infty}^{\infty} C_{ij}(t;t') e^{i\omega t'} dt' \ . \tag{A.22}$$

Note that

$$C^{>}_{ij}(t;\omega) = C^{<}_{ji}(t;-\omega) \quad , \quad C^{<}_{ij}(t;\omega) = C^{>}_{ji}(t;-\omega) \ , \tag{A.23}$$

and that if the bath density matrix at time t is of the equilibrium form described by temperature $T_e(t)$ ($\beta_e(t){=}1/k_B T_e(t)$), then the correlation functions fulfill the Kubo-Martin-Schwinger detailed balance condition (see e.g. [143]):

$$C^{>}_{ij}(t;\omega) = e^{\beta_e(t)\hbar\omega} C^{<}_{ij}(t;\omega) \ . \tag{A.24}$$

We also write

$$\begin{aligned} \int_0^\infty C_{ij}(t;t') e^{i\omega_{nm} t'} dt' &= \int_{-\infty}^{\infty} \frac{d\omega}{2\pi} \frac{i C_{ij}(t;\omega)}{\omega_{nm} - \omega + i\eta} \\ &= i\mathcal{P} \int_{-\infty}^{\infty} \frac{d\omega}{2\pi} \frac{C_{ij}(t;\omega)}{\omega_{nm} - \omega} \ + \ \frac{1}{2} C_{ij}(t;\omega_{nm}) \ . \end{aligned} \tag{A.25}$$

where $\mathcal{P}$ denotes the principle values of the integral.

We are mostly interested in the dynamics of the diagonal elements of the density matrix, since they determine the average $\langle S_z \rangle$. Although generally $\hat{\rho}^{S}_{nn}$ can be driven by $\hat{\rho}^{S}_{ab}$ (with $a{\neq}b$) on the right-hand side of Equation (A.19), below we will show that this is not the case here. Thus, for the dynamics of $\hat{\rho}^{S}_{nn}$ only the "diagonal" elements of the Redfield tensor are important, and we write them as

$$\mathcal{R}_{nnaa}(t) = -\delta_{na} \sum_{k} W_{kn}(t) + W_{na}(t) \ , \tag{A.26}$$

where we have defined the transition rates

$$W_{nm}(t) = \Gamma^{+}_{mnnm}(t) + \Gamma^{-}_{mnnm}(t) \ . \tag{A.27}$$

Using Equations (A.21a-A.21b), (A.23) and (A.25) we get

$$W_{nm}(t) = \frac{1}{\hbar^2} \sum_{ij} S^i_{mn} S^j_{nm} C^{>}_{ij}(t;\omega_{mn}) \ . \tag{A.28}$$

Rate equation for spin-flip scattering

Let us now concentrate on our case, in which the localized spin-bath interaction is given by Eq. (A.2). In Appendix C we show that for magnetization in $\langle 100 \rangle$ and $\langle 111 \rangle$ directions only the "spin-flip" correlation functions $C_{\pm\mp}(t;t')$ are non-zero. As a result, we have

$$\Gamma_{mabn} \sim S^{+}_{ma} S^{-}_{bn} C_{-+} + S^{-}_{ma} S^{+}_{bn} C_{+-} \ , \tag{A.29}$$

and it is easy to see that the rate equations for the diagonal elements of the density matrix involve only the diagonal elements, and the equations for off-diagonal elements involve only off-diagonal ρ^S_{nm}. The rate equation for ρ^S_{nn} is

$$\frac{d}{dt}\rho^S_m = -(W_{m-1,m} + W_{m+1,m})\rho^S_m + W_{m,m+1}\rho^S_{m+1} + W_{m,m-1}\rho^S_{m-1} \ , \tag{A.30}$$

where the t dependence is understood. The transition rates are given by Equation (A.28), which we rewrite as

$$W_{m,m\pm 1} = \frac{1}{\hbar^2} |S^{\pm}_{m\pm 1,m}|^2 \, C^{>}_{\mp\pm}(t;\pm\delta/\hbar) \ , \tag{A.31}$$

in which the localized spin splitting δ appears. The Fourier transform of the correlation function is

$$C^{>}_{\mp\pm}(t;\pm\delta) = \int_{-\infty}^{\infty} e^{\pm i\delta t'/\hbar} C^{>}_{\mp\pm}(t;t') dt' \tag{A.32}$$

with

$$C^{>}_{\mp\pm}(t;t') = \frac{\gamma^2}{4V^2} \sum_{n\mathbf{k},n'\mathbf{k}'} \sum_{l\mathbf{q},l'\mathbf{q}'} \langle n\mathbf{k}|\hat{s}^{\mp}|n'\mathbf{k}'\rangle \langle l\mathbf{q}|\hat{s}^{\pm}\,|l'\mathbf{q}'\rangle \, \langle a^{\dagger}_{n\mathbf{k}}(t') a_{n'\mathbf{k}'}(t') a^{\dagger}_{l\mathbf{q}} a_{l'\mathbf{q}'} \rangle_t \ , \tag{A.33}$$

in which the eigenstates $|n\mathbf{k}\rangle$ are taken at time t. The creation and annihilation operators have the following time-dependence in the "local" interaction picture:

$$a^{\dagger}_{n\mathbf{k}}(t') = a^{\dagger}_{n\mathbf{k}} e^{i\epsilon_{n\mathbf{k}}(t)t'} \tag{A.34a}$$

$$a_{n\mathbf{k}}(t') = a_{n\mathbf{k}} e^{-i\epsilon_{n\mathbf{k}}(t)t'} \ . \tag{A.34b}$$

Using the expression for the average of the operator product:

$$\langle a^{\dagger}{}_{\alpha} a_{\beta} a^{\dagger}{}_{\gamma} a_{\delta} \rangle_t = \delta_{\alpha\beta}\delta_{\gamma\delta} \ f_{\alpha} f_{\gamma} + \delta_{\alpha\delta}\delta_{\beta\gamma} \ f_{\alpha}(1 - f_{\beta}) \ , \tag{A.35}$$

we get

$$C^{>}_{\mp\pm}(t;t') = \frac{\gamma^2}{4} \sum_{n,n'} \int \frac{d^3k}{(2\pi)^3} \int \frac{d^3k'}{(2\pi)^3} |\langle n\mathbf{k}|\hat{s}^{\mp}|n'\mathbf{k}'\rangle|^2 \, e^{i(\epsilon_{n\mathbf{k}} - \epsilon_{n'\mathbf{k}'})t/\hbar} f_{n\mathbf{k}}(1 - f_{n'\mathbf{k}'}) \ , \tag{A.36}$$

and finally the transition rates are given by

$$W_{m,m\pm1} = \frac{2\pi}{\hbar}\frac{\gamma^2}{4} |S^{\pm}_{m\pm1,m}|^2 \sum_{n,n'} \int \frac{d^3k}{(2\pi)^3} \int \frac{d^3k'}{(2\pi)^3} |\langle n'\mathbf{k}'|\hat{s}^{\pm}|n\mathbf{k}\rangle|^2 \, f_{n\mathbf{k}}(1 - f_{n'\mathbf{k}'}) \times \delta(\epsilon_{n\mathbf{k}} - \epsilon_{n'\mathbf{k}'} \pm \delta) \ . \tag{A.37}$$

Appendix B

$\mathbf{k}\cdot\mathbf{p}$ Hamiltonian for (III,Mn)V magnetic semiconductors

The $\mathbf{k}\cdot\mathbf{p}$ theory is explained in many books and review articles (see e.g. [17]). The starting point is the set of Bloch eigenstates $e^{i\mathbf{k}_0\mathbf{r}}u_n(\mathbf{r})$ at a given point $\mathbf{k}_0$ in the Brillouin zone (here it is the Γ point, $\mathbf{k}_0$=0), with n numbering the bands which we take into account. The $\mathbf{k}\cdot\mathbf{p}$ effective Hamiltonian is a $\mathbf{k}$-dependent $n\times n$ matrix, which gives us the energies and eigenvectors at a $\mathbf{k}$ point close to $\mathbf{k}_0$. We use the following set of basis states at Γ point of the III-V semiconductor:

$$
\begin{aligned}
u_1 &= |S\rangle|\uparrow\rangle \ , \\
u_2 &= i|S\rangle|\downarrow\rangle \ , \\
u_3 &= \frac{1}{\sqrt{2}}(|X\rangle + i|Y\rangle)|\uparrow\rangle = |\frac{3}{2}\ \frac{3}{2}\rangle \ , \\
u_4 &= \frac{i}{\sqrt{6}}\Big[(|X\rangle + i|Y\rangle)|\downarrow\rangle - 2|Z\rangle|\uparrow\rangle\Big] = |\frac{3}{2}\ \frac{1}{2}\rangle \ , \\
u_5 &= \frac{1}{\sqrt{6}}\Big[(|X\rangle - i|Y\rangle)|\uparrow\rangle + 2|Z\rangle|\downarrow\rangle\Big] = |\frac{3}{2} - \frac{1}{2}\rangle \ , \\
u_6 &= \frac{i}{\sqrt{2}}(|X\rangle - i|Y\rangle)|\downarrow\rangle = |\frac{3}{2} - \frac{3}{2}\rangle \ , \\
u_7 &= \frac{1}{\sqrt{3}}\Big[(|X\rangle + i|Y\rangle)|\downarrow\rangle + |Z\rangle|\uparrow\rangle\Big] = |\frac{1}{2}\ \frac{1}{2}\rangle \ , \\
u_8 &= -\frac{i}{\sqrt{3}}\Big[(|X\rangle - i|Y\rangle)|\uparrow\rangle - |Z\rangle|\downarrow\rangle\Big] = |\frac{1}{2} - \frac{1}{2}\rangle \ .
\end{aligned}
$$

The first two are the conduction band states, and the remaining 6 functions are the valence band states. The phases of these functions are chosen so that u_2, u_4, u_6, and u_8 are the time-reversal counterparts of the u_1, u_3, u_5, and u_7 functions, respectively (the time reversal operator is $\hat{\sigma}_y\hat{K}$, where $\hat{K}$ is the complex conjugation operator). In this basis, the Kane Hamiltonian is given by

$$\begin{pmatrix} E_g+\frac{\hbar^2k^2}{2\tilde{m}_e} & 0 & \frac{i}{\sqrt{2}}Vk_+ & \sqrt{\frac{2}{3}}Vk_z & \frac{i}{\sqrt{6}}Vk_- & 0 & \frac{i}{\sqrt{3}}Vk_z & \frac{1}{\sqrt{3}}Vk_- \\ 0 & E_g+\frac{\hbar^2k^2}{2\tilde{m}_e} & 0 & \frac{i}{\sqrt{6}}Vk_+ & \sqrt{\frac{2}{3}}Vk_z & \frac{i}{\sqrt{2}}Vk_- & \frac{1}{\sqrt{3}}Vk_+ & \frac{i}{\sqrt{3}}Vk_z \\ -\frac{i}{\sqrt{2}}Vk_- & 0 & P+Q & L & M & 0 & \frac{i}{\sqrt{2}}L & -i\sqrt{2}M \\ \sqrt{\frac{2}{3}}Vk_z & -\frac{i}{\sqrt{6}}Vk_- & L^* & P-Q & 0 & M & -i\sqrt{2}Q & i\sqrt{\frac{3}{2}}L \\ -\frac{i}{\sqrt{6}}Vk_+ & \sqrt{\frac{2}{3}}Vk_z & M^* & 0 & P-Q & -L & -i\sqrt{\frac{3}{2}}L^* & -i\sqrt{2}Q \\ 0 & -\frac{i}{\sqrt{2}}Vk_+ & 0 & M^* & -L^* & P+Q & -i\sqrt{2}M^* & -\frac{i}{\sqrt{2}}L^* \\ -\frac{i}{\sqrt{3}}Vk_z & \frac{1}{\sqrt{3}}Vk_- & -\frac{i}{\sqrt{2}}L^* & i\sqrt{2}Q & i\sqrt{\frac{3}{2}}L & i\sqrt{2}M & P-\Delta_{so} & 0 \\ \frac{1}{\sqrt{3}}Vk_+ & -\frac{i}{\sqrt{3}}Vk_z & i\sqrt{2}M^* & -i\sqrt{\frac{3}{2}}L^* & i\sqrt{2}Q & \frac{i}{\sqrt{2}}L & 0 & P-\Delta_{so} \end{pmatrix} \tag{B.1}$$

where we have defined

$$\begin{aligned} V &= -i\frac{\hbar}{m_0}\langle S|\hat{p}_x|X\rangle = \sqrt{E_p\frac{\hbar^2}{2m_0}} \ , \\ P &= -\frac{\hbar^2}{2m_0}\tilde{\gamma}_1k^2 \ , \\ Q &= -\frac{\hbar^2}{2m_0}\tilde{\gamma}_2(k_x^2+k_y^2-2k_z^2) \ , \\ L &= i\frac{\hbar^2}{m_0}\sqrt{3}\tilde{\gamma}_3k_zk_- \\ M &= -\frac{\hbar^2}{2m_0}\sqrt{3}(\tilde{\gamma}_2(k_x^2-k_y^2)-i2\tilde{\gamma}_3k_xk_y) \ , \\ &= -\frac{\hbar^2}{2m_0}\sqrt{3}(\tilde{\gamma}k_-^2-\tilde{\mu}k_+^2) \ , \end{aligned}$$

with electron mass m_0, bandgap energy E_g, energy E_p associated with the momentum matrix element between the conduction and the valence bands, spin-orbit splitting Δ_{so}, $\tilde{\gamma}=(\tilde{\gamma}_3+\tilde{\gamma}_2)/2$, and $\tilde{\mu}=(\tilde{\gamma}_3-\tilde{\gamma}_2)/2$. In the above Hamiltonian we have neglected the terms linear in **k** in the valence band submatrix (see e.g. Ref. [17]

ch. 3.3). Because we use 8 bands, the conduction band effective mass $\tilde{m}_e$ is renormalized:

$$\frac{1}{\tilde{m}_e} = \frac{1}{m_e} - \frac{1}{m_0}\frac{E_p}{3}\left(\frac{2}{E_g} + \frac{1}{E_g + \Delta_{so}}\right) , \tag{B.2}$$

where m_e is the effective mass in the single band model. Similarly, the renormalized Luttinger parameters $\tilde{\gamma}_i$ are related to the usual γ_i by

$$\tilde{\gamma}_1 = \gamma_1 - \frac{E_p}{3E_g} , \tag{B.3a}$$

$$\tilde{\gamma}_2 = \gamma_2 - \frac{E_p}{6E_g} , \tag{B.3b}$$

$$\tilde{\gamma}_3 = \gamma_3 - \frac{E_p}{6E_g} , \tag{B.3c}$$

The γ_i parameters are used in the 6 band Luttinger Hamiltonian [219, 220], which has the same form as the 6×6 valence band submatrix of the Hamiltonian (B.1), only with $\tilde{\gamma}_i$ replaced by γ_i. The band parameters for GaAs (InAs) are: E_g=1.52 eV (0.42 eV), Δ_{so}=0.34 eV (0.39 eV), E_p=28.8 eV (21.5 eV), m_e=0.067 (0.026), γ_1=6.98 (20.0), γ_2=2.06 (8.5), γ_3=2.93 (9.2).

The sp-d exchange Hamiltonian in the mean-field approximation is given by

$$\hat{H}_{s-d} = -n_i\gamma\langle\hat{\mathbf{S}}\rangle \cdot \hat{\mathbf{s}} , \tag{B.4}$$

where γ is the exchange constant (equal to α for the conduction band and β for the valence band), n_i is the density of the localized spins and $\langle\hat{\mathbf{S}}\rangle$ is the average localized spin. The matrix of the spin operator in the basis of the 8 states given above has a block-diagonal form, with the conduction band spin 2×2 matrix $\hat{\mathbf{s}}$=$\hat{\sigma}/2$, and the 6×6 valence band matrices:

$$\hat{s}_+ = \begin{pmatrix} 0 & \frac{i}{\sqrt{3}} & 0 & 0 & \sqrt{\frac{2}{3}} & 0 \\ 0 & 0 & \frac{2}{3}i & 0 & 0 & -\frac{\sqrt{2}}{3} \\ 0 & 0 & 0 & \frac{i}{\sqrt{3}} & 0 & 0 \\ 0 & 0 & 0 & 0 & 0 & 0 \\ 0 & 0 & \frac{\sqrt{2}}{3} & 0 & 0 & \frac{i}{3} \\ 0 & 0 & 0 & -\sqrt{\frac{2}{3}} & 0 & 0 \end{pmatrix} \tag{B.5}$$

$$\hat{s}_- = \begin{pmatrix} 0 & 0 & 0 & 0 & 0 & 0 \\ -\frac{i}{\sqrt{3}} & 0 & 0 & 0 & 0 & 0 \\ 0 & -\frac{2}{3}i & 0 & 0 & \frac{\sqrt{2}}{3} & 0 \\ 0 & 0 & \frac{-i}{\sqrt{3}} & 0 & 0 & -\sqrt{\frac{2}{3}} \\ \sqrt{\frac{2}{3}} & 0 & 0 & 0 & 0 & 0 \\ 0 & -\frac{\sqrt{2}}{3} & 0 & 0 & -\frac{i}{3} & 0 \end{pmatrix} \tag{B.6}$$

and

$$\hat{s}_z = \begin{pmatrix} \frac{1}{2} & 0 & 0 & 0 & 0 & 0 \\ 0 & \frac{1}{6} & 0 & 0 & i\frac{\sqrt{2}}{3} & 0 \\ 0 & 0 & -\frac{1}{6} & 0 & 0 & -i\frac{\sqrt{2}}{3} \\ 0 & 0 & 0 & -\frac{1}{2} & 0 & 0 \\ 0 & -i\frac{\sqrt{2}}{3} & 0 & 0 & -\frac{1}{6} & \frac{i}{3} \\ 0 & 0 & i\frac{\sqrt{2}}{3} & 0 & 0 & \frac{1}{6} \end{pmatrix} . \tag{B.7}$$

The operators of the spin in directions other than $\hat{z}$ are given by

$$\hat{s}_x = \frac{1}{2}(\hat{s}_+ + \hat{s}_-) \ , \tag{B.8a}$$

$$\hat{s}_y = -\frac{i}{2}(\hat{s}_+ - \hat{s}_-) \ . \tag{B.8b}$$

Appendix C

Some symmetry properties of exchange-split bands in a cubic semiconductor

The addition of a mean-field exchange interaction with localized spins $\Delta\langle\mathbf{S}\rangle\cdot\hat{\mathbf{s}}$ (with $\langle\mathbf{S}\rangle$ the average localized spin and $\hat{\mathbf{s}}$ the carrier spin operator) to the carriers' Hamiltonian lowers its symmetry. Let us take the full cubic group O_h as the initial symmetry. This is an approximation for zinc-blende crystals which lack the center of inversion, but we are not concerned here with small effects brought by this lowered symmetry. When the average localized spin $\langle\mathbf{S}\rangle$ is parallel to one of $\langle 100\rangle$ directions (we denote the magnetization direction as $\mathbf{n}$), the order of the group drops from 48 to 8, with the remaining symmetry operations being the identity, rotations by $\frac{\pi}{2}$,π,$\frac{3\pi}{2}$ around $\mathbf{n}$ axis and inversion multiplying all the previous operations. Analogously, for magnetization in $\langle 111\rangle$ direction there are 6 remaining symmetry operations (with rotations by $\frac{2\pi}{3}$ and $\frac{4\pi}{3}$ around $\mathbf{n}$), and for $\mathbf{n}$ parallel to $\langle 110\rangle$ there are only 4 operations (with rotation by π around $\mathbf{n}$).

In the following we assume that the carriers' density matrix is diagonal in the basis of the energy eigenstates, giving the occupation function f_α for the energy ϵ_α (α=$n\mathbf{k}$). First, let us prove that the average of the carrier spin-flip operators $\hat{F}^{\pm}$ is zero, as we asserted in Appendix A. Denoting the carrier average by $\langle ...\rangle_C$

we have

$$\langle \hat{F}^{\pm} \rangle_C \sim \sum_{\alpha\beta} \langle \alpha | \hat{s}^{\pm} | \beta \rangle \langle a^{\dagger}{}_{\alpha} a_{\beta} \rangle_C = \sum_{\alpha} \langle \alpha | \hat{s}^{\pm} | \alpha \rangle f_{\alpha} \ . \tag{C.1}$$

Now we change the sum over all states α to a sum over an "irreducible" set of states (e.g. an irreducible Brillouin Zone (IBZ)), and generate the symmetry-equivalent states by rotations. For example, for a given state $|\alpha\rangle$ we have symmetry-equivalent states $|\alpha_n\rangle$=exp$(-i\phi_n \hat{s}^z)|\alpha\rangle$, with allowed set of angles ϕ_n depending on the orientation of the localized spin magnetization (defining the $\hat{z}$ axis) with respect to crystal axes. The ladder operators transform in the following way:

$$e^{i\phi\hat{s}^z} \hat{s}^{\pm} e^{-i\phi\hat{s}^z} = e^{\pm i\phi} \hat{s}^{\pm} \ . \tag{C.2}$$

For the localized spin along the $\langle 100 \rangle$ directions, we get

$$\langle \hat{F}^{\pm} \rangle \sim \sum_{\alpha \in \mathrm{IBZ}} f_{\alpha} \langle \alpha | \hat{s}^{\pm} | \alpha \rangle (1 \pm i - 1 \mp i) = 0 \ , \tag{C.3}$$

and similarly we get zero for other high-symmetry directions: $\langle 111 \rangle$ and $\langle 110 \rangle$.

Let us look now at the correlation function $C_{ij}(t)$ (see Appendix A) for i=j. It is proportional to

$$C_{\pm\pm}(t) \sim \sum_{\alpha\beta} f_{\alpha} f_{\beta} \langle \alpha | \hat{s}^{\pm} | \alpha \rangle \langle \beta | \hat{s}^{\pm} | \beta \rangle + \sum_{\alpha\beta} e^{i\omega_{\alpha\beta} t} f_{\alpha} (1 - f_{\beta}) \langle \alpha | \hat{s}^{\pm} | \beta \rangle \langle \beta | \hat{s}^{\pm} | \alpha \rangle \ . \tag{C.4}$$

The first term is a product of two $\langle \hat{F}^{\pm} \rangle_C$, and so it vanishes in the cases discussed above. In the second term we have to transform pairs of states α,β simultaneously, and the resulting phase factors are now $e^{2i\phi_n}$. As a consequence, it vanishes for $\mathbf{n}$ parallel to $\langle 100 \rangle$ and $\langle 111 \rangle$, but not $\langle 110 \rangle$ (this was also noted in Ref. [222]) . In all the calculations in Chapter 10 we always assume that the magnetization is along one of the $\langle 100 \rangle$ directions, so that the C_{ii} correlation functions are zero. Only the "spin-flip" correlations

$$C_{\pm\mp} \sim \sum_{\alpha,\beta} e^{i\omega_{\alpha\beta} t} f_{\alpha} (1 - f_{\beta}) |\langle \alpha | \hat{s}^{\pm} | \beta \rangle|^2 \tag{C.5}$$

remain.

Appendix D

Spin-flip transition rate in the 4 band spherical Luttinger model

The 4 band Luttinger Hamiltonian in spherical approximation is given by

$$\hat{H}_{\rm sph} = -\frac{\hbar^2}{2m_0}[(\gamma_1 + \frac{5}{2}\gamma_2)k^2 - 2\gamma_2(\mathbf{k}\cdot\hat{\mathbf{j}})^2], \tag{D.1}$$

where γ_1,γ_2 are Luttinger parameters and $\hat{\mathbf{j}}$ is the spin-3/2 operator. The γ_2 parameter in the above Hamiltonian is best approximated by an average of γ_2 and γ_3 used in non-spherical Luttinger Hamiltonian. This Hamiltonian corresponds to the limit of infinite spin-orbit splitting energy, and it is quite accurate for states close in energy to the top of the valence band. Its diagonalization is easily done for $\mathbf{k}$ parallel to $\hat{z}$ (j quantization) axis. The eigenvectors are the eigenstates of $\hat{j}_z$, and the energies are

$$\epsilon_{hh}(k) = \frac{-\hbar^2 k^2}{2m_{hh}} \quad , \quad \epsilon_{lh}(k) = \frac{-\hbar^2 k^2}{2m_{lh}} \tag{D.2}$$

with m_{hh}=$m_0/(\gamma_1 - 2\gamma_2)$ (for j_z=$\pm 3/2$) and m_{lh}=$m_0/(\gamma_1 + 2\gamma_2)$ (for j_z=$\pm 1/2$). Spherical symmetry of the Hamiltonian allows us to generate all the $|n\mathbf{k}\rangle$ eigenvectors from $|j_z\rangle$ states by a rotation in spin-3/2 space:

$$|n\mathbf{k}\rangle = e^{-i\phi\hat{j}_z}e^{-i\theta\hat{j}_y}|j_z\rangle \ , \tag{D.3}$$

where $\mathbf{k}$ vector is pointing in the direction described by (θ,ϕ) angles in the spherical coordinate system.

We use the following basis of $|j_z\rangle$ states:

$$\begin{aligned}
|3/2\rangle &= \frac{1}{\sqrt{2}}|(X+iY)\uparrow\rangle\ , \\
|1/2\rangle &= \frac{i}{\sqrt{6}}|(X+iY)\downarrow -2Z\uparrow\rangle\ , \\
|-1/2\rangle &= \frac{1}{\sqrt{6}}|(X-iY)\uparrow +2Z\downarrow\rangle\ , \\
|-3/2\rangle &= \frac{i}{\sqrt{2}}|(X-iY)\downarrow\rangle\ .
\end{aligned}$$

In this basis the Hamiltonian (D.1) reads:

$$\hat{H}_{\text{sph}} = -\frac{\hbar^2}{2m_0}\begin{pmatrix} P+Q & M & L & 0 \\ M^* & P-Q & 0 & -L \\ L^* & 0 & P-Q & M \\ 0 & -L^* & M^* & P+Q \end{pmatrix}\ , \tag{D.4}$$

where

$$\begin{aligned}
P &= \gamma_1 k^2\ , \\
Q &= \gamma_2(k_x^2+k_y^2-2k_z^2)\ , \\
M &= \sqrt{3}\gamma_2 k_-^2\ , \\
L &= -2i\sqrt{3}\gamma_2 k_- k_z\ ,
\end{aligned}$$

where $k_-{=}k_x - ik_y$.

From Wigner-Eckart theorem [223] we have that the spin operator $\hat{s}^-{=}\frac{1}{3}\hat{j}^-$, and in the above basis it is given by

$$\hat{s}^- = \begin{pmatrix} 0 & 0 & 0 & 0 \\ -i/\sqrt{3} & 0 & 0 & 0 \\ 0 & -2i/3 & 0 & 0 \\ 0 & 0 & -i/\sqrt{3} & 0 \end{pmatrix}\ . \tag{D.5}$$

The non-trivial operation in Equation (D.3) is the rotation about the $\hat{y}$ axis,

$\hat{d}(\theta)$=exp$(-i\theta\hat{j}_y)$, the matrix of which is given by

$$\hat{d}(\theta) = \begin{pmatrix} c^3 & -i\sqrt{3}c^2 s & -\sqrt{3}cs^2 & is^3 \\ -i\sqrt{3}c^2 s & c(c^2-2s^2) & -is(2c^2-s^2) & -\sqrt{3}cs^2 \\ -\sqrt{3}cs^2 & -is(2c^2-s^2) & c(c^2-2s^2) & -i\sqrt{3}c^2 s \\ is^3 & -\sqrt{3}cs^2 & -i\sqrt{3}c^2 s & c^3 \end{pmatrix}, \tag{D.6}$$

where c=cos $\theta/2$ and s=sin $\theta/2$.

Using all this we arrive at the following form of the spin-flip matrix element

$$\langle n'\mathbf{k}'|\hat{s}^-|n\mathbf{k}\rangle = -\frac{i}{3}e^{-i\phi}\sum_{m=-3/2\ldots1/2}\sqrt{15/4-m(m+1)} \times e^{i(\phi'-\phi)m}\ d_{n',m}(\theta')\ d_{m+1,n}(\theta)\ . \tag{D.7}$$

In the following we calculate analytically the spin-flip transition rate in the limit of zero spin splitting of the valence band (Δ=0 and thus δ=0). The W_{+-} matrix element is given by the following formula

$$W_{+-} = \frac{\gamma^2}{4}\frac{2\pi}{\hbar}\sum_{nn'}\int\frac{\mathrm{d}^3k}{(2\pi)^3}\int\frac{\mathrm{d}^3k'}{(2\pi)^3}|\langle n'\mathbf{k}'|\hat{s}^{\pm}|n\mathbf{k}\rangle|^2 \times f_{n\mathbf{k}}(1-f_{n'\mathbf{k}'})\,\delta(\tilde{\epsilon}_{n\mathbf{k}}-\tilde{\epsilon}_{n'\mathbf{k}'})\ , \tag{D.8}$$

where γ is the exchange constant and $f_{n\mathbf{k}}$ is the occupation of the $|n\mathbf{k}\rangle$ state. Using the simple energy dispersion of spherical Hamiltonian we arrive at

$$W_{+-} = \frac{\gamma^2}{4}\frac{2\pi}{\hbar}\sum_{nn'}I_{n'n}\int_0^\infty dED_n(E)D_{n'}(E)f(E)(1-f(E))\,, \tag{D.9}$$

where $D_n(E)$ is the density of states for the n-th subband and

$$I_{n'n} = \frac{1}{(4\pi)^2}\int d\Omega\int d\Omega'\ |\langle n'\mathbf{k}'|\hat{s}^-|n\mathbf{k}\rangle|^2\ , \tag{D.10}$$

where $\int d\Omega$ is the integral over all the possible directions of $\mathbf{k}$. Because of the double averaging over all possible directions of $\mathbf{k}$ and $\mathbf{k}'$, the $I_{n'n}$ factor is actually independent of n and n', and is equal to 5/72. So we finally get

$$W_{+-} = \frac{\gamma^2}{4}\frac{2\pi}{\hbar}\ \frac{5}{72}\int_0^\infty dED(E)D(E)f(E)(1-f(E))\ , \tag{D.11}$$

with the total density of states

$$D(E) = \frac{1}{\pi^2\hbar^2}\left(m_{hh}\sqrt{\frac{2m_{hh}}{\hbar^2}E} + m_{lh}\sqrt{\frac{2m_{lh}}{\hbar^2}E}\right) . \qquad \text{(D.12)}$$

In the limit of no spin splitting, the density of states for one spin is 1/2 of the above $D(E)$. Thus, in the naive calculation disregarding the matrix elements, one would have a factor of 1/4 instead of 5/72 in Equation (D.11). This reduction of W_{+-} by 5/18 compared to the result obtained from densities of states is expected to be weaker in 6 band Luttinger model, where a finite value of spin-orbit splitting is used. Our numerical integration procedures described in Appendix E were tested on the spherical 4 band model, reproducing the above results with high accuracy.

Appendix E

Numerical calculations of densities of states and transition rates in a $\mathbf{k} \cdot \mathbf{p}$ model

We have calculated the valence bandstructure of (III,Mn)V ferromagnetic semiconductor using an effective $\mathbf{k} \cdot \mathbf{p}$ Hamiltonian approach [175]. The explicit forms of the 8×8 Kane Hamiltonian, the 6×6 Luttinger Hamiltonian, and the H_{p-d} matrix are given in Appendix B (see also Refs. [180, 29, 222]). In the presence of exchange splitting the symmetry of the Hamiltonian is lowered, and the irreducible part of the Brillouin zone (IBZ) is 1/8 of the entire zone (assuming that the magnetization is in one of $\langle 100 \rangle$ directions). Since the $\mathbf{k} \cdot \mathbf{p}$ model that we use is accurate up to wave-vectors about 1/4 of the BZ away from the Γ point [221], and we restrict all the $\mathbf{k}$-space integrals to this region, we can choose our effective IBZ to be a cube (e.g. $k_i{\geq}0$, $i{=}x{,}y{,}z$). We have divided this IBZ into N^3 cubic cells, and diagonalized the $\mathbf{k} \cdot \mathbf{p}$ Hamiltonian for $\mathbf{k}$ vectors located at the centers of the cells.

An example of spin-split bandstructure for GaMnAs with Δ=0.15 eV is plotted in Figure 10.6 The spin-projected densities of states D_s in this Figure have been

calculated from the formula

$$D_s(E) = \sum_n \int \frac{\mathrm{d}^3k}{(2\pi)^3}\, \delta(E-\epsilon_{n\mathbf{k}})\, \langle n\mathbf{k}|\hat{P}_s|n\mathbf{k}\rangle \ , \tag{E.1}$$

where $\epsilon_{n\mathbf{k}}$ is the energy of the $|n\mathbf{k}\rangle$ eigenstate, and $\hat{P}_s$ is the operator projecting on a given spin direction s=↑,↓:

$$\hat{P}_s = |s\rangle\langle s| \ .$$

We have numerically evaluated the Equation (E.1) using Gilat's method [224, 225]. In this method, the isoenergy surfaces within each cell are approximated by planes. The area of such a plane of energy E for N-th band intersecting the **k**-th cell is given by $S_{n\mathbf{k}}(E)$, which is a function of energy gradient $\nabla_{\mathbf{k}}\epsilon_{n\mathbf{k}}$ calculated at the **k** point [224]. If we treat the matrix elements as constant within each cell, we have then

$$D_s(E) \approx \frac{8}{(2\pi)^3} \sum_n \sum_{\mathbf{k}\in\mathrm{IBZ}} \langle n\mathbf{k}|\hat{P}_s|n\mathbf{k}\rangle \frac{S_{n\mathbf{k}}(E)}{|\nabla_{\mathbf{k}}\epsilon_{n\mathbf{k}}|} \ . \tag{E.2}$$

At the additional computational expense of calculating the gradients of the spin-projection operator matrix elements, we have employed a generalization of this method [225], which takes into account the variation of these matrix elements inside the cell. The resulting $D_s(E)$ are practically free of visible numerical inaccuracies for $N \geq 30$.

The calculation of the transition rate W_{+-} (Eq. (10.29)) which involves a double integration over the relevant part of Brillouin Zone (restricted by occupation factors), is performed in the following way. Omitting the overall constant, we write the transition rate as

$$W_{+-} = \sum_n \int \frac{\mathrm{d}^3k}{(2\pi)^3} f_{n\mathbf{k}} \sum_{n'} \int \frac{\mathrm{d}^3k'}{(2\pi)^3} \left(1-f_{n'\mathbf{k}'}\right) |\langle n'\mathbf{k}'|\hat{s}^-|n\mathbf{k}\rangle|^2\, \delta(\epsilon_{n\mathbf{k}}-\epsilon_{n'\mathbf{k}'}-\delta) \ . \tag{E.3}$$

For the numerical calculation, we approximate it by

$$W_{+-} \approx \frac{8\Delta k^3}{(2\pi)^6} \sum_{n,\mathbf{k}\in\mathrm{IBZ}} f(\epsilon_{n\mathbf{k}})(1-f(\epsilon_{n\mathbf{k}}-\delta)) \sum_{n',\mathbf{k}'} |\langle n'\mathbf{k}'|\hat{s}^-|n\mathbf{k}\rangle|^2 \frac{S_{n'\mathbf{k}'}(E-\delta)}{|\nabla_{\mathbf{k}'}\epsilon_{n'\mathbf{k}'}|} \ , \tag{E.4}$$

where Δk^3 is the volume of the cell in $\mathbf{k}$-space. The integral with respect to $\mathbf{k}$ has been converted to a sum over the cells in IBZ (times the symmetry factor of 8). The domain of the second integral is a full Brillouin Zone, and we evaluate it by Gilat's method, with matrix elements taken as constant inside the cells. For the evaluation of matrix elements, we use only the eigenvectors obtained by diagonalization of the Hamiltonian within the IBZ, and transform them into other parts of BZ using symmetry transformations (four-fold rotation around $\hat{z}$ axis and inversion, all having simple representations in $|jm\rangle$ basis). The accuracy of this numerical approach has been tested by numerical calculation of W_{+-} for the spherical 4 band Luttinger model, which is done analytically in Appendix D. With N=30, we have achieved 5 digit accuracy in reproducing the reduction factor of 5/18. We have also checked how the transition rates calculated in 6 band model change with N. The difference between results for N=20 and 30 is about 2%. Taking into account all the other approximations used by us and uncertainties in values of some of the parameters (e.g. hole concentration), we have used N=20 for the calculations presented in this dissertation.

Bibliography

[1] A. Aharoni, *Introduction to the Theory of Ferromagnetism* (Oxford University Press, New York, 1996).

[2] M. N. Baibich, J. M. Broto, A. Fert, F. Nguyen Van Dau, F. Petroff, P. Eitenne, G. Creuzet, A. Friederich, and J. Chazelas, Phys. Rev. Lett. **61**, 2472 (1988).

[3] G. Binasch, P. Grünberg, F. Saurenbach, and W. Zinn, Phys. Rev. B **39**, 4828 (1989).

[4] P. M. Levy, in *Solid State Physics* (Academic, New York, 1994), Vol. 47, pp. 367–462.

[5] S. S. P. Parkin, N. More, and K. P. Roche, Phys. Rev. Lett. **64**, 2304 (1990).

[6] P. Bruno, Phys. Rev. B **52**, 411 (1995).

[7] G. A. Prinz, Science **282**, 1660 (1998).

[8] J. C. Slonczewski, J. Magn. Magn. Mat. **159**, L1 (1996).

[9] L. Berger, Phys. Rev. B **54**, 9353 (1996).

[10] M. Tsoi, A. G. M. Jansen, J. Bass, W. C. Chiang, M. Seck, V. Tsoi, and P. Wyder, Phys. Rev. Lett, **80**, 4281 (1998).

[11] M. D. Stiles and J. Miltat, Top. Appl. Phys. **202**, 225 (2006).

[12] T. Gerrits, H. A. M. van den Berg, J. Hohlfeld, L. Bar, and T. Rasing, Nature **418**, 509 (2002).

[13] E. Beaurepaire, J. C. Merle, A. Daunois, and J.-Y. Bigot, Phys. Rev. Lett. **76**, 4250 (1996).

[14] J. S. Moodera, L. R. Kinder, T. M. Wong, and R. Meservey, Phys. Rev. Lett. **74**, 3273 (1995).

[15] S. Tehrani, B. Engel, J. M. Slaughter, E. Chen, M. DeHerrera, M. Durlam, P. Naji, R. Whig, J. Janesky, and J. Calder, IEEE Trans. Magn. **36**, 2752 (2000).

[16] S. Datta and B. Das, Appl. Phys. Lett **56**, 665 (1990).

[17] R. Winkler, *Spin-Orbit Coupling Effects in Two-Dimensional Electron and Hole Systems* (Springer-Verlag, Berlin, 2003).

[18] M. Johnson and R. H. Silsbee, Phys. Rev. Lett. **55**, 1790 (1985).

[19] *Optical Orientation*, edited by F. Meier and B. P. Zakharchenya (North-Holland, New York, 1984).

[20] J. M. Kikkawa and D. D. Awschalom, Phys. Rev. Lett. **80**, 4313 (1998).

[21] J. M. Kikkawa and D. D. Awschalom, Nature **397**, 139 (1999).

[22] R. Fiederling, M. Keim, G. Reuscher, W. Ossau, G. Schmidt, A. Waag, and L. W. Molenkamp, Nature **402**, 787 (1999).

[23] Y. Ohno, D. K. Yound, B. Beschoten, F. Matsukura, H. Ohno, and D. D. Awschalom, Nature **402**, 790 (1999).

[24] M. Oestreich, J. Hübner, D. Hägele, P. J. Klar, W. Heimbrodt, W. W. Rühle, D. E. Ashenford, and B. Lunn, Appl. Phys. Lett. **74**, 1251 (1999).

[25] H. J. Zhu, M. Ramsteiner, H. Kostial, M. Wassermeier, H.-P. Schonherr, and K. H. Ploog, Phys. Rev. Lett. **87**, 016601 (2001).

[26] H. Ohno, H. Munekata, T. Penney, S. von Molnar, and L. L. Chang, Phys. Rev. Lett. **68**, 2664 (1992).

[27] H. Ohno, A. Shen, F. Matsukura, A. Oiwa, A. Endo, S. Katsumoto, and Y. Iye, Appl. Phys. Lett. **69**, 363 (1996).

[28] T. Dietl, H. Ohno, F. Matsukura, J. Cibert, and D. Ferrand, Science **287**, 1019 (2000).

[29] T. Dietl, H. Ohno, and F. Matsukura, Phys. Rev. B **63**, 195205 (2001).

[30] J. Fernández-Rossier and L. J. Sham, Phys. Rev. B **64**, 235323 (2001).

[31] H. Ohno, D. Chiba, F. Matsukura, T. Omiya, E. Abe, T. Dietl, Y. Ohno, and K. Ohtani, Nature **408**, 944 (2000).

[32] S. A. Wolf, D. D. Awschalom, R. A. Buhrman, J. M. Daughton, S. von Molnar, M. L. Roukes, A. Y. Chtchelkanova, and D. M. Treger, Science **294**, 1488 (2001).

[33] I. Žutić, J. Fabian, and S. D. Sarma, Rev. Mod. Phys. **76**, 323 (2004).

[34] *Magnetoelectronics*, edited by M. Johnson (Elsevier, Amsterdam, 2004).

[35] F. X. Bronold, A. Saxena, and D. L. Smith, in *Solid State Physics* (Elsevier, New York, 2004), Vol. 58, pp. 73–166.

[36] A. T. Hanbicki, O. M. J. van't Erve, R. Magno, G. Kioseoglou, C. H. Li, B. T. Jonker, G. Itskos, R. Mallory, M. Yasar, and A. Petrou, Appl. Phys. Lett. **82**, 4092 (2003).

[37] J. Strand, B. D. Schultz, A. F. Isakovic, C. J. Palmstrom, and P. A. Crowell, Phys. Rev. Lett. **91**, 036602 (2003).

[38] S. A. Crooker, M. Furis, X. Lou, C. Adelmann, D. L. Smith, C. J. Palmstrom, and P. A. Crowell, Science **309**, 2191 (2005).

[39] P. C. van Son, H. van Kempen, and P. Wyder, Phys. Rev. Lett **58**, 2271 (1987).

[40] H. A. Engel, E. I. Rashba, and B. I. Halperin, cond-mat/0603306v2 (2006).

[41] X. Lou, C. Adelmann, M. Furis, S. A. Crooker, C. J. Palmstrom, and P. A. Crowell, Phys. Rev. Lett. **96**, 176603 (2006).

[42] X. Lou, C. Adelmann, S. A. Crooker, E. S. Garlid, J. Zhang, K. M. Reddy, S. D. Flexner, C. J. Palmstrom, and P. A. Crowell, Nature Physics **3**, 197 (2007).

[43] B. Koopmans, J. J. M. Ruigrok, F. D. Longa, and W. J. M. de Jonge, Phys. Rev. Lett. **95**, 267207 (2005).

[44] J. Wang, C. Sun, Y. Hashimoto, J. Kono, G. A. Khodaparast, Ł. Cywiński, L. J. Sham, G. D. Sanders, C. J. Stanton, and H. Munekata, J. Phys.: Condens. Matter **18**, R501 (2006).

[45] S. A. Crooker and D. L. Smith, Phys. Rev. Lett. **94**, 236601 (2005).

[46] Y. V. Pershin, Physica E **23**, 226 (2004).

[47] S. Saikin, J. Phys.: Condens. Matter **16**, 5071 (2004).

[48] J. E. Hirsch, Phys. Rev. Lett. **83**, 1834 (1999).

[49] J. Sinova, D. Culcer, Q. Niu, N. A. Sinitsyn, T. Jungwirth, and A. H. MacDonald, Phys. Rev. Lett. **92**, 126603 (2004).

[50] Y. K. Kato, R. C. Myers, A. C. Gossard, and D. D. Awschalom, Science **306**, 1910 (2004).

[51] N. W. Ashcroft and N. D. Merlin, *Solid State Physics* (Saunders College Publishing, New York, 1976).

[52] I. D'Amico and G. Vignale, Europhys. Lett. **55**, 566 (2001).

[53] C. P. Weber, N. Gedik, J. E. Moore, J. Orenstein, J. Stephens, and D. D. Awschalom, Nature **437**, 1330 (2005).

[54] T. Valet and A. Fert, Phys. Rev. B **48**, 7099 (1993).

[55] D. R. Penn and M. D. Stiles, Phys. Rev. B **72**, 212410 (2005).

[56] Y. Qi and S. Zhang, Phys. Rev. B **67**, 052407 (2003).

[57] Z. G. Yu and M. E. Flatté, Phys. Rev. B **66**, 235302 (2002).

[58] R. A. Smith, *Semiconductors* (Cambridge University Press, Cambridge, England, 1978).

[59] S. Hershfield and H. L. Zhao, Phys. Rev. B **56**, 3296 (1997).

[60] L. Villegas-Lelovsky, J. Appl. Phys. **101**, 053707 (2007).

[61] S. R. in 't Hout, J. Appl. Phys. **79**, 8435 (1996).

[62] I. Žutić, J. Fabian, and S. D. Sarma, Phys. Rev. Lett. **88**, 066603 (2002).

[63] J. Fabian, I. Žutić, and S. D. Sarma, Appl. Phys. Lett. **84**, 85 (2004).

[64] M. E. Flatté, Z. G. Yu, , E. Johnston-Halperin, and D. D. Awschalom, Appl. Phys. Lett. **82**, 4740 (2003).

[65] T. Dietl, Semicond. Sci. Technol. **17**, 377 (2002).

[66] J. Fabian, I. Žutić, and S. D. Sarma, Phys. Rev. B **66**, 165301 (2002).

[67] D. Csontos and S. E. Ulloa, Phys. Rev. B **74**, 155207 (2006).

[68] M. Johnson and R. H. Silsbee, Phys. Rev. B **37**, 5326 (1988).

[69] V. V. Osipov, N. A. Viglin, I. V. Kochev, and A. A. Samokhvalov, JETP Lett. **52**, 386 (1990).

[70] B. T. Jonker, Y. D. Park, B. R. Bennett, H. D. Cheong, G. Kioseoglou, and A. Petrou, Phys. Rev. B **62**, 8180 (2000).

[71] A. T. Hanbicki, B. T. Jonker, G. Itskos, G. Kioseoglou, and A. Petrou, Appl. Phys. Lett. **80**, 1240 (2002).

[72] C. Adelmann, X. Lou, J. Strand, C. J. Palmstrom, and P. A. Crowell, Phys. Rev. B **71**, 121301 (2005).

[73] B. T. Jonker, Proceedings of the IEEE **91**, 727 (2003).

[74] C. Adelmann, J. Q. Xie, C. J. Palmstrom, J. Strand, X. Lou, J. Wang, and P. A. Crowell, J. Vac. Sci. Technol. B **23**, 1747 (2005).

[75] J. Stephens, J. Berezovsky, J. P. McGuire, L. J. Sham, A. C. Gossard, and D. D. Awschalom, Phys. Rev. Lett. **93**, 097602 (2004).

[76] G. Schmidt, D. Ferrand, L. W. Molenkamp, A. T. Filip, and B. J. van Wees, Phys. Rev. B **62**, R4790 (2000).

[77] E. I. Rashba, Phys. Rev. B **62**, R16267 (2000).

[78] M. Johnson and R. H. Silsbee, Phys. Rev. B **35**, 4959 (1987).

[79] S. M. Sze, *Physics of Semiconductor Devices* (John Wiley, New York, 1981).

[80] M. Zachau, F. Koch, K. Ploog, P. Roentgen, and H. Beneking, Solid State Commun. **59**, 591 (1986).

[81] J. M. Geraldo, W. N. Rodrigues, G. Medeiros-Ribeiro, and A. G. de Oliveira, J. Appl. Phys. **73**, 820 (1993).

[82] V. I. Shashkin, A. V. Murel, V. M. Daniltsev, and O. K. Khrykin, Semiconductors (translated from Fizika i Tekhnika Poluprovodnikov **36**, 505 (2002).

[83] V. V. Osipov and A. M. Bratkovsky, Phys. Rev. B **70**, 205312 (2004).

[84] J. D. Albrecht and D. L. Smith, Phys. Rev. B **66**, 113303 (2002).

[85] J. D. Albrecht and D. L. Smith, Phys. Rev. B **68**, 035340 (2003).

[86] H. Dery and L. J. Sham, Phys. Rev. Lett. **98**, 046602 (2007).

[87] S. Saikin, M. Shen, and M.-C. Cheng, J. Phys.: Condens. Matter **18**, 1535 (2006).

[88] J. C. Slonczewski, Phys. Rev. B **39**, 6995 (1989).

[89] C. Ciuti, J. P. McGuire, and L. J. Sham, Phys. Rev. Lett. **89**, 156601 (2002).

[90] C. Ciuti, J. P. McGuire, and L. J. Sham, Appl. Phys. Lett. **81**, 4781 (2002).

[91] W. H. Butler, X.-G. Zhang, X. Wang, J. van Ek, and J. M. MacLaren, J. Appl. Phys. **81**, 5518 (1997).

[92] T. J. Zega, A. T. Hanbicki, S. C. Erwin, I. Žutić, G. Kioseoglou, C. H. Li, B. T. Jonker, and R. M. Stroud, Phys. Rev. Lett. **96**, 196101 (2006).

[93] D. A. Papaconstantopoulos, *Handbook of the Band Structure of Elemental Solids* (Plenum, New York, 1986).

[94] *Tunneling Phenomena in Solids*, edited by E. Burstein and S. Lundqvist (Plenum Press, New York, 1969).

[95] A. Fert and H. Jaffrès, Phys. Rev. B **64**, 184420 (2001).

[96] B. Dieny, V. S. Speriosu, S. S. P. Parkin, B. A. Gurney, D. R. Wilhoit, and D. Mauri, Phys. Rev. B **43**, 1297 (1991).

[97] J. Nogués and I. K. Schuller, J. Magn. Magn. Mat. **192**, 203 (1999).

[98] J. P. McGuire, C. Ciuti, and L. J. Sham, Phys. Rev. B **69**, 115339 (2004).

[99] F. J. Jedema, A. T. Filip, and B. J. van Wees, Nature **410**, 345 (2001).

[100] Y. Ji, A. Hoffman, J. E. Pearson, and S. D. Bader, Appl. Phys. Lett. **88**, 052509 (2006).

[101] B.-C. Min, K. Motohashi, C. Lodder, and R. Jansen, Nature Materials **5**, 817 (2006).

[102] I. Appelbaum, B. Huang, and D. J. Monsma, Nature **447**, 295 (2007).

[103] G. Schmidt, G. Richter, P. Grabs, C. Gould, D. Ferrand, and L. W. Molenkamp, Phys. Rev. Lett. **87**, 227203 (2001).

[104] J. Hamrle, T. Kimura, Y. Otani, K. Tsukagoshi, and Y. Aoyagi, Phys. Rev. B **71**, 094402 (2005).

[105] S. Takahashi and S. Maekawa, Phys. Rev. B **67**, 052409 (2003).

[106] H. Dery, Ł. Cywiński, and L. J. Sham, Phys. Rev. B **73**, 041306(R) (2006).

[107] J. Schliemann, J. C. Egues, and D. Loss, Phys. Rev. Lett. **90**, 146801 (2003).

[108] M. E. Flatté and G. Vignale, Appl. Phys. Lett. **78**, 1273 (2001).

[109] J. Fabian and I. Žutić, Phys. Rev. B **69**, 115314 (2004).

[110] K. C. Hall, W. H. Lau, K. Gündogdu, M. E. Flatté, and T. F. Boggess, Appl. Phys. Lett. **83**, 2937 (2003).

[111] H. Dery, Ł. Cywiński, and L. J. Sham, Phys.Rev. B **73**, 161307(R) (2006).

[112] M. Johnson, Science **260**, 320 (1993).

[113] T. Kimura, Y. Otani, and J. Hamrle, Phys. Rev. Lett. **96**, 037201 (2006).

[114] A. Ney, C. Pampuch, R. Koch, and K. H. Ploog, Nature **425**, 485 (2003).

[115] B. C. Choi and M. R. Freeman, in *Ultrathin Magnetic Structures III*, edited by B. Heinrich and J. A. C. Bland (Springer-Verlag, Berlin, 2004), pp. 211–232.

[116] A. Brataas, Y. V. Nazarov, and G. E. W. Bauer, Phys. Rev. Lett. **84**, 2481 (2000).

[117] A. Brataas, Y. V. Nazarov, and G. E. W. Bauer, Eur. Phys. J. B **22**, 99 (2001).

[118] H. Dery, P. B. Dalal, Ł. Cywiński, and L. J. Sham, Nature **447**, 573 (2007).

[119] K. W. Hipps and G. A. Crosby, J. Phys. Chem. **83**, 555 (1979).

[120] I. Žutić, J. Fabian, and S. D. Sarma, Phys. Rev. B **64**, 121201 (2001).

[121] T. Kondo, J. Hayafuji, and H. Munekata, Jpn. J. Appl. Phys., Part 1 **45**, 663 (2006).

[122] A. F. Isakovic, D. M. Carr, J. Strand, B. D. Schultz, C. J. Palmstrom, and P. A. Crowell, J. Appl. Phys. **91**, 7261 (2002).

[123] A. Hirohata, Y. B. Xiu, C. M. Guertler, J. A. C. Bland, and S. N. Holmes, Phys. Rev. B **63**, 104425 (2001).

[124] S. Steinmuller, C. M. Gürtler, C. Wastlbauer, and J. A. C. Bland, Phys. Rev. B **72**, 045301 (2005).

[125] A. Vaterlaus, T. Beutler, and F. Meier, Phys. Rev. Lett. **67**, 3314 (1991).

[126] A. Vaterlaus, T. Beutler, D. Guarisco, M. Lutz, and F. Meier, Phys. Rev. B **46**, 5280 (1992).

[127] W. Hübner and K. H. Bennemann, Phys. Rev. B **53**, 3422 (1996).

[128] J. Hohlfeld, E. Matthias, R. Knorren, and K. H. Bennemann, Phys. Rev. Lett. **78**, 4861 (1997).

[129] B. Koopmans, M. van Kampen, J. T. Kohlhepp, and W. J. M. de Jonge, Phys. Rev. Lett. **85**, 844 (2000).

[130] H. S. Rhie, H. A. Dürr, and W. Eberhardt, Phys. Rev. Lett. **90**, 247201 (2003).

[131] E. Beaurepaire, G. M. Turner, S. M. Harrel, M. C. Beard, J.-Y. Bigot, and C. A. Schmuttenmaer, Appl. Phys. Lett. **84**, 3465 (2004).

[132] D. Cheskis, A. Porat, L. Szapiro, O. Potashnik, and S. Bar-Ad, Phys. Rev. B **72**, 014437 (2005).

[133] T. Kampfrath, R. G. Ulbrich, F. Leuenberger, M. Münzenberg, B. Sass, and W. Felsch, Phys. Rev. B **65**, 104429 (2002).

[134] D. J. Hilton, R. P. Prasankumar, S. A. Trugman, A. J. Taylor, and R. D. Averitt, J. Phys. Soc. Jpn. **75**, 011006 (2006).

[135] M. Vomir, L. H. F. Andrade, L. Guidoni, E. Beaurepaire, and J. Y. Bigot, Phys. Rev. Lett. **94**, 237601 (2005).

[136] M. Cinchetti, M. S. Albaneda, D. Hoffman, T. Roth, J. P. Wüstenberg, M. Krauß, O. Andreyev, H. C. Schneider, M. Bauer, and M. Aeschlimann, Phys. Rev. Lett. **97**, 177201 (2006).

[137] E. Beaurepaire, M. Maret, V. Halté, J.-C. Merle, A. Daunois, and J.-Y. Bigot, Phys. Rev. B **58**, 12134 (1998).

[138] L. Guidoni, E. Beaurepaire, and J.-Y. Bigot, Phys. Rev. Lett. **89**, 017401 (2002).

[139] J. Y. Bigot, L. Guidoni, E. Beaurepaire, and P. N. Saeta, Phys. Rev. Lett. **93**, 077401 (2004).

[140] B. Koopmans, Top. Appl. Phys. **87**, 253 (2003).

[141] P. M. Oppeneer and A. Liebsch, J. Phys.: Condens. Matter **16**, 5519 (2004).

[142] G. Zhang, W. Hübner, E. Beaurepaire, and J.-Y. Bigot, Top. Appl. Phys. **83**, 245 (2002).

[143] G. D. Mahan, *Many-Particle Physics* (Kluwer Academic, New York, 2000).

[144] P. B. Allen, Phys. Rev. Lett. **59**, 1460 (1987).

[145] B. Koopmans, H. H. J. E. Kisken, M. van Kampen, and W. J. M. de Jonge, J. Magn. Magn. Mat. **286**, 271 (2005).

[146] G. P. Zhang and W. Hübner, Phys. Rev. Lett. **85**, 3025 (2000).

[147] R. Gómez-Abal, O. Ney, K. Satitkovitchai, and W. Hübner, Phys. Rev. Lett. **92**, 227402 (2004).

[148] A. V. Kimel, A. Kirilyuk, P. A. Usachev, R. V. Pisarev, A. M. Balbashov, and T. Rasing, Nature **435**, 655 (2005).

[149] R. J. Elliott, Phys. Rev. **96**, 266 (1954).

[150] Y. Yafet, *Solid State Physics* (Academic, New York, 1963), Vol. 14.

[151] B. Heinrich, in *Ultrathin Magnetic Structures III*, edited by B. Heinrich and J. A. C. Bland (Springer-Verlag, Berlin, 2004), pp. 143–210.

[152] P. Mohn, *Magnetism in the Solid State: An Introduction* (Springer, New York, 2003).

[153] C. Herring, in *Magnetism*, edited by G. T. Rado and H. Suhl (Academic Press, New York, 1966), Vol. IV.

[154] L. Berger, J. Phys. Chem. Solids **38**, 1321 (1977).

[155] O. Gunnarsson, J. Phys. F: Metal Phys. **6**, 587 (1976).

[156] T. Moriya, *Spin Fluctuations in Itinerant Electron Magnetism* (Springer-Verlag, Berlin, 1985).

[157] R. H. M. Groeneveld, R. Sprik, and A. Lagendijk, Phys. Rev. B **51**, 11433 (1995).

[158] M. Bauer and M. Aeschlimann, J. Electron Spectrosc. Relatn Phenom. **124**, 225 (2002).

[159] M. van Kampen, J. T. Kohlhepp, W. J. M. de Jonge, B. Koopmans, and R. Coehoorn, J. Phys.: Condens. Matter **17**, 6823 (2005).

[160] M. van Kampen, Ph.D. thesis, Thechnische Universiteit Eindhoven, 2003, http://alexandria.tue.nl/extra2/200312043.pdf.

[161] G. L. Krasko, Phys. Rev. B **36**, 8565 (1987).

[162] G. Fabricius, A. M. Llois, and H. Dreysseé, Phys. Rev. B **48**, 6665 (1993).

[163] C. S. Wang and J. Callaway, Phys. Rev. B **9**, 4897 (1974).

[164] J. Fabian and S. D. Sarma, Phys. Rev. Lett. **83**, 1211 (1999).

[165] J. Bass and W. P. Pratt., Jr, J. Phys. Condens. Matter **19**, 183201 (2007).

[166] P. Holody, W. C. Chiang, R. Loloee, J. Bass, W. P. Pratt, Jr, and P. A. Schroeder, Phys. Rev. B **58**, 12230 (1998).

[167] C. Vouille, A. Barthélémy, F. E. Mpondo, A. Fert, P. A. Schroeder, S. Y. Hsu, A. Reilly, and R. Loloee, Phys. Rev. B **60**, 6710 (1999).

[168] J. Fernández-Rossier, M. Braun, A. S. Núñez, and A. H. MacDonald, Phys. Rev. B **69**, 174412 (2004).

[169] *Handbook of Mathematical Functions*, edited by A. Abramowitz and I. A. Stegun (Dover, New York, 1965).

[170] J. Wang, C. Sun, J. Kono, A. Oiwa, H. Munekata, Ł. Cywiński, and L. J. Sham, Phys. Rev. Lett. **95**, 167401 (2005).

[171] S. V. Vonsovskii, *Magnetism* (J. Wiley, New York, 1974).

[172] C. Zener, Phys. Rev. **81**, 440 (1951).

[173] C. Zener, Phys. Rev. **83**, 299 (1951).

[174] B. König, I. A. Merkulov, D. R. Yakovlev, W. Ossau, S. M. Ryabchenko, M. Kutrowski, T. Wojtowicz, G. Karczewski, and J. Kossut, Phys. Rev. B **61**, 16870 (2000).

[175] T. Jungwirth, J. Sinova, J. Mašek, J. Kučera, and A. H. MacDonald, Rev. Mod. Phys. **78**, 809 (2006).

[176] E. L. Nagaev, *Physics of Magnetic Semiconductors* (Mir Publishers, Moscow, 1983).

[177] J. Wang, I. Cotoros, K. M. Dani, D. S. Chemla, X. Liu, and J. K. Furdyna, Phys. Rev. Lett. **98**, 217401 (2007).

[178] Y. Tserkovnyak, A. Brataas, G. E. W. Bauer, and B. I. Halperin, Rev. Mod. Phys. **77**, 1375 (2005).

[179] J. K. Furdyna, J. Appl. Phys. **64**, R29 (1988).

[180] J. Kossut, Semicond. Semimetals **25**, 183 (1988).

[181] P. Kacman, Semicond. Sci. Technol. **16**, R25 (2001).

[182] T. Dietl, A. Haury, and Y. Merle d'Aubigné, Phys. Rev. B **55**, R3347 (1997).

[183] A. Haury, A. Wasiela, A. Arnoult, J. Cibert, S. tatarenko, T. Dietl, and Y. Merle d'Aubigné, Phys. Rev. Lett. **79**, 511 (1997).

[184] S. Koshihara, A. Oiwa, M. Hirasawa, S. Katsumoto, Y. Iye, C. Urano, H. Takagi, and H. Munekata, Phys. Rev. Lett. **78**, 4617 (1997).

[185] D. Chiba, M. Yamanouchi, F. Matsukura, and H. Ohno, Science **301**, 943 (2003).

[186] K. S. Burch, D. B. Shrekenhamer, E. J. Singley, J. Stephens, B. L. Sheu, R. K. Kawakami, P. Schiffer, N. Samarth, D. D. Awschalom, and D. N. Basov, Phys. Rev. Lett. **97**, 087208 (2006).

[187] A. A. Abrikosov and L. P. Gorkov, Sov. Phys. JETP **16**, 1575 (1963).

[188] T. Jungwirth, W. A. Atkinson, B. H. Lee, and A. H. MacDonald, Phys. Rev. B **59**, 9818 (1999).

[189] J. Szczytko, W. Bardyszewski, and A. Twardowski, Phys. Rev. B **64**, 075306 (2001).

[190] T. Komori, T. Ishikawa, T. Kuroda, J. Yoshino, F. Minami, and S. Koshihara, Phys. Rev. B **67**, 115203 (2003).

[191] E. J. Singley, K. S. Burch, R. Kawakami, J. Stephens, D. D. Awschalom, and D. N. Basov, Phys. Rev. B **68**, 165204 (2003).

[192] R. Lang, A. Winter, H. Pascher, H. Krenn, X. Liu, and J. K. Furdyna, Phys. Rev. B **72**, 024430 (2005).

[193] E. M. Hankiewicz, T. Jungwirth, T. Dietl, C. Timm, and J. Sinova, Phys. Rev. B **70**, 245211 (2004).

[194] E. H. Hwang, A. J. Millis, and S. D. Sarma, Phys. Rev. B **65**, 233206 (2002).

[195] K. Hirakawa, A. Oiwa, and H. Munekata, Physica E **10**, 215 (2001).

[196] P. Fumagalli and H. Munekata, Phys. Rev. B **53**, 15045 (1996).

[197] M. Woerner and T. Elsaesser, Phys. Rev. B **51**, 17490 (1995).

[198] J. Shah, *Ultrafast Spectroscopy of Semiconductors and Semiconductor Heterostructures* (Springer, Berlin, 1999).

[199] K. Blum, *Density Matrix Theory and Applications* (Plenum Press, New York, 1981).

[200] J. Korringa, Physica **16**, 601 (1950).

[201] R. Orbach, J. Magn. Magn. Mat. **15-18**, 706 (1980).

[202] A. Abragam, *The Principles of Nuclear Magnetism* (Oxford University Press, New York, 1983).

[203] G. Feher, Phys. Rev. Lett. **3**, 135 (1959).

[204] W. G. Clark and G. Feher, Phys. Rev. Lett. **10**, 134 (1963).

[205] H. Suhl, cond-mat/0206215 (2002).

[206] D. W. Bailey, C. J. Stanton, and K. Hess, Phys. Rev. B **42**, 3423 (1990).

[207] D. J. Hilton and C. L. Tang, Phys. Rev. Lett. **89**, 146601 (2002).

[208] T. Jungwirth, M. Abolfath, J. Sinova, J. Kučera, and A. H. MacDonald, Appl. Phys. Lett **81**, 4029 (2002).

[209] T. Uenoyama and L. J. Sham, Phys. Rev. Lett. **64**, 3070 (1990).

[210] R. Ferreira and G. Bastard, Phys. Rev. B **43**, 9687 (1991).

[211] T. C. Damen, L. Viña, J. E. Cunningham, J. Shah, and L. J. Sham, Phys. Rev. Lett. **67**, 3432 (1991).

[212] J. Wang, G. A. Khodaparast, J. Kono, T. Slupinski, A. Oiwa, and H. Munekata, Physica E **20**, 412 (2004).

[213] J. Wang, G. A. Khodaparast, J. Kono, T. Slupinski, A. Oiwa, and H. Munekata, Physica E **25**, 681 (2005).

[214] A. V. Kimel, G. V. Astakhov, G. M. Schott, A. Kirilyuk, D. R. Yakovlev, G. Karczewski, W. Ossau, G. Schmidt, L. W. Molenkamp, and T. Rasing, Phys. Rev. Lett. **92**, 237203 (2004).

[215] M. U. Wehner, M. H. Ulm, D. S. Chemla, and M. Wegener, Phys. Rev. Lett. **80**, 1992 (1998).

[216] E. Kojima, R. Shimano, Y. Hashimoto, S. Katsumoto, Y. Iye, and M. Kuwata-Gonokami, Phys. Rev. B **68**, 193203 (2003).

[217] A. G. Redfield, IBM J. Res. Dev. **1**, 19 (1957).

[218] C. P. Slichter, *Principles of Magnetic Resonance* (Springer-Verlag, Berlin, 1978).

[219] J. M. Luttinger and W. Kohn, Phys. Rev. **97**, 869 (1955).

[220] J. M. Luttinger, Phys. Rev. **102**, 1030 (1956).

[221] I. Vurgaftman and J. R. Meyer, J. Appl. Phys. **89**, 5815 (2001).

[222] J. König, T. Jungwirth, and A. H. MacDonald, Phys. Rev. B **64**, 184423 (2001).

[223] J. J. Sakurai, *Modern Quantum Mechanics* (Addison-Wesley, Reading, MA, 1995).

[224] G. Gilat and L. J. Raubenheimer, Phys. Rev. **144**, 390 (1966).

[225] G. Gilat and Z. Kam, Phys. Rev. Lett. **22**, 715 (1969).